Visualizing Protein-Specific Post-Translational Modifications with FLIM-FRET Microscopy

Dissertation zur Erlangung des

akademischen Grades eines Doktors der

Naturwissenschaften (Dr.rer.nat.)

vorgelegt von

Doll, Franziska

an der

Universität Konstanz

Mathematisch-Naturwissenschaftliche Sektion

Fachbereich Chemie

Konstanz, 2018

Tag der mündlichen Prüfung: 30. November 2018
1. Referent: Prof. Dr. Andreas Zumbusch
2. Referent: Prof. Dr. Valentin Wittmann
3. Referent: Prof. Dr. Christof R. Hauck

Danksagung

Die vorliegende Arbeit entstand zwischen Juni 2014 und Mai 2018 in der Arbeitsgruppe von Prof. Dr. Andreas Zumbusch am Fachbereich Chemie der Universität Konstanz.
Mein besonderer Dank gilt Prof. Dr. Andreas Zumbusch für die Betreuung und Unterstützung während meiner Promotion. Insbesondere möchte ich mich für das mir zugebrachte Vertrauen und die Möglichkeit, meinen Ideen freien Lauf zu lassen, bedanken.
Prof. Dr. Valentin Wittmann danke ich für die vielen Diskussionen und Anregungen, für die Möglichkeit für ein Forschungsvorhaben nach Portugal zu reisen, sowie für die Übernahme des Zweitgutachtens.
Ebenso danke ich Prof. Dr. Christof R. Hauck für die Möglichkeit, sein Labor zu nutzen, die Betreuung im Rahmen meines Thesis Committees und für die Erstellung des dritten Gutachtens.
Allen aktuellen und ehemaligen Mitgliedern der Arbeitsgruppe Zumbusch danke ich für die gute Zusammenarbeit, angenehme Arbeitsatmosphäre und gemeinsamen Aktivitäten. Besonders danke ich Dr. Annette S. Indlekofer für die Einarbeitung in die Zellkultur und ihr Weitfeld-FLIM-Setup, für die vielen Diskussionen und die Unterstützung im Glykosylierungprojekt sowie für die außerfachlichen Gespräche. Dr. Martin J. Winterhalder danke ich für Hilfen bei Problemen an Mikroskopen. Patricia Scheel und Dr. Christoph Kölbl danke ich für die gemeinsamen Ausflüge, ihr offenes Ohr und die vielen lustigen Stunden im Büro. Bernhard U. Conrads, Franziska Rabold und insbesondere Brunhilde Anna Kottwitz danke ich für ihre hervorragende Unterstützung im Laboralltag.
Dr. Anne-Katrin Späte, Dr. Verena F. Schöwe und Jessica Hassenrück danke ich für die Synthese modifizierter Monosaccharide und die gute Zusammenarbeit bei den Glykosylierungsprojekten.
Zudem danke ich PD Dr. Dietmar Funck für die Einführung in das Arbeiten mit *A. thaliana* und sein Interesse am Projekt.
Prof. Dr. Celso Reis vom i3s Institut Porto danke ich für die freundliche Aufnahme in seine Arbeitsgruppe und Betreuung im Rahmen eines Kooperationsprojekts. Bei Dr. Ana Magalhães und Dr. Stefan Mereiter möchte ich mich für die tolle Einarbeitung, Unterstützung und das enorme Interesse am Projekt bedanken. Der ganzen Glycobiology in Cancer Gruppe danke ich für die interessanten, abwechslungsreichen und schönen Wochen in Portugal.
Mein Dank gilt auch den Studenten, die meine Forschung während ihrer Mitarbeiterpraktika (Anna Burrichter, Laura Scheinost, Hannah Bronner, Wolfgang Hinze und Jessica Dröden), Bachelorarbeiten (Wolfgang Hinze und Eliane Landwehr) sowie Masterarbeiten (Pia Widder und Raphael R. Steimbach) unterstützt haben.
Ferner bedanke ich mich bei Jessica Hassenrück, Dr. Matthias Klein und Dr. Katharina Doll für das Korrekturlesen dieser Arbeit.
Darüber hinaus danke ich der Studienstiftung des Deutschen Volkes für die ideelle Förderung und finanzielle Unterstützung meines Studiums sowie der Konstanzer Research School Chemical Biology und dem Zukunftskolleg der Universität Konstanz für Promotionsstipendien und ausgezeichnete Rahmenbedingungen.
Großer Dank gilt meinen Eltern und fünf Geschwistern, die mich sowohl im Studium als auch während der Promotion stetig unterstützt und bestärkt haben. Mein innigster Dank gilt

meinem Freund Matthias, der mich seit Beginn meiner Promotion bedingungslos unterstützt hat, bei chemischen Arbeiten mit Rat und Tat zur Seite stand und mir in turbulenten Zeiten stets Halt gegeben hat.

Zusammenfassung

Modifikationen von Proteinen mit funktionellen Gruppen, die als post-translationale Modifikationen (PTMs) bezeichnet werden, beeinflussen die Struktur, Funktion, Stabilität und Lokalisation eines Proteins erheblich. Es existieren verschiedenste Methoden zur Identifizierung und Untersuchung von PTMs. Jedoch beruhen die meisten auf Proteinaufreinigungen, die den zellulären Kontext zerstören. Die vorliegende Arbeit befasst sich mit der Entwicklung und Anwendung neuartiger Ansätze zur Visualisierung proteinspezifischer PTMs in Säugetierzellen. Dabei werden Analoga der PTM Substrate, die zusätzlich eine chemische Gruppe tragen, in Zellen eingebracht. Diese chemischen Reporter werden von zellulären Enzymen metabolisiert und an Proteine angehängt. In einem weiteren Schritt werden die chemischen Gruppen über bioorthogonale Ligationsreaktionen fluoreszenzmarkiert. Parallel dazu wird das zu untersuchende Protein verknüpft mit einem grün fluoreszierenden Protein (GFP) in Zellen expremiert. Die Modifikation dieses Proteins mit dem PTM-Analogon kann über das Auftreten von Förster-Resonanzenergietransfer (FRET) von dem als Donor fungierenden GFP zu dem an den Reporter gehefteten Akzeptorfarbstoff ermittelt werden. FRET wird am robustesten und genausten über die Fluoreszenzlebenszeit des Donorfluorophors bestimmt, welche durch FRET abnimmt.

Mit dieser Strategie wurde proteinspezifische Glykosylierung untersucht. Dazu wurde zunächst das Verbleiben des ausgewählten chemischen Glykosylierungreporters (Ac_4GlcNCyoc) nach Aufnahme in Zellen näher beleuchtet. Es wurde festgestellt, dass dieser Reporter in eine spezielle Form der intrazellulären Proteinglykosylierung, die sogenannte *O*-GlcNAcylierung, eingebaut wird. Indem diese Reporterstrategie mit GFP-markierten Proteinen und der Bildgebung über Fluoreszenzlebenszeiten (*fluorescence lifetime imaging*, FLIM) kombiniert wurde, wurde der erste Ansatz zur Visualisierung des Glykosylierungszustands einzelner Proteine in lebenden Zellen geschaffen. Dessen generelle Anwendbarkeit wurde durch die Bildgebung der Glykosylierung von fünf GFP-gekennzeichneten Proteine nachgewiesen. Studien mit der Kinase Akt1 offenbarten die Möglichkeit der Methode, räumliche Unterschiede im Glykosylierungszustand eines Proteins aufzulösen. Versuche zur Anwendung des Ansatzes zur Lösung biologischer Fragestellungen zeigten dessen Limitierungen auf, welche die Notwendigkeit der Nähe der PTM Stelle zum GFP und die Glykosylierung der zu untersuchenden Proteine mit einer hohen Stöchiometrie einschließen.

Neben der Bildgebung proteinspezifischer Glykosylierung wurden chemische Glykosylierungreporter auch zur Untersuchung von Glykanen in Wurzeln der Modellpflanze *Arabidopsis thaliana* sowie Membranglykanen von Magenkrebszellen eingesetzt.

Ähnliche Visualisierungsstrategien, wie für die Glykosylierung, wurden für die PTMs Acetylierung und Methylierung realisiert. Im Falle der Proteinacetylierung wurde für den gewählten chemischen Reporter Natrium 4-Pentynoat die Prozessierung durch Acetyltransferasen und Deacetylasen demonstriert. Dabei wurden die 4-Pentynoylgruppen an Proteine angehängt und mit azidfunktionalisierten Farbstoffen fluoreszenzmarkiert, was über Fluoreszenzmikroskopie sichtbar gemacht wurde. Allerdings war deren Einbau in das zelluläre Acetylom zu schwach, sodass kein effizienter FRET über FLIM detektiert werden konnte. Der chemische Reporter ProSeAM, welcher für Methylierungsexperimente

ausgewählt wurde, wurde erfolgreich mittels Elektroporation in Zellen eingebracht. Die anschließende bioorthogonale Ligationsreaktion ermöglichte die Visualisierung der Methylierung innerhalb von Zellen durch Fluoreszenzmikroskopie. Des Weiteren wurde ein FLIM-FRET-basierter Ansatz zur Bildgebung proteinspezifischer Methylierung in Zellen erarbeitet. Die geschaffene, generell anwendbare Methode ermöglichte die Visualisierung des Methylierungszustands von vier GFP-Fusionsproteinen in zwei verschiedenen Zelllinien sowie die Auflösung des räumlichen Methylierungsmusters eines einzelnen Proteins.

Abstract

Modifications of proteins with functional groups, better known as post-translational modifications (PTMs), tremendously affect a protein's structure, function, stability, and localization. Although various methods for the identification and investigation of protein PTMs exist, most of them require the isolation of proteins and thus disturb their cellular context. The present thesis deals with the development and application of novel strategies for imaging of protein-specific PTMs inside mammalian cells. Thereto, PTM substrate analogs carrying a chemical handle are introduced in cells. These chemical reporters are metabolized and attached to proteins by cellular enzymes. In a second step, chemical handles are fluorescently labeled via bioorthogonal ligation reactions. In addition, the protein of interest is expressed with a green fluorescent protein (GFP)-tag in cells. The modification of this protein with the PTM analog can be assessed by measuring the occurrence of Förster resonance energy transfer (FRET) from the donor GFP to the reporter-anchored acceptor fluorophore. FRET is most robustly and accurately detected via the fluorescence lifetime of the donor fluorophore, which decreases due to FRET.

Using this strategy, protein-specific intracellular glycosylation has been studied. Firstly, the metabolic fate of the chemical glycosylation reporter of choice (Ac_4GlcNCyoc) was investigated. It was shown to most likely end up in a special type of intracellular protein glycosylation termed *O*-GlcNAcylation. By combining this chemical reporter with GFP-tagged proteins and fluorescence lifetime imaging (FLIM) microscopy, the first approach for visualizing glycosylation states of individual proteins inside living cells was established. Its general applicability was demonstrated by imaging the glycosylation of five different GFP-fusion proteins. Studies on the kinase Akt1 revealed the potential of the established approach to resolve spatial differences in a protein's glycosylation state. Attempts to apply this strategy to biological investigations of selected proteins showed its limitations, which include the need of the PTM site to be in close proximity to the GFP-tag and the glycosylation of proteins of interest with a high stoichiometry.

Besides imaging protein-specific glycosylation, chemical glycosylation reporters were utilized to examine glycans in roots of the model plant *Arabidopsis thaliana* and membrane glycans of gastric cancer cells.

Protein-specific imaging strategies similar to those for glycosylation were developed for the PTMs acetylation and methylation. Regarding protein acetylation, the selected chemical reporter sodium 4-pentynoate was shown to be processed by acetyltransferases and deacetylases. Its 4-pentynoyl groups were attached to proteins and fluorescently labeled with azide-functionalized dyes, which were visualized by fluorescence microscopy. However, its incorporation in the cellular acetylome was too weak to allow for the detection of efficient FRET by FLIM. The chemical reporter chosen for protein methylation studies (ProSeAM) was successfully delivered into cells by electroporation. Subsequent bioorthogonal labeling enabled in cell imaging of a whole cell's methylation with fluorescence microscopy. Moreover, a FLIM-FRET-based approach for in cell imaging of protein-specific methylation was created. This generally applicable method allowed for the visualization of the methylation state of four GFP-fusion proteins in two different cell lines and enabled resolving the spatial methylation pattern of an individual protein.

Table of Contents

1. Introduction ..... - 1 -
2. State of Knowledge ..... - 3 -
   2.1. Post-Translational Protein Modifications ..... - 3 -
   2.1.1. Protein Glycosylation ..... - 3 -
   2.1.2. Protein Acetylation ..... - 7 -
   2.1.3. Protein Methylation ..... - 10 -
   2.2. Chemical Reporters ..... - 14 -
   2.2.1. Chemical Reporters for Protein Glycosylation ..... - 15 -
   2.2.2. Chemical Reporters for Protein Acetylation ..... - 17 -
   2.2.3. Chemical Reporters for Protein Methylation ..... - 18 -
   2.2.4. Delivery of Chemical Reporters into Cells ..... - 20 -
   2.3. Bioorthogonal Ligation Reactions ..... - 21 -
   2.4. FLIM-FRET Microscopy ..... - 26 -
   2.4.1. Fluorescence ..... - 26 -
   2.4.2. Fluorescent Proteins ..... - 28 -
   2.4.3. Fluorescence Microscopy ..... - 29 -
   2.4.4. Förster Resonance Energy Transfer ..... - 30 -
   2.4.5. Fluorescence Lifetime Imaging Microscopy ..... - 34 -
   2.5. Detection of Protein-Specific PTMs ..... - 37 -
3. Objectives ..... - 39 -
4. Results and Discussion ..... - 41 -
   4.1. Protein Glycosylation ..... - 41 -
   4.1.1. Ac_4GlcNCyoc ..... - 41 -
   4.1.2. Protein-Specific Imaging of Glycosylation ..... - 51 -
   4.1.3. *O*-GlcNAcylation of Kif18A ..... - 61 -
   4.1.4. *O*-GlcNAcylation of α-synuclein ..... - 64 -
   4.1.5. *O*-GlcNAcylation of β-catenin ..... - 67 -
   4.1.6. Glycosylation in *A. thaliana* ..... - 74 -
   4.1.7. Visualizing the Sialyl Tn Antigen ..... - 79 -
   4.1.8. Conclusions ..... - 86 -
   4.2. Protein Acetylation ..... - 89 -
   4.2.1. Evaluation of Na4P as Chemical Reporter for Protein Acetylation ..... - 89 -

4.2.2. Synthesis of New Reporters for Protein Acetylation ..... - 90 -
4.2.3. Biological Evaluation of Na4P, M4P, and AM4P ..... - 91 -
4.2.4. Protein-Specific Imaging of Protein Acetylation ..... - 102 -
4.2.5. Conclusions ..... - 112 -
4.3. Protein Methylation ..... - 113 -
4.3.1. Evaluation of ProSeAM as Chemical Reporter for Protein Methylation ..... - 113 -
4.3.2. Delivery of ProSeAM in Mammalian Cells ..... - 115 -
4.3.3. Protein-Specific Imaging of Protein Methylation ..... - 119 -
4.3.4. Conclusions ..... - 130 -
5. Outlook ..... - 131 -
6. Materials and Methods ..... - 133 -
6.1. Materials ..... - 133 -
6.1.1. Organisms ..... - 133 -
6.1.2. Media ..... - 134 -
6.1.3. Buffers and Solutions ..... - 135 -
6.1.4. Chemicals ..... - 136 -
6.1.5. Enzymes ..... - 138 -
6.1.6. Plasmids ..... - 138 -
6.1.7. Oligonucleotides ..... - 140 -
6.1.8. Antibodies ..... - 141 -
6.1.9. Kits ..... - 142 -
6.1.10. Equipment ..... - 142 -
6.1.11. Consumables ..... - 142 -
6.1.12. Software ..... - 143 -
6.2. Biochemical Methods for Mammalian Cells ..... - 143 -
6.2.1. Cell Culture ..... - 143 -
6.2.2. Transient Transfection of Mammalian Cells ..... - 143 -
6.2.3. Cell Lysis ..... - 144 -
6.2.4. Immunoprecipitation ..... - 144 -
6.2.5. SDS-PAGE and Western Blotting ..... - 145 -
6.2.6. Cell Seeding for Microscopy ..... - 147 -
6.2.7. Metabolic Labeling of Mammalian Cells for Protein Glycosylation ..... - 147 -
6.2.8. Metabolic Labeling of Mammalian Cells for Protein Acetylation ..... - 147 -

6.2.9. Metabolic Labeling of Mammalian Cells for Protein Methylation ..... - 147 -
6.2.10. DAinv Reaction ..... - 148 -
6.2.11. CuAAC ..... - 148 -
6.2.12. Dual Labeling of Membrane Glycans via SPAAC and DAinv Reactions ..... - 149 -
6.2.13. Immunocytochemistry ..... - 150 -
6.2.14. Viability Tests ..... - 150 -
6.3. Biochemical Methods for *E. coli* ..... - 151 -
6.3.1. Cultivation of *E. coli* ..... - 151 -
6.3.2. Transformation of Competent *E. coli* ..... - 151 -
6.3.3. Plasmid Preparation ..... - 152 -
6.3.4. Restriction Digest of Plasmid DNA ..... - 153 -
6.3.5. Hot-Start Gradient PCR ..... - 154 -
6.3.6. Ligation Independent Cloning (LIC) ..... - 154 -
6.3.7. Site Directed Mutagenesis of Plasmid DNA ..... - 154 -
6.3.8. Cre-LoxP Recombination ..... - 155 -
6.3.9. Agarose Gel Electrophoresis ..... - 156 -
6.3.10. Isolation of DNA from an Agarose Gel ..... - 156 -
6.3.11. Sequencing of Plasmid DNA ..... - 156 -
6.4. Biochemical Methods for *A. thaliana* ..... - 157 -
6.4.1. Seeding *A. thaliana* ..... - 157 -
6.4.2. Treatment of *A. thaliana* with Chemical Reporters ..... - 157 -
6.4.3. Lysis of *A. thaliana* ..... - 157 -
6.4.4. DAinv Reaction ..... - 158 -
6.4.5. CuAAC ..... - 158 -
6.4.6. Seedling Preparation for Microscopy ..... - 159 -
6.5. Chemical Synthesis ..... - 159 -
6.5.1. OSMI-1 ..... - 159 -
6.5.2. M4P ..... - 160 -
6.5.3. AM4P ..... - 161 -
6.6. Microscopy ..... - 161 -
6.6.1. Confocal Fluorescence Microscopy ..... - 161 -
6.6.2. Acceptor Photobleaching ..... - 162 -
6.6.3. Wide-field Frequency Domain FLIM ..... - 162 -

6.7. Statistics ..... - 164 -
7. Publications ..... - 165 -
8. Conference Contributions ..... - 167 -
9. List of Abbreviations ..... - 169 -
10. References ..... - 173 -
11. Appendix ..... - 195 -

1. Introduction

Next to lipids, nucleic acids, and carbohydrates, proteins are one of the four major classes of organic macromolecules. Proteins are responsible for almost all cellular tasks. They serve as enzymes for catalyzing biochemical reactions, as hormones for transmitting signals, as cytoskeleton for maintaining and changing a cell's shape, as molecular motors for transporting cargo, as contractile proteins to enable movements, or as antibodies to recognize and remove foreign molecules.

The information encoding proteins is stored as deoxyribonucleic acid (DNA) in the cellular nucleus. It is transcribed into messenger ribonucleic acid (mRNA) and additionally processed. mRNA is the template for protein biosynthesis, which takes place at ribosomes in the cytoplasm. This process is called translation. Thereby, an amino acid chain is formed according to the mRNA's code. This chain represents the primary structure of a protein and can fold autocatalytically or with the help of chaperones into various secondary and tertiary protein structures.

According to the central dogma of molecular biology "DNA gives RNA gives proteins",[1] it was speculated that the code of life could be read as soon as the human genome was deciphered. It was hoped that this code would provide all necessary information to elucidate the molecular causes of diseases and easily find therapeutic approaches to cure them. However, only 20,000 to 25,000 genes were identified in the human genome.[2] This small value was surprising, as the number of genes has been believed to be a measure of organismal complexity, but also 13,000, 19,000, and 30,000 genes have been located in the genomes of the fruit fly *Drosophila melanogaster*, the nematode *Caenorhabditis elegans*, and the grapevine, respectively.[3–6] The number of distinct covalent forms of proteins, collectively referred to as the proteome, is larger than one million and thus exceeds the amount of proteins predicted by the coding capacity of the DNA by two orders of magnitude.[7] While alternative splicing of mRNA contributes to the diversification of proteins on the transcriptional level,[8] the complexity of the human proteome is mainly generated by attachments of chemical groups to protein termini or amino acid side chains.[9] These protein alterations are summarized with the term post-translational modifications (PTMs). Until now, hundreds of different protein PTMs have been identified,[10] which tremendously affect all properties of proteins and are linked to numerous diseases.[9]

Consequently, knowing when and where which protein is present in cells is not sufficient to fully elucidate basic cellular processes. This requires a profound understanding of protein interactions and protein PTMs. For this purpose, mass spectrometry as well as biochemical and bioinformatic methods are usually utilized. Although these techniques have been valuable for the identification of thousands of modified proteins, exact modification sites, and biological effects of these modifications,[11,12] most work has been performed outside the cellular context. Since Robert Hooke's first detection of cells with an optical microscope in

the early 17th century,[13,14] the field of light and especially fluorescence microscopy has emerged rapidly.[15,16] Nowadays, microscopes enable imaging of cellular and subcellular processes. The discovery of the green fluorescent protein from the jellyfish *Aequorea victoria* has revolutionized the application of fluorescence microscopy in biological studies.[17,18] The genetic fusion of a protein's DNA with that of a fluorescent protein allows for in cell expression and investigation of fluorescently marked proteins. However, PTMs are secondary gene products and thus cannot be expressed with a fluorescent protein tag in cells. To fluorescently label and image PTMs, several methods utilizing chemical biology approaches have been developed in the last two decades.[19] Whereas many of them allowed studying PTMs on the whole proteome level, only few approaches gave insights on modification states of individual proteins.[20]

The present thesis deals with developing and applying novel strategies for imaging protein-specific PTMs inside cells that are based on a combination of chemical biology and microscopy. It is structured as follows: Chapter 2 covers the basics and the state of the art of PTMs studied in this thesis, chemical reporter strategies, associated bioorthogonal ligation reactions, and the microscopy techniques used. Following, known methods for the detection of protein-specific PTMs are summarized and lead to the formulation of the objectives of this work in chapter 3. In chapter 4, achieved results are presented, discussed, and summarized for each examined PTM individually. Finally, an outlook on further possible experiments on presented topics and possible follow-up projects is given (chapter 5). Materials and methods employed within this thesis are listed in chapter 6.

2. State of Knowledge

2.1. Post-Translational Protein Modifications

Until now, more than 430 PTMs have been identified.[10] Functional groups attached to proteins range in their size from small methyl groups to huge oligosaccharides. Modifications of proteins with PTMs can be covalent or noncovalent and are often catalyzed by enzymes. Whereas some PTMs are irreversible, for example myristoylation[21], many PTMs can be removed by cellular enzymes rendering them dynamic, such as phosphorylation[22]. In addition, PTMs can occur substoichiometric and can possess heterogeneous structures.[23]

PTMs increase the complexity of the cellular proteome by several orders of magnitude compared to the genome's coding capacity.[24] They change the biochemical and biophysical properties of the targeted protein and thereby affect for instance the activity, function, stability, structure, and localization of proteins and modulate protein-protein interactions, signaling cascades, DNA transcription, DNA repair, and cell division.[7,24,25] Moreover, PTMs are involved in the regulation of the circadian clock and transmit information on the cellular environment, such as the presence of nutrients or stressors.[26–29] As a consequence of its manifold effects, it barely astonishes that PTM disorders are associated with severe ailments including diabetes, Alzheimer's and Huntington's disease, cardiovascular diseases, and cancer.[30–34]

15 out of the 20 standard amino acids have been shown to be post-translationally modified (neglecting acetylation of N-termini).[7] Often, multiple residues of a protein carry the same or different PTMs. Several cases of competition among PTMs for the same or adjacent amino acids have been reported, which frequently yield opposing functions of the target protein. Examples for competing PTMs include phosphorylation and *O*-linked *N*-acetylglucosamine at threonine 41 of β-catenin[35] or acetylation and methylation at lysine 382 of the tumor protein p53[36].

A quantification of experimentally observed PTMs revealed that the most prevalent PTMs are phosphorylation, acetylation, *N*-linked glycosylation, amidation, hydroxylation, methylation, *O*-linked glycosylation, and ubiquitination.[10] Three of these modifications, namely glycosylation, acetylation, and methylation, were studied within this thesis. Accordingly, their mechanisms and functions are explained in more detail in the following chapters.

2.1.1. Protein Glycosylation

The attachment of sugar moieties to proteins is termed protein glycosylation. Early bioinformatic studies suggested that approximately half of all proteins are glycosylated.[37] A recent analysis of experimental data demonstrated that at most every fifth protein is glycosylated, but still lists glycosylation among the three most common PTMs.[10] Glycosylation is a multifaceted co- and post-translational modification of lipids and proteins.

Eukaryotic glycans are made up from the eight monosaccharides D-glucose (Glc), D-galactose (Gal), D-mannose (Man), L-fucose (Fuc), D-xylose, *N*-acetyl-D-glucosamine (GlcNAc), *N*-acetyl-D-galactosamine (GalNAc), and *N*-acetyl-neuraminic acid (Neu5Ac) (Figure 2.1).[38] These sugars can be attached to different protein sides and linked in various ways, resulting in an enormous structural complexity.

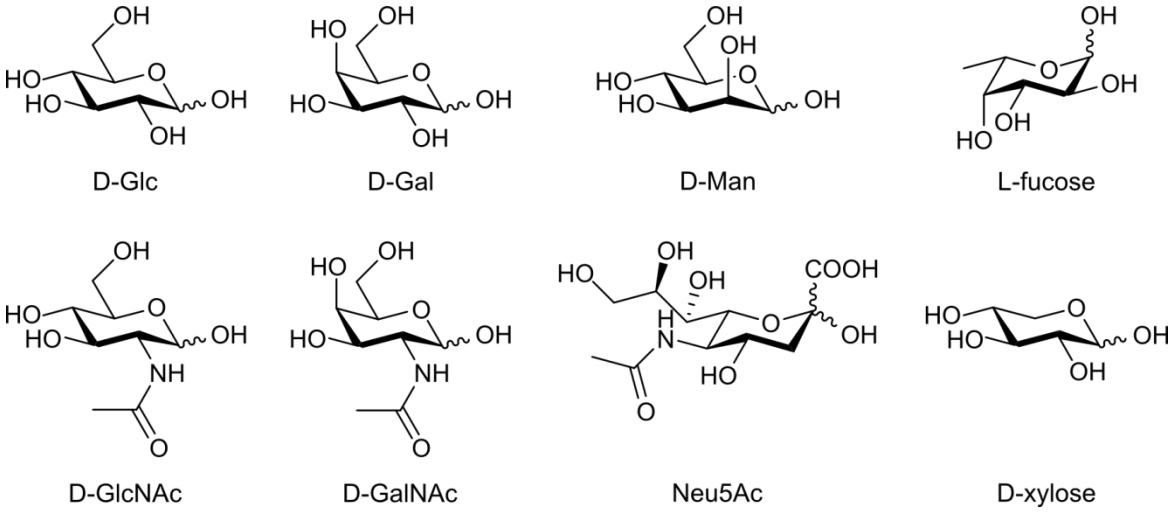

Figure 2.1: Chemical structures of monosaccharides present in eukaryotic glycans.

The two main types of protein glycosylation are *N*-glycans and *O*-glycans. *N*-glycans are oligosaccharides linked via a *N*-glycosidic bond to asparagine residues in the consensus sequence motif (asparagine)-(any amino acid besides proline)-(serine/threonine).[39] The common sugar structure shared by all *N*-glycans is Manα1-6(Manα1-3)Manβ1-4GlcNAc β1-4GlcNAcβ1-asparagine, which can be enlarged in many ways.[38] *O*-glycans are linked to hydroxy groups of serine and threonine residues and possess no common core structure. Different *O*-glycan types are defined by the first sugar attached to proteins and include mucin-type *O*-glycans, which are oligosaccharides starting with α-linked GalNAc, β-linked *O*-GlcNAc, β-linked *O*-Glc, α-linked *O*-Man, and α-linked *O*-Fuc.[40]

N-glycans and mucin-type *O*-glycans are accomplished in the endoplasmic reticulum and Golgi apparatus. Proteins modified with these complex oligosaccharides are present on the cell surface or secreted into the extracellular space. At the cell surface, *N*- and *O*-glycans function in cell-cell adhesion, signal transduction, immune response, endocytosis, and interaction with pathogens.[41,42]

Of special interest is protein *O*-GlcNAcylation, which has been discovered in 1982 and has meanwhile been shown to be nearly as dynamic as protein phosphorylation.[43–45] Compared to phosphorylation, where many protein kinases are known, intracellular *O*-GlcNAcylation is solely catalyzed by one enzyme: *O*-GlcNAc transferase (OGT).[46] It uses uridine diphosphate (UDP)-GlcNAc as substrate and transfers GlcNAc onto serine and threonine residues of cytoplasmic, nuclear, and mitochondrial proteins.[47,48] In humans, one single gene encodes three splice versions of OGT: the nucleocytoplasmic OGT (116 kDa), the mitochondrial OGT (103 kDA), and the small OGT (78 kDa).[49] All of them own a N-terminal domain with different amounts of tetratricopeptide repeat motifs, a linker domain, and a C-terminal catalytic domain. OGT is an essential enzyme, as its knockout in mice has been reported to be

embryonically lethal.[50] Apart from intracellular *O*-GlcNAcylation, also secreted and membrane proteins owing an epidermal growth factor-like repeat domain have recently been proven to become *O*-GlcNAcylated by another enzyme, the epidermal growth factor domain-specific OGT.[51] The enzyme rendering *O*-GlcNAcylation dynamic is *O*-GlcNAcase (OGA).[52] OGA hydrolyzes the *O*-glycosidic bond while retaining the configuration at the anomeric center of the monosaccharide.[53] Both OGT and OGA are evolutionary well conserved.[54] Until now, thousands of proteins from almost all functional protein classes have been identified to become *O*-GlcNAcylated.[55] *O*-GlcNAcylation influences the stability, structure, function, and localization of proteins and has impacts on protein-protein interactions, transcription, translation, cell division, and metabolism.[54,56–59] Moreover, *O*-GlcNAcylation responses to nutrients and oxidative stress.[28,60] As a result of its many tasks, malfunctions of protein *O*-GlcNAcylation have been reported to be associated with severe ailments including cancer, Alzheimer's disease, cardiovascular diseases, neurodegenerative diseases, and diabetes type 2.[30,59,61] A widespread crosstalk between protein *O*-GlcNAcylation and phosphorylation has been found.[54,62,63] Both modifications can compete for certain serine/threonine residues or influence one another at adjacent residues. For example, the *O*-GlcNAcylation of RAC-α serine/threonine-protein kinase (Akt1) following an insulin stimulus inhibits its phosphorylation at threonine 308, thereby terminating its kinase activity.[64] In addition, protein *O*-GlcNAcylation interacts with ubiquitination, for instance in case of p53,[65] and OGT overexpression influences the methylation and acetylation patterns of histones[66].

In this thesis, glycosylation studies mainly focused on *O*-GlcNAc, but chapter 4.1.7 also deals with the imaging of cell surface-localized GalNAc in mucin-type *O*-glycans and Neu5Ac. For a more comprehensive understanding of the origin of these three glycoconjugates, biosynthesis pathways of their precursors are outlined in the following section (Figure 2.2).

The precursor for protein *O*-GlcNAcylation is UDP-GlcNAc, which is generated in six steps from Glc. Thereby, Glc is phosphorylated at is C-6´ by glucokinase. Glc6P isomerase converts Glc6P into Fru6P, which further reacts to GlcN6P with the help of glutamine-Fru6P aminotransferase. GlcN6P *N*-acetyltransferase adds an acetyl group to give GlcNAc6P. This compound can also be generated from GlcNAc, which is a product from the hexosamine salvage pathway, through phosphorylation by GlcNAc kinase. The C-6´ phosphate group of GlcNAc6P is transferred to its C-1´ via GlcNAc phosphomutase. The sugar is activated through the addition of UDP by UDP-GalNAc/UDP-GlcNAc pyrophosphorylase yielding UDP-GlcNAc, which serves as substrate for OGT. OGA removes *O*-linked GlcNAc by hydrolyzation yielding the free hydroxy group of the serine or threonine residue and GlcNAc. As approximately two to five percent of intracellular glucose end up as UDP-GlcNAc after metabolism via the hexosamine biosynthetic pathway, it is obvious that changes in the glucose level alter cellular amounts of UDP-GlcNAc and thus affect protein *O*-GlcNAcylation.[67] This further underlines the linkages of the presence of nutrients and dynamic protein *O*-GlcNAcylation.

All mucin-type *O*-glycans bear a GalNAc that is α-linked to the hydroxy group of a serine or threonine amino acid via an *O*-glycosidic linkage. For this purpose, GalNAc from the hexosamine salvage pathway is phosphorylated at its C-1´ by GalNAc-1-kinase to give

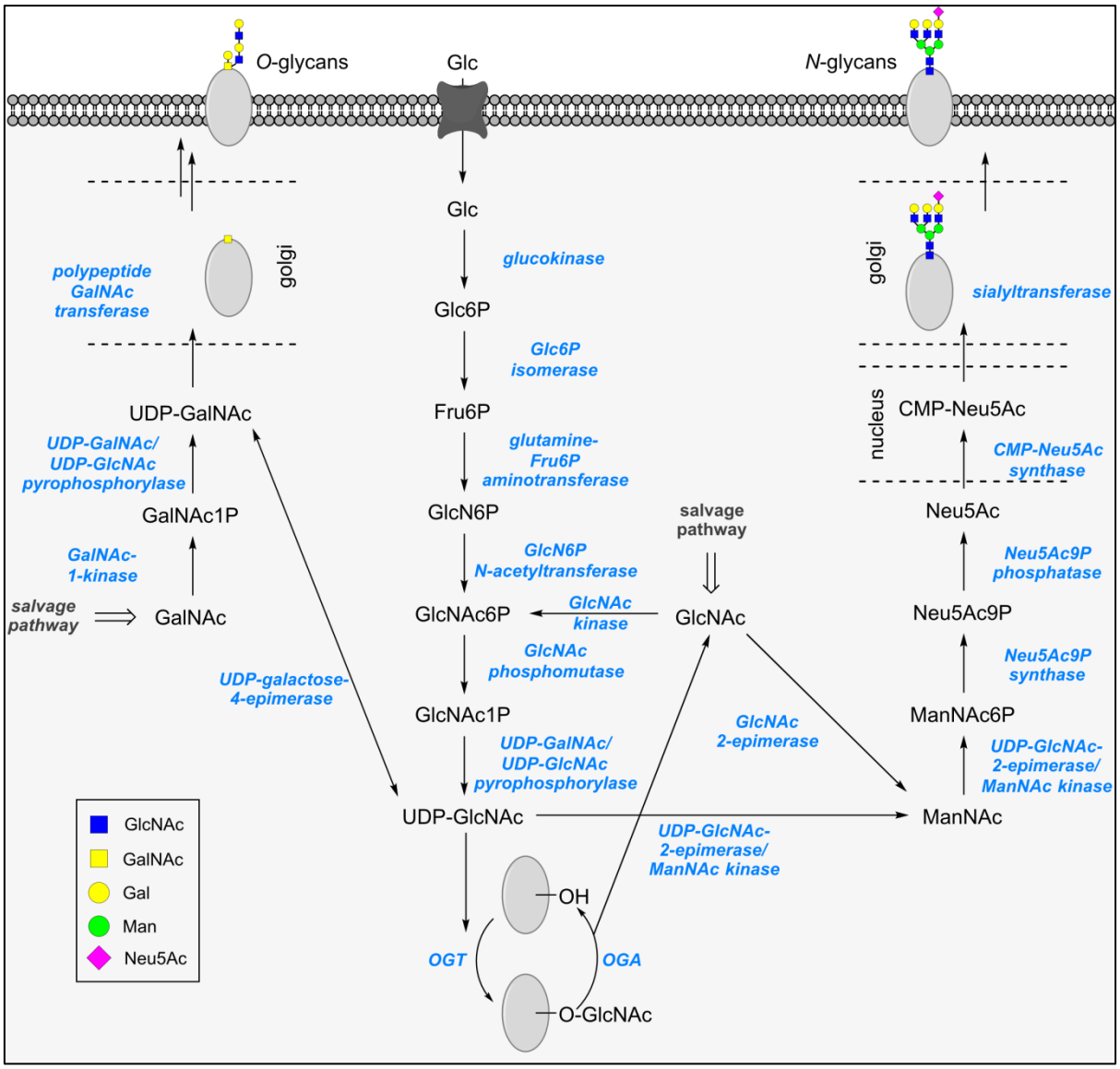

Figure 2.2: Biosynthesis pathways for UDP-GalNAc, UDP-GlcNAc, and CMP-Neu5Ac.

GalNAc1P. This compound is activated by addition of UDP, which is mediated by UDP-GalNAc/UDP-GlcNAc pyrophosphorylase. UDP-GalNAc is transported into the Golgi apparatus, where it is attached to proteins by polypeptide GalNAc transferase. Afterwards, various glycosyltransferases can add further monosaccharides to form different mucin-type *O*-glycans.[68] The resulting *O*-glycoproteins are then localized to the plasma membrane or secreted in the extracellular space.

Neu5Ac is one of over 50 monosaccharides belonging to the family of *N*-acylneuraminic acids, also termed sialic acids.[69] These monosaccharides mainly occur at ends of *N*-glycans, *O*-glycans, and glycolipids and are important for cell-cell interactions, signal transductions, protein stabilization, immunoregulation, ion binding, and ion transport.[70,71] The precursor for Neu5Ac is ManNAc, which is first phosphorylated at its C-6´ by UDP-GlcNAc-2-epimerase/ManNAc kinase. In a next step, ManNAc6P is converted to Neu5Ac9P by a synthase. Its phosphate residue is removed by Neu5Ac9P phosphatase to give Neu5Ac, which is transported into the nucleus, where cytidine monophosphate (CMP)-Neu5Ac synthase

activates Neu5Ac by linking it to CMP. Subsequently, CMP-Neu5Ac is transported to the Golgi apparatus and transferred to glycoproteins and glycolipids by sialyltransferases.
Metabolic pathways of GlcNAc, GalNAc, and ManNAc are interconnected. UDP-galactose-4-epimerase converts UDP-GlcNAc in UDP-GalNAc as well as UDP-Glc in UDP-Gal and *vice versa*.[72] GlcNAc can enter the Neu5Ac biosynthetic pathway via two routes: It can be directly transformed into ManNAc by the GlcNAc-2-epimerase or ManNAc can be obtained from UDP-GlcNAc through catalysis by UDP-GlcNAc-2-epimerase/ManNAc kinase.[73,74] Further possible conversions have been summarized elsewhere.[75]

2.1.2. Protein Acetylation

The modification of proteins with acetyl groups is among the most prevalent PTMs. The substrate for protein acetylation is acetyl-linked coenzyme A (acetyl-CoA, Figure 2.3A),[76,77] which is present in mitochondria, the cytoplasm, and the nucleus of a cell. In mammals, acetyl-CoA is produced in mitochondria from pyruvate, itself generated from glucose via glycolysis, by the pyruvate dehydrogenase complex or from fatty acids by β-oxidation (Figure 2.4). Acetyl-CoA can be converted into citrate via the citric acid cycle. Citrate can be actively transported into the cytoplasm, where it serves as substrate for adenosine triphosphate (ATP) citrate lyase, which produces acetyl-CoA. In the cytoplasm, acetyl-CoA can be synthesized from acetate by acetyl-CoA synthetase. Citrate freely diffuses in and out of the nucleus, where it can also be converted to acetyl-CoA by ATP citrate lyase.[78]

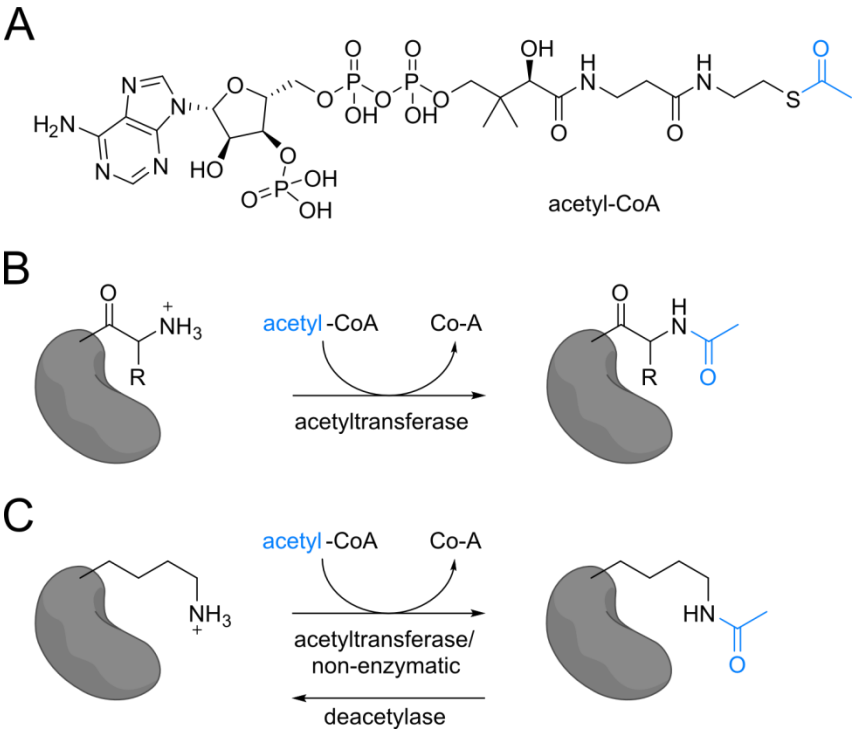

Figure 2.3: (A) Chemical structure of acetyl-CoA. (B) Mechanism of irreversible N-terminal protein acetylation. (C) Mechanism of reversible protein acetylation at the ε-amino group of lysine residues.

The first proteins identified to be acetylated have been histones in 1963.[79] For a long time, acetylation has been believed to be solely a histone modification. With the discovery of

further acetylated proteins, such as tubulin[80], tumor suppressor p53[81], and transcription factor NF-κB[82], the field was opened to investigations of non-histone acetylation targets. The first proteomics study on protein acetylation in 2006 has revealed that many nuclear, cytoplasmic, and even mitochondrial proteins are acetylated.[83]

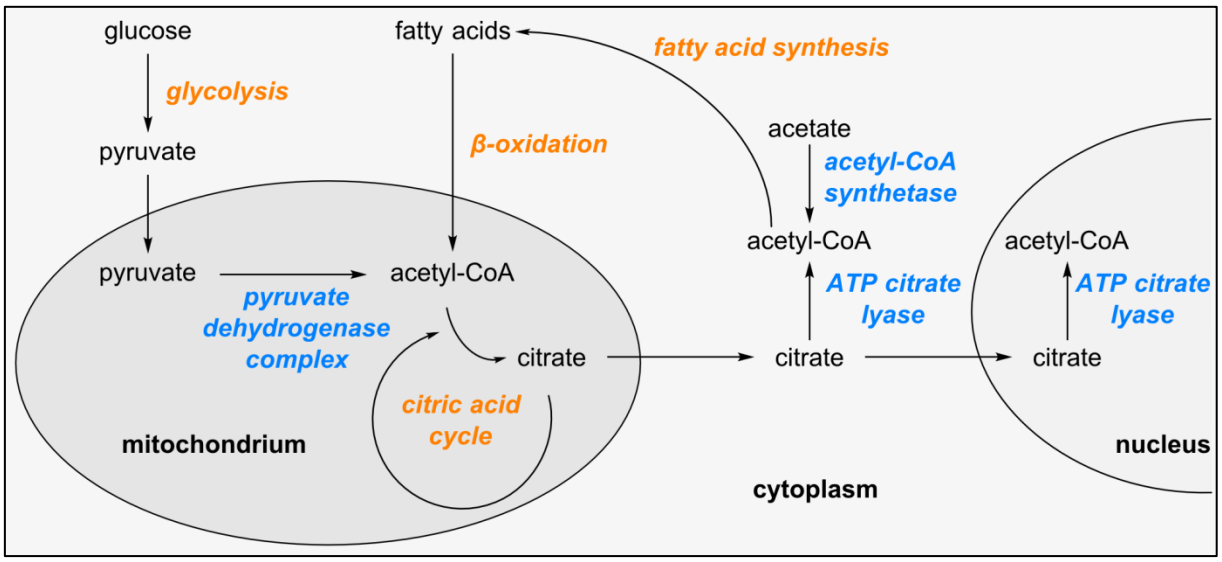

Figure 2.4: Biosynthesis pathways for acetyl-CoA. This drawing is based on[78].

Protein acetylation can occur at N-terminal α-amino groups or at lysine ε-amino groups of proteins (Figure 2.3B and C). Acetylation neutralizes the positive charge of amino groups and thereby inhibits further or other PTMs at these residues.[84] Approximately 80-90 % of all human proteins are co- and post-translationally acetylated at their N-termini.[85,86] In mammals, six different N-terminal acetyltransferases have been found.[87] This type of protein acetylation is assumed to be irreversible and serves many functions. For instance, it influences a protein's lifetime, folding, localization, and interaction partners.[84,87] Acetylation of lysine ε-amino groups is well conserved from bacteria to humans.[88] It is catalyzed by lysine acetyltransferases and can be reversed by lysine deacetylases, which render lysine ε-amino acetylation a dynamic PTM. 22 different lysine acetyltransferases have been listed for humans, but no clear acetylation sequence motifs have been found.[78,84] In addition, eleven Zn^{2+}-dependent lysine deacetylases and seven NAD^{+}-dependent deacetylases (named sirtuins) exist.[84] Whereas sirtuins are present in the mitochondria, cytoplasm, and nucleus, Zn^{2+}-dependent deacetylases are solely localized in the cytoplasm and nucleus.[78] Proteins that recognize and bind acetylated lysines often bear a so called bromodomain, which consists of approximately 120 amino acids forming small helical structures. A summary of bromodomain-containing proteins and their acetylated interaction partners has been published by Filippakopoulos and Knapp.[89] As a result of lysine acetylation, the positive charge of amino groups is eliminated and some steric hindrance is introduced, which affects the interaction of proteins with nucleic acids and with other proteins. In 1964, it has been proposed that histone acetylation regulates gene expression.[90] Meanwhile, it has been proven that acetylation and deacetylation finely regulate nucleosomal assembly of histones and DNA, chromosomal condensation, and gene transcription.[91] For example, acetylation of histone 4

at lysine 16 influences the structure of nucleosomes and its interaction with external proteins, both resulting in the activation of transcription.[92,93] Moreover, lysine acetylation is involved in the regulation of the subcellular localization of proteins, their enzymatic activity, intracellular pH, metabolism, apoptosis, and stress response.[83,94–96]

Malfunctions of protein acetylation have been linked to several cardiovascular and neurodegenerative diseases as well as to cancer.[97] As an example, acetylation at N-terminal lysine residues of the huntingtin protein associated with Huntington's disease affects the protein's interaction with lipid bilayers and retards fibril formation, which results in larger fibrillar aggregates.[31]

Besides enzyme-catalyzed acetylation, lysine ε-amino groups are also non-enzymatically acetylated.[98] This is especially important in mitochondria, where a slightly increased pH value (7.9) and a higher acetyl-CoA concentration favor non-enzymatic acetylation.[99] In line with these observations, a low stoichiometry of acetylation sites and a strong correlation of acetylation levels with acetyl-CoA levels have been found for mitochondrial and cytoplasmic proteins in *S. cerevisiae*.[100] Thus, the presence of the deacetylases sirtuin 3 and 5 in mitochondria has been suggested to regulate non-enzymatic acetylation of proteins.[99] Recently, it has been reported that non-enzymatic acetylation of lysine residues by acetyl-CoA frequently takes place via a *S*-acetylated thiol intermediate in close proximity to the lysine.[101]

In addition to acetylation, further acylations of lysine ε-amino groups have been discovered within the last decade. These comprise lysine formylation[102], propionylation[103], butyrylation[103], crotonylation[104], malonylation[105], succinylation[106], and glutarylation[107] (Figure 2.5). Similar to acetylation, protein formylation, propionylation, butyrylation, and crotonylation neutralize the positive charge of the ε-amino group of a lysine residue. In contrast, malonylation, succinylation, and glutarylation add a negative charge to lysines, which alters the proteins surface charge landscape and consequently its interaction partners. So far, no lysine acyltransferases have been detected for most acylations. However, propionylation and butyrylation of histones have been shown to be catalyzed by the histone acetyltransferase p300 and the CREB-binding protein.[103] Besides this, the weak deacetylase sirtuin 5, which is present in mitochondria and the cytoplasm, has been reported to possess orders of magnitudes higher activity towards malonyl, succinyl, and glutary groups than towards acetyl groups.[105,107] Details of the biological functions of these modifications are still unknown.

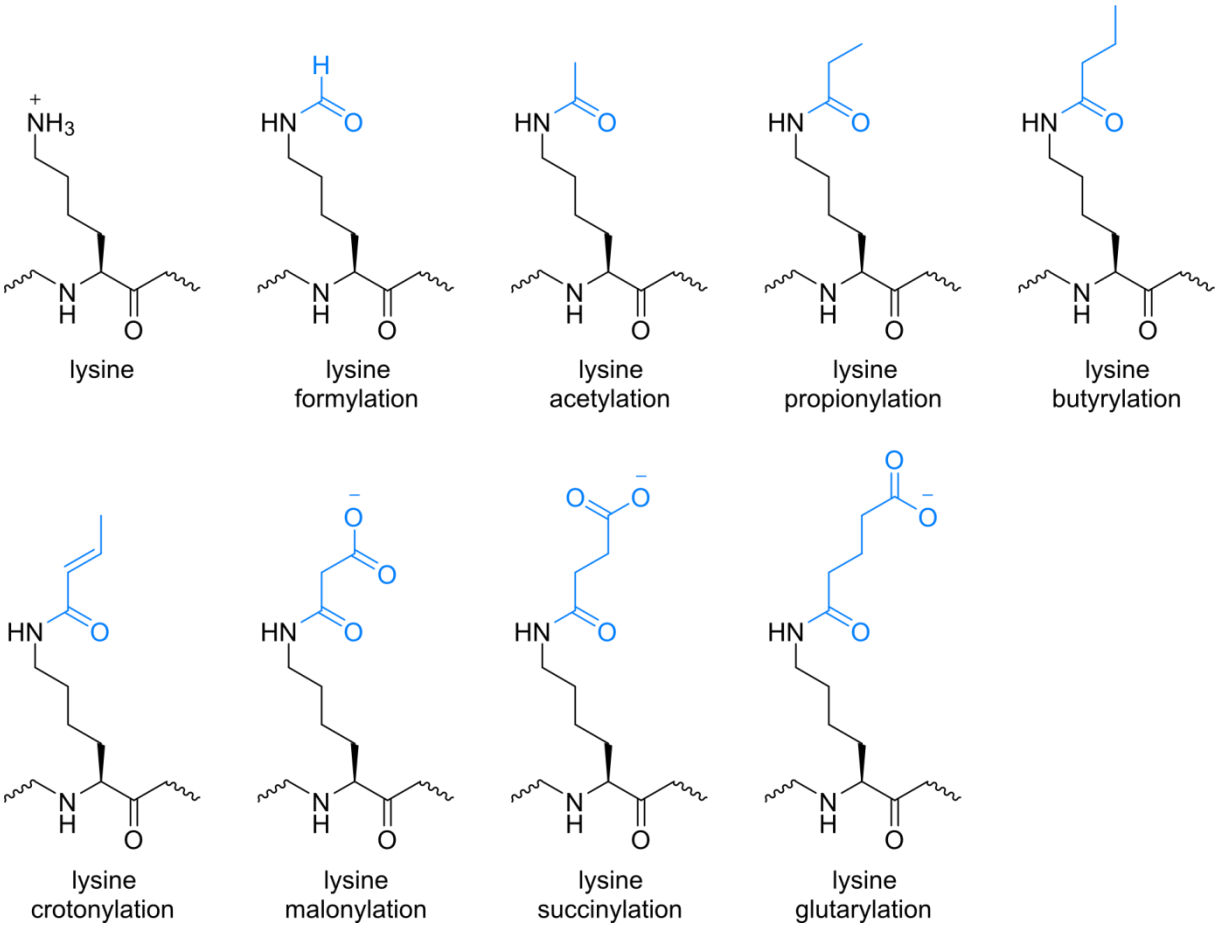

Figure 2.5: Chemical structures of formylated, acetylated, propionylated, butyrylated, crontonylated, malonylated, succinylated, and glutarylated ε-amino groups of lysine side chains.

2.1.3. Protein Methylation

Protein methylation is the smallest PTM known, but it is of immense importance. The universal substrate for protein, DNA, RNA, and small molecule methylation is *S*-adenosyl-L-methionine (SAM),[108] which has been discovered in 1952 and is the second most consumed enzyme substrate next to ATP.[109,110] SAM is only accepted as methylation donor in its (*S*,*S*) configuration. Epimerization under physiological conditions leads to (*R*,*S*)-SAM, which is not accepted by methyltransferases and inhibits them.[111] The transfer of SAM's methyl group is thermodynamically preferred, as it is exothermic.[110] As a consequence of SAM's high reactivity, it is generally directly consumed in methylation reactions after its biosynthesis. SAM is produced from methionine and ATP by the methionine adenosyltransferase. Following the transfer of its methyl group to nucleophiles by methyltransferases, *S*-Adenosyl-L-homocysteine (SAH) is generated, which can be cleaved by SAH hydrolase into adenosine and homocysteine. The latter can be converted to methionine by either methionine synthase utilizing 5-methyltetrafolate or by betaine-homocysteine methyltransferase. This metabolic SAM pathway is illustrated in Figure 2.6.[112,113] The cleavage of SAH must be tightly regulated, since SAH inhibits methyltransferases and in this manner controls their activities.[113]

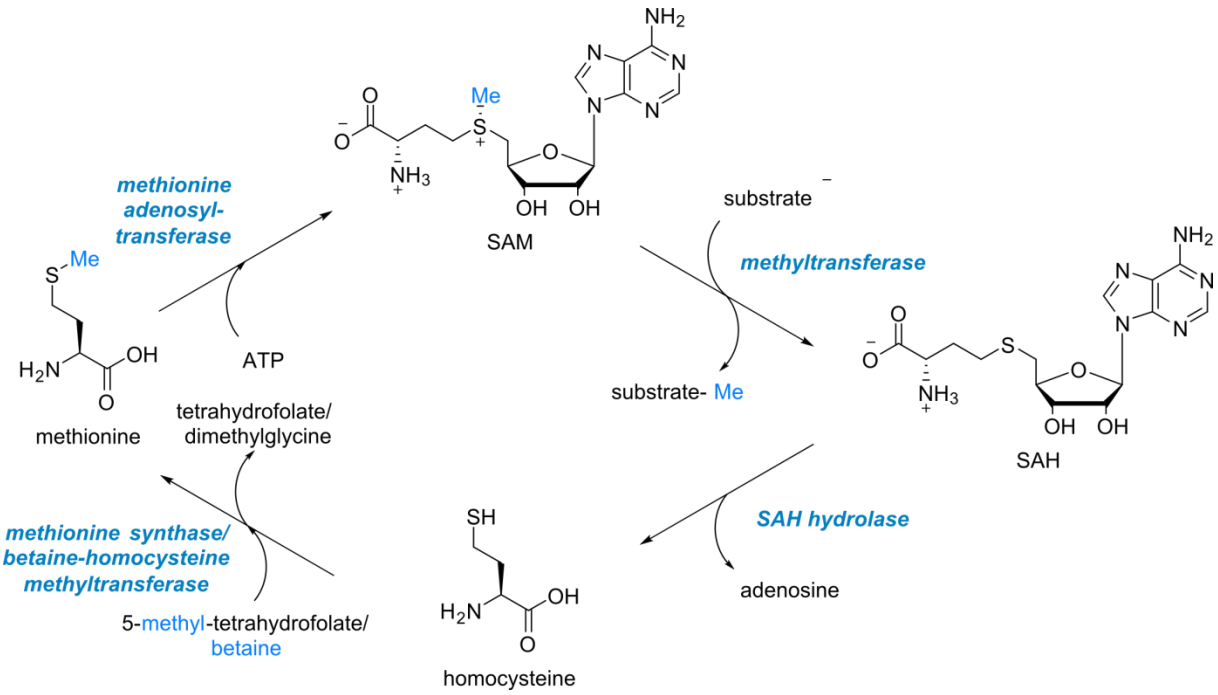

Figure 2.6: Metabolic pathway for SAM.

Protein methylation at lysine and arginine side chains is most common, but also *N*-, *C*-, *O*-, and *S*-methylations at glutamine, glutamic acid, histidine, cysteine, asparagine, and aspartic acid as well as N-terminal protein methylation have been reported.[7,9,114–116] The lysine ε-amino group can be mono-, di-, or trimethylated (Figure 2.7A), while the guanidine group of arginine can be monomethylated, symmetrically dimethylated, or asymmetrically dimethylated (Figure 2.7B).

Until now, more than fifty protein lysine methyltransferases have been detected, which mono-, di-, or trimethylate lysine ε-amino groups.[117] Firstly, most lysine methyltransferases have been shown to act on histones, but nowadays many non-histone target proteins are known.[117] Besides lysine methyltransferases, ten different protein arginine methyltransferases exist in humans, which catalyze the methylation of cytoplasmic and nuclear proteins.[33] They can be classified according to their methylarginine product. Class I transferases catalyze N^{ω}-monomethylation and asymmetric N^{ω}-$N^{\omega'}$-dimethylation, class II N^{ω}-monomethylation and symmetric N^{ω}-N^{ω}-dimethylation, and class III only N^{ω}-monomethylation. N^{δ}-monomethylation is catalyzed by class IV methyltransferases, but these have solely been found in yeast and are possibly present in plants.[33,118]

For a long time, it has been believed that protein methylation is irreversible.[119] Meanwhile, two classes of lysine demethylases have been identified, which oxidize the methyl groups and release formaldehyde.[120] Flavin-dependent amine oxidases demethylate mono- and dimethylated lysines, while iron-dependent oxygenases demethylate all three lysine methylation states.[121] Mechanistic details on the demethylation reactions of lysines have been summarized by Fischle and Schwarzer.[117] Arginine demethylases have also been reported.[122,123] Besides demethylation, demethylimination of arginine residues by the human enzyme PAD4 has been described.[124,125] Thereby, the methylated N^{ω}-amino group is

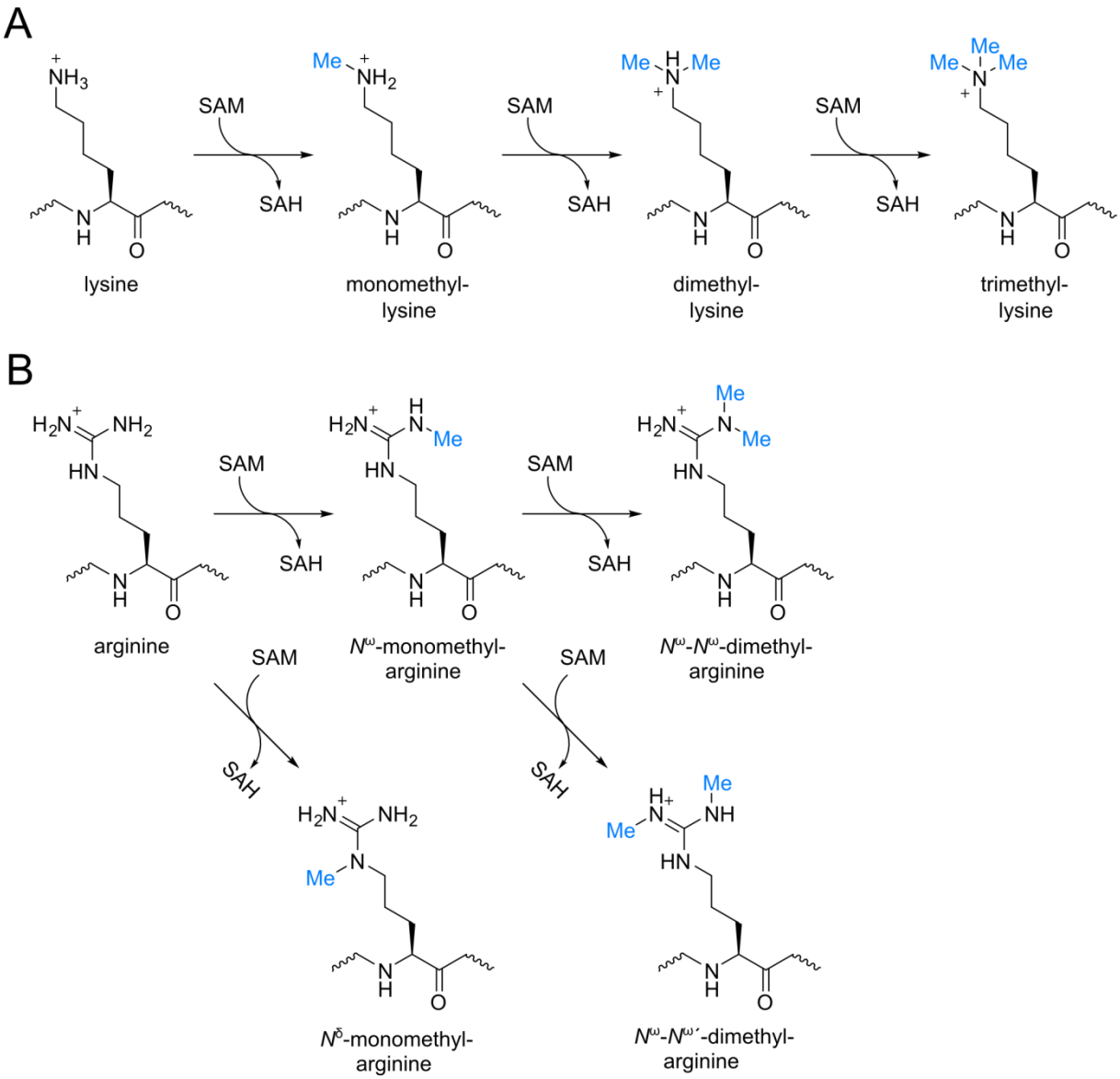

Figure 2.7: Known (A) lysine and (B) arginine methylation sites.

removed, which results in methylamine and a citrulline residue. Whether the resulting citrulline-containing proteins are degraded or restored by a hitherto unknown mechanism is still not clear.[126] The ability of PAD4 to demethyliminate arginine has also been questioned.[127]

Methylation fulfills crucial functions in all life forms. Protein lysine methylation has been shown to influence chromatin remodeling, protein stability, and biomineralization. Protein arginine methylation affects mRNA splicing, signal transduction, cell proliferation, chromatin remodeling, the cell cycle, DNA repair, transcription, protein-protein interactions, and protein localization.[33,126] Furthermore, many diseases including prostate and breast cancer, cardiovascular diseases, viral pathogenesis, multiple sclerosis, and spinal muscular atrophy have been linked to protein arginine methylation.[126,128] In addition, protein lysine methylation has been reported to be involved in various types of cancer and bacterial pathogenicity.[129]

Protein methylation achieves further biological outcomes in combination with other PTMs.[121] For instance, the interplay of methylation and phosphorylation regulates the transcriptional activity of NF-κB[130] and the crosstalk of methylation and acetylation modulates gene expression and activation of p53 upon DNA damage.[34,131]

2.2. Chemical Reporters

Since the discovery of protein PTMs, research focused on answering the following question: Which proteins are when, where, and how modified and re-modified by which enzymes? To answer this question, a repertoire of biochemical techniques has been established, which includes radioactive isotope-labeled PTM substrates, antibody-based approaches, many mass spectrometry methods, protein arrays, and, solely for protein glycosylation, carbohydrate-binding proteins (lectins).[11,132–135] While all these methods have been valuable for the identification of modified proteins and their PTM sites, they suffer from certain shortcomings. The generally used radio-isotopes ^{3}H and ^{14}C are weak radio emitters rendering an efficient detection of modified proteins difficult.[11] As antibodies recognize a certain epitope and PTMs are often very small and present in different amino acid sequence surroundings, pan-specific antibodies are not available for every PTM, laborious to be prepared, and sometimes lack specificity.[11,136] Lectins are cytotoxic and are not cell permeable, which limits their *in vivo* application.[137] Additionally, lectins have usually low target affinities.[138,139] Moreover, most of these techniques require the isolation of proteins from cells and thus disturb the cellular context which contains further information, e.g. on the localization of the protein in its modified state. Even imaging mass spectrometry, which combines mass spectrometry with a surface sampling process with resolutions down to 100 nm,[140,141] or the application of antibodies for immunocytochemistry restricts the detection of PTMs to proteins in fixed cells or tissue samples, therewith losing information on PTM dynamics.

An alternative approach overcoming some of the above mentioned limitations and allowing for the detection of PTMs inside living cells and even organisms relies on chemical reporters.[142–146] These are analogs of the corresponding PTM substrates bearing an unnatural chemical handle, for example an azide (Az), alkyne (Alk), or alkene. Chemical reporters are commonly employed in a two-step labeling approach. The first step comprises their delivery into cells, subsequent processing by cellular enzymes, and attachment to protein side chains. The cellular processing should preferably occur in the same way as it would be the case for the native PTM substrate. In a second step, the chemical handle of the reporter can be labeled with an exogenously delivered tag (e.g. biotin or a fluorophore) via a bioorthogonal ligation reaction (see chapter 2.3) for the enrichment, isolation, detection, or visualization of the PTM via mass spectrometry, fluorescence microscopy, or on Western blot membranes. Furthermore, one-step labeling approaches based on chemical reporter strategies have been developed. Thereby, either the chemical reporter is modified with a larger tag suitable for standard detection methods[147] or the small chemical handle itself is sensed via advanced microspectroscopic techniques,[148–150] such as coherent anti-Stokes Raman scattering[151,152] or stimulated Raman scattering[153]. The key to chemical reporter strategies lies in the acceptance of the modified substrate by native enzymes. If the chemical handle is too large to fit the enzymes' substrate pocket, enzymes can be genetically engineered.[154] As chemical reporters can be introduced in cells and labeled at freely defined time points, newly synthesized biomolecules can be easily separated from the steady-state PTM population, which enables monitoring dynamic changes of PTMs in living cells and organisms.[19]

Suitable chemical reporters for the three post-translational modifications glycosylation, acetylation, and methylation are discussed below in detail. Apart from these, chemical

reporters have been designed and applied to study protein malonylation[155], crotonylation[156], propionylation[157], butyrylation[157], *N*-myristoylation[158], *S*-palmitoylation[159], further lipidations[160,161], PARylation[147,162,163], AMPylation[164], and phosphorylation[165].

2.2.1. Chemical Reporters for Protein Glycosylation

The usage of chemical reporters for the detection of protein glycosylation is better known as metabolic glycoengineering (MGE) or metabolic oligosaccharide engineering (MOE). Chemical glycosylation reporters are precursors of the monosaccharide of interest modified with a chemical handle. ManNAc, GalNAc, and GlcNAc derivatives are utilized as chemical reporters to target sialic acids, mucin-type *O*-glycans, and *O*-GlcNAc, respectively.[166] However, it has to be taken into account that natural sugars are interconverted into one another, as explained above. These interconversions might also occur for unnatural sugars, but the chemical handle attached might influence the acceptance by cellular enzymes. As monosaccharide derivatives are poorly cell permeable, peracetylated reporters are usually employed.[167,168] Peracetylation enables the diffusion of chemical glycosylation reporters into cells, where they are expected to be rapidly deacetylated by esterases.[169] In a next step, modified monosaccharides are enzymatically processed and attached to proteins. Their chemical handles can subsequently be labeled via ligation reactions with suitable tags for detection.

The first chemical glycosylation reporters have been presented by Reutter et al. in the early 1990s. Based on their findings that *N*-modified ManNAc derivatives are metabolized and end up as sialic acids, they have used *N*-propanoyl-, *N*-butanoyl, or *N*-pentanoyl-tagged ManNAc derivatives and have detected their incorporation as sialic acids *in vitro* and *in vivo*.[170–172] This pioneering work proved that *N*-acyl modified ManNAc analogs are accepted by the cells' enzymatic machinery and opened a new field in glycobiology. The group of Bertozzi has been the first to use ManNAc derivatives with chemical handles, which can be labeled after incorporation into the cellular glycome with ligation reactions, for the detection or purification of glycosylation targets.[173,174] Meanwhile, reporters targeting Neu5Ac or GalNAc with various chemical handles, including ketones[173], azides[167,175], alkynes[176,177], terminal alkenes[178,179], strained alkenes[180–183], nitrones[184], or diazo-groups[185], have been developed and summarized elsewhere.[186]

Chemical glycosylation reporters developed to target protein *O*-GlcNAcylation are depicted in Figure 2.8. The first reporter presented by Bertozzi and coworkers in 2003 has been a peracetylated GlcNAc derivative bearing an azide at the *N*-acetyl side chain (Ac_4GlcNAz).[187] They have proven that this azide-derivative is well accepted by all enzymes required to form UDP-GlcNAz from GlcNAz *in vitro*, i.e. GlcNAc kinase, GlcNAc phosphomutase, and UDP-GalNAc/UDP-GlcNAc pyrophosphorylase, as well as by OGT and OGA. Moreover, cells treated with Ac_4GlcNAz have been shown to incorporate it into nuclear and cytoplasmic proteins. In 2011, the same group has reported on the usage of peracetylated azide-tagged GalNAc (Ac_4GalNAz) for the purification and identification of many *O*-GlcNAcylated proteins.[72] Bertozzi and coworkers have demonstrated that GalNAz is converted by endogenous cellular enzymes into UDP-GalNAz, which can be epimerized to UDP-GlcNAz by UDP-galactose-4-epimerase. In comparison to Ac_4GlcNAz, Ac_4GalNAz turned out to

mimic *O*-GlcNAc more faithfully, as its incorporation responded to changes of OGT, OGA, and *O*-GlcNAc levels. Yet, Ac_4GalNAz also ends up in mucin type *O*-glycans.[188] The third reporter was an peracetylated *N*-pentynoyl-GlcNAc derivative (Ac_4GlcNAlk).[189] Cells treated with Ac_4GlcNAlk attached it to many intracellular proteins allowing for the identification of many novel presumably *O*-GlcNAcylated proteins. The authors have assumed that GlcNAlk is a more specific *O*-GlcNAc reporter than GlcNAz, as the latter, but not GlcNAlk, can be interconverted to the GalNAc-derivative. To date, peracetylated GlcNAc with a methylcyclopropenylmethylcarbamate-tag at the *N*-acetyl side chain (Ac_4GlcNCyoc) is the only reporter designed for *O*-GlcNAc allowing labeling with a fluorophore via a bioorthogonal ligation reaction inside living cells. It has been reported by two groups independently.[180,182] Ac_4GlcNCyoc has been shown to mainly end up in intracellular proteins, but to some extent also in glycans on cell membranes.

Recently, five additional chemical reporters for *O*-GlcNAc have been reported. Peracetylated 6-azido-6-dexoy-GlcNAc ($Ac_3$6AzGlcNAc) and its alkynyl analog ($Ac_3$6AlkGlcNAc) bypass the standard hexosamine pathway, as they cannot be phosphorylated at the 6-hydroxy group and instead are directly phosphorylated by phospho-GlcNAc mutase at the 1-hydroxy group.[190,191] Both sugars have been shown to solely end up in protein *O*-GlcNAcylation and not, as reported for Ac_4GlcNAz, Ac_4GalNAz, and Ac_4GalNAlk, in *N*-glycans or mucin-type *O*-glycans. Thus, the authors claimed that $Ac_3$6AzGlcNAc and $Ac_3$6AlkGlcNAc are the most selective *O*-GlcNAc reporters outperforming the others. In addition, differences found in the enzymatic processing of these chemical reporters revealed a certain metabolic flexibility within the biosynthesis of carbohydrates. In 2016, Wang and coworkers presented peracetylated 4-deoxy GlcNAz ($Ac_3$4dGlcNAz) as potent and selective *O*-GlcNAc reporter.[192] The lack of the 4-hydroxy group results in less incorporation of $Ac_3$4dGlcNAz in cell surface glycoconjugates[193] and renders it resistant against hydrolysis by OGA. Thus, $Ac_3$4dGlcNAz accumulates as *O*-GlcNAc. Following bioorthogonal labeling of incorporated 4dGlcNAz, imaging, purification, and identification of *O*-GlcNAcylated proteins has been achieved. Two additional reporters, peracetylated 2-azido-2-deoxy-glucose ($Ac_4$2AzGlc) and peracetylated 6-azido-6-deoxy-glucose ($Ac_4$6AzGlc), have been introduced by Pratt and coworkers.[194,195] $Ac_4$2AzGlc and $Ac_4$6AzGlc were only found to very low extents in cell

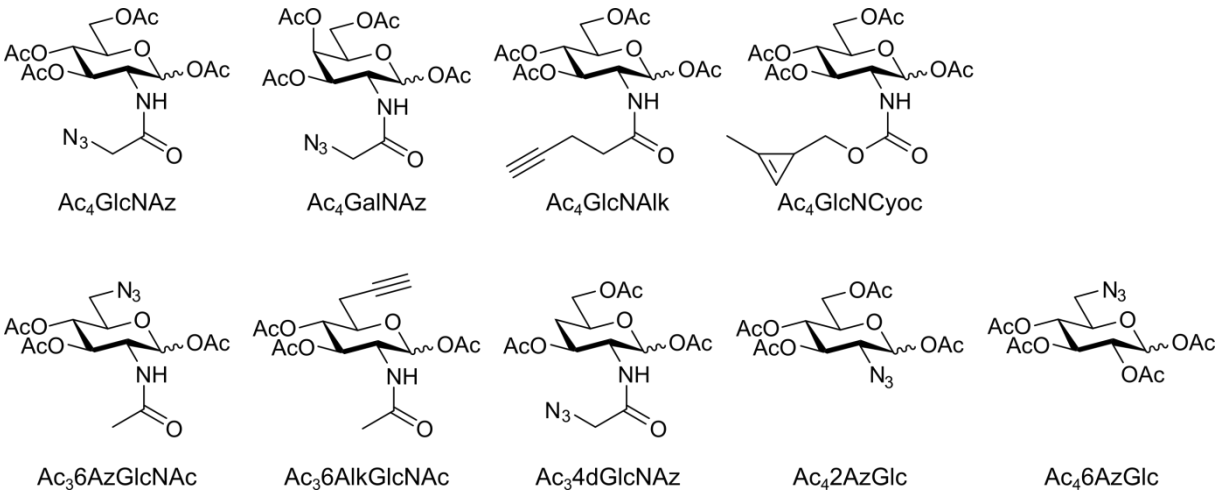

Figure 2.8: Chemical structures of reporters designed to target protein *O*-GlcNAcylation.

surface glycans in levels comparable to those of Ac_4GlcNAz and $Ac_3$6AzGlcNAc. Proteomics data revealed the sugars' specific incorporation as *O*-GlcNAc by OGT. Like $Ac_3$4dGlcNAz, $Ac_4$2AzGlc and $Ac_4$6AzGlc cannot be removed by OGA.
Besides targeting *O*-GlcNAc, Neu5Ac, or GalNAc, chemical reporters have been developed to study protein fucosylation and xylose, rhamnose, as well as arabinose in plant cell walls.[196–198] Chemical glycosylation reporters have not only been applied *in vitro* and in cell culture, but also *in vivo*, for instance in mice[144], *Caenorhabditis elegans*[146], Zebra fish embryos[145], and *Arabidopsis thaliana* (*A. thaliana*)[196,197,199].

2.2.2. Chemical Reporters for Protein Acetylation

The first chemical reporter for monitoring protein acetylation was developed by Yang et al. in 2010.[157] Their reporter is based on the native acetylation substrate acetyl-CoA, but is additionally tagged with a terminal alkyne for detection. Among several chain lengths tested *in vitro* (3-butynoyl-, 4-pentynoyl, and 5-hexynoyl-CoA), 4-pentynoyl-CoA was well accepted by the acetyltransferase p300 and transferred to lysine residues of histone 3. For in cell application followed by cell lysis and detection of alkyne-modified proteins on Western blots or via mass spectrometry, sodium 4-pentynoate (Figure 2.9A) has been selected. It has been metabolically processed and attached to lysine residues of many proteins including histones 2B, 3, and 4 and has been accepted by acetyltransferases, such as p300. However, concentrations as high as 10 mM needed to be employed, which might be due to a weak cellular uptake of the salt.
Three years later, an alkyne-modified aspirin (Figure 2.9B) has been presented for in cell detection of aspirin-dependent protein acetylation.[200] While this provides a nice tool to study effects of aspirin, this reporter is not suitable for studying protein acetylation in general.
A third probe was published by the Pratt group in 2014: 1-deoxy-*N*-pentynoylglucosamine (Figure 2.9C).[201] This molecule lacks the 1-hydroxyl group, which is indispensable for its processing by enzymes and incorporation into glycans, but instead has been shown to end up, at least partially, in the protein acetylation pathway. More than 60 known acetylated proteins were detected with 1-deoxy-*N*-pentynoylglucosamine. Comparison with sodium 4-pentynoate, however, revealed a different modification pattern of labeled proteins on Western blots and demonstrated that the incorporation of sodium 4-pentynoate was stronger.
Recently, sodium 4-pentenoate and two of its esters have been used for monitoring protein acetylation in cells and *in vitro* (Figure 2.9D).[202] Nevertheless, these alkene-modified reporters were less accepted and incorporated than sodium 4-pentynoate.

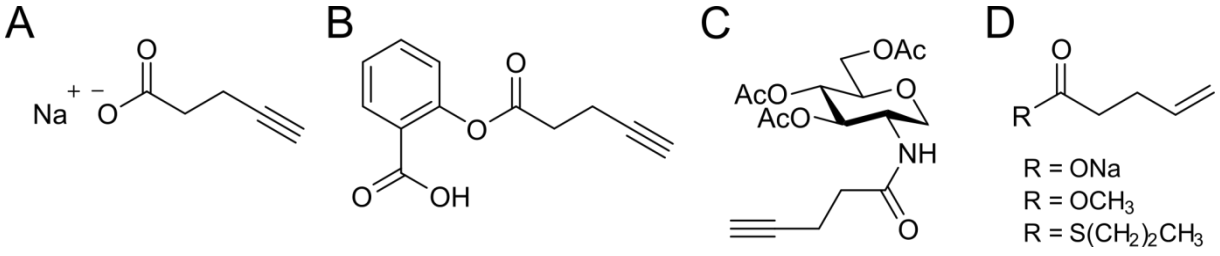

Figure 2.9: Chemical structures of the acetylation reporters (A) sodium 4-pentynoate, (B) aspirin-alkyne, (C) 1-deoxy-*N*-pentynoylglucosamine, (D) sodium 4-pentenoate, methyl 4-pentenoate, and *S*-propyl pent-4-enethioate.

These observations support the conclusion that sodium 4-pentynoate is the best known chemical reporter for monitoring protein acetylation.

2.2.3. Chemical Reporters for Protein Methylation

Chemical reporters for monitoring methylation have been based on the structure of the common cofactor SAM. In the last two decades, a huge variety of chemical methylation reporters has been developed.[203–205]

To establish the first methylation reporters, the sulfonium and methionine of SAM have been replaced by an aziridin.[206] Following its protonation, methylation substrates can attack the aziridinium ion and thereby attach themselves to the reporter (Figure 2.10A). The DNA methyltransferase from *Thermus aquaticus* has been shown to catalyze this reaction *in vitro*.[206] Further aziridin-based chemical methylation reporters have been developed, as summarized elsewhere.[207] They are for instance modified with azides or fluorophores enabling the detection of modified substrates.[208,209] However, these reporters are not suited for cellular applications, as methyltransferases cannot dissociate from substrate-reporter conjugates and consequently high concentrations are needed.[210] This can also be an advantage, as a methyltransferase responsible for a certain modification can be easily purified and identified, if it is linked to its substrate. Noteworthy, aziridin-based reporters are highly reactive. This results in their degradation and in non-specific alkylation, even in the absence of methyltransferases.[204,207]

The second class of chemical methylation reporters comprises SAM analogs bearing a chemical handle instead of the methyl group at the sulfonium center, which is transferred by methyltransferases to their targets (Figure 2.10B). It is known that SAM analogs with longer alkyl chains are accepted by methyltransferases, but reaction rates are much lower compared to native SAM, which has been explained by steric hindrance.[211] Early synthesized chemical methylation reporters have carried an allyl or propargyl group.[212,213] The allylic or propargylic carbon-carbon bond in β-position of the sulfonium atom stabilizes the transition state of the S_N2 reaction and in this way recovers good reaction rates.[204,212,213] Many more SAM analogs with diverse groups for detection (alkynes, ketones, or azides) differently accepted by methyltransferases and with altered reaction rates have been published.[214–219] Reporters with chemical handles larger than the pent-2-en-4-ynyl group[214] have not been accepted by native methyltransferases and required genetically engineered methyltransferases to recognize and transfer bulky SAM analogs.[215] Although smaller reporters such as ProSAM (Figure 2.10C) are better tolerated by methyltransferases, they have half-life times lower than one minute under physiological conditions, rendering their application difficult.[216,220] Decomposition pathways of SAM analogs include the racemization at the sulfonium center, the deprotonation at the C-5´ followed by elimination of the adenine base (depurination), and loss of methionine as homoserine lactone after a nucleophilic attack of the α-carboxylate at the γ-carbon atom.[204,221] In addition, the alkyl side chain can decompose. For example, the propargyl group of ProSAM can hydratase, presumably via an allene intermediate.[220] A chemical reporter with increased stability and a half-life time of around 60 min under physiological conditions is the selenium-based ProSeAM (Figure 2.10D).[220,222] Selenium analogs are more electrophilic than sulfonium analogs and for this reason more

reactive towards a nucleophilic attack resulting in increased reaction rates.[204,220,223] In addition, selenium analogs possess a reduced C-5´ acidity compared to sulfonium analogs.[223] Thus, they are more stable towards deprotonation at the 5´-H.[220] Moreover, ProSeAM's propargyl group does not undergo hydratization.[220] ProSeAM has been shown to be well accepted by a wide variety of native protein methyltransferases,[220,222] but also by DNA and RNA methyltransferases.[222,224] This reporter has been employed for the isolation of modified proteins from cell lysates followed by mass spectrometry and for the identification of substrates of certain methyltransferases *in vitro*.[220,222] Besides ProSeAM, three further SeAM analogs have been synthesized carrying a 3-butynyl, 2-azidoethyl, or 3-azidopropyl group, but all of them have been less reactive in an enzymatic methylation assay than ProSeAM.[225,226]

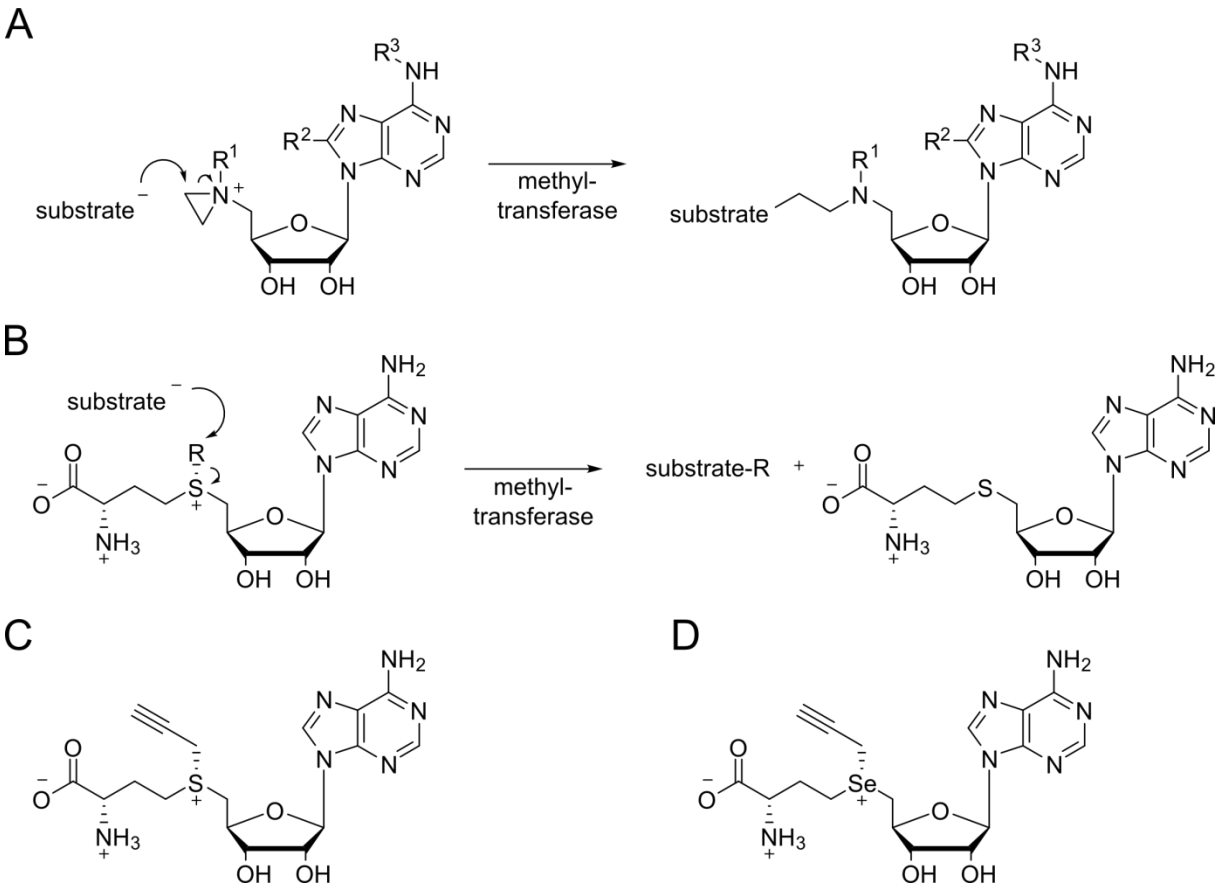

Figure 2.10: (A) Mechanism of the reaction of nucleophilic substrates with aziridin-based chemical reporters. R^1, R^2, R^3 = H/chemical handle/fluorophore. (B) Mechanism of the reaction of nucleophilic substrates with SAM-based chemical reporters. R = chemical handle. (C) Chemical structure of ProSAM. (D) Chemical structure of ProSeAM.

The application of methylation reporters is largely restricted to experiments in cell lysates. The lack of in cell experiments is mainly due to the low cellular permeability of SAM analogs and the absence of a proper transport system in mammalian cells. A unique SAM transporter system exists in *S. cerevisiae*, which has allowed the delivery of chemical methylation reporters in yeast.[227] So far, the only methylation reporters having been used in mammalian cells are methionine analogs, which have been taken up by cells and have been converted into the corresponding SAM analogs by engineered SAM synthetases.[154,228]

2.2.4. Delivery of Chemical Reporters into Cells

As chemical reporters need to be processed by cellular enzymes to become attached to proteins, reporters have to be delivered into cells. Ideally, the chemical reporter is cell permeable and simply diffuses in the cytoplasm. However, most chemical reporters are polar and thus can hardly pass cellular membranes. As a consequence, polar groups, such as alcohols, are often protected with acetyl- or acetoxymethyl-groups making reporters more hydrophobic and therefore better cell permeable.[155,167–169] It is assumed that cellular esterases remove these protecting groups inside cells.[169]

If chemical reporters cannot pass cell membranes, several methods exist to introduce them into cells:

- Electroporation. An external electrical field can be applied that leads to the temporary formation of membrane pores through which reporters can diffuse.[229] This technique can be performed with adherent cells or cells in suspension and allows for homogenous introduction.[230] Electroporation conditions need to be adapted for each reporter and cell line individually to ensure a proper delivery with minimal effects on cellular integrity.
- Microinjection. Thereby, the amount of reporters present in cells can be clearly defined.[231] Correct microinjection of many cells requires expertise and is time-consuming.
- Triton X-100. Low concentrations of this detergent can be used to transiently permeabilized cellular membranes without breaking up the membranes' structure completely.[232] Triton permeabilization delivers compounds homogenously into cells, but cells die rapidly within the next two hours. This restricts its application in living samples to short-term studies.
- Peptide carriers. A short amphipathic peptide can be employed, which has been shown to efficiently deliver peptides, proteins, and chemical reporters into cells.[147,233] This peptide is not toxic and leads to the homogenous delivery of probes in cell, but it is relatively expensive.
- Cell squeezing. Cells are rapidly and dynamically deformed by cell squeezing, which enables the diffusion of macromolecules or nanomaterial into cells.[234] Whereas many cells can be easily processed at once and are not affected in their viability, cell squeezing is done with cells in suspension. Hence it does not allow monitoring the incorporation of chemical reporters into adherent cells by microscopy subsequently.
- Liposomes. Chemical reporters encapsulated in liposomes can be taken up by cells via endocytosis. Recently, this liposome-assisted bioorthogonal reporter strategy has been applied to deliver chemical glycosylation reporters in mouse brains *in vivo* and to target different cell types by using ligand-functionalized liposomes.[143,235,236]

As all aforementioned delivery methods exhibit different advantages and disadvantages, the appropriate method has to be chosen carefully according to the respective experimental demands.

2.3. Bioorthogonal Ligation Reactions

Chemical handles of reporters presented in the last chapters need to be labeled with tags for the purification and detection of targeted biomolecules. Examples for possible tags are biotin or fluorophores. Labeling reactions between chemical reporters and tags should be selective, fast, irreversible, give ideally no side products, and proceed with high yields. As the reaction must occur in the cellular environment, all reaction partners should be stable under physiological conditions (ambient temperature, aqueous solution, pH 7 to 8). In addition, reagents should not be present in cells naturally, should be non-toxic, and inert towards biological compounds. These properties are summarized with the term "bioorthogonal". Within the last two decades, various bioorthogonal ligation reactions have been developed and applied.[237–240] Selected ones are presented within this chapter.

The first labeling reaction applied has been the ketone-hydrazine-ligation.[173] Thereby, a ketone or aldehyde reacts with a hydrazide forming a stable hydrazone (Figure 2.11A). As the pH optimum for this reaction lies between 5 and 6, its application in living samples is not possible.[241] In addition, the ketone-hydrazine-ligation is limited in its use to cell surfaces,[173] which are, in contrast to the intracellular space, free of native aldehydes and ketones. Aldehydes and ketones can also react with other groups present inside cells including alcohols, amines and thiols. Thus, the ketone-hydrazide-ligation is in fact not bioorthogonal.

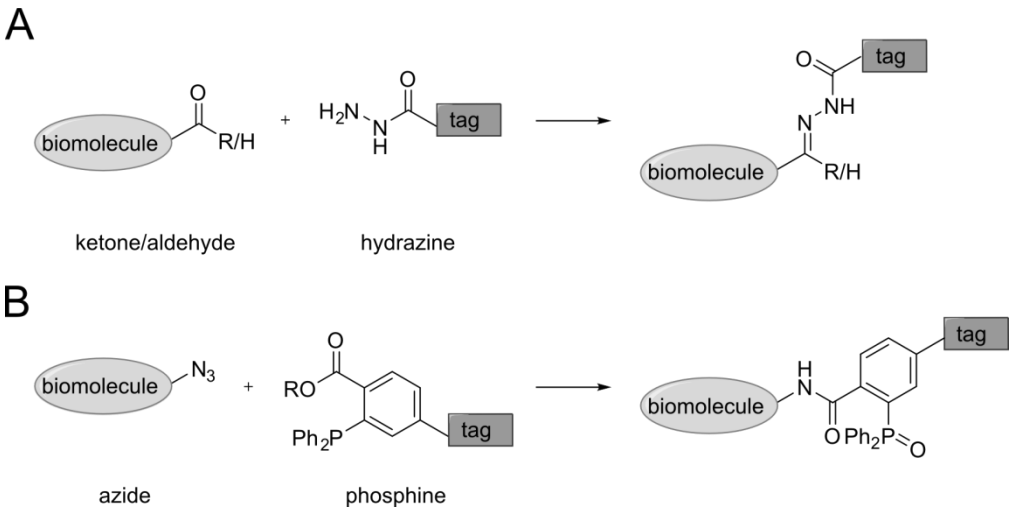

Figure 2.11: Reaction schemes for (A) the ketone-hydrazide ligation and (B) the Staudinger ligation.

The first "real" bioorthogonal ligation reaction established has been the Staudinger ligation, which uses an azide as chemical handle. The azide is very small and does naturally not occur in cells, making it perfectly suitable for cellular applications. The Staudinger ligation is based on the classical Staudinger reduction of azides with triphenylphosphines forming an aza-ylide hydrolyzing into an amine and phosphine oxide.[242] To avoid this hydrolysis, Bertozzi and coworkers positioned an ester group at one of the phosphine's aryl substituents to enable the intramolecular conversion of the aza-ylide to a stable amide (Figure 2.11B).[167] This reaction can proceed in aqueous solution, at physiological pH, and at ambient temperature.[188] However, phosphines are prone to oxidation and have low reactivities,[243,244] which is why high concentrations of phosphines (>250 µM) need to be employed.

A further ligation reaction utilizing the small azide, but proceeding faster than the Staudinger ligation is the Cu(I)-catalyzed azide-alkyne cycloaddition (CuAAC). It is often named "click-reaction" or "click-chemistry" and based on the [3+2] cycloaddition of azides and alkynes introduced by Huisgen.[245] Following his approach, high temperatures are needed rendering its application in cellular systems impossible. Such harsh reaction conditions can be avoided by addition of Cu(I) as catalyst.[246,247] In the CuAAC, the azide and alkyne react to a triazole with 1,4 regioselectivity (Figure 2.12A). Both the azide and the alkyne can be placed at the chemical reporter or the tag, as they are very small. Cu(I) is usually produced in the reaction mixture from $CuSO_4$ using the reducing agents tris(2-carboxyethyl)phosphine (TCEP) or sodium ascorbate. As Cu(I) is cytotoxic and therefore cannot be used for the labeling of living samples, ligands chelating Cu(I) ions have been developed (Figure 2.12B). They accelerate the CuAAC by maintaining the Cu(I) oxidation state and furthermore protect biomolecules from oxidative damage. Common Cu(I) ligands are the poorly water soluble tris((1-benzyl-1H-1,2,3-triazol-4-yl)methyl)amine (TBTA)[248] and the water soluble tris(3-hydroxypropyltriazolylmethyl)amine (THPTA).[249] Compared to TBTA and THPTA, the ligands 2-(4-((bis((1-(tert-butyl)-1H-1,2,3-triazol-4-yl)methyl)amino)methyl)-1H-1,2,3-triazol-1-yl)ethyl hydrogen sulfate (BTTES)[250] and 2-(4-((bis((1-(tert-butyl)-1H-1,2,3-triazol-4-yl)methyl)amino)methyl)-1H-1,2,3-triazol-1-yl)acetic acid (BTTAA)[142] enhance reaction rates markedly. Moreover, aminoguanidine has been described to be a suitable additive in CuAACs to prevent the formation of byproducts of ascorbate oxidation.[251]

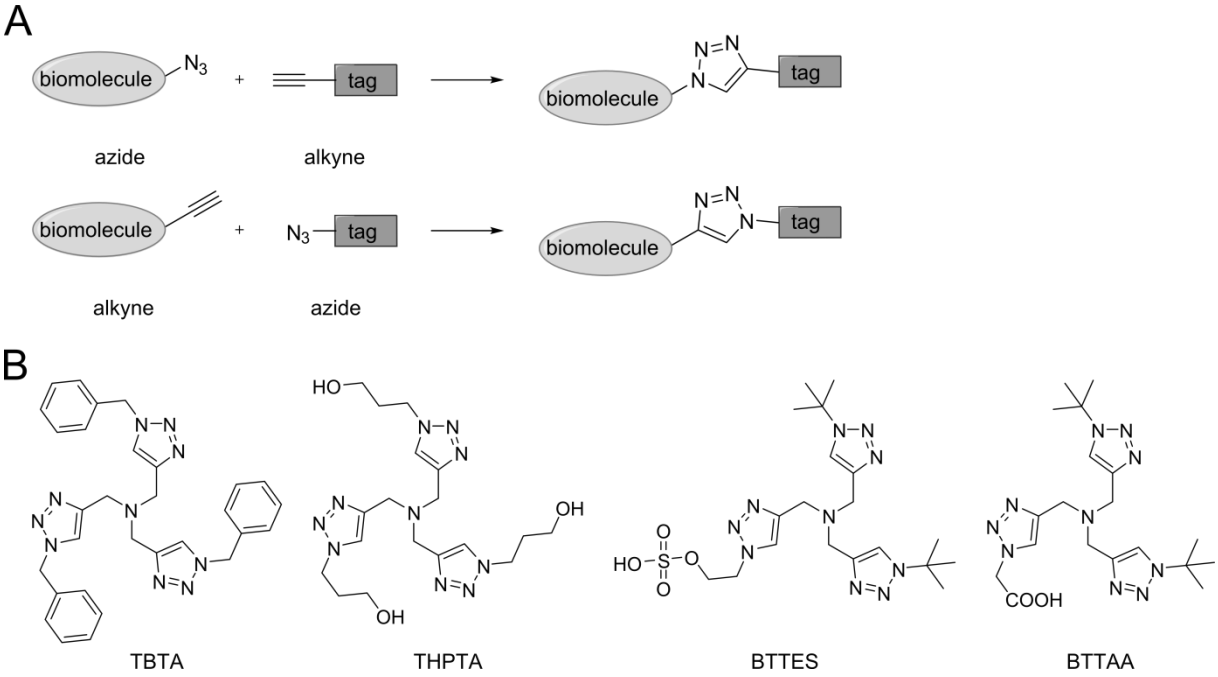

Figure 2.12: (A) Reaction scheme for the CuAAC. (B) Chemical structures of selected Cu(I) ligands.

To overcome the requirement of cytotoxic Cu(I) in azide-alkyne cycloadditions, the strain-promoted azide-alkyne cycloaddition (SPAAC) of azides and strained cycloalkynes can be applied (Figure 2.13A).[252] Reagents for this reaction are not cytotoxic, but SPAACs proceed slower than CuAACs in general.[253] The first strained alkyne employed has been the cyclooctyne (OCT).[253] Until now, more than ten different cyclooctynes for SPAAC have

been reported,[254] including dibenzocyclooctyne (DIBO)[255], bicyclo[6.1.0]non-4-yne (BCN)[255], and biarylazacyclooctynone (BARAC)[256] (Figure 2.13B). Among them, DIBO and BARAC react fastest in SPAAC, but have an increased hydrophobicity due to their aromatic character resulting in their non-specific attachment to other biomolecules.[239,257] Cyclooctynes are prone to react with thiols.[258] Thus, the application of SPAAC requires capping thiols with acylating agents or limits its usage to extracellular spaces that are free of thiols.[239]

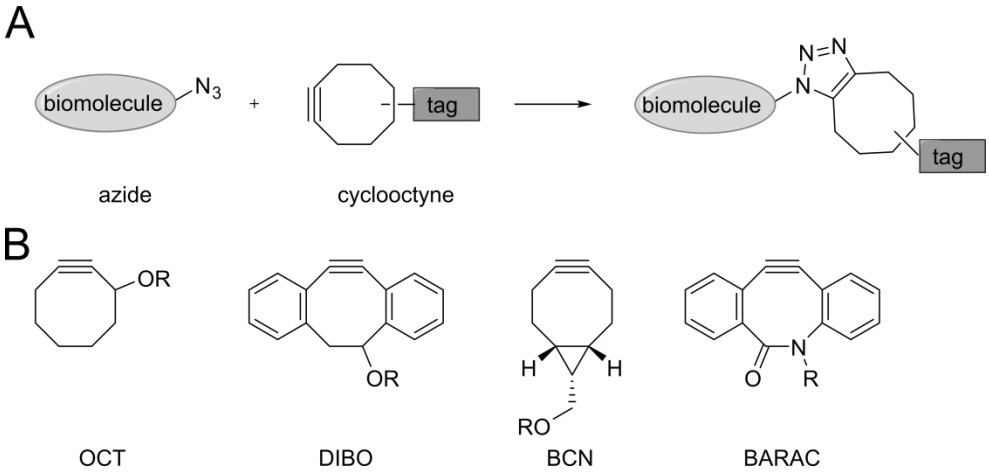

Figure 2.13: (A) Reaction scheme for SPAAC. (B) Chemical structures of selected cyclooctynes.

Owing to its fast kinetics and excellent biocompatibility, the inverse-electron-demand Diels-Alder (DAinv) reaction, firstly reported in 1956,[259] has set a new standard in bioorthogonal ligation chemistry.[237,260] The DAinv reaction is a [4+2] cycloaddition of a 1,2,4,5-tetrazine (Tz) and an alkene forming an intermediate state, which reacts in a retro-Diels-Alder reaction to a 4,5-dihydropyridazine (Figure 2.14).[261] The latter emerges as different isomers and can be oxidized to a pyridazine. The DAinv reaction does not need toxic catalysts and is irreversible due to release of nitrogen.[262] Thus, it is perfectly suited for live cell applications.

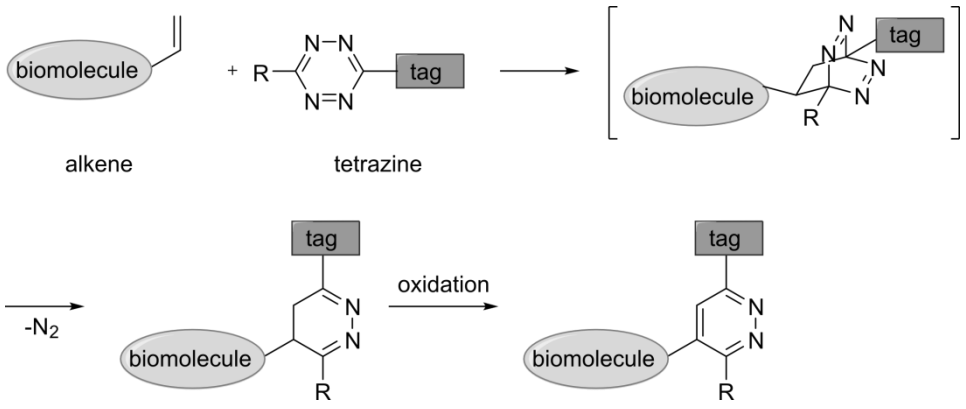

Figure 2.14: Reaction scheme for the DAinv reaction.

In a Diels-Alder reaction with normal electron demand, the highest occupied molecular orbital (HOMO) of the diene (tetrazine) overlaps with the lowest unoccupied molecular orbital (LUMO) of the dienophile (alkene). In contrast, the HOMO of the dienophile overlaps with

the LUMO of the diene in a DAinv reaction (Figure 2.15).[262] Residues of diene and dienophile determine whether the reaction of an alkene with a tetrazine takes place with normal or inverse electron demand. To achieve a DAinv reaction, the diene should be electron poor and the dienophile electron rich. Hence, the DAinv reaction is accelerated by the presence of electron withdrawing groups at the diene and electron donating groups at the dienophile.[262,263] The reactivities of differently substituted tetrazines have been summarized by Chen and Wu.[240] Suitable alkenes for the DAinv reaction are norbornenes[183,264], *trans*-cyclooctenes[261], *trans*-biocyclo[6.1.0]nonenes[265], cyclopropenes[180–182,266–268], and terminal alkenes.[178] Whereas alkenes with strained rings react faster than unstrained ones, as their ring strain is released within the reaction,[240,269] smaller alkenes are better tolerated by cellular enzymes.[179,270] Besides alkenes, also several strained alkynes, such as OCT or BCN, have been shown to react with tetrazines in a DAinv reaction.[145,271]

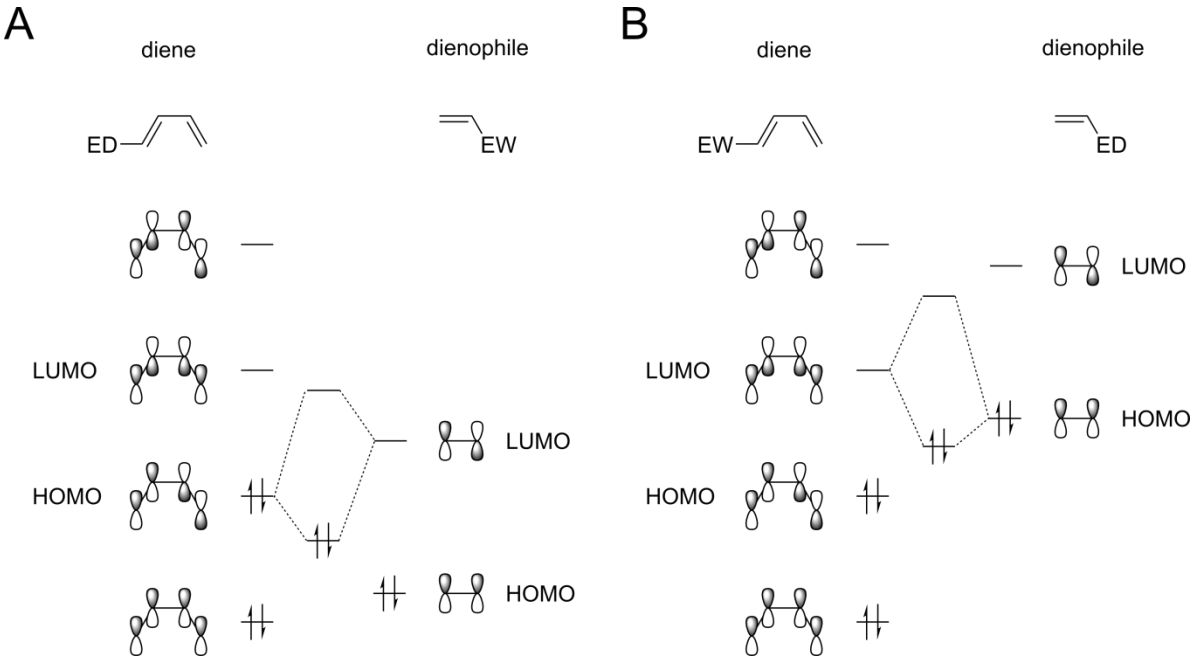

Figure 2.15: Orbital schemes for Diels-Alder reactions with (A) normal and (B) inverse electron demand. ED = electron donating substituent, EW = electron withdrawing substituent. Based on [272].

In several cases, labeling of two chemical reporters is required. For this purpose, two bioorthogonal ligation reactions need to proceed without disturbing one another. Dual labeling was achieved by combining the ketone-hydrazide-ligation with the Staudinger ligation[175], the CuAAC with the SPAAC (although labeling was performed sequentially)[273,274], the SPAAC with the DAinv reaction[178,181], as well as two orthogonal selectively enhanced DAinv reactions[275]. For the combination of SPAAC and DAinv reaction, a strained alkyne not reacting with tetrazines, such as DIBO, must be selected.[276]
Probes fluorescing only upon completion of the ligation reaction have been developed for the Staudinger ligation[277,278], the CuAAC[198,279–281], the SPAAC[282,283], and the DAinv reaction[284–287]. Since only reacted molecules contribute to the fluorescence and unreacted labels do not, the fluorescence signal to background ratio is dramatically increased.

Consequently, the usage of turn-on probes circumvents the need of washing steps after labeling, which might affect cellular viabilities and removes for instance mitotic cells.
The choice of the "right" bioorthogonal ligation reaction needs to consider various parameters including the selectivity and speed of reactions, but also possible cytotoxic effects of reaction partners for applications *in vivo* or in cell culture.[239] Additionally, sizes of chemical handles and tags should be as small as possible to be tolerated by native enzymes. Otherwise, engineered enzymes can be employed.[215] More importantly, the availability of PTM analogs with defined chemical handles and corresponding tags is often limiting.

2.4. FLIM-FRET Microscopy

2.4.1. Fluorescence

Early observations of compounds in solution that "change" ultraviolet light into visible blue light have been made by Clarke, Brewster, and Herschel.[288] In 1852, Stokes reported similar experiments and named this effect fluorescence.[289,290] Fluorescence is one of several luminescence processes, whereby the transition of a molecule from the electronically excited state to the electronic ground state is connected with the emission of light. Luminescence processes differ in their excitation pathways resulting in the occupation of the electronically excited state, which include among others chemical reactions (chemiluminescence), ionizing radiation (radioluminescence), or the absorption of photons (photoluminescence).
The transitions of molecules between electronic states are commonly illustrated in a Jablonski diagram (Figure 2.16).[291] According to the Boltzmann distribution, almost all molecules reside at room temperature in the electronic and vibrational ground state. Absorption of a photon transfers a molecule into the electronically excited state. This process is very fast and occurs on the time-scale of femtoseconds. Which vibrational state of the electronically excited state becomes populated depends on the energy of the photon and the overlap of vibrational wave functions of the electronic ground and excited state. The larger the overlap of the wave functions, the more likely is the population of a certain vibrational state. This rule is known as Franck-Condon principle. Once a molecule is in the electronically excited state, several radiative or non-radiative relaxation pathways are possible, which compete with one another. Internal conversion describes a process of radiation-less relaxation via several vibrational modes based on an energy loss through collisions with other molecules. As internal conversion to the vibrational ground state of the first electronically excited state occurs on a picosecond time-scale, all other relaxation processes start from there and are mostly independent of the excitation pathway (Kasha's rule). Fluorescence is the transition of a molecule from the electronically excited state to the electronic ground state accompanied by the emission of a photon and occurs on the nanosecond time-scale. Due to the fast internal conversion to the vibrational ground state of the electronically excited state, the energy of the

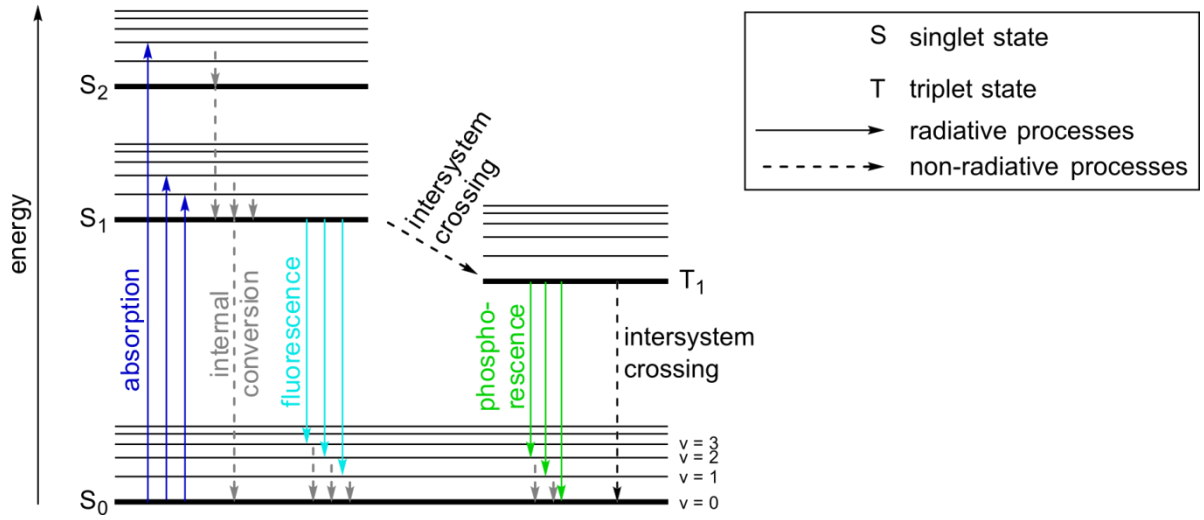

Figure 2.16: Jablonski diagram.

emitted fluorescence photon is generally lower than that of the absorbed photon resulting in a red-shifted wavelength as compared to the excitation (Stoke's shift). In most cases, absorption and fluorescence emission spectra are mirror symmetric, as vibrational wave functions of electronic ground and excited state are similar. Besides internal conversion and fluorescence, non-radiative intersystem crossing to a triplet state depopulates the electronically excited singlet state. The molecule can return from the triplet state in the electronic singlet ground state, which is connected with the emission of phosphorescence. As this process requires a change in spin multiplicity and is consequently formally not allowed, phosphorescence occurs on time-scales of microseconds to seconds.[292]
Both radiative (r) and non-radiative (nr) processes lead to the depopulation of the electronically excited state with different rate constants k_{nr} (including internal conversion and intersystem crossing) and k_r. The number N of molecules in the excited state at a time point t can be calculated according to

$$N(t) = N_0 \cdot e^{(-t \cdot (k_{nr} + k_r))}. \tag{2.1}$$

Thereby, N_0 is the initial number of molecules present in the excited state. The time until the number of molecules in the excited state has dropped to the *1/e*-fraction of N_0 is the fluorescence lifetime τ, which can be calculated from the reciprocal of the sum over all rate constants involved in the depopulation of the excited state:

$$\tau = \frac{1}{k_{nr} + k_r} \tag{2.2}$$

The fluorescence lifetime is an intrinsic property of a fluorophore. However, it also depends on the fluorophore's environment, as temperature, pH, viscosity, or refractive index can affect fluorescence lifetimes.[293] Since the number of fluorophores in the excited state is proportional to the fluorescence intensity I, the time-dependent fluorescence intensity $I(t)$ can be written as

$$I(t) = I_0 \cdot e^{\left(\frac{-t}{\tau}\right)}. \tag{2.3}$$

If several fluorophores are present in a sample or a fluorophore exists in different states, the fluorescence intensity follows a multiexponential decay

$$I(t) = \sum_{i=1}^{n} a_i \cdot e^{\left(\frac{-t}{\tau_i}\right)}. \tag{2.4}$$

In this equation, the preexponential factor a_i accounts for the fractional contribution of a component with the fluorescence lifetime τ_i to the time-resolved decay.[294] The fluorescence quantum yield Φ is directly linked to the fluorescence lifetime and is defined by the ratio of photons emitted by fluorescence and absorbed photons:

$$\Phi = \frac{k_r}{k_{nr} + k_r} = \tau \cdot k_r \tag{2.5}$$

The fluorescence intensity can be reduced due to various processes called quenching. It opens a further depopulation pathway for a molecule in the electronically excited state. Quenching results in an additional rate constant k_Q, which leads to a reduction of both the fluorescence lifetime and the fluorescence quantum yield Φ.[292] Förster resonance energy transfer (FRET) is one possible quenching process and discussed in chapter 2.4.4. Within this thesis, FRET was assessed via fluorescence lifetime measurements (see section 2.4.5) to image PTMs of proteins, as explained in chapter 3.

2.4.2. Fluorescent Proteins

Organic fluorophores possess a π-electron system capable of absorbing light of a certain wavelength. Both the size of the π-electron system and nearby functional groups influence the wavelength range of absorption. For biological applications, genetically encoded fluorophores, so called fluorescent proteins, have gained immense importance in the last two decades. The first fluorescent protein, aequorin, has been isolated from the jellyfish *Aequorea victoria* by Shimomura et al.[17] This protein has been named green fluorescent protein (GFP). It has a molecular weight of 238 kDa and forms a β-barrel structure with an interior α-helix. The chromophore of GFP is autocatalytically formed in the α-helix from the three amino acids serine 65, tyrosine 66, and glycine 67 (Figure 2.17).[295–298] This has enabled the expression of the GFP gene in cells and whole organisms and to attach it genetically to proteins.[296,298–300] Native GFP has a major absorption maximum at 395 nm and a minor one at 475 nm. Its fluorescence emission peak lies at 504 nm. Through mutations changing amino acids close to the chromophore, GFP derivatives with altered spectral and physical properties have been generated.[301] For example, the two point mutations F64L and S65T resulted in enhanced GFP (EGFP). Its absorption maximum is shifted to 488 nm. In addition, EGFP possesses an

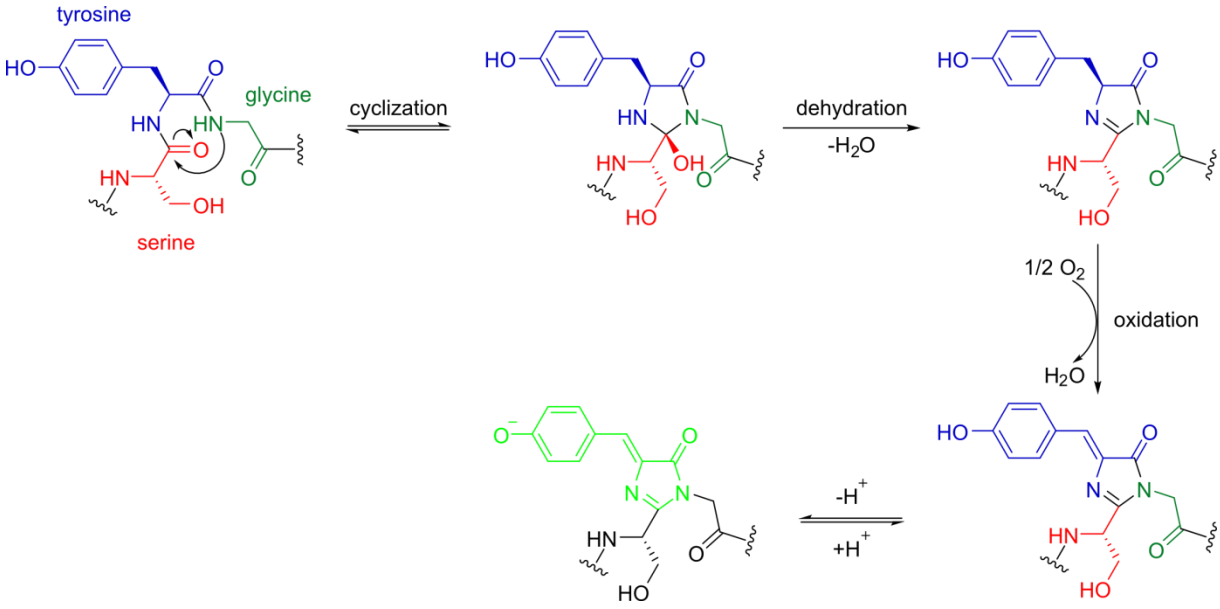

Figure 2.17: Spontaneous formation of the chromophore of GFP.

improved protein maturation efficiency and a more stabilized hydrogen-bonding network compared to native GFP.[302,303] Hence, most plasmids encoding fluorescent protein-fusion proteins available from nonprofit plasmid repositories carry EGFP. Meanwhile, a whole color pallet of genetically encodable fluorophores derived from native fluorescent proteins from jellyfish or anthozoa corals with various physical, photochemical, and biological properties has been established.[304–308]

2.4.3. Fluorescence Microscopy

Hundreds of years ago, first microscopes for the magnified imaging of structures or compounds not visible by human eyes have been developed. Microscopy relies on the generation of contrast, which can be achieved for example from differences in absorption, phase, or polarization.[293] Microscopes are tools employed in biology, material science, and medicine. The best achievable resolution, defined as the distance d between two structures required to distinguish them, can be calculated via Abbe's diffraction limit:

$$d = \frac{0.61 \cdot \lambda}{n \cdot \sin \alpha} \tag{2.6}$$

The distance d depends on the wavelength of light λ, the refractive index n of the medium through which the light travels, and half the opening angle of the objective α. The product $n \cdot \sin \alpha$ is also known as numerical aperture. Meanwhile, several modern microscopic techniques "overcome" the resolution limit given by diffraction and can be utilized to resolve structures in the nanometer range.[309–315]

Fluorescence microscopes use the fluorescence signal for the generation of contrast. The excitation light from a lamp, diode, or laser is passed via mirrors to an objective, which focusses it onto the sample. In epifluorescence microscopy, the emitted fluorescence is collected with the same objective. Due to the Stoke's shift, the fluorescence signal can be easily separated from the excitation light by dichroic mirrors and filters before being detected. As nearly no background is present, the detection of fluorescence is very sensitive.

Two main types of fluorescence microscopes exist: wide-field and confocal scanning microscopes (Figure 2.18).[15,316] Wide-field microscopes allow the illumination of a large area at once, which can be imaged with an area detector, such as a charge-coupled device (CCD) camera.[317] This allows the temporal resolution of fast processes, but also requires high powers of excitation light. As wide-field microscopes hardly suppress out-of-focus light, their axial resolution is weak. The development of the confocal microscope has overcome this obstacle.[318,319] In this technique, excitation light is focused diffraction-limited onto the sample. Thus, only a small volume of the sample is illuminated at once. Additionally, a pinhole is placed in front of the detector to suppress out-of-focus light. The excitation light is scanned over the sample and fluorescence from each pixel is acquired with point detectors separately. Whereas confocal scanning microscopes achieve a much better axial resolution than wide-field microscopes and enable three-dimensional imaging, they suffer from poor temporal resolution.

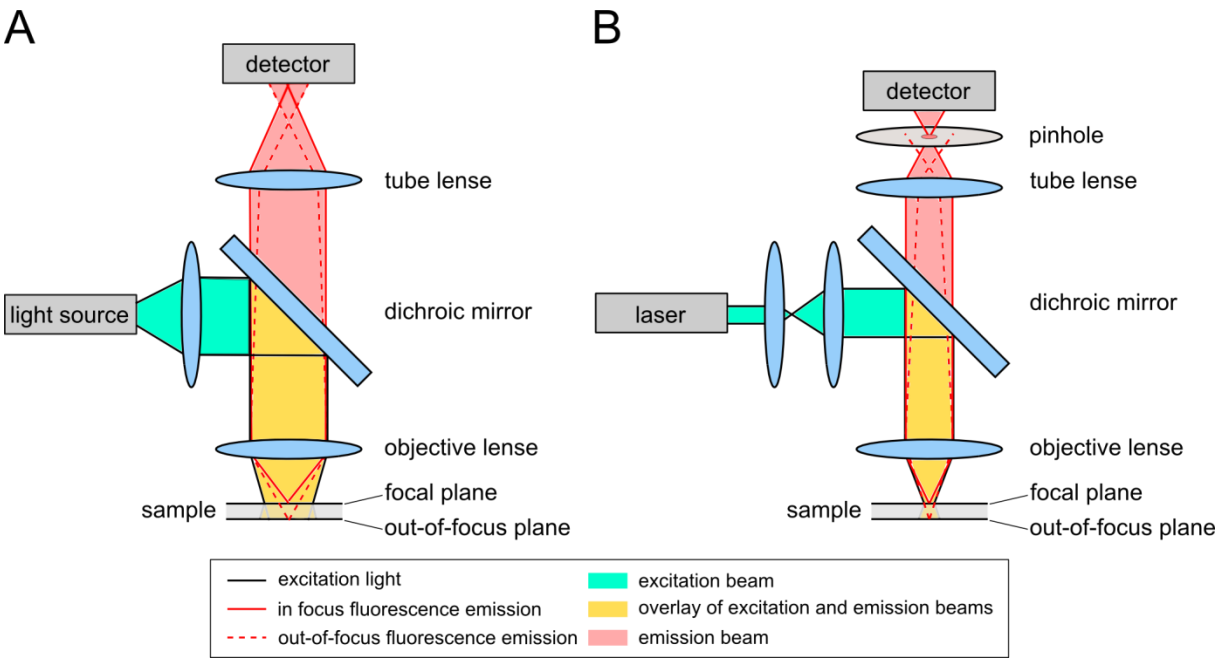

Figure 2.18: Schematic drawing of (A) a wide-field and (B) a confocal fluorescence microscope. Based on[320,321].

2.4.4. Förster Resonance Energy Transfer

FRET is a radiation-less energy transfer from a donor fluorophore in the electronically excited state to an acceptor fluorophore in the electronic ground state via dipole-dipole coupling (Figure 2.19) and has first been described by Förster.[322–324]

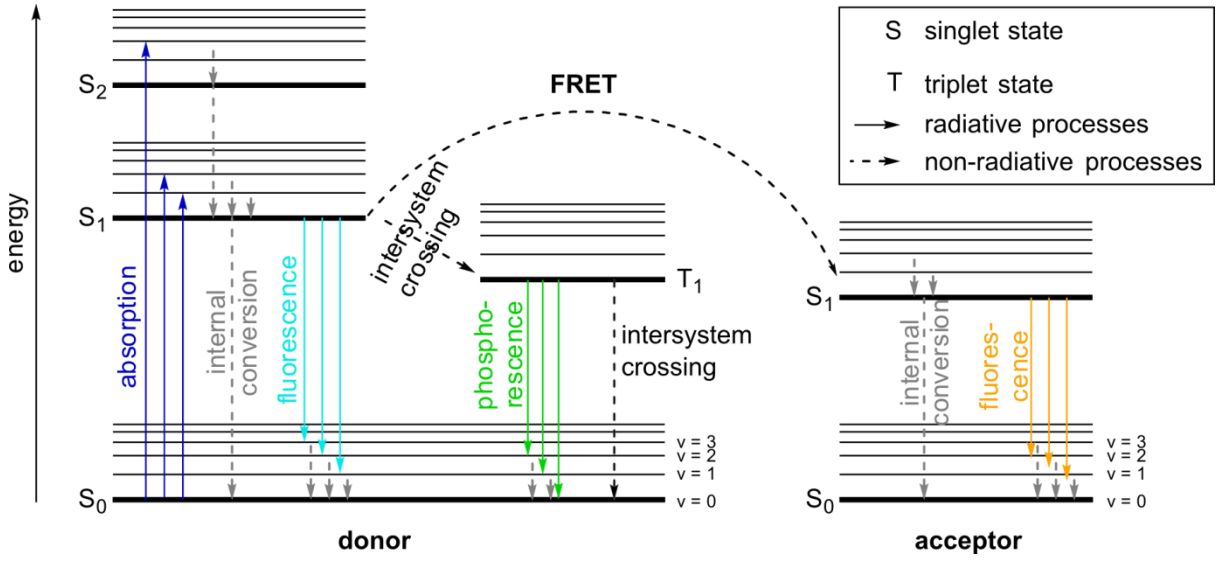

Figure 2.19: Jablonski diagram with FRET from the donor to the acceptor fluorophore.

The efficiency of FRET E_{FRET} strongly depends on the distance r of donor and acceptor fluorophore and can be calculated according to

$$E_{FRET} = \frac{R_0^6}{R_0^6 + r^6}. \tag{2.7}$$

R_0 is the Förster radius and is defined as the distance r at which the FRET efficiency of a certain donor-acceptor pair equals 50 %. The Förster radius is given as

$${R_0}^6 = \frac{9000 \cdot \ln 10 \cdot \Phi_D \cdot \kappa^2}{128 \cdot N_A \cdot \pi^5 \cdot n^4} \cdot J(\lambda), \tag{2.8}$$

where Φ_D is the quantum yield of the donor in absence of the acceptor, κ^2 the orientation factor, N_A Avogadro's number, n the refractive index of the medium, and $J(\lambda)$ the wavelength-dependent overlap integral of the donor's emission and the acceptor's absorption spectra. The latter is calculated from the normalized fluorescence intensity of the donor $F(\lambda)$ and the extinction coefficient of the acceptor $\varepsilon(\lambda)$ via

$$J(\lambda) = \int_0^\infty F(\lambda)\, \varepsilon(\lambda) \lambda^4 \mathrm{d}\lambda. \tag{2.9}$$

The orientation factor κ^2 describes the relative orientation of donor and acceptor transition dipole moments in space. It can be calculated from the angle between both transition dipoles θ_T and the angles between each dipole and the separation vector between donor and acceptor θ_D / θ_A (Figure 2.20) with the following equation:

$$\kappa^2 = (\cos\theta_T - 3\cos\theta_D \cos\theta_A)^2 \tag{2.10}$$

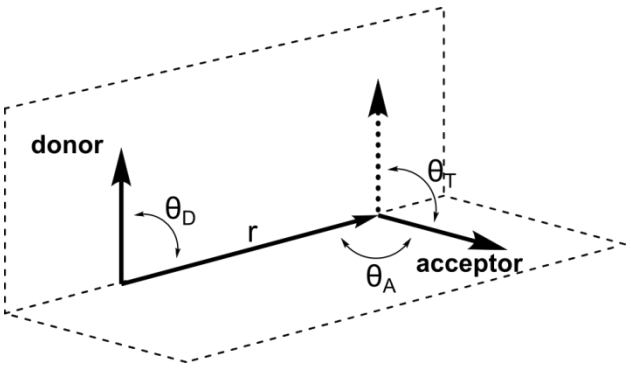

Figure 2.20: Schematic representation of angles between donor and acceptor transition dipole moments used to calculate κ^2.

Based on these equations, three preconditions for efficient FRET can be formulated. Firstly, the distance between donor and acceptor fluorophore must be very small. As a rule of thumb, it should be between 2 nm and 10 nm. An increase of r to two times R_0 already results in FRET efficiencies of only 1.5 % (Figure 2.21). Secondly, the emission spectrum of the donor

must overlap with the acceptor's excitation spectrum. As FRET is a dipolar interaction, the third precondition is the proper orientation of the transition dipole moments of donor and acceptor fluorophore, which can hardly be influenced. κ^2 can range from 0 to 4. For donor-acceptor pairs with random orientation and high mobility, an average value for κ^2 is 2/3.[325,326]

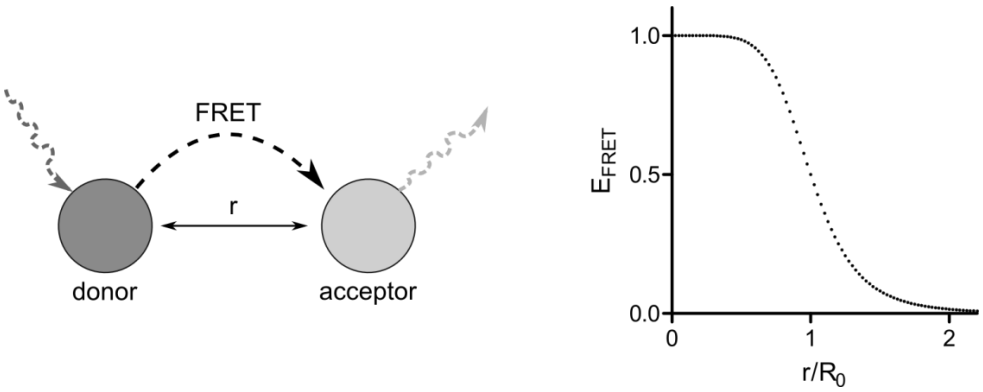

Figure 2.21: Dependency of the FRET efficiency E_{FRET} on the sixth power of the donor-acceptor distance *r*.

Due to its strong distance-dependency, FRET is an ideal tool to investigate processes based on changes of intra- or intermolecular distances.[293,327] For example, conformational changes of single biomolecules can be monitored by attaching two fluorophores forming a FRET pair at different sites of a molecule.[328] In cellular biology, FRET is often used to assess the interaction of two partners, e.g. a protein and lipid, a protein and DNA, or two different proteins. As such samples contain several donor and acceptor fluorophores and a Förster radius is not known for every FRET pair, exact distances are seldom calculated from these FRET experiments. However, FRET measurements yield valuable information on the close proximity of donor- and acceptor-tagged molecules allowing for conclusions on molecular interactions.[329] As FRET only occurs if both molecules are closer than roughly 10 nm, it allows much higher spatial localization than studies purely based on the diffraction of light. If protein interactions are studied, fluorescent protein-fusion proteins are often used.

Several techniques with different advantages and disadvantages have been established to measure FRET.[320,326,330–332] They are based on fluorescence intensities, anisotropies, or lifetimes. The usage of fluorescence lifetimes to detect FRET is separately discussed in the next chapter. Both the decrease of the donor's fluorescence intensity and the increase in the acceptor's fluorescence intensity accompanying FRET can be employed to determine its efficiency. Traditionally, FRET is detected by measuring the acceptor fluorescence (sensitized emission) after donor excitation.[333] A quantitative analysis of such experiments requires several controls to correct for artifacts arising from spectral bleed-through due to excitation of the acceptor at the donor's excitation wavelength and emission of the donor at the acceptor's emission wavelengths. As a consequence, excitation and emission spectra of donor and acceptor should not be too close to one another. Conversely, this reduces the Förster radius and thus the sensitivity of the FRET measurement. To solve this discrepancy, some correction procedures have been established.[333,334] They are based on the examination of samples containing only donor, only acceptor, or both fluorophores combined with different filter

settings. Sensitized emission can be performed as cuvette experiment, but also via spectral imaging.[335,336] Besides the detection of the acceptor's fluorescence, the donor's fluorescence intensity can be assessed, as it decreases due to FRET. This is the most direct approach to quantify FRET.[331] As only the donor's emission is detected, spectral bleed-through is not obstructive and FRET pairs with a larger spectral overlap and accordingly higher Förster radii can be used. Moreover, experiments with an excess of acceptor fluorophores can be performed. One facile implementation of a FRET measurement based on the fluorescence intensity of the donor is acceptor photobleaching.[337] Thereby, images of both the donor and the acceptor emission are taken before and after photochemically destroying acceptor fluorophores. If FRET occurred before bleaching, the donors' fluorescence intensity will increase afterwards. FRET efficiencies can be calculated from the average donor fluorescence intensities before I_{DA} and after I_D bleaching the acceptor via

$$E_{FRET} = 1 - \frac{I_{DA}}{I_D}. \tag{2.11}$$

For FRET experiments with equal amounts of donor and acceptor fluorophores, such as intramolecular applications, the measured FRET efficiency corresponds to the actual FRET efficiency. If the stoichiometry of both fluorophores changes, for instance in the case of intermolecular interaction studies, the FRET efficiency derived from the measurement is the apparent FRET efficiency $E_{FRET,app}$, which is the product of the "real" FRET efficiency E_{FRET} and the fraction of interacting donor fluorophores α:[338]

$$E_{FRET,app} = 1 - \frac{I_{DA}}{I_D} = \alpha \cdot E_{FRET} \tag{2.12}$$

Acceptor photobleaching is usually performed with fixed samples, as data acquisition takes some minutes. Movements of fluorophores in living samples would influence the result. Additionally, bleaching destroys the acceptor fluorophore and in this way prevents repeated measurements.

Furthermore, FRET can be detected by measuring fluorescence anisotropy following the excitation of samples with linearly polarized light.[329,339] This leads to the selective excitation of fluorophores, whose absorption transition dipole moments are approximately parallel to the electric field vector of the excitation light. Hence, immediately after excitation also the polarization of the fluorescence emission is parallel to the excitation light.[292] Rotations of fluorophores can decrease the fluorescence anisotropy, but are rather slow if large fluorophores such as fluorescent proteins are used.[340] If FRET occurs, the excitation energy of the donor can be transferred to a slightly differently oriented acceptor fluorophore. The fluorescence emission can thus occur at a different angle resulting in fluorescence depolarization. This approach can be applied to study FRET between two identical (homo FRET) or different fluorophores.[341–343]

2.4.5. Fluorescence Lifetime Imaging Microscopy

The measurement of the donor's fluorescence lifetime is considered to be the most robust and accurate way to determine FRET.[293,329,330,344] It circumvents several drawbacks of other FRET detection schemes. As the fluorescence lifetime is an intrinsic property of a fluorophore, it is theoretically independent of variations in fluorophore concentrations, illumination intensity, light pathlength, scattering, and to some extent even photobleaching.[293] Similar to equation 2.12, apparent FRET efficiencies can be calculated from fluorescence lifetimes of samples with donor and acceptor fluorophores τ_{DA} and such with only donor fluorophores τ_D according to

$$E_{FRET,app} = 1 - \frac{\tau_{DA}}{\tau_D} = \alpha \cdot E_{FRET}. \tag{2.13}$$

Fluorescence lifetime imaging (FLIM) microcopy allows for the spatially resolved detection of FRET. Thereby, the image contrast is generated from fluorescence lifetimes. FLIM techniques can be grouped into time- or frequency-domain, photon counting or analog, and point-scanning or wide-field approaches.[293,345,346] Almost all technical combinations are used.[346]

In the time-domain, samples are excited with a sharp laser pulse and fluorescence is detected over time (Figure 2.22A). Fluorescence lifetimes can be derived from the exponential decay of the fluorescence intensity using equation 2.4. Time-domain FLIM can be performed with a confocal scanning or wide-field microscope. Confocal time-domain FLIM is better known as time-correlated single photon counting (TCSPC).[347] Thereby, fluorescence lifetimes are recorded pixel by pixel. Samples are excited with pulsed lasers and the arrival time of single photons is detected in relation to the excitation pulse with point detectors. Subsequently, histograms of the arrival times of single photons are created for each pixel. Fluorescence decays can be fitted to exponential functions in order to derive fluorescence lifetime components. TCSPC is considered as gold standard in FLIM.[348] Since all available photons are detected, it has an optimal signal-to-noise ratio, good reproducibility and spatial resolution, linear recording characteristics, and can be used to resolve complex decay profiles.[293,346,349–351] However, pulsed lasers are needed and the acquisition is rather slow (generally some minutes per image), as each photon at each pixel has to be measured individually.[293] Wide-field time-domain FLIM microscopy is faster than conventional TCSPC, as it allows for the parallel acquisition of all pixels.[346] Samples are excited with laser pulses and snap shots of the fluorescence decay are acquired with a CCD camera coupled to a gated image intensifier, whose detection window is temporally shifted in relation to the excitation after each pulse.[352,353] As the whole frame is illuminated simultaneously, higher laser powers are needed. In addition, wide-field time-domain FLIM is less sensitive than TCSPC, as the photon efficiency is lower and its temporal resolution is limited to approximately 80 ps.[351,354]

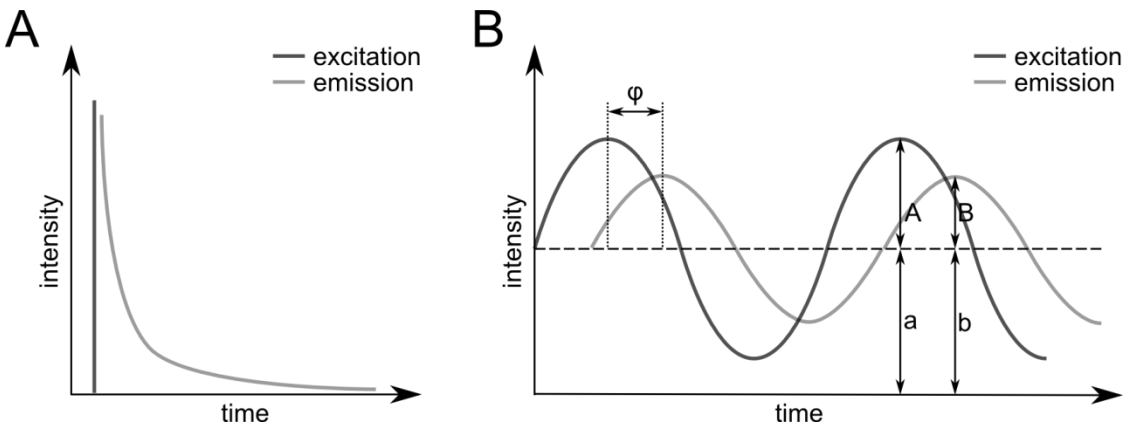

Figure 2.22: Fluorescence lifetime measurements (A) in the time-domain and (B) in the frequency domain. The intensities of excitation light (dark grey) and emitted fluorescence (light gray) are drawn over time. (B) is reprinted (adapted) with permission from Doll et al.[355] Copyright (2018) Elsevier Inc.

For frequency-domain measurements, fluorophores are excited with a sinusoidally intensity modulated continuous wave laser at a MHz frequency ω (Figure 2.22B). As a consequence, the fluorescence emission is modulated in its intensity at the same frequency, but with a decreased modulation depth m and a shifted phase φ compared to the excitation light. Both the relative demodulation (equation 2.14) and the phase shift (equation 2.15) can be used to derive fluorescence modulation τ_m and phase τ_φ lifetimes.

$$m = \frac{m_{em}}{m_{ex}} = \frac{B/b}{A/a} \tag{2.14}$$

$$\varphi = \varphi_{ex} - \varphi_{em} \tag{2.15}$$

In these equations, *em* stands for emission light and *ex* for excitation light. For a mono-exponential decay, fluorescence modulation and phase lifetimes are equal and given by the following equations:

$$\tau_m = \frac{1}{\omega}\sqrt{\left(\frac{1}{m}\right)^2 - 1} \tag{2.16}$$

$$\tau_\varphi = \frac{1}{\omega}\tan\varphi \tag{2.17}$$

For more complex decays, fluorescence phase lifetimes are shorter than fluorescence modulation lifetimes.[293,356] Lifetime components of multiexponential decays can be analyzed by measuring at several modulation frequencies.[345] The optimal modulation frequency depends on the fluorescence lifetime of the donor fluorophore τ and can be calculated according to equation 2.18.[357]

$$\omega_{optimal} = \frac{1}{\tau}\sqrt{\left(\frac{1+\sqrt{3}}{2}\right)}. \tag{2.18}$$

For EGFP, whose fluorescence lifetime has been reported to range from 2.1 ns to 2.6 ns,[358,359] optimal modulation frequencies lie between 70 MHz and 90 MHz. A detailed theoretical description of frequency-domain FLIM can be found in literature.[326,353,360,361]
Frequency-domain FLIM can be detected with gain-modulated cameras following wide-field excitation or gain-modulated point detectors after scanning.[346,362] The latter approach is faster than TCSPC.[363] Its optimization led to the development of "digital FLIM", which possesses an improved photon efficiency.[364] However, the wide-field frequency-domain approach is preferred for real-time fluorescence lifetime imaging applications.[360] Following wide-field excitation, emitted fluorescence is detected with a CCD camera coupled to an image intensifier, which is modulated at the same frequency as the excitation light.[292] A series of images is acquired, while the detection window is shifted in phase with respect to the excitation light from 0 ° to 360 °. The fluorescence signal is accumulated for 1 ms to 100 ms per image. This approach can easily be implemented and allows for fast FLIM, as all pixels are illuminated simultaneously. Data analysis can be performed graphically with so-called phasor plots.[365] The poor axial resolution arising from the wide-field setup can be improved by combining frequency-domain FLIM with other microscopic approaches, such as spinning disk[366,367] or lightsheet microscopy[368].
As a side note it should be mentioned that apart from FRET, FLIM microscopy has been used to investigate the local environment of fluorophores yielding information on the refractive index of the medium, viscosity, temperature, oxygen and ion concentrations, and local pH values.[293]

2.5. Detection of Protein-Specific PTMs

Tens of thousands of protein PTM sites have been identified[10] raising questions on the influence of a certain PTM on a protein's function. For this purpose, methods probing a PTM at the single protein level are indispensable. In general, protein-specific PTMs are assessed via biochemical approaches applying antibody-enrichment protein purification in combination with immunoblotting or mass spectrometry.[11,369] However, these methods disrupt the cellular context. In order to unravel the function of PTMs in signaling cascades and decipher when and where a certain PTM occurs, strategies to visualize the PTM-state of a specific protein inside cells are of fundamental importance.[20] They would allow obtaining information on how PTMs regulate the subcellular localization of proteins with ideally temporal resolution.
In principle, fluorescent antibodies or Fab fragments directed against a protein only in its post-translationally modified state can be employed to this end. Such antibodies have been used to visualize protein-specific phosphorylation[370–373], methylation[374], acetylation[375], and lipidation[376]. Yet, antibodies are not available for every protein and PTM, as their preparation is challenging and laborious. For this reason, two more general approaches have been developed, which rely on the investigation of the proximity between the PTM and the protein of interest (POI).
The first approach is the proximity ligation assay (Figure 2.23A),[377] which requires two antibodies: one detecting the PTM and one against the specific POI. These antibodies are tagged with DNA strands, which are ligated together when present in close proximity. The circular DNA formed in this manner is amplified using fluorescent nucleotides enabling the visualization of the proximity ligation product. Following this strategy, protein-specific glycosylation[378,379], phosphorylation[380–383], and lipidation[159,384] have been studied. Disadvantages of this method are the need of specific antibodies for the POI and the PTM, the laborious procedure, a low spatial resolution, and the fact that it cannot be used *in vivo*.[385] Especially the generation of pan-specific PTM antibodies is difficult, since many PTMs are very small, but need to be selectively detected in different amino acid sequence surroundings.[11]

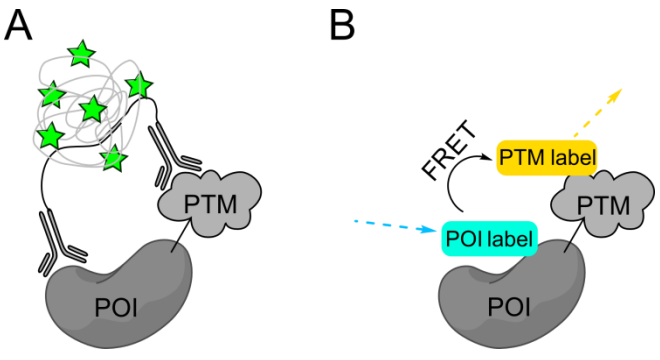

Figure 2.23: Proximity-dependent imaging of protein-specific PTMs via (A) a proximity ligation assay or (B) FRET.

The second method relies on FRET and requires both the PTM and the POI to be fluorescently labeled with different fluorophores forming a FRET pair (Figure 2.23B). As FRET strongly depends on the distance between donor and acceptor fluorophore,

intramolecular interactions are favored over intermolecular ones.[386] The POI can be tagged with a fluorescent protein, a protein-specific and fluorophore-functionalized antibody, or any kind of protein-specific tag[240] that can be modified with a fluorophore, such as SNAP-, Halo-, LAP-tags, aptamers, or unnatural amino acids. The PTM can either be labeled with fluorophore-functionalized antibodies or chemical reporters labeled with fluorophores via bioorthogonal ligation reactions. By combining tagged POIs with metabolic reporters for protein glycosylation, visualizing protein-specific glycosylation of cell-membrane proteins has been achieved.[387–390] In addition, FRET has been used to investigate protein-specific phosphorylation[391–395] and poly(ADP-ribosyl)ation[147]. The major difficulty of the FRET-based approach is the detection of FRET in the presence of a large excess of PTM labels. This can be overcome by using the fluorescence lifetime of the donor fluorophore as readout, which enables a robust and accurate detection of FRET.[293] For this purpose, the protein is tagged with the FRET donor and the PTM label bears the FRET acceptor.

Moreover, genetically encoded sensors have been used to study PTMs of selected proteins in living cells. In the case of FRET sensors, a construct comprising two fluorescent proteins forming a FRET pair, a peptide sequence known to be post-translationally modified, and a sensing protein domain binding to the PTM-modified peptide is genetically encoded in cells. Once the peptide is modified, the sensing domain binds to the PTM-peptide resulting in a conformational change of the whole sensor construct, which brings the two fluorescent proteins in close proximity and enables FRET. Furthermore, sensors based on bioluminescence, dimerization-dependent fluorescent proteins, or split fluorescence proteins have been developed.[396] PTM sensors have been established to visualize for instance protein *O*-GlcNAcylation of casein kinase II[397,398], acetylation of histones 3 and 4 [399,400], methylation of histone 3[401–403], and phosphorylation of many proteins including protein kinase A[404], aurora B kinase[371], and Akt1[405]. While these sensors are valuable tools for in cell imaging of protein-specific PTMs, they detect only a predefined PTM site on a short peptide of the POI. Sensors need to be prepared for each POI and each PTM site individually. Besides this, it is questionable whether the PTM of the peptide in the context of a many tens of kDa large sensor construct behaves in the same way as in its native protein surrounding.

More recently, two additional approaches have been presented for protein-specific imaging of glycosylation. One of them relies on surface-enhanced Raman scattering, which occurs if both an aptamer-modified gold nanoparticle targeting the POI and a functionalized gold nanoparticle attached to azide-tagged glycans installed by MGE are present in close proximity.[406] The other method allows for the simultaneous detection of two different monosaccharides on a single glycoprotein. It is based on duplexed luminescence resonance energy transfer from luminescence upconversion nanoparticles binding to the POI via aptamers to acceptor fluorophores ligated to chemical glycosylation reporters.[273] However, both approaches were confined to applications on cell surfaces due to the usage of azide-alkyne cycloadditions.

3. Objectives

Protein PTMs are essential, as they influence biological (e.g. function or interaction partners), chemical (e.g. involvement in biochemical reactions), and physical (e.g. structure and localization) properties of proteins and are associated with multiple diseases.[25,407] Thus, it is of fundamental importance to investigate PTMs of individual proteins in their native context, the cell. The aforementioned approaches for studying protein-specific PTMs are limited in their usage, as they are either designed for a certain protein-PTM pair and are not generally applicable (such as FRET sensors) or restricted to applications on cell surfaces or fixed cells due to poor cellular permeability or toxicity of reagents used (such as proximity ligation assays or most existing FRET-based approaches).

The main aim of this thesis was the development of a more generally applicable approach for imaging protein-specific PTMs inside, preferably living, cells. For this purpose, the POI should be expressed with an EGFP tag. Chemical reporters targeting the desired PTM should be introduced in cells and after their incorporation by the cells' enzymatic machinery labeled via a suitable bioorthogonal ligation reaction. The proximity of EGFP at the POI and the modification-anchored fluorophore should be detected by FRET (Figure 3.1). To this end, an existing frequency-domain wide-field FLIM microscope should be employed, which enables a fast and accurate acquisition of fluorescence lifetime data from single living cells.[320]

The modification to be studied was intracellular protein *O*-GlcNAcylation. To establish this method, the known chemical reporter Ac_4GlcNCyoc should be used. So far, it is the only known reporter for monitoring intracellular protein glycosylation capable of being bioorthogonally labeled inside living cells. This can be achieved via a DAinv reaction with tetrazine-functionalized fluorophores. As it was solely proposed that Ac_4GlcNCyoc ends up as *O*-GlcNAc, its cellular incorporation should be investigated in a first step. Thereafter, the protein-specific approach should be established for the glycosyltransferase OGT, which was chosen as model protein. The method's general applicability and meaningfulness should be demonstrated by visualizing the glycosylation state of further proteins in living cells.

Furthermore, the developed imaging strategy should be applied to study the glycosylation of individual proteins in cells and optimally resolve spatial differences in glycosylation patterns. Suggested proteins were the microtubule-associated kinesin-like protein Kif18A and the multifunctional protein β-catenin.

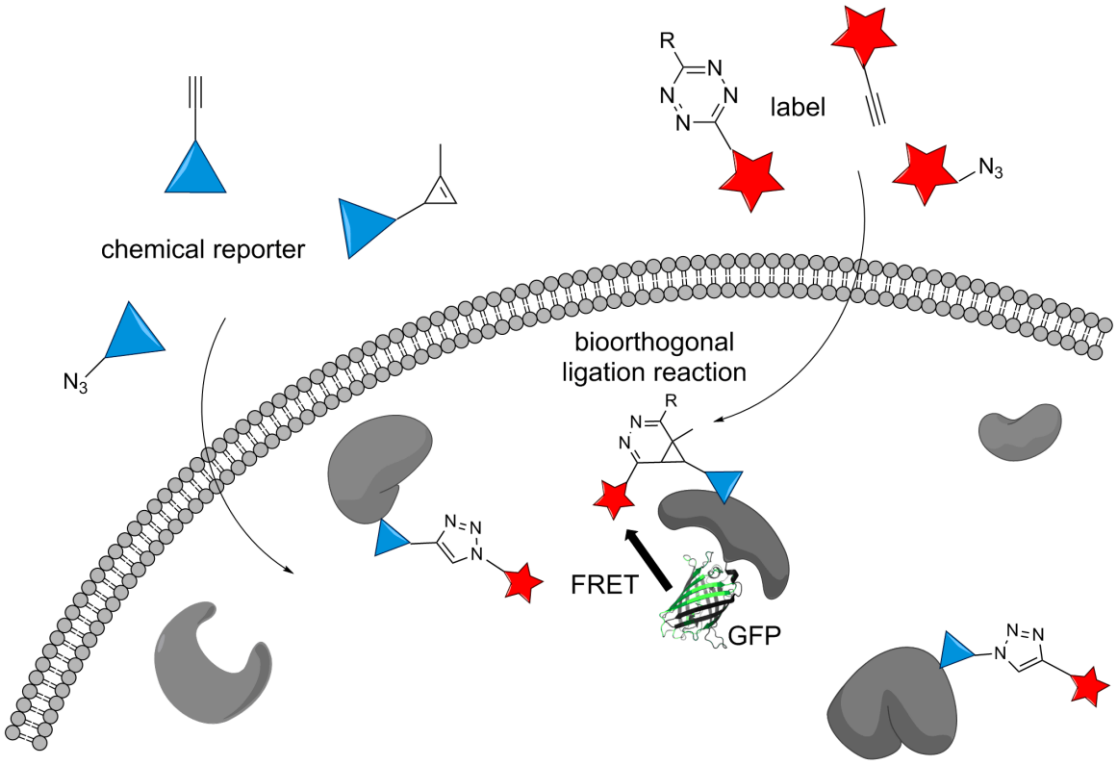

Figure 3.1: Experimental strategy for protein-specific imaging of PTMs by combining chemical reporter strategies with FRET.

Besides studying protein-specific intracellular protein glycosylation, a similar strategy should be established to image other PTMs, namely protein acetylation and methylation. As described in chapters 2.1.2 and 2.1.3, these PTMs have huge biological impacts and are associated with severe diseases. For both modifications, several chemical reporters have been described in literature (see chapters 2.2.2 and 2.2.3), but none of them has been used to visualize acetylation or methylation of the whole proteome or in a protein-specific manner inside cells with microscopic approaches. To this end, suitable methods for the delivery of the respective chemical reporters into cells should be identified and conditions for the required bioorthogonal ligation reaction should be optimized. Afterwards, these PTMs should be imaged proteome-wide with fluorescence microcopy. For protein-specific applications, plasmids encoding EGFP-fusions of selected proteins should be cloned. The combination of EGFP-tagged proteins, chemical reporter strategies, and FLIM-FRET microscopy should then allow for protein-specific imaging of acetylation and methylation within single cells.

4. Results and Discussion

4.1. Protein Glycosylation

This chapter comprises different projects dealing with the imaging of protein glycosylation. Firstly, studies on the incorporation of the chemical reporter Ac_4GlcNCyoc into the cellular glycome are described (chapter 4.1.1). After this, the development of an approach for visualizing protein-specific glycosylation inside living cells and its application to various proteins of interest are presented (chapters 4.1.2 to 4.1.5). Finally, attempts towards the investigation of protein *O*-GlcNAcylation in *A. thaliana* and the visualization of the sialyl Tn antigen on membranes of cancer cells are explained in chapters 4.1.6 and 4.1.7.
Results included in chapters 4.1.1 and 4.1.2 have been published.[355,408]

4.1.1. Ac_4GlcNCyoc

The chemical reporter of choice for studying intracellular protein glycosylation was Ac_4GlcNCyoc[180,182] (Figure 4.1A). The chemical handle of Ac_4GlcNCyoc is a carbamate-linked methylcyclopropene, which reacts faster than terminal alkenes, isonitriles, or amide-linked cyclopropenes in DAinv reactions with tetrazines.[181,266–268] Späte et al. could demonstrate that human embryonic kidney (HEK) 293T cells and cervical cancer cells taken from Henrietta Lacks (HeLa) S3 treated with 50 µM Ac_4GlcNCyoc displayed only weak membrane fluorescence after labeling with Tz-biotin and streptavidin-Alexa Fluor 647.[182] In contrast, lysates of such Ac_4GlcNCyoc-treated cells labeled with Tz-biotin and streptavidin-Alexa Fluor 647 showed strong signals. Based on these results, it has been suggested that Ac_4GlcNCyoc ends up as *O*-GlcNAc.[180,182]
Thus, the first aim was to investigate whether Ac_4GlcNCyoc is indeed incorporated as *O*-GlcNAc. Cyanine (Cy) 3-Tz (Figure 4.1B) was selected for DAinv reactions to avoid the necessity of two reagents for labeling Ac_4GlcNCyoc. This dye has already been utilized to mark peracetylated methylcyclopropene-tagged ManNAc (Ac_4ManNCyoc).[181,409] At the beginning, DAinv reaction parameters were optimized. To this end, HEK293T cells were treated with 100 µM Ac_4GlcNCyoc or peracetylated *N*-acetylglucosamine (Ac_4GlcNAc) as control for 20 h and lysed. Proteins modified with the chemical reporter were labeled with different concentrations of Cy3-Tz for different periods of time and separated with sodium dodecylsulfate-polyacrylamide gelelectrophoresis (SDS-PAGE). The degree of Ac_4GlcNCyoc incorporation was determined by reading out fluorescence of Cy3 from Western blots. Fluorescence signals of Ac_4GlcNCyoc-treated cells were much stronger than those of Ac_4GlcNAc-treated ones for all Cy3-Tz concentrations tested (Figure 4.1C+D). This states that Ac_4GlcNCyoc is indeed metabolized in cells and attached to proteins. Fluorescence intensities did not vary much among different Cy3-Tz concentrations and always led to the same level of fluorescence background detected for Ac_4GlcNAc-treated samples. The DAinv

reaction between the Cyoc-derivative and Cy3-Tz proceeded very fast, as fluorescence signals were already present after an incubation time of 15 min. However, Cy3 signals increased with longer incubation times, while the background fluorescence of Ac_4GlcNAc-treated samples did not change markedly. Useful DAinv reaction parameters for Ac_4GlcNCyoc and Cy3-Tz were found to be 10 µM Cy3-Tz and a reaction time of 90 min, which were used for further lysate experiments.

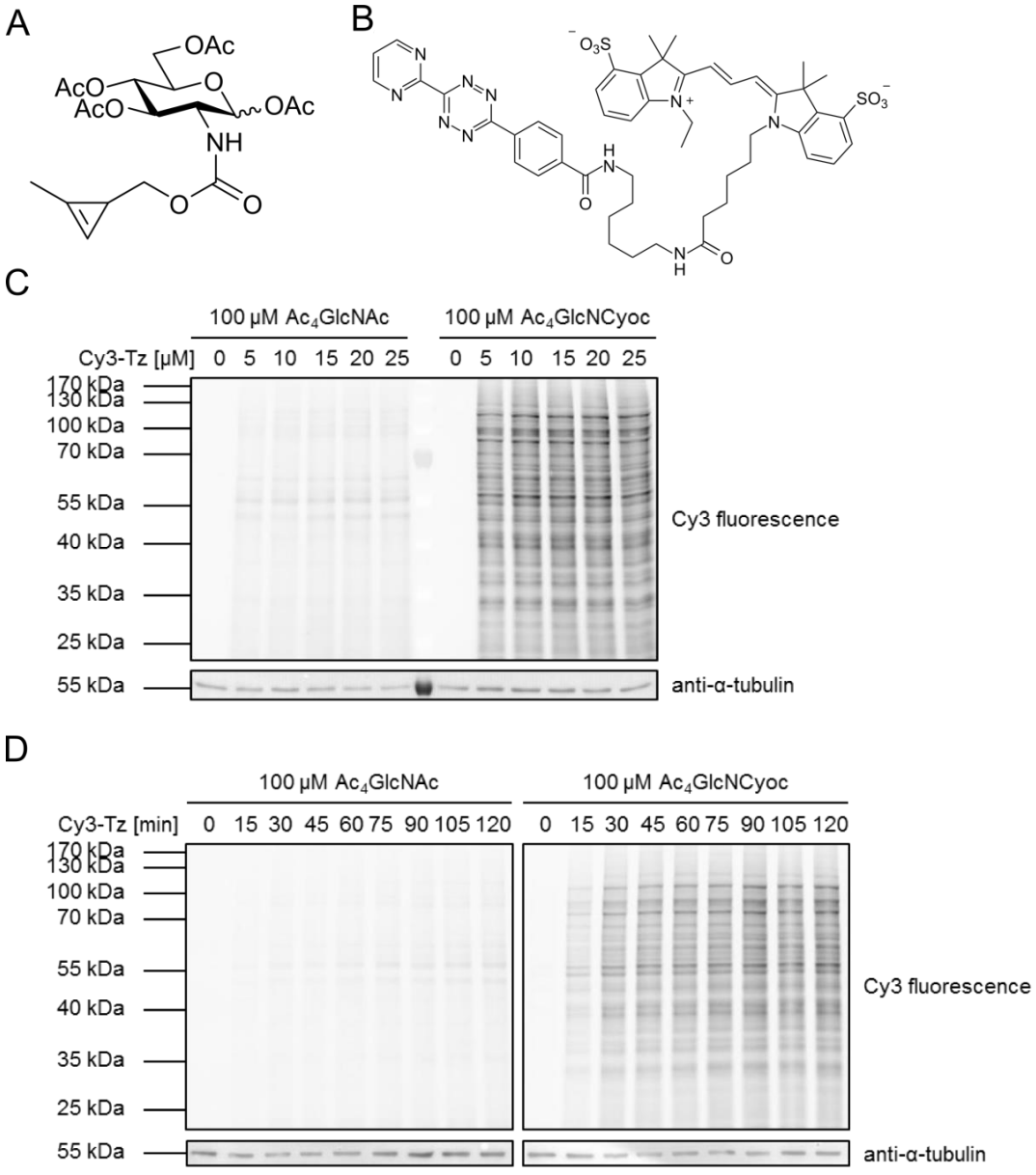

Figure 4.1: DAinv reaction of Ac_4GlcNCyoc and Cy3-Tz. Chemical structures of (A) Ac_4GlcNCyoc and (B) Cy3-Tz are shown. (C+D) HEK293T cells were treated with 100 µM Ac_4GlcNCyoc or Ac_4GlcNAc for 20 h, lysed, and labeled (C) with different concentrations of Cy3-Tz for 90 min or (D) with 10 µM Cy3-Tz for different durations at 25 °C. Protein samples were separated by SDS-PAGE and fluorescence of Cy3 was read out from Western blots. Reprinted (adapted) with permission from Doll et al.[408] Copyright (2016) WILEY-VCH Verlag GmbH & Co. KGaA, Weinheim.

As it was aimed to perform glycosylation studies within living cells, possible cytotoxic effects of $Ac_4GlcNCyoc$ were investigated. HEK293T cells were treated with up to 200 µM $Ac_4GlcNCyoc$ for 20 h or 48 h. Dimethyl sulfoxide (DMSO) was used as solvent control and $Ac_4GlcNAc$ to account for effects not arising from the chemical handle, but from increased intracellular GlcNAc levels. Viabilities were quantified with AlamarBlue assays. Whereas the treatment of cells with DMSO did not affect their integrity, increasing concentrations of $Ac_4GlcNAc$ and $Ac_4GlcNCyoc$ as well as longer incubation times impaired cells (Figure 4.2). For 100 µM $Ac_4GlcNAc$ and $Ac_4GlcNCyoc$, viabilities dropped to 74 % and 52 % after 20 h and to 35 % and 13 % after 48 h, respectively. Thus, concentrations of $Ac_4GlcNCyoc$ should not exceed 100 µM and the incubation time should be as short as possible in order to receive meaningful results.

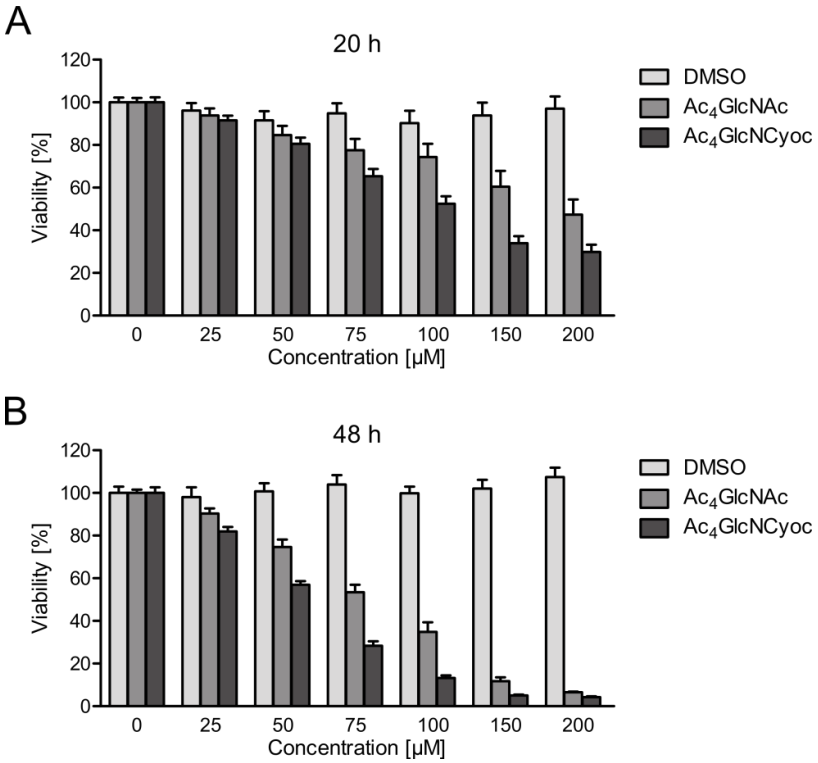

Figure 4.2: $Ac_4GlcNAc$ and $Ac_4GlcNCyoc$ affect cellular viabilities. HEK293T cells were treated with different concentrations of $Ac_4GlcNAc$ or $Ac_4GlcNCyoc$ for (A) 20 h or (B) 48 h. DMSO was used as solvent control and added to 0–0.2 V-%. Viabilities were assessed with AlamarBlue assays. Columns correspond to average values from three independent experiments with four replicates each and error bars to standard errors of the means (SEMs). Reprinted (adapted) with permission from Doll et al.[408] Copyright (2016) WILEY-VCH Verlag GmbH & Co. KGaA, Weinheim and Doll et al.[355] Copyright (2018) Elsevier Inc.

Next, the temporal and concentration-dependent incorporation of $Ac_4GlcNCyoc$ was examined. HEK293T cells were either treated with 100 µM of the monosaccharide for different time spans or with different concentrations of $Ac_4GlcNCyoc$ for 20 h. Cells were lysed and Cyoc-derivatives were labeled with Cy3-Tz. Although a weak incorporation of the chemical reporter could already be detected after 5 min, much stronger fluorescence signals were found for proteins from cells treated with $Ac_4GlcNCyoc$ for 19 h (Figure 4.3A).

Prolonged incubation resulted in slightly decreased Cy3 signals, which might be a result of the increased cytotoxicity of Ac_4GlcNCyoc. For following experiments, it was decided to use incubation times of approximately 20 h. As expected, highest concentrations of Ac_4GlcNCyoc resulted in strongest incorporation of Ac_4GlcNCyoc. However, also lower concentrations such as 25 µM or 50 µM displayed Cy3 signals significantly larger than background signals of samples not treated with Ac_4GlcNCyoc but still incubated with Cy3-Tz. Apart from HEK293T cells, Ac_4GlcNCyoc was found to be well incorporated in HeLa and human non-small cell lung carcinoma (H1299) cells (Figure 4.3B+C). Maximal Cy3 fluorescence was observed with 100 µM Ac_4GlcNCyoc for both cell lines after roughly 19 h. The decrease of Ac_4GlcNCyoc incorporation for incubation times longer than 19 h was stronger for these two

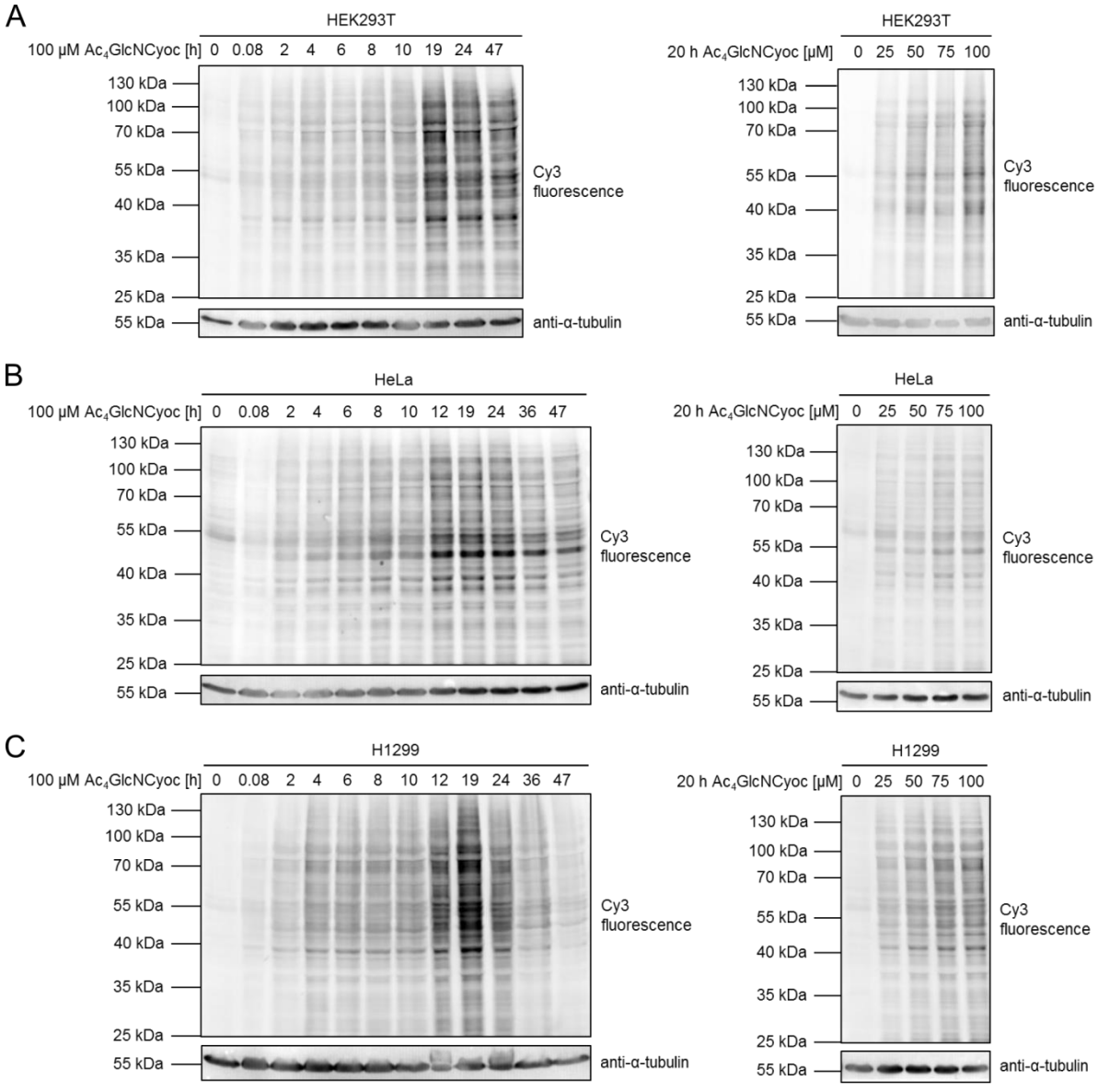

Figure 4.3: Time- and concentration-dependent incorporation of Ac_4GlcNCyoc into the cellular glycome of (A) HEK293T, (B) HeLa, and (C) H1299 cells. Fluorescence readouts of Western blots of Cy3-marked lysates from cells treated for different times with 100 µM Ac_4GlcNCyoc or with different concentrations of Ac_4GlcNCyoc for 20 h are displayed. Reprinted (adapted) with permission from Doll et al.[355] Copyright (2018) Elsevier Inc.

cell lines than for HEK293T cells. Although HeLa and H1299 cells nicely incorporated Ac_4GlcNCyoc, HEK293T cells were chosen for setting up the glycosylation imaging approach, as they grow rapidly, are easy to handle, can be transfected via calcium phosphate co-precipitation in bulk, and have already been shown to accept Ac_4GlcNCyoc.[182]
Having determined optimal incorporation and labeling parameters for Ac_4GlcNCyoc, its metabolic fate was investigated. Once present in cells, Ac_4GlcNCyoc is assumed to be rapidly deacetylated by unspecifically acting esterases.[169] Thereafter, it needs to be processed by several enzymes in order to be converted to UDP-GlcNCyoc, which could then serve as substrate for OGT. To prove that the processing and incorporation of Ac_4GlcNCyoc depends on the activity of cellular enzymes, native and heat-denatured HEK293T cell lysates were treated with 100 µM Ac_4GlcNCyoc for 5 h or 20 h at 37 °C. After performing the DAinv reaction with Cy3-Tz and separating proteins via SDS-PAGE, fluorescence of Cy3 was read out from Western blots. Heat treatment denatures proteins and renders enzymes inactive, although some residual enzyme activity can remain.[410] Several heating procedures were tried, but most of them failed as proteins precipitated as large insoluble aggregates. Finally, lysates were incubated at 98 °C for three times 10 min followed by subsequent cooling and centrifugation of samples. Native lysates treated with Ac_4GlcNCyoc for 5 h showed little Cy3 fluorescence, which was still higher than background fluorescence of the lysate sample not treated with Ac_4GlcNCyoc at all (Figure 4.4). The 20 h sample displayed a much greater signal. However, no labeling of Cyoc-derivatives with Cy3-Tz was detected in heat-denatured lysates. This led to the conclusions that Ac_4GlcNCyoc is incorporated into the cellular glycome *in vitro* and that this process depends on the activity of enzymes.

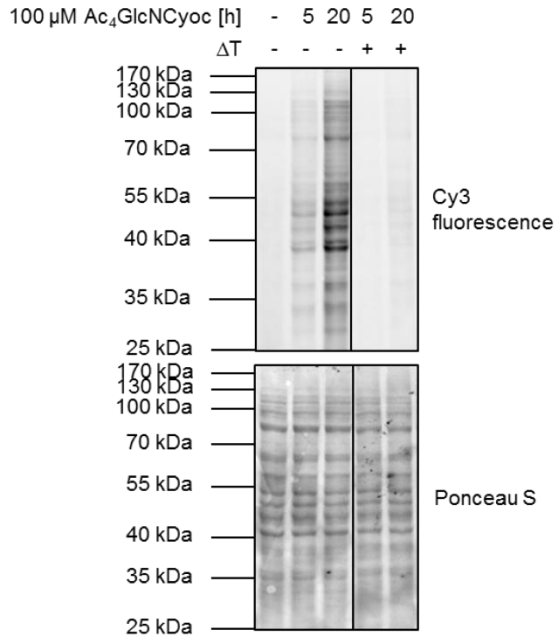

Figure 4.4: Enzyme-dependent incorporation of Ac_4GlcNCyoc. HEK293T cell lysates were heat-denatured for three times 10 min at 98 °C. Native (-) or denatured (+) lysates were treated with 100 µM Ac_4GlcNCyoc at 37 °C for 5 h or 20 h and labeled with Cy3-Tz. Fluorescence of Cy3 and Ponceau S as loading control were read out from Western blots.

Even though GlcNAc derivatives end up as *O*-GlcNAc very likely, several interconversions among GlcNAc, GalNAc, and ManNAc are possible, as elucidated in chapter 2.1.1. In addition, it has been reported that the pentynoyl group of Ac_4GlcNAlk can be transferred to lysine side chains resulting in the generation of stable amide bonds.[201] A similar transfer of the carbamate-linked methylcyclopropene to lysine residues would yield a base-stable product. To test, whether such a transfer to lysine residues might occur for Ac_4GlcNCyoc, β-elimination was performed. This relies on the removal of *O*-linked glycans attached to serine or threonine residues, but not of *N*-linked glycans or carbamates, under mild basic conditions (pH 12).[411] For this purpose, lysates of HEK293T cells treated with Ac_4GlcNAc or Ac_4GlcNCyoc were labeled with Tz-biotin (Figure 4.5A). The pH value was subsequently raised to 12 for β-elimination or left at 7.8 for control samples. Cy3-Tz could not be used, as the dye itself appeared to be affected by bases. In addition, also the cyclopropene moiety

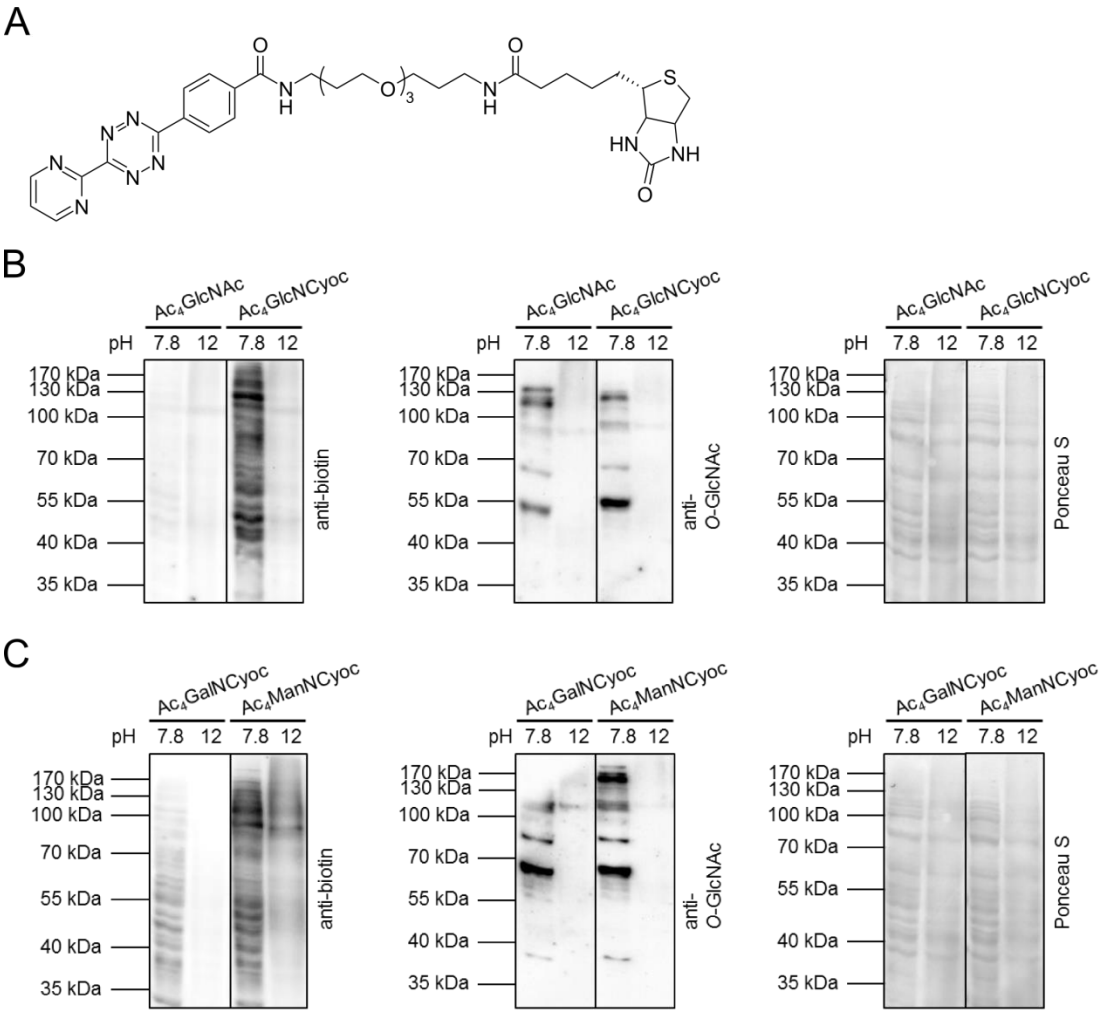

Figure 4.5: β-elimination of incorporated Cyoc derivatives. (A) Chemical structure of Tz-biotin. (B+C) HEK293T cells were treated with 100 µM Ac_4GlcNAc, Ac_4GlcNCyoc, Ac_4GalNCyoc, or Ac_4ManNCyoc for 20 h, lysed, and incubated with 150 mM Tz-biotin for 90 min. For the β-elimination, the pH of lysates (~7.8) was increased to 12 by addition of NaOH. Equal volumes of water were added to control samples. All samples were incubated at 37 °C for 90 min. Antibodies against biotin and *O*-GlcNAc were used to examine the success of the β-elimination. Ponceau S was used as loading control. Reprinted (adapted) with permission from Doll et al.[408] Copyright (2016) WILEY-VCH Verlag GmbH & Co. KGaA, Weinheim.

was destroyed under these alkaline conditions, such that the DAinv reaction with Tz-biotin had to occur before the β-elimination. Immunoblotting against *O*-GlcNAc proved the success of the β-elimination, as no antibody staining was present in pH 12 samples (Figure 4.5B). In addition, also the signals of Cyoc-anchored biotin almost completely disappeared at pH 12 stating that incorporated Cyoc derivatives are most likely bound to serine and threonine residues of proteins via an *O*-linkage. As controls, β-elimination experiments were performed with lysates from Ac_4GalNCyoc- and Ac_4ManNCyoc-treated cells. Whereas biotin signals arising from incorporated Ac_4GalNCyoc vanished completely after base treatment, those of Ac_4ManNCyoc-treated samples disappeared only partly (Figure 4.5C). These observations are in line with recent findings proposing that Ac_4GalNCyoc is most likely incorporated into mucin-type *O*-glycans and Ac_4ManNCyoc into sialoglycans,[180–182] which can be *O*-linked to serine and threonine or *N*-linked to asparagine residues.[166]

Based on the observation that Ac_4GlcNCyoc is incorporated enzymatically and is *O*-linked to proteins, the involvement of the glycosyltransferase OGT in the attachment of GlcNCyoc to proteins was studied. To this end, HEK293T cells were transfected with a plasmid encoding EGFP-OGT or an empty vector before adding 100 µM Ac_4GlcNCyoc or DMSO. After 20 h, cells were lysed and labeled with Cy3-Tz. Immunoblotting against EGFP verified the overexpression of EGFP-OGT, which resulted in strongly increased *O*-GlcNAc levels (Figure 4.6A). Importantly, the incorporation of Ac_4GlcNCyoc increased compared to empty vector-transfected samples. Moreover, the highly potent OGT inhibitor $Ac_4$5SGlcNAc was employed (Figure 4.6B).[412] Its presence resulted in reduced incorporation of Ac_4GlcNCyoc in HEK293T cell lysates (Figure 4.6C). In summary, both experiments indicated that OGT is involved in the incorporation of Ac_4GlcNCyoc or GlcNCyoc in the cellular glycome.

Recently, the synthesis and application of a new promising OGT inhibitor, termed OSMI-1 (Figure 4.7A), has been reported by Ortiz-Meoz et al.[413] Compared to $Ac_4$5SGlcNAc, OSMI-1 inhibits *O*-GlcNAcylation less, but more selectively, as $Ac_4$5SGlcNAc has been shown to block glycosyltransferases responsible for the synthesis of mucin-type *O*-glycans, too.[413] Aiming to further substantiate the obtained data, the small molecule inhibitor was synthesized in four steps according to the published procedure.[413] Firstly, possible cytotoxic effects of OSMI-1 were determined with AlamarBlue viability assays. As shown in Figure 4.7B, OSMI-1 strongly reduced cellular viabilities from 25 µM onwards. Already at 50 µM, viabilities were below 50 %. These observations are in accordance with toxicity data obtained for OSMI-1-treated Chinese hamster ovary (CHO) cells.[413] Nevertheless, an OSMI-1 concentration of 50 µM was found to be necessary to reduce cellular *O*-GlcNAc levels notably. HEK293T cells treated with 50 µM OSMI-1 and 100 µM Ac_4GlcNAc or 25 µM, 50 µM, 75 µM, or 100 µM Ac_4GlcNCyoc displayed less *O*-GlcNAcylation than cells not treated with OSMI-1 as detected with an *O*-GlcNAc-specific antibody (Figure 4.7C). Surprisingly, Cy3 signals increased in the presence of OSMI-1 significantly, which demonstrates that even more Ac_4GlcNCyoc is incorporated, if the inhibitor OSMI-1 is used. These results are not in line with other studies demonstrating the functionality of OSMI-1 in several biological studies.[414–417] Possible explanations could be that Ac_4GlcNCyoc is (1) not a substrate of OGT, which would question the OGT-dependent experiments presented above, (2) a substrate of OGT and another yet unknown enzyme, or (3) effects of OSMI-1 are a result

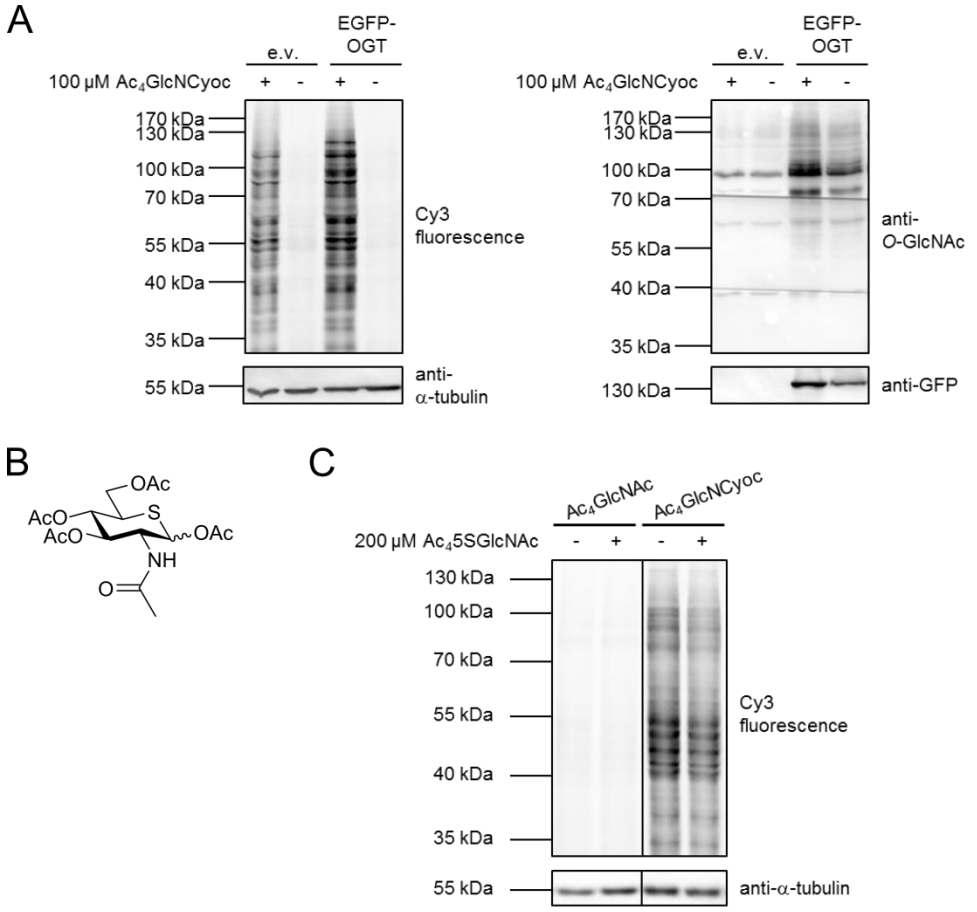

Figure 4.6: Dependence of the incorporation of $Ac_4GlcNCyoc$ on OGT. (A) HEK293T cells were transfected with a plasmid encoding EGFP-OGT or an empty vector (e.v.). After 30 h, cells were treated with 100 µM $Ac_4GlcNCyoc$ (+) or 0.1 V-% DMSO (-) as solvent control for 20 h. Cells were lysed and samples labeled with Cy3-Tz. Fluorescence of Cy3 was read out from the Western blot. Antibodies against *O*-GlcNAc and GFP were used to prove the overexpression of OGT. (B) Chemical structure of $Ac_45SGlcNAc$. (C) Lysates of HEK293T cells were incubated with 100 µM $Ac_4GlcNAc$ or $Ac_4GlcNCyoc$ and 200 µM $Ac_45SGlcNAc$ (+) or DMSO (-) as solvent control at 37 °C for 20 h. The DAinv reaction with Cy3-Tz was performed prior to SDS-PAGE, Western blotting, and fluorescence readout. Equal loading was confirmed by blotting against α-tubulin. Reprinted (adapted) with permission from Doll et al.[408] Copyright (2016) WILEY-VCH Verlag GmbH & Co. KGaA, Weinheim.

of combined toxicities of the $Ac_4GlcNCyoc$ and the inhibitor. To unravel these inconsistencies, studies with other OGT inhibitors, such as the recently presented inhibitors L01 and APNT/APBT,[418,419] alongside with *in vitro* experiments with purified OGT and UDP-GlcNCyoc could be performed. As the synthesis of UDP-GlcNCyoc is complex and challenging and was not in the focus of this thesis, it should be addressed in further studies.

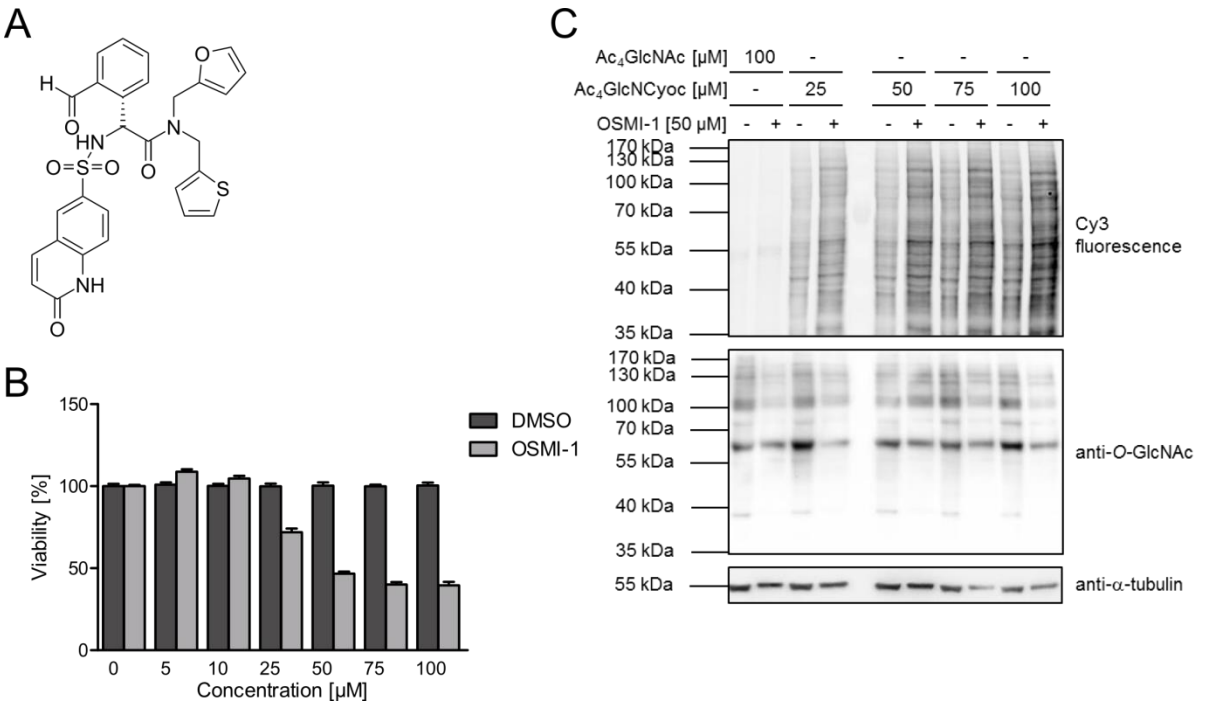

Figure 4.7: Effects of the OGT inhibitor OSMI-1 on the incorporation of Ac_4GlcNCyoc in the cellular glycome. (A) Chemical structure of OSMI-1. (B) Viabilities of HEK293T cells treated with different concentrations of OSMI-1 or 0–0.2 V-% DMSO for 20 h were determined with AlamarBlue assays. Columns represent mean values of three independent experiments with four replicates each and error bars SEMs. (C) HEK293T cells were treated with 100 µM Ac_4GlcNAc or different concentrations of Ac_4GlcNCyoc in the presence of 50 µM OSMI-1 (+) or DMSO (-). Cells were lysed and labeled with Cy3-Tz. Fluorescence of Cy3 was read out from the Western blot. Immunostaining was performed with antibodies against *O*-GlcNAc and α-tubulin.

Finally, the involvement of OGA in the removal of Ac_4GlcNCyoc from proteins was assessed. Until now, OGA is the only glycosidase known to remove *O*-GlcNAc. Many OGA inhibitors have been presented within the last years. Among them, Thiamet G (Figure 4.8A) is one of the most effective and selective ones.[420–423] It did not affect the viability of HEK293T cells, as proven with AlamarBlue assays (Figure 4.8B). Treatment of HEK293T cells with Thiamet G resulted in an increased level of cellular *O*-GlcNAc, which demonstrated the functionality of this OGA inhibitor (Figure 4.8C). To study the removal of Ac_4GlcNCyoc, pulse-chase experiments similar to those reported by Pratt and colleagues[190,194] were performed. For this purpose, HEK293T cells were treated with 100 µM Ac_4GlcNCyoc for 20 h. Subsequently, the cell culture medium was replaced with new one supplemented with 100 µM Ac_4GlcNAc and 10 µM Thiamet G. Control samples did not receive the inhibitor. After indicated time points, cells were lysed, the DAinv reaction with Cy3-Tz was performed, and samples were analyzed by SDS-PAGE and Western blotting. Cy3 fluorescence of control and Thiamet G-treated samples decreased with increasing time (Figure 4.8D). If OGA would be involved in the removal of Cyoc-derivatives attached to proteins, Cy3 signals of Thiamet G-treated samples should decrease slower than those of control samples. However, fluorescence of control and inhibitor-treated samples decreased similarly over time. Thus, the reduced Cy3 fluorescence is most likely not due to OGA, but rather the degradation of Cyoc-modified proteins over time. To confirm this result, HEK293T cells were transfected with a

plasmid encoding OGA. Cellular OGA and *O*-GlcNAc level did not decrease, stating that the overexpression of OGA was not successful (Figure 4.8E). Alterations in the transfection procedure did also not lead to the desired result. If one would like to further investigate a possible role of OGA in the removal of the incorporated Cyoc-derivative, work could be continued with purified OGA and other OGA inhibitors. Within this thesis, Ac_4GlcNCyoc should be employed to image the glycosylation state of individual proteins in cells. Due to the attachment of the bulky Cy3-Tz to Cyoc-residues via a DAinv reaction, it is unlikely that dynamic changes, which would require the involvement of OGA, could be monitored. Therefore, studies on OGA were not continued.

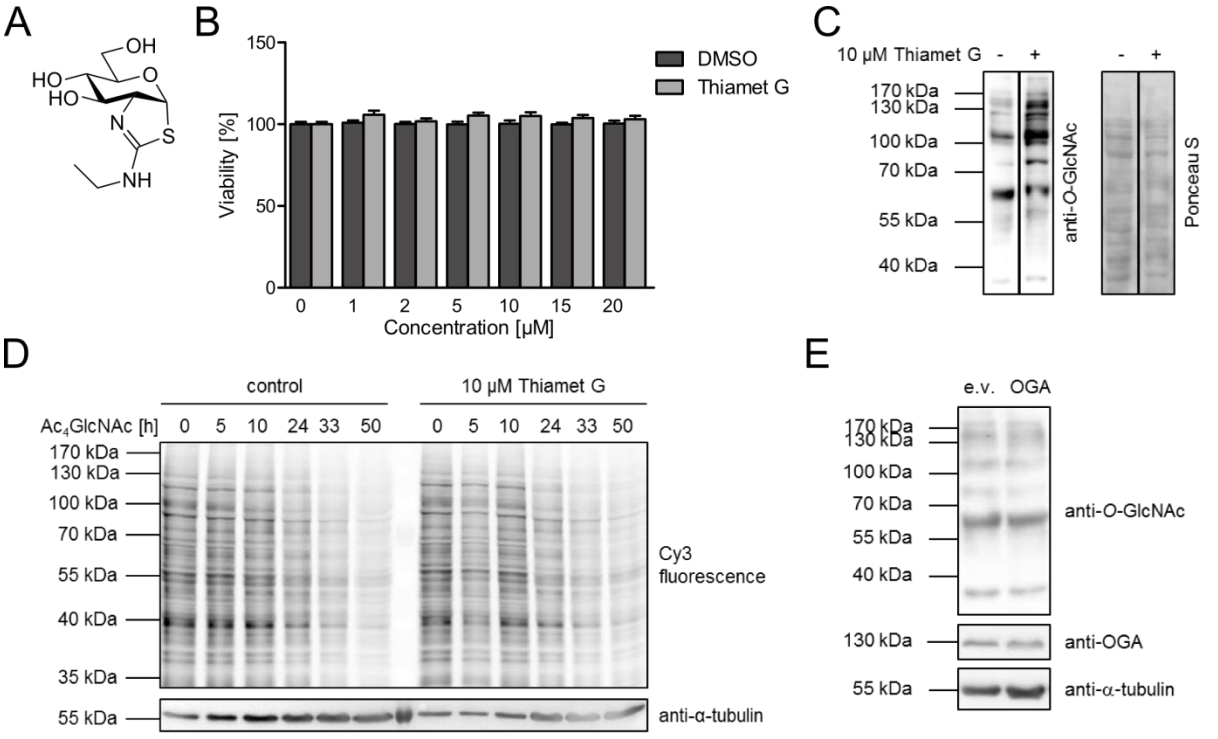

Figure 4.8: Involvement of OGA in the degradation of incorporated GlcNCyoc. (A) Chemical structure of Thiamet G. (B) Viabilities of HEK293T cells treated with different concentrations of Thiamet G or 0-0.2 V-% DMSO for 20 h were determined with AlamarBlue assays. Columns represent mean values of three independent experiments with four replicates each and error bars SEMs. (C) HEK293T cells were treated with 10 µM Thiamet G for 20 h, lysed, and cellular *O*-GlcNAc levels were detected with an anti-*O*-GlcNAc antibody. Ponceau S was used as loading control. (D) HEK293T cells were treated with 100 µM Ac_4GlcNCyoc for 20 h, washed twice with Dulbecco's phosphate buffered saline (DPBS), and fresh medium supplemented with 100 µM Ac_4GlcNAc and 10 µM Thiamet G was added. Control samples did not receive the inhibitor. Cells were lysed at different time points and labeled with Cy3-Tz. Fluorescence was read out from the Western blot in order to detect the chemical reporter still attached to proteins. An antibody against α-tubulin was used to confirm equal loading of samples. (E) HEK29T cells were transfected with an empty vector (e.v.) or a plasmid encoding OGA. After 48 h, cells were lysed. Cellular OGA and *O*-GlcNAc levels were detected with suitable antibodies.

Taken together, the results obtained in this chapter indicate that Ac_4GlcNCyoc is enzymatically incorporated as *O*-GlcNAc. This process is, at least to some extent, catalyzed by OGT. An involvement of OGA in the removal of incorporated Cyoc-derivatives was not detected.

4.1.2. Protein-Specific Imaging of Glycosylation

The development of an approach for protein-specific imaging of intracellular glycosylation was based on previous reports on the detection of protein-specific glycosylation of membrane proteins.[387–389] All of them used CuAAC chemistry, which prevents applications in living cells. The selected experimental strategy is shown in Figure 4.9 and relies on non-toxic Diels-Alder chemistry. The chemical reporter Ac_4GlcNCyoc was used, which diffuses into cells expressing an EGFP-tagged POI. Once present in cells, the monosaccharide is assumed to be rapidly deacetylated by non-specifically acting esterases. Subsequently, it is metabolized by cellular enzymes and attached to many proteins. In a second step, a fluorophore-functionalized tetrazine derivate can react with the cyclopropene moiety in a DAinv reaction. If the POI itself is modified with GlcNCyoc, EGFP gets in close proximity to the glycosylation-anchored acceptor fluorophore. This proximity can be detected by measuring FRET, which can be read out even in presence of a large excess of acceptor fluorophores via the fluorescence lifetime of the donor EGFP.

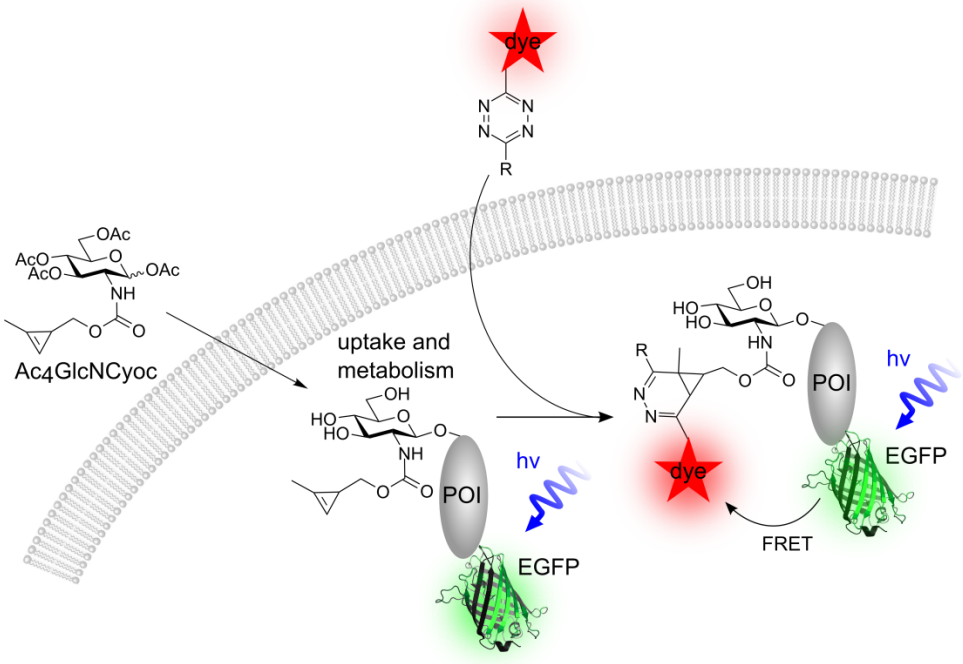

Figure 4.9: Experimental strategy for in cell imaging of protein-specific glycosylation. Reprinted (adapted) with permission from Doll et al.[408] Copyright (2016) WILEY-VCH Verlag GmbH & Co. KGaA, Weinheim.

In order to enable the DAinv reaction inside living cells, the tetrazine functionalized fluorophore needs to be cell permeable. Cy3-Tz entered cells neither by diffusion nor could it be homogenously introduced by electroporation (Figure 4.10A+B). Microinjection allowed for the delivery of Cy3-Tz into cells, but it is impossible to microinject many cells in a short time period. Thus, the commercially available fluorophore tetramethylrhodamine (TAMRA)-Tz was used (Figure 4.10C). In contrast to Cy3-Tz, it simply diffused into cells

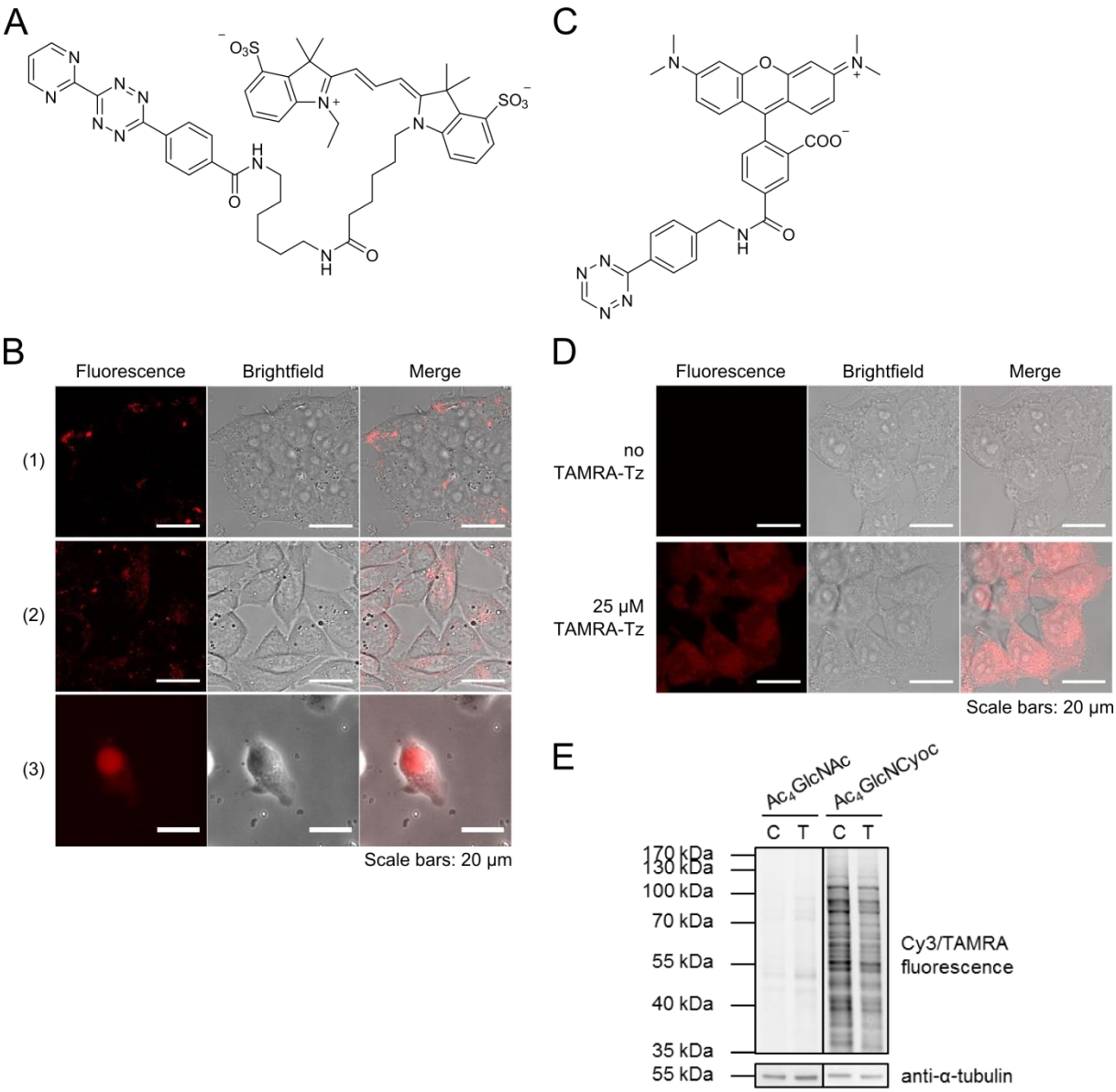

Figure 4.10: Fluorophores for the DAinv reaction. (A) Chemical structure of Cy3-Tz. (B) Confocal fluorescence, brightfield, and merged images of (1) HEK293T cells incubated with 50 µM Cy3-Tz at 37 °C for 45 min, (2) CHO cells electroporated in presence of 50 µM Cy3-Tz, or (3) HEK293T cells microinjected with a solution of 50 µM Cy3-Tz in phosphate buffered saline (PBS) are displayed. (C) Chemical structure of TAMRA-Tz. (D) Representative confocal fluorescence, brightfield, and merged images of HEK293T cells incubated without or with 25 µM TAMRA-Tz at 37 °C for 60 min and subsequently fixed are depicted. (E) HEK293T cells were treated with 100 µM Ac_4GlcNCyoc or Ac_4GlcNAc for 20 h, lysed, and labeled with 10 µM Cy3-Tz (C) or 10 µM TAMRA-Tz (T) for 90 min. Fluorescence of the respective fluorophore was read out from membranes. Equal loading of samples was verified with immunoblotting against α-tubulin. Reprinted (adapted) with permission from Doll et al.[408] Copyright (2016) WILEY-VCH Verlag GmbH & Co. KGaA, Weinheim.

(Figure 4.10D). Lysates of Ac_4GlcNCyoc-treated HEK293T cells showed similar patterns of fluorescent bands on Western blots for both fluorophores, although the recorded fluorescence of TAMRA-Tz was less intense (Figure 4.10E). Moreover, the fluorescence background of lysates from Ac_4GlcNAc-treated HEK293T cells labeled with Cy3-Tz or TAMRA-Tz was

slightly stronger for the latter dye. Hence, it was decided to continue using Cy3-Tz for lysate experiments and to employ TAMRA-Tz only for live cell imaging.
Next, possible cytotoxic effects of TAMRA-Tz were elucidated. To this end, HEK293T cells were treated with up to 30 µM TAMRA-Tz at 37 °C for 60 min. DMSO was used as solvent control. Viabilities were obtained with ATP assays, which demonstrated that TAMRA-Tz is not cytotoxic within the concentration range tested (Figure 4.11). Standard AlamarBlue-based viability assays could not be performed for two reasons. Firstly, the readout of an AlamarBlue assay is based on the fluorescence of resorufin, which spectrally overlaps with the fluorescence emission of TAMRA. In an ATP assay, chemiluminescence is generated without the need for excitation. Thus, it should not be disturbed by the presence of the fluorophore TAMRA. Secondly, the AlamarBlue assay follows the treatment with the compound of interest and takes approximately 90 min. If one is interested in time spans as short as 60 min, additional 90 min would alter the result. In contrast, cells are lysed at the beginning of an ATP assay, which allows drawing conclusions on defined incubation times.

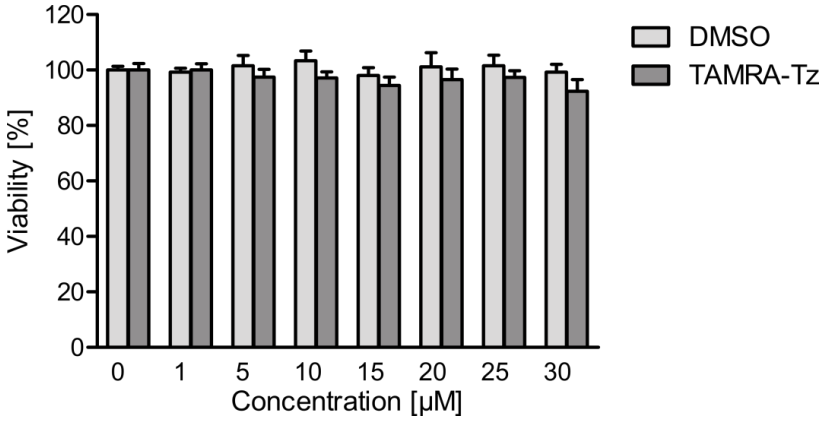

Figure 4.11: Effect of TAMRA-Tz on cellular viabilities. HEK293T cells were treated with up to 30 µM TAMRA-Tz or 0.2 V-% DMSO at 37 °C for 60 min. Cellular viabilities were assessed with an ATP-assay. Columns represent mean values and error bars SEMs. Experiments were performed three times in quadruplicates. Reprinted with permission from Doll et al.[408] Copyright (2016) WILEY-VCH Verlag GmbH & Co. KGaA, Weinheim.

The model protein used to establish the protein-specific approach was the glycosyltransferase OGT. It is present in the cytoplasm and the nucleus and is known to *O*-GlcNAcylate itself at serine 3 and serine 4.[424,425] Further glycosylation sites and types have not been reported for OGT. Firstly, the modification of OGT using Ac_4GlcNCyoc needed to be ensured. For this purpose, HEK293T cells were transfected with plasmids encoding EGFP-OGT or EGFP. The latter served as non-glycosylated control. One day after transfection, cells were treated with 100 µM Ac_4GlcNCyoc or Ac_4GlcNAc for 20 h. Cells were lysed and EGFP as well as EGFP-OGT were isolated by immunoprecipitation with anti-GFP antibodies. Samples were labeled with Cy3-Tz and subjected to SDS-PAGE and Western blotting. A strong fluorescence band was detected for EGFP-OGT samples treated with Ac_4GlcNCyoc at 130 kDa, which corresponds to the size of the fusion protein EGFP-OGT (Figure 4.12A). No fluorescence band was present for the Ac_4GlcNAc-treated EGFP-OGT sample demonstrating the selective labeling of the Cyoc-derivative attached to EGFP-OGT by the DAinv reaction. As

Ac_4GlcNCyoc-treated EGFP samples displayed no Cy3 fluorescence, it can be concluded that solely OGT and not its fusion partner EGFP was modified with the chemical reporter. Consequently, EGFP can be used as negative control in all further experiments.
Having demonstrated the utilization of Ac_4GlcNCyoc for monitoring the glycosylation state of individual proteins isolated from cell lysates, the next step was to transfer this technique to the imaging of living cells by using FLIM-FRET microscopy. Most FLIM-FRET and acceptor photobleaching experiments presented in this chapter were performed and evaluated together with Dr. Annette S. Indlekofer (group of Prof. Dr. Zumbusch, University of Konstanz).[320] EGFP-OGT- or EGFP- expressing cells were treated with 50 µM or 100 µM Ac_4GlcNCyoc or Ac_4GlcNAc for 20 h. Then, cells were labeled with TAMRA-Tz for 60 min. FLIM-FRET microscopy was performed immediately. Representative fluorescence lifetime images are shown in Figure 4.12B. In all fluorescence lifetime images displayed in this thesis, the pixel color corresponds to the fluorescence lifetime and the pixel brightness to the detected fluorescence intensity. For both concentrations used, fluorescence lifetimes of EGFP-OGT in Ac_4GlcNCyoc-treated cells were much shorter than those measured for Ac_4GlcNAc-treated cells, indicating successful FRET. Reductions in fluorescence lifetimes were also detected for EGFP, but to a lesser extent. As EGFP was not modified with Ac_4GlcNCyoc, shorter fluorescence lifetimes for EGFP must be due to unspecific FRET to TAMRA-Tz attached to nearby Cyoc-modified proteins. Interestingly, fluorescence lifetimes of EGFP-OGT and EGFP itself are different even in Ac_4GlcNAc-treated cells, likely as a result of two effects. Firstly, fluorescence lifetimes are sensitive to the local environment of a fluorophore, since they are affected by viscosity, oxygen and ion concentrations, temperature, and pH values.[293,345] The fusion of EGFP and OGT could lead to such a changed local environment. Secondly, the unspecific labeling of proteins with TAMRA-Tz gives rise to background FRET that is present in both Ac_4GlcNAc- and Ac_4GlcNCyoc-treated samples. This background could be different in close proximity to EGFP or EGFP-OGT. To determine solely FRET arising from TAMRA linked to Ac_4GlcNCyoc, average fluorescence lifetimes of Ac_4GlcNCyoc-treated and Ac_4GlcNAc-treated cells were used to calculate FRET efficiencies. Within cellular samples, fluorophores are not present in a one to one stoichiometry and fluorescence lifetimes are averaged and include values of modified and unmodified proteins. Thus, all FRET efficiencies presented in this thesis are apparent values. FRET efficiencies were determined to be 16 % and 30 % for EGFP-OGT and 6 % and 10 % for EGFP at sugar concentrations of 50 µM and 100 µM, respectively (Figure 4.12C). Since EGFP is not modified with Ac_4GlcNCyoc, FRET efficiencies of EGFP-OGT were compared with those of EGFP. Significant differences were found. Therefore, the here presented approach can be used to detect the glycosylation of a specific protein in living cells by intramolecular FRET over intermolecular FRET to nearby glycosylated proteins. It has to be mentioned that FRET from an EGFP-tagged protein to its glycosylated interaction partner in close proximity cannot be excluded.

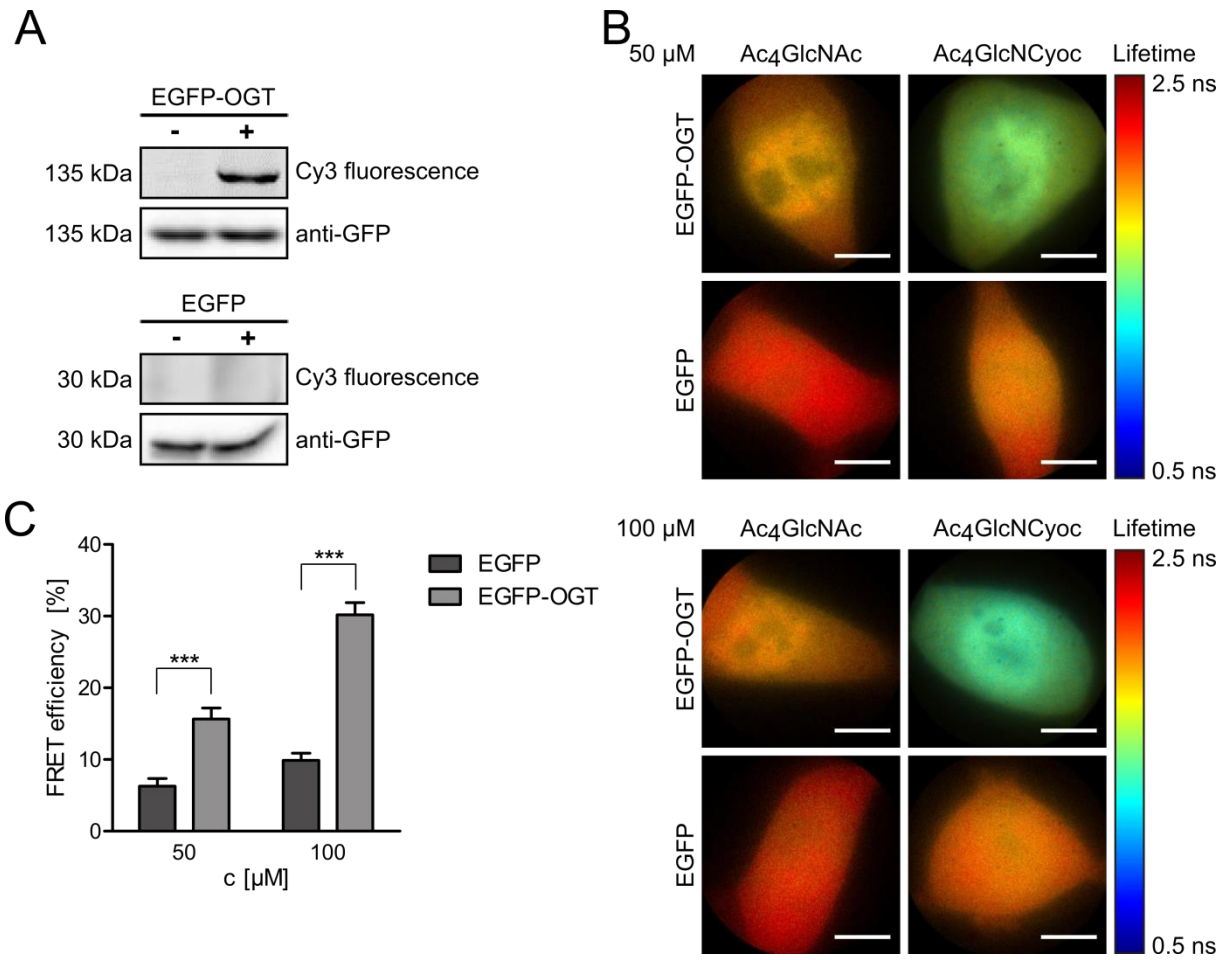

Figure 4.12: Visualization of OGT's glycosylation in living cells. HEK293T cells were transfected with plasmids encoding EGFP-OGT or EGFP. (A) Cells were treated with 100 µM $Ac_4GlcNAc$ (-) or $Ac_4GlcNCyoc$ (+) for 20 h, lysed, EGFP-OGT and EGFP were immunoprecipitated, and labeled with 10 µM Cy3-Tz at 25 °C for 90 min. Fluorescence of Cy3 was read out from Western blots to investigate the modifications state of immunoprecipitated proteins. Amounts of blotted proteins were determined with an anti-GFP antibody. (B) Cells were treated with 50 µM or 100 µM $Ac_4GlcNAc$ or $Ac_4GlcNCyoc$ for 20 h and labeled with 25 µM TAMRA-Tz at 37 °C for 60 min. Representative fluorescence modulation lifetime images of EGFP-OGT and EGFP expressing, living cells are displayed. Scale bars correspond to 10 µm. (C) FRET efficiencies were calculated from fluorescence modulation lifetimes averaged over three independent experiments with five cells each for $Ac_4GlcNCyoc$ concentrations of 50 µM and 100 µM. Statistical significance was assessed with a two-way analysis of variances (ANOVA) and a Bonferroni posttest. The degree of significance is *** $p<0.001$. Reprinted (adapted) with permission from Doll et al.[408] Copyright (2016) WILEY-VCH Verlag GmbH & Co. KGaA, Weinheim.

The presence of the acceptor fluorophore TAMRA in cells is necessary for the generation of glycosylation-specific FRET, but its unspecific attachment to proteins also results in background FRET. Thus, an optimal concentration of TAMRA-Tz allowing for the detection of protein-specific FRET over background FRET needs to be chosen. HEK293T cells expressing EGFP or EGFP-OGT were treated with 100 µM $Ac_4GlcNCyoc$ and incubated with different concentrations of TAMRA-Tz for 60 min. With increasing TAMRA-Tz concentration, fluorescence lifetimes of both EGFP and EGFP-OGT decreased (Figure 4.13). From 5 µM TAMRA-Tz onwards, calculated FRET efficiencies were significantly higher for EGFP-OGT compared to EGFP. Highest EGFP-OGT FRET efficiencies were achieved with

15 µM to 30 µM TAMRA-Tz. As FRET efficiencies of EGFP and EGFP-OGT did not vary too much within this concentration range, 25 µM were used for the following experiments.

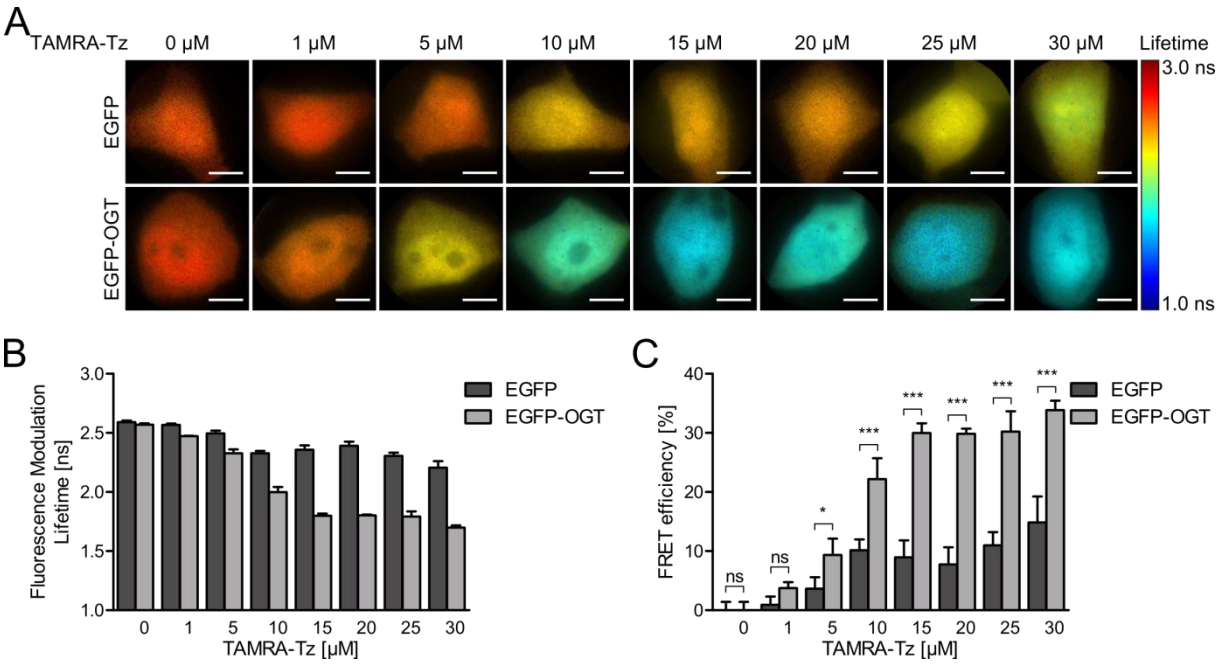

Figure 4.13: Influence of an increasing TAMRA-Tz concentration on FRET efficiencies. HEK293T cells were transfected with expression vectors encoding EGFP or EGFP-OGT and treated with 100 µM Ac_4GlcNCyoc for 20 h. The DAinv reaction in living cells was performed with different concentrations of TAMRA-Tz for 60 min. (A) Representative fluorescence modulation lifetime images are depicted. Scale bars correspond to 10 µm. (B) Fluorescence modulation lifetimes were averaged over four cells and are presented as columns. Error bars represent SEMs. (C) FRET efficiencies were calculated from averaged fluorescence modulation lifetimes. Error bars are SEMs. Degrees of statistical significances were determined with a one-way ANOVA and a Bonferroni posttest and are ns (not significant) $p>0.05$, * $p<0.05$, and *** $p<0.001$. Reprinted (adapted) with permission from Doll et al.[355] Copyright (2018) Elsevier Inc.

To substantiate the FLIM-FRET data of OGT, FRET measurements were repeated with acceptor photobleaching. For this purpose, EGFP- or EGFP-OGT-transfected HEK293T cells were treated with 100 µM Ac_4GlcNCyoc or DMSO for 20 h. Subsequently, cells were fixed to avoid the diffusion of fluorescently tagged probes in cells that would affect measurements. After permeabilization, cells were labeled with 10 µM Cy3-Tz for 60 min. Apparent FRET efficiencies obtained from acceptor photobleaching experiments were in good agreement with values from FLIM-FRET experiments (Figure 4.14). Thus, both methods can be employed to image protein-specific glycosylation in living or fixed cells.

To assess the general applicability of the established approach and verify that overexpression of EGFP-OGT, which slightly increased the incorporation of Ac_4GlcNCyoc (Figure 4.6A), is not responsible and mandatory for the detection of FRET efficiencies higher than those of EGFP, five additional EGFP-fusion proteins, besides OGT, were examined: vinculin, the calcium/calmodulin-dependent protein kinase type IV (CAMK4), the tumor suppressor p53, the forkhead box protein O1 (Foxo1), and the kinase Akt1. The only reported glycosylation

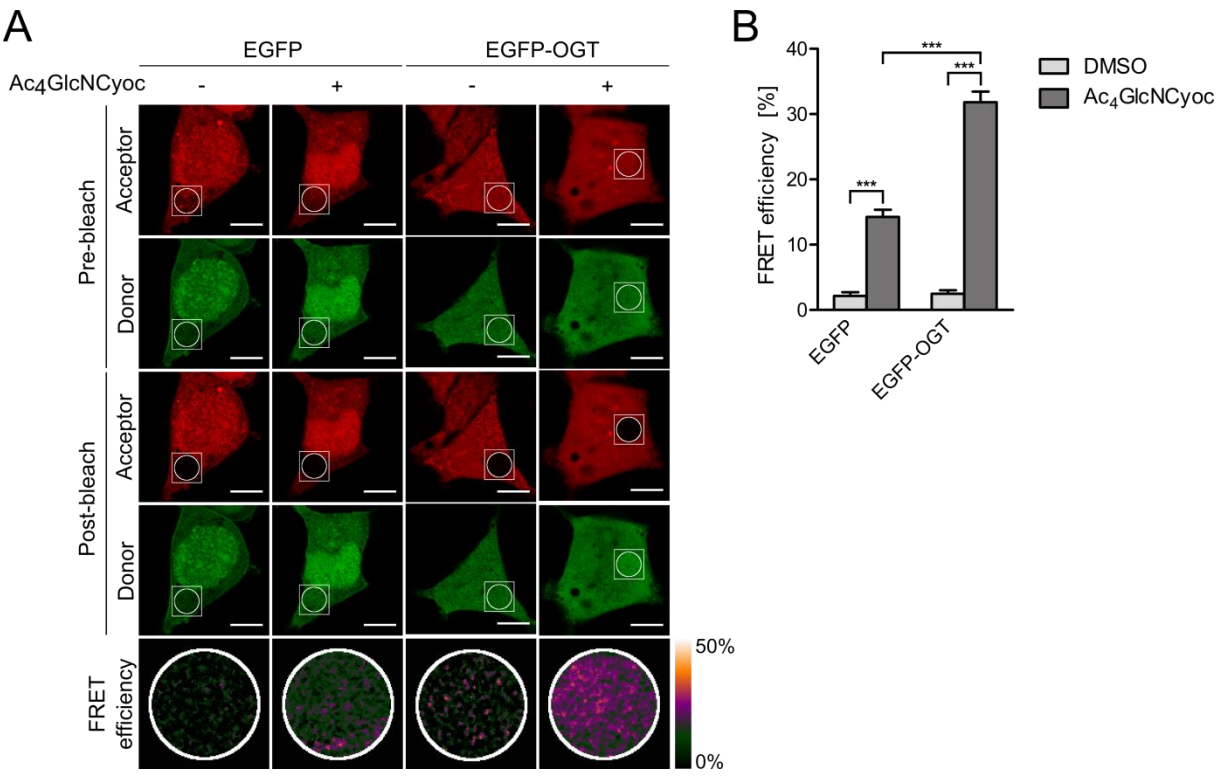

Figure 4.14: Acceptor photobleaching experiments validate FLIM-FRET data. HEK293T cells were transfected with vectors encoding EGFP or EGFP-OGT and treated with 100 µM Ac_4GlcNCyoc (+) or 0.1 V-% DMSO (-) for 18-20 h. Cells were fixed, permeabilized, and labeled with 10 µM Cy3-Tz for 60 min before performing acceptor photobleaching. (A) Representative confocal fluorescence images of donor and acceptor fluorophores before and after bleaching the acceptor are depicted. FRET efficiencies were color-coded and are shown in the lowest panel. Scale bars correspond to 10 µm. (B) FRET efficiencies were calculated for EGFP and EGFP-OGT from three independent experiments with five cells each. Columns show mean values and error bars SEMs. Statistical significances were assessed with a one-way ANOVA and a Tukey-Kramer posttest and are *** $p<0.001$. Reprinted (adapted) with permission from Doll et al.[408] Copyright (2016) WILEY-VCH Verlag GmbH & Co. KGaA, Weinheim.

form for all these proteins is *O*-GlcNAcylation. Their cellular localizations, sizes, known *O*-GlcNAc sites, and functions are summarized in Table 4.1. Initially, all EGFP-fusion proteins were immunoprecipitated from HEK293T cells, which had been transfected with the corresponding construct and treated with Ac_4GlcNCyoc or Ac_4GlcNAc, and were labeled with 10 µM Cy3-Tz. All proteins, except EGFP-vinculin, displayed Cy3 fluorescence bands on Western blots conforming their modification with the glycosylation reporter (Figure 4.15A). Although vinculin has been reported to be *O*-GlcNAcylated,[38,426] no modification with GlcNCyoc could be detected. This might be due to a very low extent of vinculin *O*-GlcNAcylation or the usage of an artificial monosaccharide, which does not need to behave as the native substrate. Next, FLIM microscopy of samples treated with 50 µM or 100 µM of monosaccharides and incubated with 25 µM TAMRA-Tz was performed. Representative fluorescence lifetime images showed the presence of EGFP-vinculin and Foxo1-EGFP in the cytoplasm, CAMK4-EGFP and Akt1-EGFP in the whole cell, and p53 solely in the nucleus (Figure 4.15B). The transcription factor Foxo1 is known to shuttle between the cytoplasm and the nucleus.[427] Indeed, also cells with nuclear accumulated Foxo1 were found, but they

Table 4.1: Information on localizations, sizes, *O*-GlcNAc sites, and functions of EGFP-fusion proteins, whose glycosylation states were examined within this thesis. The localization can be nuclear (N), cytoplasmic (C), or membranous (M). Proteins are either N-terminally (NT) or C-terminally (CT) tagged with EGFP. Reprinted (adapted) with permission from Doll et al.[408] Copyright (2016) WILEY-VCH Verlag GmbH & Co. KGaA, Weinheim.

Protein	Localization	Number of amino acids	*O*-GlcNAc sites	EGFP tag	Function
OGT	N+C[424]	1046	(S3, S4)[425]	NT	*O*-linked *N*-acetylglucosamine (GlcNAc) transferase[46]
Vinculin	C[428]	1134	sites unknown[38,426]	NT	cytoplasmic actin-binding protein[429]
CAMK4	C+N[430]	473	(T57/S58, S137, S189, S344/S345, S356)[431]	CT	member of the calcium-calmodulin-dependent protein kinase signaling cascade; regulator of several transcription activators in immune response, inflammation, and memory consolidation[432]
p53	N[433]	393	S149[65,434]	CT	tumor suppressor; regulator of cell cycle and apoptosis[435]
Foxo1	(N+)C[436]	655	(T317, S550, T648, S654)[437], S333[438], T646[439]	CT	transcription factor; main target of insulin signaling; regulates metabolic homeostasis in response to oxidative stress[440]
Akt1	C+N+M[441]	480	(S126, S129, T305, S312)[442], S473[443]	NT or CT	serine/threonine kinase; regulator of glucose metabolism, cell proliferation, apoptosis, transcription, and cell migration[444]

exhibited much higher fluorescence intensities. In order to allow for comparisons, only cells with cytoplasmic Foxo1-EGFP were measured. Notably, decreases of fluorescence lifetimes were visible for p53, Foxo1, and Akt1, which were even stronger, if concentrations of 100 µM were used. FRET efficiencies were calculated for all EGFP-fusion proteins and both sugar concentrations from averaged fluorescence lifetimes. Those of p53-EGFP, Foxo1-EGFP, and Akt1-EGFP were significantly larger than the FRET efficiency of the control EGFP, which was also the case for measurements with less cytotoxic 50 µM Ac_4GlcNCyoc (Figure 4.15C). Despite the fact that CAMK4-EGFP was found to be strongly modified with Ac_4GlcNCyoc, no significant FRET efficiencies were detected for this protein. This might be due to the fact that its *O*-GlcNAc sites are located at the N-terminus or in the middle of the protein.[431] As the EGFP-tag was attached at the C-terminus and efficient FRET requires a close proximity of both the donor EGFP and the glycosylation-anchored acceptor fluorophore, glycosylation sites might have been too far away to be imaged via this approach.

Whereas fluorescence lifetime values of all other proteins were homogenous throughout single cells indicating that the glycosylation of these proteins does not depend on their cellular localization, those of Akt1-EGFP appeared to be much shorter in the nucleus than in the

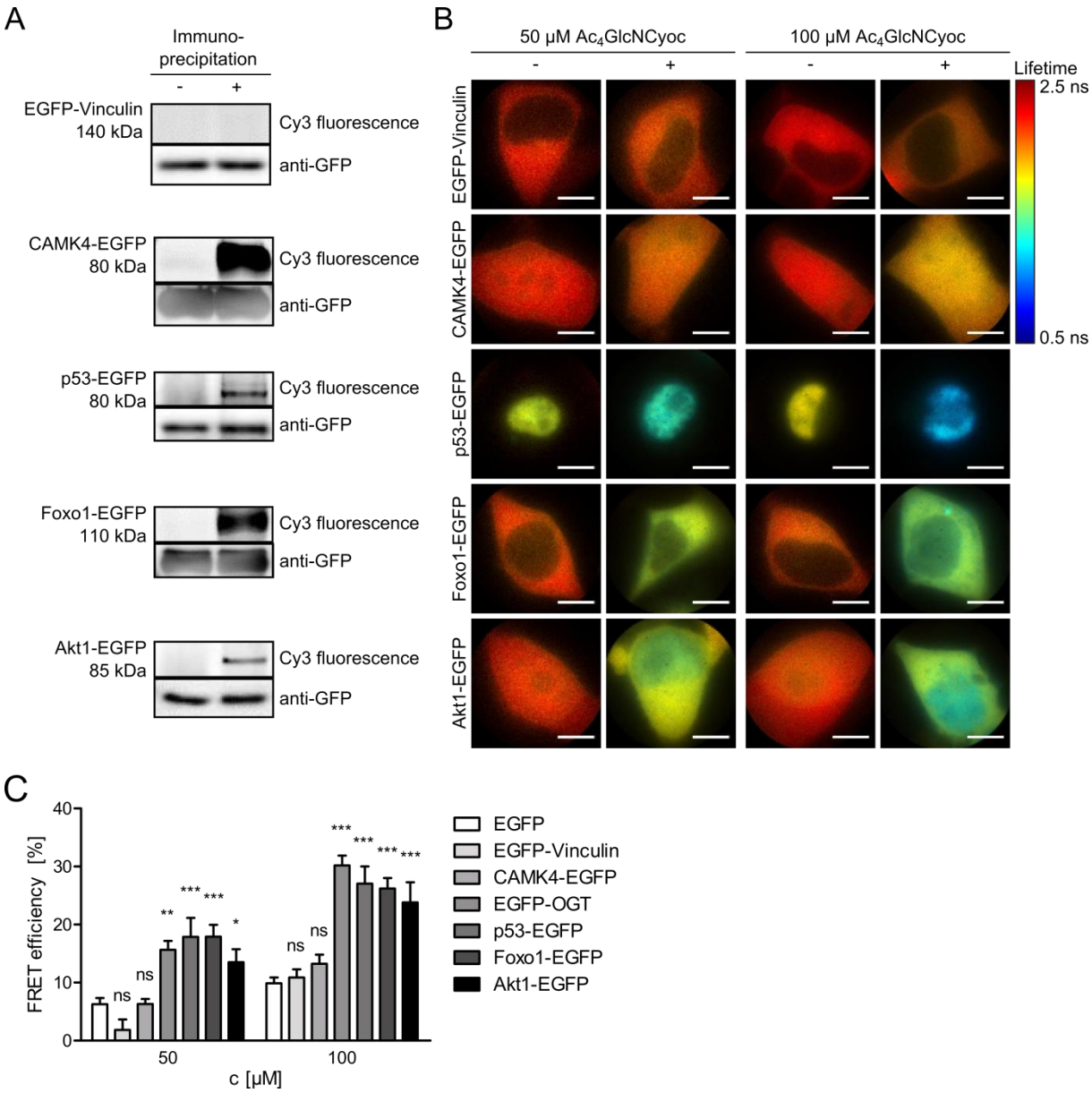

Figure 4.15: Imaging protein-specific glycosylation of further proteins. HEK293T cells were transfected with plasmids encoding various EGFP-fusion proteins. (A) Cells were treated with 100 µM $Ac_4GlcNAc$ (-) or $Ac_4GlcNCyoc$ (+) for 20 h and lysed. EGFP-fusion proteins were immunoprecipitated and the DAinv reaction was carried out with 10 µM Cy3-Tz. Fluorescence of Cy3 was read out from Western blots to assess the modification state of immunoprecipitated proteins. Equal loading of immunoprecipitated proteins was confirmed with immunoblotting against EGFP. (B) Cells were treated with 50 µM or 100 µM $Ac_4GlcNAc$ or $Ac_4GlcNCyoc$ for 20 h and labeled with 25 µM TAMRA-Tz. Representative fluorescence modulation lifetime images are shown. Scale bars correspond to 10 µm. (C) Fluorescence modulation lifetimes averaged over three independent experiments with five cells each were used to calculate FRET efficiencies for $Ac_4GlcNCyoc$ concentrations of 50 µM and 100 µM. Statistical significances compared to EGFP were determined with a two-way ANOVA and a Bonferroni posttest. Degrees of significances are ns $p>0.05$, * $p<0.05$, ** $p<0.01$, and *** $p<0.001$. Reprinted (adapted) with permission from Doll et al.[408] Copyright (2016) WILEY-VCH Verlag GmbH & Co. KGaA, Weinheim.

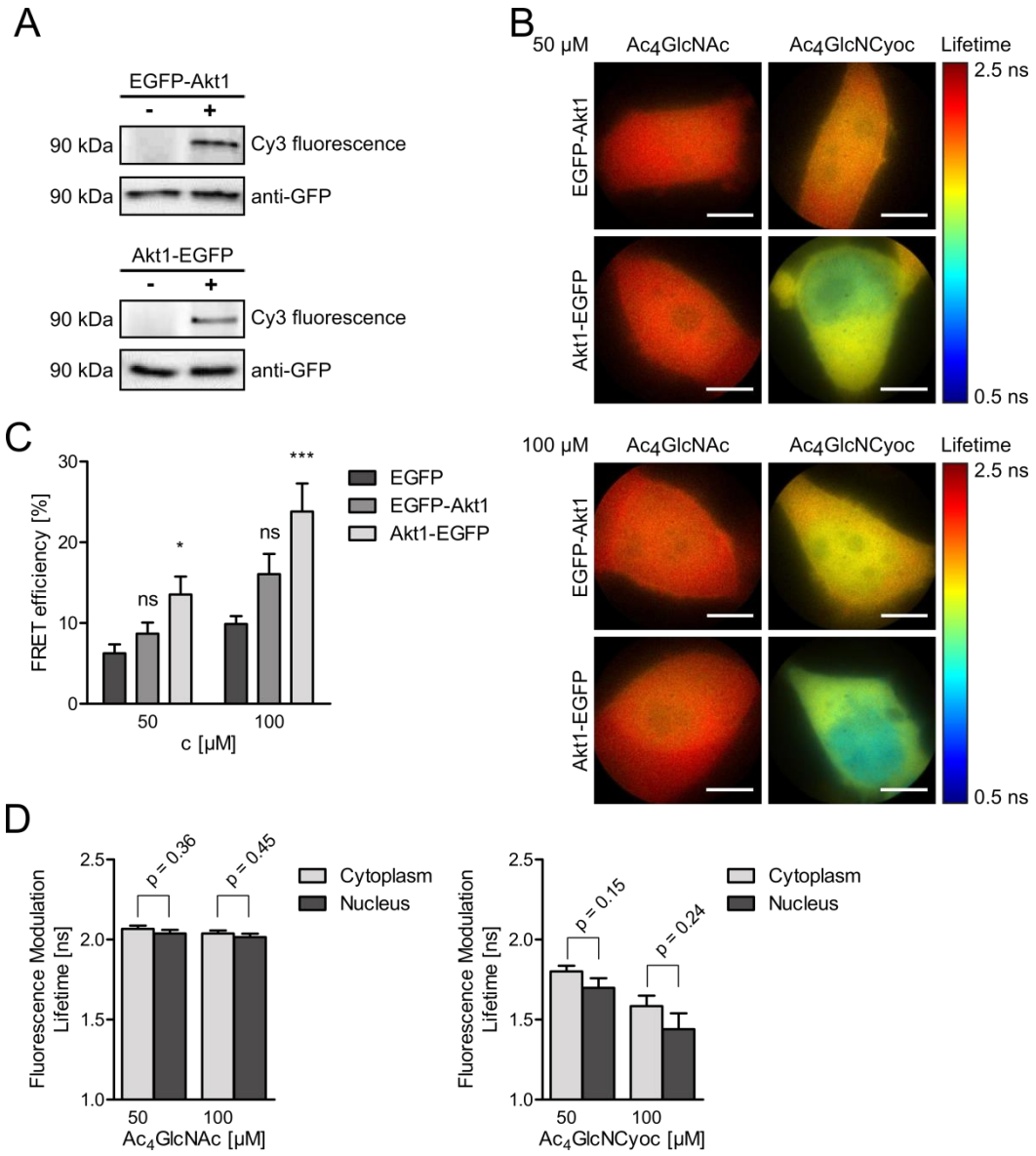

Figure 4.16: Comparison of N- and C-terminally EGFP-tagged Akt1. HEK29T cells were transfected with plasmids encoding EGFP-Akt1 or Akt1-EGFP. (A) Cells were treated with 100 µM $Ac_4GlcNAc$ or $Ac_4GlcNCyoc$ for 20 h, lysed, EGFP-Akt1 and Akt1-EGFP were isolated by immunoprecipitation, and the DAinv reaction with 10 µM Cy3-Tz was performed. Fluorescence was read out from Western blots to assess the modification state of Akt1 proteins. Equal loading was confirmed by immunoblotting against EGFP. (B) Cells were treated with 50 µM or 100 µM $Ac_4GlcNCyoc$, labeled with 25 µM TAMRA-Tz, and used for FLIM-FRET microscopy. Representative fluorescence modulation lifetimes images are depicted. Scale bars correspond to 10 µm. (C) FRET efficiencies were calculated from fluorescence modulation lifetimes averaged over three independent experiments with five cells each. Columns represent mean FRET efficiencies and error bars SEMs. Statistical significance compared to EGFP was assessed with a two-way ANOVA and a Bonferroni posttest. Degrees of significances are ns $p>0.05$, * $p<0.05$, and *** $p<0.001$. (D) Fluorescence modulation lifetimes were measured in the cytoplasm and nucleus of Akt1-EGFP expressing cells separately. Localizations of cytoplasm and nuclei were determined based on the fluorescence intensity and fluorescence lifetime of Akt1-EGFP. Columns belong to means and error bars to SEMs. P-values were calculated with two-tailed t-tests of unpaired observations. Reprinted (adapted) with permission from Doll et al.[408] Copyright (2016) WILEY-VCH Verlag GmbH & Co. KGaA, Weinheim and Doll et al.[355] Copyright (2018) Elsevier Inc.

cytoplasm. The N-terminally tagged EGFP-Akt1 was also found to be modified with Ac_4GlcNCyoc, but did not exhibit FRET efficiencies significantly different from those of EGFP (Figure 4.16A-C). Most probably, donor and acceptor fluorophores are again too far apart from each other. In addition, its fluorescence lifetimes did not vary as much as those of Akt1-EGFP within single cells. Fluorescence lifetimes of nuclear and cytoplasmic Akt1-EGFP were determined and analyzed separately. Those of nuclear Akt1-EGFP were indeed shorted than cytoplasmic lifetimes in Ac_4GlcNCyoc-treated cells (Figure 4.16D). Although differences in nuclear and cytoplasmic fluorescence lifetimes were obvious in several cells, not all cells showed differences in lifetimes, which might explain why fluorescence lifetimes were not significantly different. Nevertheless, these findings imply that Akt1 is stronger *O*-GlcNAcylated if present in the nucleus, which is in line with reports suggesting a role of Akt1's *O*-GlcNAcylation in its nuclear localization.[441]

FLIM-FRET measurements of vinculin, CAMK4, p53, Foxo1, and Akt1 clearly demonstrated the general applicability of the established approach. It not only allows imaging the glycosylation state of a selected protein inside living cells, but also to determine spatial differences in the glycosylation of a protein. The two fusion proteins EGFP-vinculin and CAMK4-EGFP did not own FRET efficiencies significantly greater than those measured for EGFP and thus further indicate that unspecific and intermolecular FRET do not hinder measurements of protein-specific glycosylation by FLIM-FRET microscopy.[408]

In summary, the first functional and general applicable approach for imaging protein-specific glycosylation inside living cells was established. In the following, it was employed to study the *O*-GlcNAcylation of the proteins Kif18A, α-synuclein, and β-catenin in more detail.

4.1.3. *O*-GlcNAcylation of Kif18A

The human kinesin-8 Kif18A is a microtubule-associated motor protein.[445] It accumulates at plus ends of microtubules in mitosis and acts as microtubule depolymerase.[446–448] Furthermore, Kif18A suppresses chromosome oscillatory movements, which occur upon congression of chromosomes around the spindle equator in metaphase and decline towards anaphase.[449,450] Such oscillations of chromosomes attached to microtubules via kinetochores protect chromosomes against damage and entanglements, but need to be terminated in order to enable the progression of mitosis.[451,452] HeLa cells lacking Kif18A have been shown to be unable to enter mitosis, because its depletion prevents a correct chromosome congression.[446,449,450] Moreover, elevated expression of Kif18A has been found to be associated with an increased risk for multiple myeloma and enhanced cell proliferation in other cancer types.[453–456]

It has been suggested that both the function and the localization of Kif18A are regulated by its PTMs, such as phosphorylation and *O*-GlcNAcylation.[457] Phosphorylation of serine 674 and serine 684 by cycline-dependent kinase 1 in early metaphase has been demonstrated to promote chromosome oscillations, while its dephosphorylation in late metaphase by protein phosphatase 1 results in metaphase plate thinning and suppressed chromosome oscillations.[452] In addition, Kif18A's *O*-GlcNAcylation has been detected with an *O*-GlcNAc-specific antibody in bone marrow stromal cells.[457] Recently, also sumoylation of Kif18A has been shown to regulate the activity of Kif18A during mitotic progression.[458]

Protein phosphorylation and *O*-GlcNAcylation are known to compete for the same or adjacent serine and threonine residues in a dynamic manner.[47,459] This could also be the case for Kif18A. Within this thesis, the modification of Kif18A with *O*-GlcNAc should be detected using Ac_4GlcNCyoc.

To be able to perform FLIM-FRET experiments later, HeLa cells stably expressing EGFP or EGFP-Kif18A under a tetracycline-inducible promotor were used. Firstly, the incorporation of Ac_4GlcNCyoc in EGFP and EGFP-Kif18A HeLa cell lines was investigated in a time- and concentration-dependent manner. Cy3 signals resulting from Cyoc-derivatives attached to proteins were highest for incubation times of 22 h and concentrations of ~100 µM Ac_4GlcNCyoc (Figure 4.17). These data are in good agreement with similar experiments performed in HEK293T, HeLa S3, and H1299 cells (Figure 4.3).

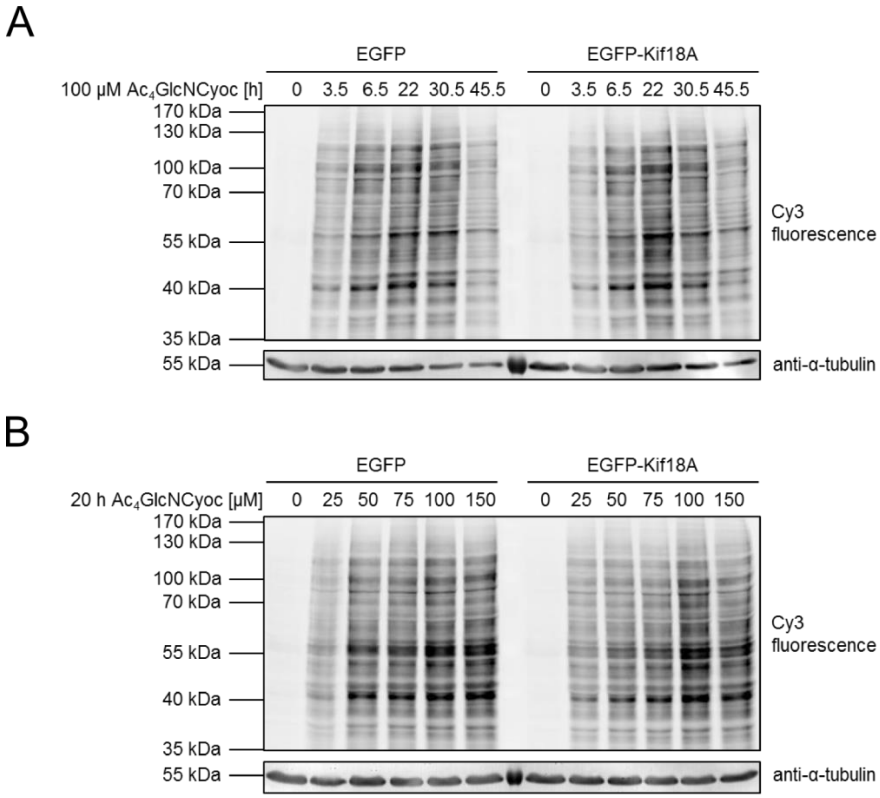

Figure 4.17: Incorporation of Ac_4GlcNCyoc in stable HeLa cell lines. HeLa cells capable of expressing EGFP or EGFP-Kif18A were (A) treated with 100 µM Ac_4GlcNCyoc for different periods of time or (B) treated with different concentrations of Ac_4GlcNCyoc for 20 h. Fluorescence readouts of Western blots from lysates of Ac_4GlcNCyoc-treated cells labeled with Cy3-Tz are shown. Equal loading was assessed by immunoblotting against α-tubulin.

As different expression levels were expected for both proteins, tetracycline concentrations had to be adjusted in order to achieve nearly equal amounts of EGFP and EGFP-Kif18A in HeLa cells. Both the expression of EGFP-Kif18A and EGFP could be induced by tetracycline (Figure 4.18A). Whereas high tetracycline concentrations led to only small quantities of EGFP-Kif18A, tenfold lower concentrations resulted in a strong expression of EGFP. Comparable protein levels were achieved with tetracycline concentrations of 2 µg ml^{-1} and 0.01 µg ml^{-1} for EGFP-Kif18A and EGFP, respectively. Cellular levels of EGFP-Kif18A

could be further increased by synchronizing cell cycles. Kif18A is degraded in interphase, but larger amounts of this protein are present in mitosis, where Kif18A is functionally active.[446] EGFP-Kif18A HeLa cells were treated with 2 µg ml^{-1} tetracycline and synchronized in S-phase with thymidine. Approximately 8 h to 10 h after releasing cells from thymidine arrest, they enter mitosis.[446] Samples were taken at different time points after thymidine release. Indeed, amounts of EGFP-Kif18A detected with an anti-GFP antibody increased upon thymidine release (Figure 4.18B).

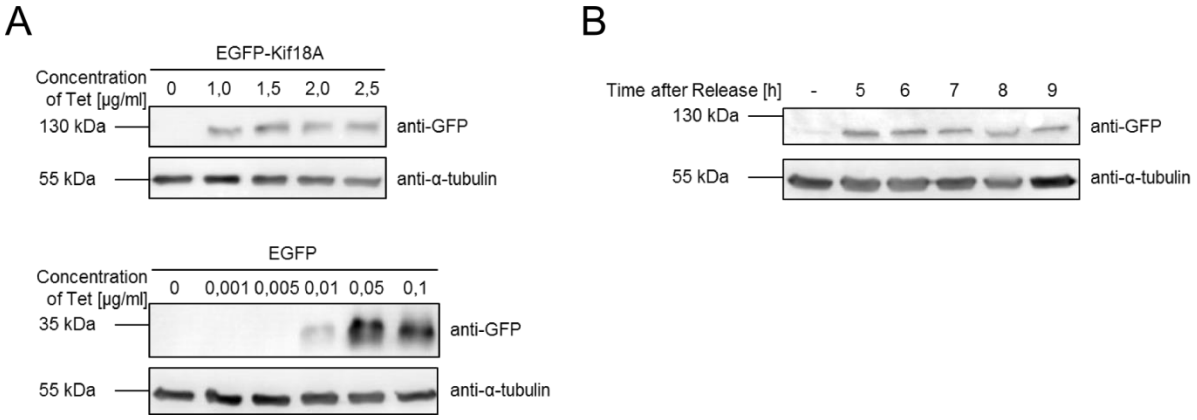

Figure 4.18: Optimizing the expression of EGFP and EGFP-Kif18A. (A) Lysates of HeLa cells treated for 12 h with different concentrations of tetracycline (Tet) were analyzed upon SDS-PAGE by immunoblotting against GFP. (B) EGFP-Kif18A HeLa cells treated with 2 µg ml^{-1} tetracycline and synchronized in S-phase with 2 mM thymidine were released and lysed at indicated time points. Cellular amounts of EGFP-Kif18A were detected with a GFP antibody. Blotting against α-tubulin served as loading control.

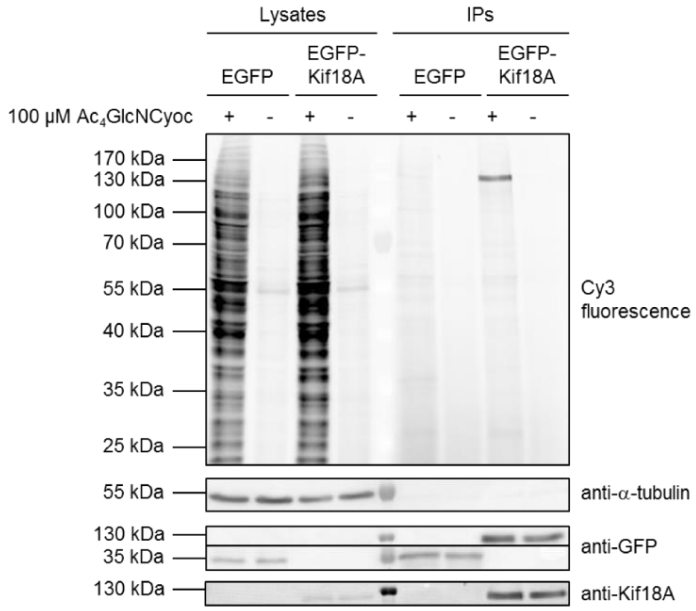

Figure 4.19: Modification of Kif18A with GlcNCyoc. Tetracycline-treated EGFP and EGFP-Kif18A HeLa cells were synchronized in prometaphase by successive treatment with thymidine and nocodazole. Additionally, cells were treated with 100 µM Ac_4GlcNCyoc (+) or 0.1 V-% DMSO (-) for 20 h. The Cy3 fluorescence readout from a blot of lysates and immunoprecipitates performed to isolate EGFP and EGFP-Kif18A is depicted. Antibodies detecting α-tubulin, GFP derivatives, and Kif18A verified equal loading of samples.

To study the modification of Kif18A with Ac_4GlcNCyoc in mitosis, HeLa cells treated with tetracycline were blocked in S-phase with 2 mM thymidine for 20 h and, following a release of 2 h, arrested in prometaphase with 0.15 µg ml^{-1} nocodazole for 16 h. During the second blocking step, 100 µM Ac_4GlcNCyoc were added to the medium for metabolic glycolabeling. After collecting mitotic cells, cells were incubated in fresh medium for 20 min to allow them to enter in metaphase. Upon cell lysis and immunoprecipitation of EGFP and EGFP-Kif18A, the DAinv reaction was performed with Cy3-Tz. Only one strong fluorescence band is visible for all immunoprecipitation samples and belongs to EGFP-Kif18A-expressing cells treated with Ac_4GlcNCyoc (Figure 4.19). Its size at approximately 130 kDa as well as immunoblots against GFP and Kif18A clearly demonstrated that this band corresponds to EGFP-Kif18A modified with Cyoc-anchored Cy3. Hence, the glycosylation of Kif18A with GlcNCyoc was successfully detected. This result substantiates the previous report on the *O*-GlcNAcylation of Kif18A.[457]

Towards characterizing the *O*-GlcNAcylation of Kif18A, next steps would comprise following the *O*-GlcNAcylation of Kif18A over the cell cycle, imaging it by FLIM-FRET microscopy in cells, identifying Kif18A's *O*-GlcNAc sites by mass spectrometry, mutating them, and analyzing the phenotypes of these mutants. This project was and will further be continued by Lisa Haiber within her master's thesis and PhD thesis in the group of Prof. Dr. Wittmann, University of Konstanz.[460]

4.1.4. *O*-GlcNAcylation of α-synuclein

The small protein α-synuclein has been found to be enriched in pre-synaptic neurons in the central nervous system.[461] There, α-synuclein is involved in remodeling and trafficking of vesicles.[462] α-Synuclein mainly exists as intrinsically disordered monomer in the cytoplasm, but, when bound to membranes, it forms a large α-helix that can cause membrane bending.[463–465] Moreover, α-synuclein can arrange in toxic β-sheet aggregates, which have been identified in synucleinopathies, such as Parkinson's disease.[466,467] Many different PTMs, including phosphorylation, ubiquitination, and nitration, have been reported for α-synuclein.[468] In addition, nine *O*-GlcNAc sites (T33, T44, T54, T59, T64, T72, T75, T81, and S87) have been detected for rodent and human α-synuclein.[469–472] To study the effect of *O*-GlcNAcylation on α-synuclein's properties, Pratt and coworkers have synthesized α-synuclein proteins carrying *O*-GlcNAc at either threonine 72 or serine 87. Using these proteins, they have found that *O*-GlcNAcylation of both residues inhibits the formation of aggregates, but does not affect the membrane binding and bending characteristics of α-synuclein.[467,473] Recently, the inhibition of the aggregate formation has also been shown for enzymatically *O*-GlcNAcylated α-synuclein.[474]

All of these studies on *O*-GlcNAcylated α-synuclein have been performed *in vitro*. To investigate this biological and medically interesting PTM of α-synuclein in the context of living cells, the established approach for protein-specific imaging of glycosylation should be employed. This project was carried out in cooperation with Petra Chovancova from the group of Prof. Dr. Leist, University of Konstanz. The final aim was imaging the *O*-GlcNAcylation of EGFP-tagged α-synuclein in neuronal cells. Nevertheless, work was started with HEK293T cells, as the approach was established for this cell line.

In a first step, the modification of EGFP-tagged α-synuclein with Ac_4GlcNCyoc was investigated. To this end, HEK293T cells were transiently transfected with plasmids encoding EGFP or α-synuclein-EGFP, treated with 100 µM Ac_4GlcNCyoc or Ac_4GlcNAc for 20 h, and lysed. Lysates and immunoprecipitates of EGFP and α-synuclein-EGFP were labeled with Cy3-Tz. Whereas the fluorescence readout of a Western blot with lysate samples clearly demonstrated the incorporation of GlcNCyoc into the cellular glycome and its labeling with Cy3-Tz via the DAinv reaction, no fluorescence band was visible on a Western blot of immunoprecipitation samples (Figure 4.20). In addition, no *O*-GlcNAcylation could be detected with an anti-*O*-GlcNAc antibody. Repetitions of this experiment always led to the same result. Thus, it was concluded that α-synuclein-EGFP is modified with GlcNCyoc or native *O*-GlcNAc to a very low extent or not at all. Studies, in which *O*-GlcNAcylation sites of α-synuclein have been determined, have been based on an enrichment of *O*-GlcNAcylated proteins and peptides. However, the approach developed here combines chemical reporter strategies and GFP-fusion proteins and averages over all proteins of interest. Consequently, no statements can be made on the modification state of a small portion of proteins. Upon affinity purification and enriching samples, Petra Chovancova demonstrated that less than 1 % of native α-synuclein is *O*-GlcNAcylated in HEK293T cells.[475] Thus, it is not surprising that the detection of the modification of α-synuclein with Ac_4GlcNCyoc or its native *O*-GlcNAcylation with an anti-*O*-GlcNAc antibody was not successful.

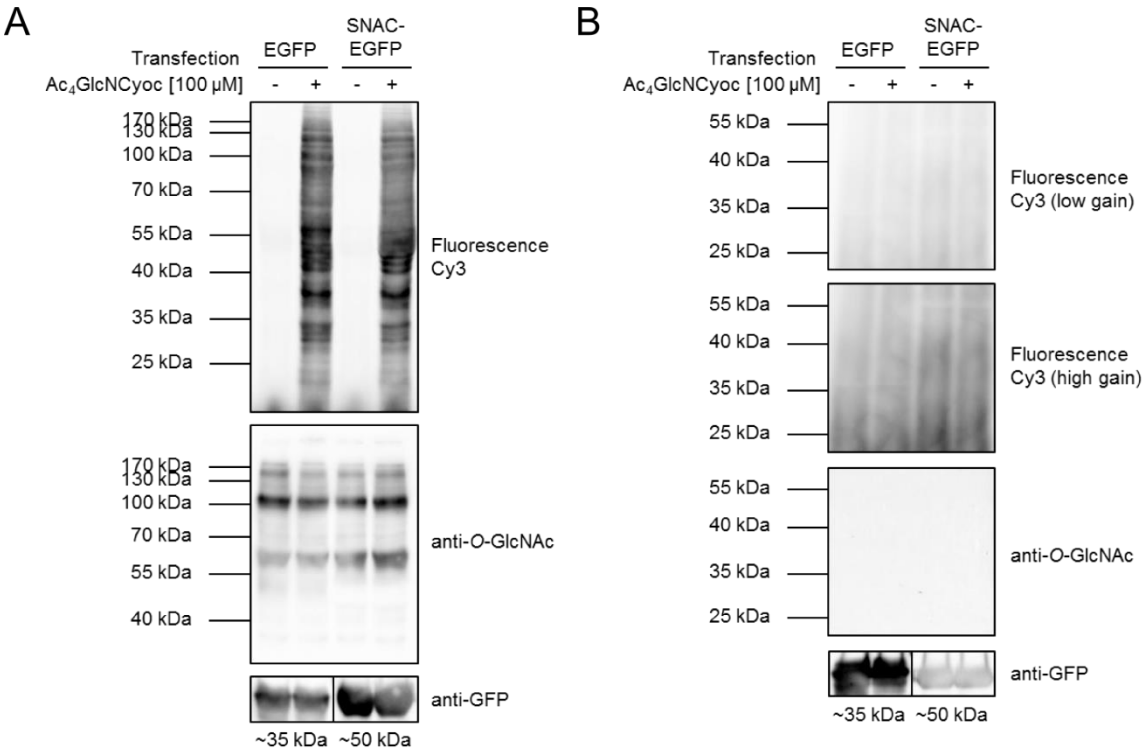

Figure 4.20: Modification of α-synuclein with GlcNCyoc. HEK293T cells transfected with plasmids encoding EGFP or α-synuclein (SNAC)-EGFP were treated with 100 µM Ac_4GlcNCyoc (+) or Ac_4GlcNAc (-) and lysed after 20 h. EGFP and SNAC-EGFP were isolated by immunoprecipitation. Lysates and immunoprecipitates were labeled with Cy3-Tz and analyzed on Western blots. Fluorescence readouts of (A) lysate samples and (B) immunoprecipitates are displayed. EGFP and *O*-GlcNAc were detected with antibodies.

Concurrently with the development of the DAinv chemistry-based imaging approach for protein-specific glycosylation presented in this thesis, Chen and coworkers reported on a similar strategy.[476] As they used $Ac_4GalNAz$, which was fluorescently labeled via a cytotoxic CuAAC, the application of their method was restricted to fixed cells. To investigate, whether α-synuclein's *O*-GlcNAcylation could be detected following their approach, $Ac_4GalNAz$ was employed (Figure 4.21A). It did not affect cellular viabilities and was well incorporated in the cellular glycome (Figure 4.21B+C). The background fluorescence

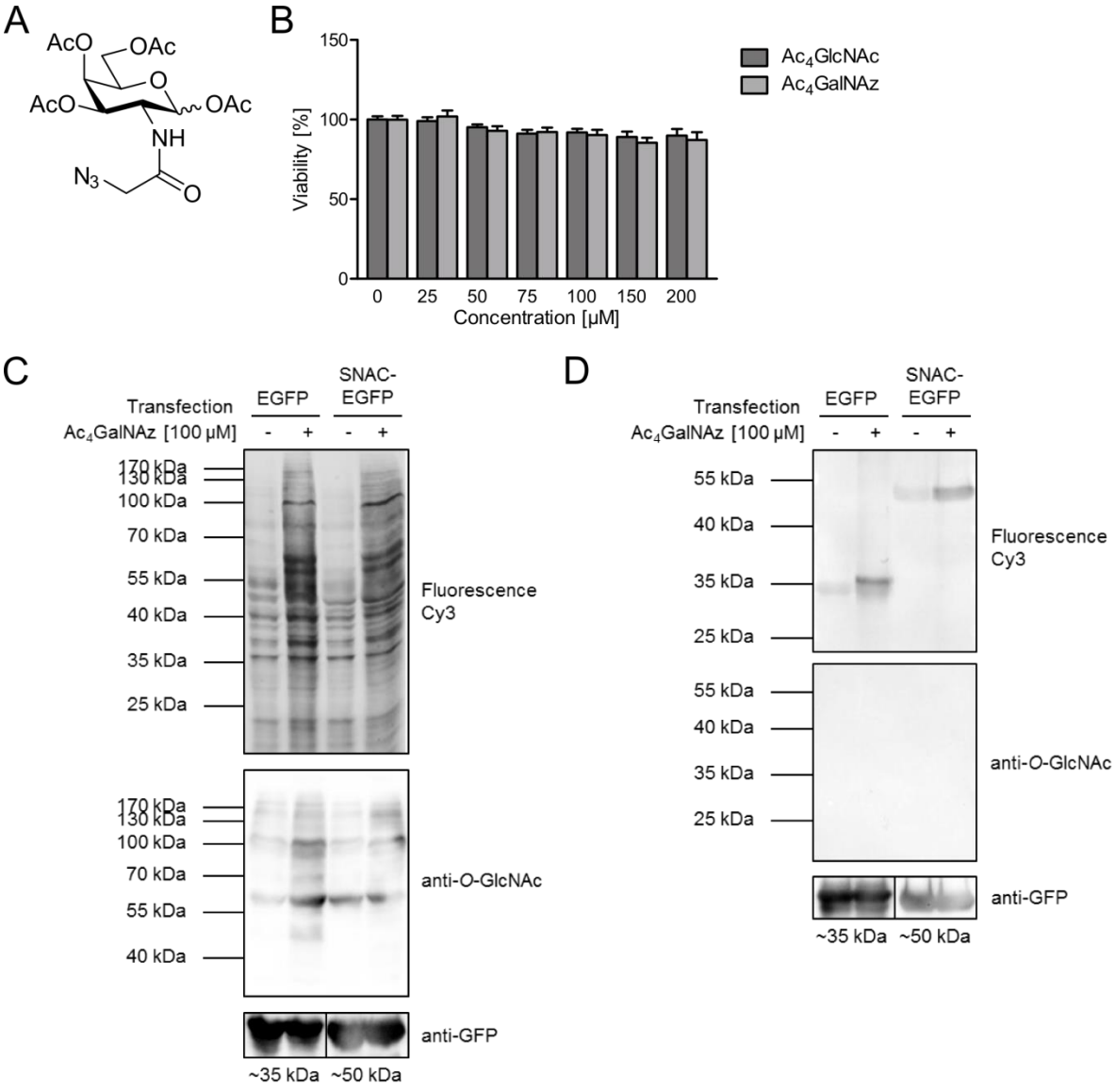

Figure 4.21: Metabolic labeling of both SNAC-EGFP and EGFP with $Ac_4GalNAz$. (A) Chemical structure of $Ac_4GalNAz$. (B) Viabilities of HEK293T cells treated with different concentrations of $Ac_4GalNAz$ or $Ac_4GlcNAc$ for 20 h were assessed with AlamarBlue assays. Columns belong to mean values calculated from three independent experiments with four replicates each. Error bars are SEMs. (C+D) HEK293T cells transiently expressing EGFP or SNAC-EGFP were treated with 100 µM $Ac_4GalNAz$ (+) or $Ac_4GlcNAc$ (-) for 20 h. Subsequently, cells were lysed and EGFP and SNAC-EGFP isolated by immunoprecipitation. Cy3-labeled lysates and immunoprecipitates were analyzed on Western blots. Fluorescence readouts of (C) lysate samples and (D) immunoprecipitates are presented. Immunoblotting was performed with anti-GFP and anti-*O*-GlcNAc antibodies.

detected for Ac_4GlcNAc was higher in case of the CuAAC performed with Cy3-alkyne than for the DAinv reaction with Cy3-Tz. Interestingly, the modification of proteins with GlcNAz, which is the metabolized form of Ac_4GalNAz attached by OGT,[72] was detected with *O*-GlcNAc antibodies. Its signal was stronger for Ac_4GalNAz- than for Ac_4GlcNAc-treated samples. This was not the case for Ac_4GlcNCyoc, which can be explained by a larger size of its chemical handle compared to the azide that might no longer be recognized by the antibody. Next, immunoprecipitates of EGFP and α-synuclein-EGFP were prepared and labeled with Cy3-alkyne to analyze the proteins' modification with GlcNAz. Stronger Cy3 fluorescence bands were observed for both EGFP and α-synuclein-EGFP in samples that received Ac_4GalNAz compared to those treated with Ac_4GlcNAc (Figure 4.21D). To exclude non-covalent attachments of Cy3-alkyne to EGFP, experiments were repeated several times using harsh washing conditions after the CuAAC (buffers with up to 1 V-% Triton X-100). However, fluorescence bands of EGFP and α-synuclein-EGFP were always stronger for Ac_4GalNAz than for Ac_4GlcNAc samples. Thus, it must be concluded that both proteins are somehow modified with an azide-tagged monosaccharide. The modification of EGFP itself prohibits conclusions on its fusion partner and the application of Ac_4GalNAz for studying protein-specific glycosylation in HEK293T cells. This is not in line with results presented by Chen and coworkers on the utilization of Ac_4GalNAz for in cell imaging of protein-specific *O*-GlcNAcylation. They also did control experiments with EGFP, but performed them in a different cell line than experiments with EGFP-fusion proteins.[476] It is known that chemical glycosylation reporters are incorporated to a different extent in diverse cell lines.[477] Hence, it is possible that cells used to estimate the modification of EGFP by Lin et al. incorporated less Ac_4GalNAz than cells used for positive experiments with EGFP-fusion proteins. Moreover, their fluorescence readout from Western blots of immunoprecipitated EGFP of cells treated with Ac_4GlcNAc or Ac_4GalNAz is doubtful, because it lacks a positive control. Therefore, it cannot be excluded that the CuAAC with alkyne-TAMRA did not work or that the gain was not adjusted correctly. Furthermore, statistical tests on the difference of fluorescence lifetimes measured for Ac_4GlcNAc- and Ac_4GalNAz-treated cells were only implemented for the positively tested EGFP-fusion proteins and not for EGFP. In conclusion, results presented here suggest that Ac_4GalNAz can, at least in HEK293T cells, not be used to study the *O*-GlcNAcylation of EGFP-fusion proteins.

Since the final aim was to image α-synuclein's *O*-GlcNAcylation in neuronal cells, work was directly continued with neuronal precursor Lund human mesencephalic (LUHMES) cells. However, Petra Chovancova found that Ac_4GlcNCyoc dramatically reduces viabilities of these cells, even at concentrations as low as 10 µM.[475] Therefore, it was concluded that a less toxic, but still specific, chemical reporter targeting *O*-GlcNAc needs to be developed in future before the continuation of this project.

4.1.5. *O*-GlcNAcylation of β-catenin

β-Catenin is a multifunctional intracellular protein consisting of 781 amino acids. It contains flexible N- and C-terminal domains as well as a central domain, which comprises twelve armadillo repeats (Figure 4.22A).[478,479] β-Catenin possesses a structural function at the adherens junctions, where it interacts with the cell adhesion protein E-cadherin and the actin

cytoskeleton (Figure 4.22B).[480] In addition, it mediates the signal transduction in the Wnt/wingless canonical pathway. The presence of Wnt leads to a stabilization and accumulation of β-catenin in the cytoplasm. Subsequently, β-catenin localizes to the nucleus, where it executes its regulatory function as a transcriptional co-activator of Wnt target genes, which are for instance associated with cell proliferation and metastasis.[481–483] In the absence of Wnt, β-catenin is part of a multiprotein complex, is phosphorylated by casein kinase 1 at serine 45 and by glycogen synthase kinase-3β (GSK-3β) at the threonine residues 33, 37, and 41, ubiquitinated, and degraded by the proteasome.[484] While the N-terminal domain of β-catenin is involved in the regulation of the protein's stability, its C-terminal domain is important for transcriptional activation and the armadillo repeats serve as binding platform for interaction partners.[479] Cellular levels of β-catenin need to be tightly regulated, since increased nuclear amounts of β-catenin are associated with several cancer types.[485–487] Phosphorylation as well as *O*-GlcNAcylation are known to alter the function and localization of β-catenin.[488,489] *O*-GlcNAcylation has been detected at the N- and C-terminal domain, but not at the armadillo repeats. Whereas C-terminal *O*-GlcNAc sites have been identified to be

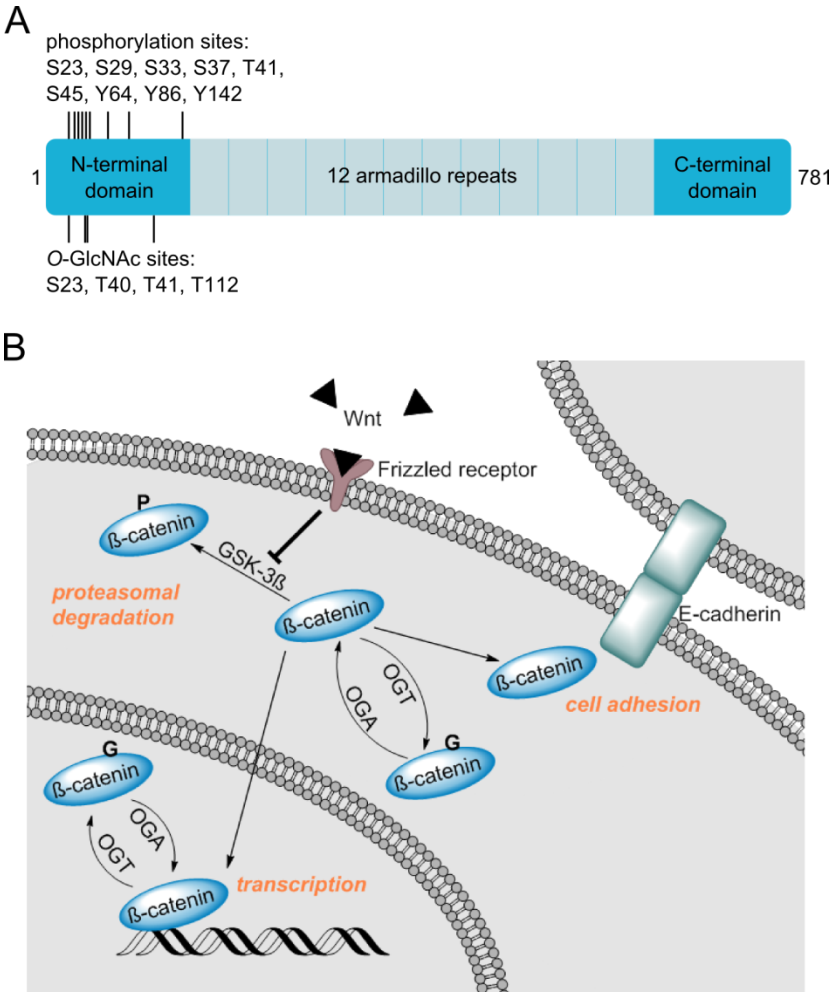

Figure 4.22: Structure, PTMs, and cellular functions of β-catenin. (A) The schematic structure and known N-terminal phosphorylation and *O*-GlcNAc sites of β-catenin are shown. (B) β-catenin serves functions in cell adhesion when interacting with E-cadherin and in transcription of DNA. It can be *O*-GlcNAcylated (G) in the cytoplasm and nucleus. Its phosphorylation (P) by GSK-3β initiates the proteasomal degradation of β-catenin. GSK-3β is inhibited by Wnt signaling.

static, N-terminal *O*-GlcNAcylation has been reported to be highly dynamic.[490] Until now, four N-terminal *O*-GlcNAc sites of β-catenin (S23, T40, T41, and T112) have been discovered (Figure 4.22A).[35,490] *O*-GlcNAc at serine 23 has been shown to result in the nuclear export of β-catenin as well as its accumulation at the plasma membrane and in the cytoplasm. Consequently, this modification reduced β-catenin's transcription activity, but increased its interaction with E-cadherin.[490] In contrast, Harosh-Davidovich and Khalaila have detected increased nuclear levels and transcriptional activity for *O*-GlcNAcylated β-catenin.[491] Moreover, *O*-GlcNAcylation at threonine 41 has been demonstrated to increase the stability of β-catenin, as it directly competes with the phosphorylation of this residue by GSK-3β.[35]

Most investigations of β-catenin's *O*-GlcNAcylation have been based on biochemical studies. Still, concrete effects of all modified residues on the function and localization of β-catenin are not completely understood. To shed more light onto the effect of β-catenin's *O*-GlcNAcylation and to decipher spatial *O*-GlcNAcylation patterns for each modified amino acid, the established approach for the visualization of protein-specific glycosylation was employed. It was of advantage that all known *O*-GlcNAc sites are close to the N-terminus of the protein, to which EGFP can be easily fused. This project was partially carried out by Pia Widder in the context of her master's thesis in the group of Prof. Dr. Zumbusch, University of Konstanz.[492]

In a first step, DNA of wild type (WT) β-catenin from the plasmid pcDNA3.0-β-catenin was amplified and integrated into the pDNR-Dual vector via ligation independent cloning (LIC). DpnI-mediated site directed mutagenesis of pDNR-Dual β-catenin was used to create the point mutants S23A, T40A, T41A, T112A, and T40AT41A. The triple mutants S23AT40AT41A and T40AT41AT112A were prepared from the double mutant T40AT41A. The quadruple mutant S23AT40AT41AT112A (Δ4) was generated from S23AT40AT41A. To be able to assess the correctness of all point mutations, additional restriction sites for common enzymes were introduced via designed primers during site directed mutagenesis. Besides restriction digestion followed by agarose gel electrophoreses, the presence of correct point mutations was verified by sequencing. Finally, DNAs encoding WT β-catenin and its mutants were integrated in the mammalian expression vector pEGFP-C1-loxP by Cre-LoxP recombination. Correct DNA sequences of all EGFP-plasmids were proven by restriction digestion, agarose gel electrophoresis, and sequencing. Test expressions of EGFP-WT β-catenin and all mutants were carried out in HEK293T cells. The presence of EGFP fluorescence was checked by fluorescence microscopy and the right size of the fusion proteins on Western blots using an antibody against GFP. All proteins, except EGFP-T40A, were correctly expressed. However, sequencing of both the promotor region and the EGFP-T40A gene confirmed its correctness.[492]

Having plasmids for the expression of EGFP-WT β-catenin and nearly all desired mutants at hands, the proteins' modification with Ac_4GlcNCyoc was investigated. For this purpose, HEK293T cells transiently transfected with plasmids encoding EGFP, EGFP-WT β-catenin, or EGFP-Δ4 β-catenin were treated with Ac_4GlcNCyoc or Ac_4GlcNAc and lysed. EGFP and both EGFP-fusion proteins were isolated by immunoprecipitation and labeled with Cy3-Tz. The modification of WT and Δ4 β-catenin with GlcNCyoc was detected via the fluorescence of Cy3 on a Western blot (Figure 4.23). Although Δ4 β-catenin does not possess any (known)

N-terminal *O*-GlcNAc site anymore, it might still be *O*-GlcNAcylated at its C-terminus. As fluorescence bands of WT and Δ4 β-catenin displayed similar intensities, it can be assumed that GlcNCyoc at S23, T40, T41, and T112 did not contribute to a great extent to the detected Cy3 fluorescence.

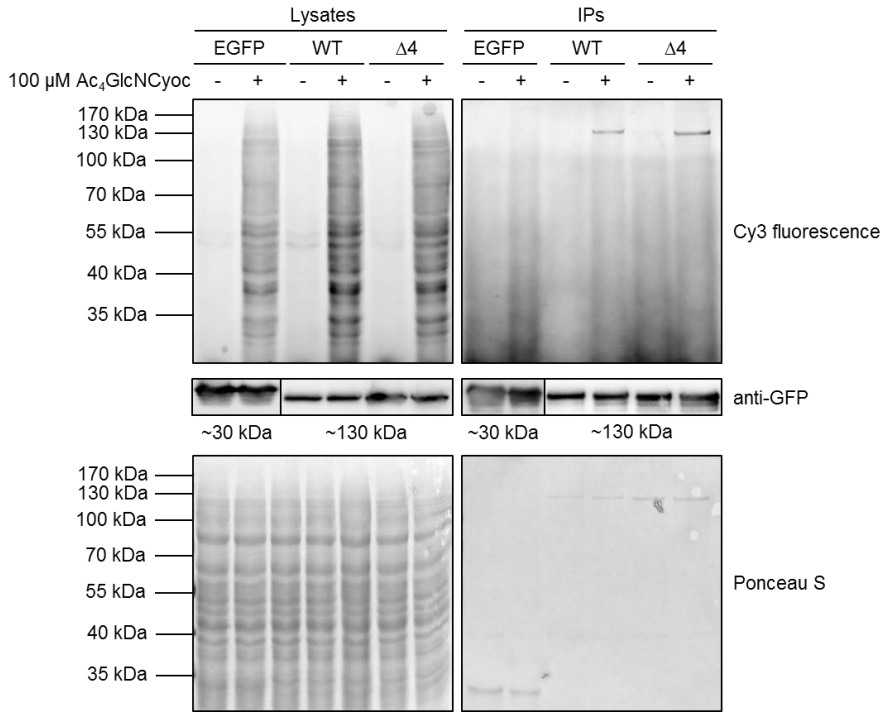

Figure 4.23: Modification of WT β-catenin and the Δ4 mutant with Ac_4GlcNCyoc. Lysates of HEK293T cells transiently transfected with vectors encoding EGFP, EGFP-WT β-catenin, or EGFP-Δ4 β-catenin and treated with 100 µM Ac_4GlcNCyoc (+) or Ac_4GlcNAc (-) for 20 h were used to isolate EGFP and EGFP-fusion proteins by immunoprecipitation. Samples were labeled with Cy3-Tz before being analyzed on a Western blot. Cy3 fluorescence was read out to investigate the glycosylation state of immunoprecipitated proteins. Ponceau S staining and immunoblotting against GFP were used as loading controls. Data underlying this figure were acquired by Pia Widder,[492] but processed and analyzed by myself.

Next, *O*-GlcNAcylation states of WT β-catenin and all mutants were imaged with FLIM-FRET microscopy in single cells. For ease of implementation, living HEK293T cells transiently transfected with EGFP, EGFP-WT β-catenin, or EGFP-β-catenin mutants and treated with Ac_4GlcNCyoc or Ac_4GlcNAc were labeled with TAMRA-Tz, but were fixed with paraformaldehyde afterwards. Thus, many samples could be prepared simultaneously to be consecutively measured at the FLIM microscope. Obtained results are summarized in Figure 4.24. Representative fluorescence modulation lifetime images displayed only very small decreases in fluorescence lifetimes of cells treated with Ac_4GlcNCyoc compared to control cells. The same trend was observed for fluorescence lifetimes averaged over three independent experiments with ten cells each. Accordingly, also FRET efficiencies calculated for each EGFP-fusion protein did not differ significantly from those of EGFP. Thus, it must be concluded that the N-terminal *O*-GlcNAcylation of β-catenin could not be detected with the established FLIM-FRET-based approach. Possible explanations could be the

decomposition of the chemical reporter $Ac_4GlcNCyoc$ or problems within the DAinv reaction with TAMRA-Tz.

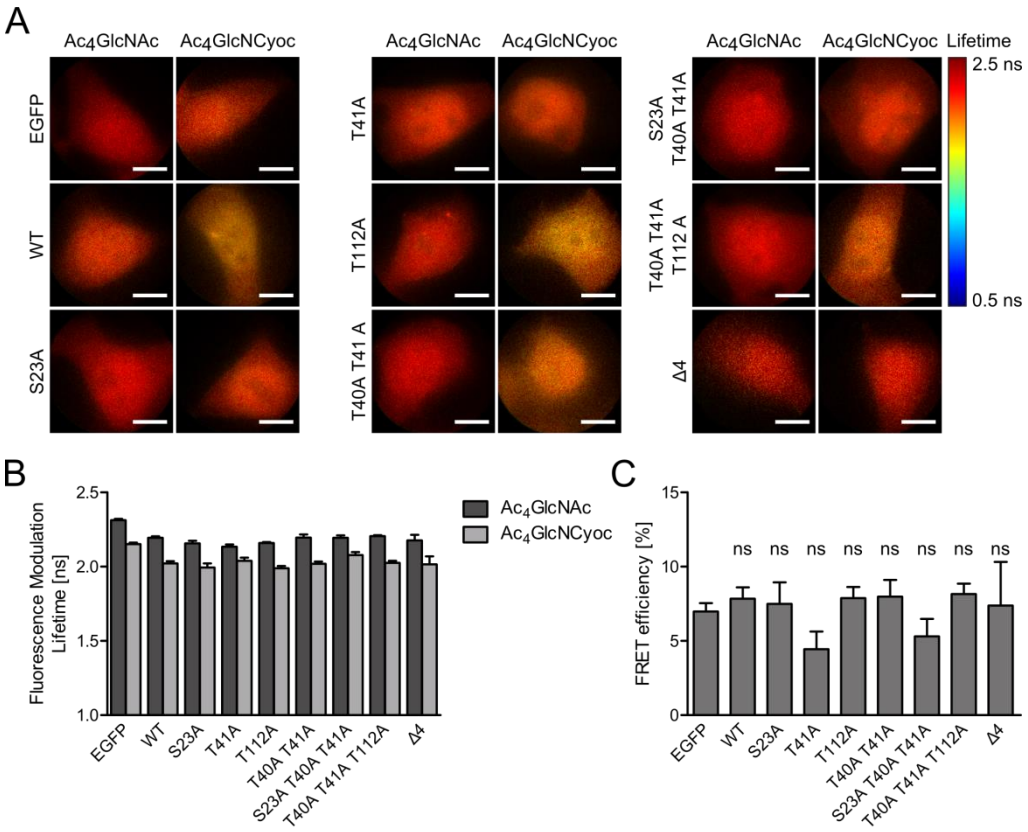

Figure 4.24: Assessing the glycosylation of EGFP-β-catenin and its mutants with FLIM-FRET microscopy. (A) Representative fluorescence modulation lifetime images of HEK293T cells expressing EGFP, EGFP-tagged WT β-catenin, or its mutants, treated with 100 µM $Ac_4GlcNAc$ or $Ac_4GlcNCyoc$ for 20 h, labeled with TAMRA-Tz, and fixed are displayed. Scale bars: 10 µm. (B) Fluorescence modulation lifetimes were averaged over three (for Δ4 only two) independent experiments with ten cells each. Columns represent mean values and error bars SEMs. (C) FRET efficiencies calculated from averaged fluorescence lifetimes are presented. Error bars are SEMs. None of the β-catenin FRET efficiencies was significantly different compared to EGFP as determined with a one-way ANOVA and a Bonferroni posttest of selected columns. ns $p>0.05$. Data were acquired by Pia Widder,[492] but processed and analyzed by myself.

To exclude any faults arising from sample preparation or chemicals, experiments in HEK293T cells were repeated with the negative control EGFP, the positive control EGFP-OGT, and the protein of interest EGFP-WT β-catenin. Representative fluorescence modulation lifetime images and averaged fluorescence lifetimes show a noticeable decrease of fluorescence lifetimes for EGFP-OGT in cells treated with $Ac_4GlcNCyoc$ compared to those treated with $Ac_4GlcNAc$. However, this was not the case for EGFP and EGFP-WT β-catenin (Figure 4.25A+B). Calculated FRET efficiencies of EGFP differed significantly from those of EGFP-OGT, but not for EGFP-WT β-catenin (Figure 4.25C). Yet, FRET efficiencies for EGFP-OGT were smaller than in initial experiments (Figure 4.12). This can be due to fixation of samples upon TAMRA-Tz labeling, as this has been found to affect fluorescence lifetimes.[493,494] In addition, it is possible that $Ac_4GlcNCyoc$ was decomposed to some extent at this time point. This cannot be assessed with Western blot experiments absolutely, as the

detection of the fluorescence of Cy3 attached to the cyclopropene does not allow for quantification among different readouts. As Western blots from β-catenin lysates treated with Ac_4GlcNCyoc still reveal fluorescence labeling of incorporated GlcNCyoc (Figure 4.23), the chemical reporter must have been functional at least to a certain degree. Despite detecting lower FRET efficiencies for EGFP-OGT than in earlier experiments, they are significantly higher compared to FRET efficiencies calculated for EGFP. Hence, any possible failures arising from sample preparation, chemicals, or the FLIM microscope can be excluded as reason for the inability to image the N-terminal *O*-GlcNAcylation of β-catenin. It is unlikely that the distance between the donor fluorophore EGFP and presumably acceptor fluorophore-labeled glycosylated N-terminal residues is too large to enable efficient FRET. Two explanations for the lack of signal remain: On the one hand, β-catenin might only be substoichiometrically *O*-GlcNAcylated at the N-terminal residues. As fluorescence lifetimes are averaged over all proteins giving rise to fluorescence detected in a single pixel in FLIM microscopy, FRET of a subpopulation can hardly be determined. On the other hand, GlcNCyoc might solely be attached to static C-terminal glycosylation sites. Since N-terminal *O*-GlcNAcylation of β-catenin has been reported to be highly dynamic,[490] it could be the case that OGT prefers native GlcNAc over artificial GlcNCyoc to modify these residues.

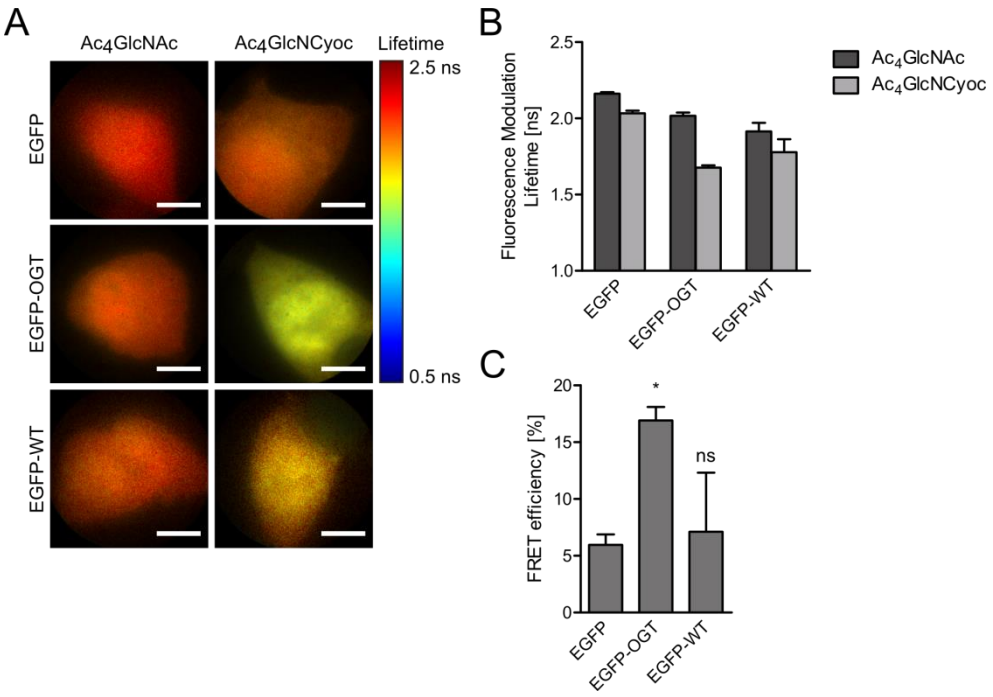

Figure 4.25: Imaging the glycosylation of EGFP-OGT but not EGFP-β-catenin by FLIM-FRET microscopy. (A) Representative fluorescence modulation lifetime images of HEK293T cells expressing EGFP, EGFP-OGT, or EGFP-WT β-catenin, treated with 100 µM Ac_4GlcNAc or Ac_4GlcNCyoc for 20 h, labeled with TAMRA-Tz, and fixed are depicted. Scale bars: 10 µm. (B) Fluorescence modulation lifetimes were averaged over three independent experiments with five cells each. Columns correspond to mean values and error bars to SEMs. (C) FRET efficiencies were calculated from averaged fluorescence lifetimes. Columns are means and error bars SEMs. Statistical analysis was performed with a one-way ANOVA and a Bonferroni posttest. Degrees of significances in comparison to EGFP are given as ns $p>0.05$ and * $p<0.05$. Data underlying this figure were acquired by Pia Widder,[492] but processed and analyzed by myself.

Since the glycosylation of N-terminal β-catenin could not be imaged using Ac_4GlcNCyoc, other chemical glycosylation reporters might be better suited. Although Ac_4GalNAz was used by the Chen group to image the glycosylation of EGFP-β-catenin in fixed cell,[476] results of this thesis (chapter 4.1.4) indicate that this monosaccharide may not be used without restrictions. A possible alternative was the chemical reporter Ac_4GlcNCp (Figure 4.26A), which has been synthesized by Jessica Hassenrück recently (group of Prof. Dr. Wittmann, University of Konstanz).[495] As its chemical handle is much smaller than that of Ac_4GlcNCyoc, it might be better accepted and incorporated by cellular enzymes. Viability tests were carried out with HEK293T cells to assess potential cytotoxic effects of this new compound. Interestingly, Ac_4GlcNCp did not affect cellular viabilities at all when applied for 20 h and it was even less toxic than the control compound Ac_4GlcNAc after an incubation time of 48 h (Figure 4.26B). Nevertheless, no fluorescence signal higher than the fluorophore's background could be detected on Western blots of lysates from Ac_4GlcNCp-treated HEK293T cells (Figure 4.26C), which hinders its usage for studying the glycosylation of β-catenin. As TAMRA signals were detected for Ac_4GlcNCyoc-treated HEK293T cells, failures of the DAinv reaction could be excluded. These data suggest that Ac_4GlcNCp is

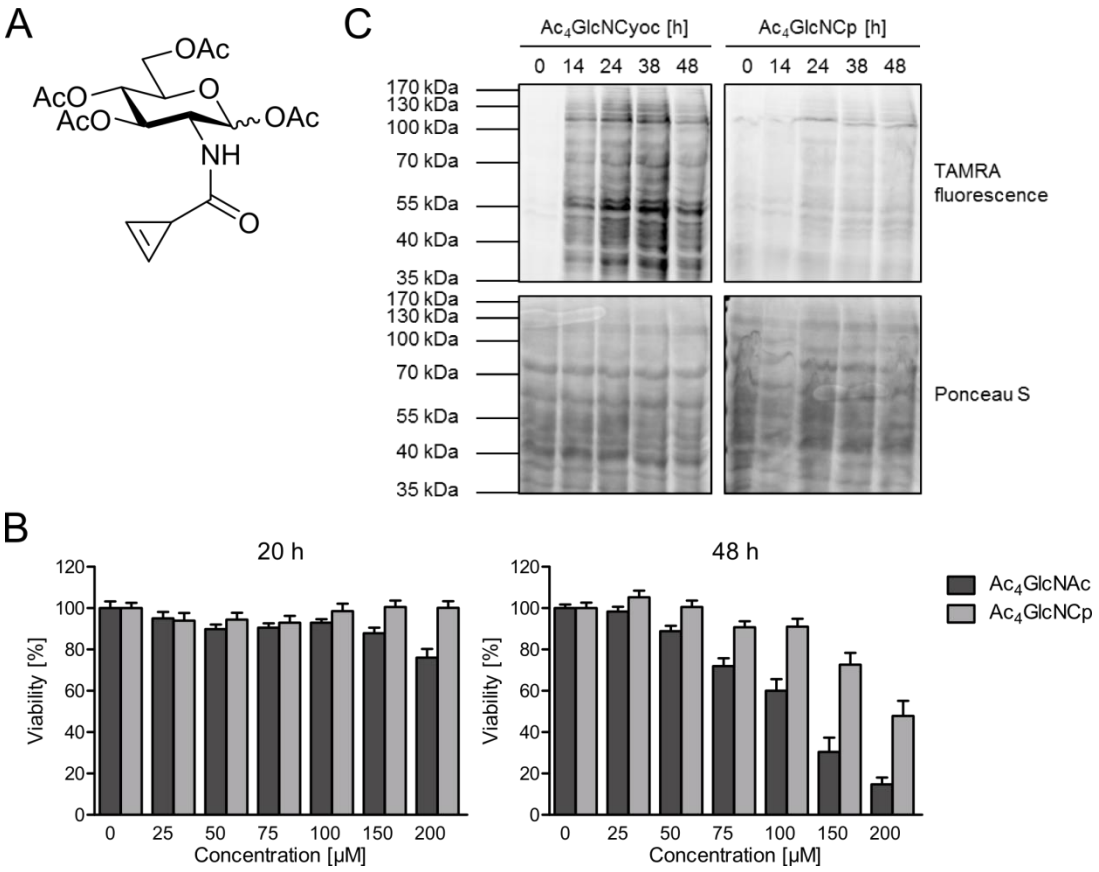

Figure 4.26: Incorporation of Ac_4GlcNCp in the cellular glycome. (A) Chemical structure of Ac_4GlcNCp. (B) Viabilities of HEK293T cells treated with different concentrations of Ac_4GlcNAc or Ac_4GlcNCp for 20 h or 48 h were assessed with AlamarBlue assays. Columns represent mean values of three independent experiments performed in quadruplicates and error bars SEMs. (C) HEK293T cells were treated for different times with 100 µM Ac_4GlcNCyoc or Ac_4GlcNCp, lysed, and labeled with 10 µM TAMRA-Tz. The fluorescence readout allowed for the detection of incorporated Ac_4GlcNCyoc, but not of Ac_4GlcNCp. Ponceau S served as loading control.

either not metabolized and attached to proteins by cellular enzymes or does not react with the tetrazine derivative. The latter possibility could be excluded, because its reactivity in the DAinv reaction was demonstrated by J. Hassenrück.[495] Further studies will clarify, why Ac_4GlcNCp is not accepted by enzymes involved in the glycosylation of intracellular proteins.

4.1.6. Glycosylation in *A. thaliana*

Plants synthesize and incorporate many different glycans. Their cell wall mainly consists of polysaccharides with high molecular weights, such as cellulose, hemicellulose, or pectins.[496] Next to glycans present in cell walls, also plant proteins are glycosylated. Thousands of secreted and membrane proteins carrying asparagine-linked *N*-glycans are known. In contrast to animals, *N*-glycans of plants are not extensively branched and do not carry sialic acids. They serve important functions in protein folding, quality control in the endoplasmic reticulum, and affect the stability and interaction partners of proteins.[497] In addition, hundreds of glycosylphosphatidylinositol-anchored proteins have been identified on plant cell membranes.[497,498] Mucin-type *O*-glycans do not exist in plants, but single galactose residues can be attached to serine residues or chains of arabinose to hydroxyprolines.[497,499,500] Moreover, nuclear and cytoplasmic proteins can be modified with *O*-GlcNAc. In the model plant *A. thaliana*, two *O*-GlcNAc transferases have been identified, which have been named Spindly and Secret Agent.[501,502] Functions of both enzymes overlap, but are not identical.[502] Similar to animal *O*-GlcNAcylation, the knockout of both *A. thaliana O*-GlcNAc transferases is lethal.[503] Plant *O*-GlcNAc has been shown to affect signaling cascades of gibberellin plant hormones, growth and differentiation of cells via the cytokine response, the circadian rhythm of plants, the development of roots, and probably the transport of proteins through plasmodesmata.[503] As no *O*-GlcNAcase has been identified in plants yet, it is unclear whether plant *O*-GlcNAcylation is dynamic.[504] Proteins known to become *O*-GlcNAcylated in plants include the glycosyltransferase Secret Agent, transcription factors involved in the cytokine signaling, and DELLA proteins, which negatively regulate gibberellin signaling cascades.[502,503,505,506] In addition, a recent study has revealed more than 900 *O*-GlcNAc sites on 262 proteins in *A. thaliana*.[507]

Since 2012, chemical reporter strategies have been used to image distinct plant glycans, which can help to decipher the biosynthesis and biological functions of plant glycans.[199] 3-Deoxy-D-manno-oct-2-ulosonic acid (Kdo) and fucose of cell walls have been targeted with the chemical reporters 8-azido 8-deoxy Kdo and 6-alkynyl fucose, respectively.[508,509] Chen and coworkers have made use of Ac_4GlcNAz to label *N*-glycans of proteins on cell membranes.[199] Shortly afterwards, the Wennekes group has demonstrated the visualization of cell wall and/or membrane glycans of living *A. thaliana* roots by using Ac_4GlcNAz, Ac_4GalNAz, Ac_4FucAz, or Ac_3ArabAz and CuAAC or SPAAC as bioorthogonal ligation reaction.[197] In addition, they imaged the incorporation of Ac_4GlcNCyoc, which had been fluorescently labeled via a DAinv reaction, and have demonstrated that even deacetylated GlcNAz can be taken up, metabolized, and incorporated by *A. thaliana*. The latter observation is in line with work from 1970 on the ability of plant roots to efficiently take up glucosamine.[510] Another study has reported the screening of 19 chemical reporters that comprise analogs of Glc, xylose, rhamnose, fucose, Kdo, L-arabinose, Man, GlcNAc, and

GalNAc.[196] Five of them, namely Ac_4GlcNAz, Ac_4GalNAz, Ac_4FucAl, Ac_4FucAz, and Ac_4Me8AzKdo, could be detected on cell walls/membranes.
After the first publication by Chen and coworkers,[199] we also started using chemical glycosylation reporters to study the glycosylation in *A. thaliana*. Initially, similar imaging experiments with azide-functionalized GlcNAc, GalNAc, and ManNAc derivatives were performed. To this end, four days old seedlings were treated with 100 µM of the monosaccharides for 48 h, fixed, and labeled with the CuAAC reaction mixture used by Zhu et al. (1 mM $CuSO_4$, 1 mM sodium ascorbate, and 1 µM sulfo-Cy3-alkyne)[199]. In Ac_4GlcNAz and Ac_4GalNAz samples, fluorescence of Cy3 was detected at cell walls/membranes and very weakly inside plant cells by fluorescence microscopy of roots (Figure 4.27). Intensities arising from incorporated Ac_4GlcNAz were higher compared to Ac_4GalNAz. Fluorescence intensities detected for peracetylated *N*-azido-ManNAz (Ac_4ManNAz)-treated samples were much lower than those of the Ac_4GlcNAz- or Ac_4GalNAz-treated roots and differed not much from the background fluorescence measured for Ac_4GlcNAc-treated samples. This finding is consistent with unsuccessful attempts from others to detect a metabolized form of Ac_4ManNAz in *A. thaliana* and the fact that sialic acids are not present in plants.[196,197]

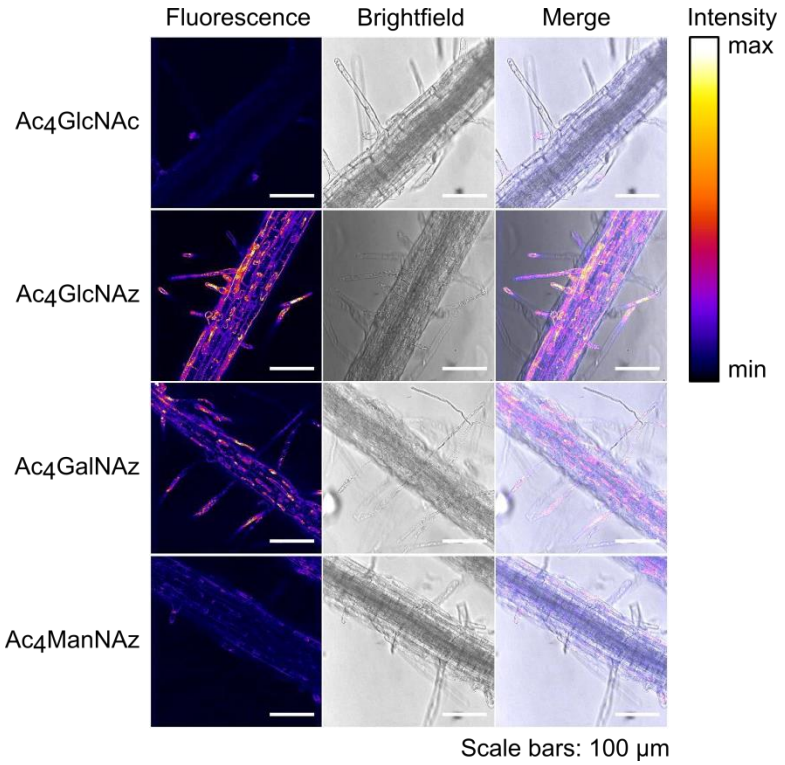

Figure 4.27: Incorporation of Ac_4GlcNAz and Ac_4GalNAz in glycoconjugates of *A. thaliana* roots. Representative confocal fluorescence and brightfield images of roots from *A. thaliana* seedlings treated with 100 µM of the indicated monosaccharide for 48 h, fixed, and labeled with sulfo-Cy3-alkyne via a CuAAC are presented.

The CuAAC mixture used by Chen and coworkers did not contain any Cu(I) chelating ligand, which was surprising, since such ligands are commonly used to increase reaction rates and protect biological molecules from oxidative damage caused by copper ions.[251] To examine

this issue, seedlings treated with $Ac_4GlcNAc$ or $Ac_4GlcNAz$ were labeled with 1 µM sulfo-Cy3-alkyne in different CuAAC reaction mixtures detailed in Figure 4.28. Brightest fluorescence was observed for azide derivatives labeled with the commercial Click-iT kit, which has also been utilized by Hoogenboom et al.[197] Fluorescence resulting from labeling with Chen's CuAAC mixture (number 1 in Figure 4.28) is less intense, but still detectable. However, no fluorescence signals were detected for the reaction mixtures 2 and 3, which both contained the Cu(I) chelating ligand THPTA. Later, also Zhu and Chen reported on the absence of fluorescence upon labeling of Ac_4FucAl-treated seedlings with CuAAC mixtures containing the Cu(I) ligands BTTPS or BTTAA, which was suggested to be due to repulsion of negatively charged Cu(I)-chelating ligands by negatively charged cell walls.[196]

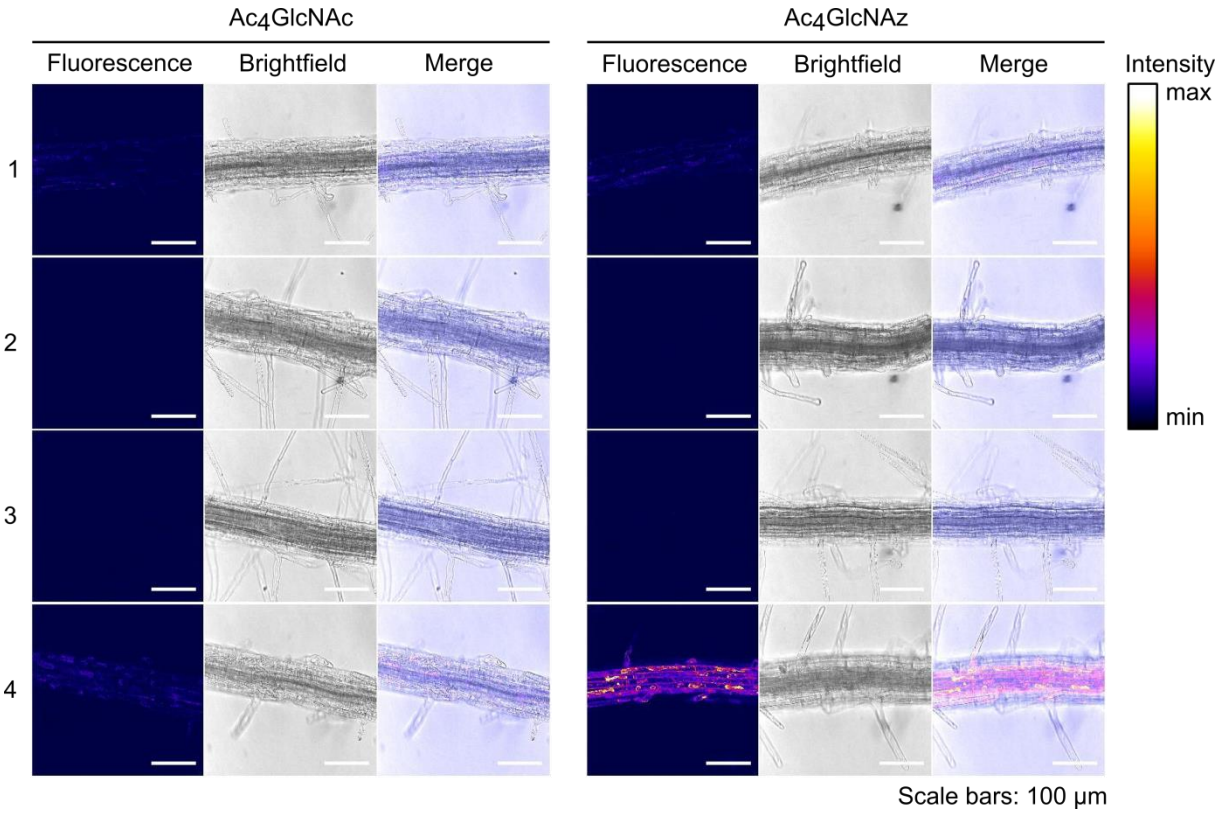

Figure 4.28: Optimizing CuAAC labeling condition in *A. thaliana*. Four days old seedlings were treated with 100 µM $Ac_4GlcNAc$ or $Ac_4GlcNAz$ for 48 h, fixed, and labeled with 1 µM sulfo-Cy3-alkyne in different CuAAC reaction mixtures (1: 1 mM $CuSO_4$, 1 mM sodium ascorbate; 2: 0.5 mM $CuSO_4$, 0.5 mM THPTA, 5 mM sodium ascorbate; 3: 1 mM $CuSO_4$, 1 mM THPTA, 5 mM aminoguanidine, 5 mM sodium ascorbate; 4: Click-iT Cell Reaction Buffer Kit). Representative confocal fluorescence and brightfield images are displayed.

Next, the incorporation of $Ac_4GlcNCyoc$ in the glycome of *A. thaliana* was investigated. Seedlings were treated with $Ac_4GlcNCyoc$ or $Ac_4GlcNAc$, fixed, and incubated with 1 µM or 10 µM TAMRA-Tz. For both concentrations, fluorescence intensities detected by confocal microscopy were much higher in $Ac_4GlcNCyoc$- than in $Ac_4GlcNAc$-treated roots (Figure 4.29) allowing for the conclusion that $Ac_4GlcNCyoc$ is metabolized and incorporated by *A. thaliana*. Signals were solely present on cell walls/membranes. These data are in accordance with findings from the Wennekes group.[197]

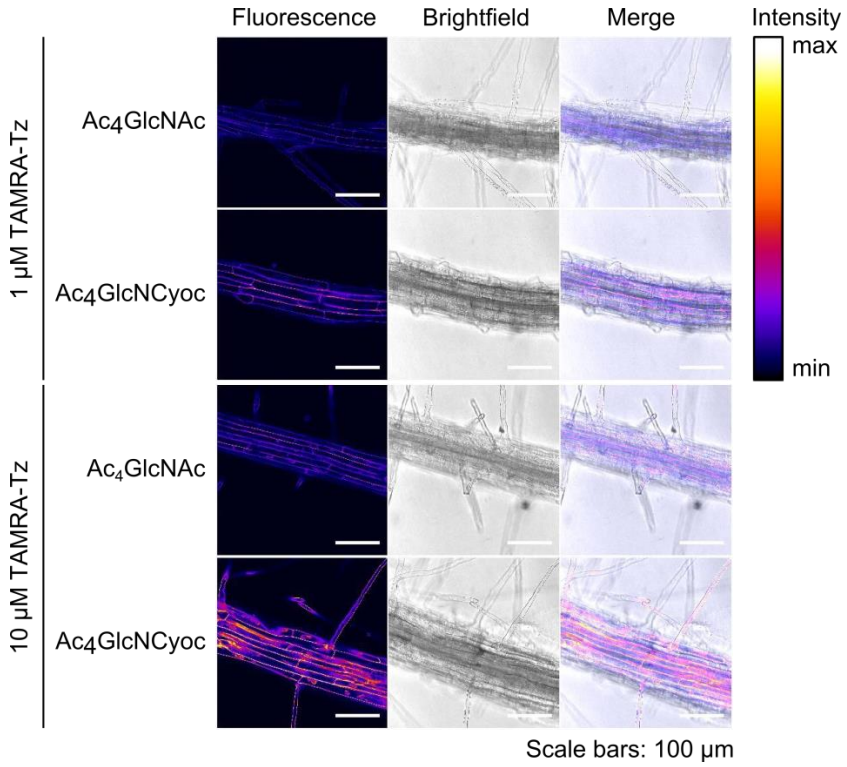

Figure 4.29: Incorporation of Ac_4GlcNCyoc in glycoconjugates of *A. thaliana*. Representative confocal fluorescence and brightfield images of roots from *A. thaliana* seedlings, which had been treated for 48 h with Ac_4GlcNAc or Ac_4GlcNCyoc, fixed, and labeled with TAMRA-Tz, are depicted.

To assess whether the chemical reporters used ended up in cell walls or were attached to proteins, lysates of *A. thaliana* seedlings treated with Ac_4GlcNAc, Ac_4GlcNCyoc, Ac_4GlcNAz, or Ac_4GalNAz were prepared. Roots and leaves were lysed separately, and labeled with Tz-biotin via a DAinv reaction or with biotin-alkyne via a CuAAC. Biotin attached to proteins was detected with an antibody on a Western blot. Fluorophores were not used for lysate experiments, as their fluorescence readout on Western blots might be disturbed in presence of chlorophyll. Signals higher than those of Ac_4GlcNAc-treated control samples were only present for Ac_4GlcNAz- and slightly also for Ac_4GalNAz-treated root samples (Figure 4.30A). To ensure the proper functionality of all reporters and labeling reagents used, control experiments were performed in HEK293T cells. As expected from earlier studies, the incorporation of Ac_4GlcNCyoc upon DAinv reaction as well as Ac_4GlcNAz and Ac_4GalNAz upon CuAAC could be unambiguously proven (Figure 4.30B). Consequently, it can be concluded that Ac_4GlcNAz and to some extent also Ac_4GalNAz, but not Ac_4GlcNCyoc, are metabolized and attached to proteins in *A. thaliana* roots. No biotin signals were present in any leave sample. As whole seedlings were in contact with liquid Murashige and Skoog (MS) medium containing the artificial monosaccharide during the incubation period of 48 h, chemical glycosylation reporters must have been predominantly taken up and metabolized by root cells.

Studying *O*-GlcNAcylated proteins in plants has been reported to be difficult, since many *N*-glycans of plants carry terminal GlcNAcs. Thus, simple detection approaches based on the labeling of native GlcNAc residues, for instance with GalNAz catalyzed by a mutated

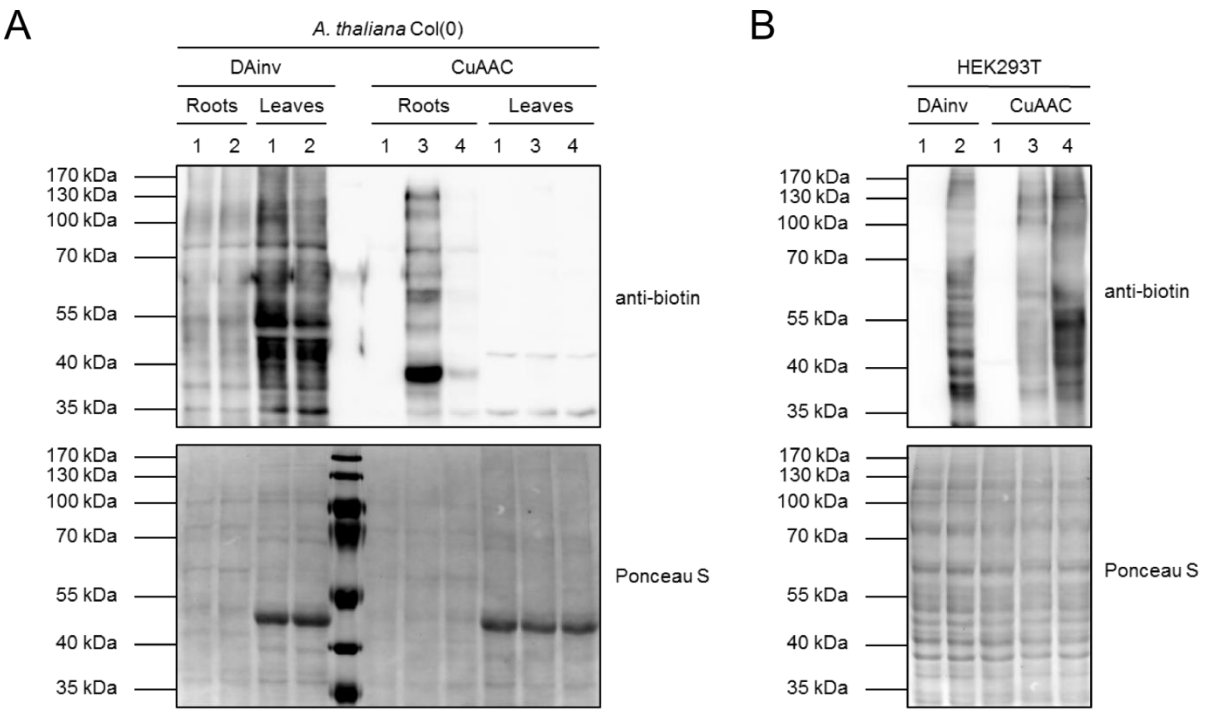

Figure 4.30: Attachment of GlcNAz to proteins. (A) Lysates of roots and leaves from *A. thaliana* seedlings treated with 100 µM of a monosaccharide (1: Ac_4GlcNAc, 2: Ac_4GlcNCyoc, 3: Ac_4GlcNAz, 4: Ac_4GalNAz) for 48 h were labeled with Tz-biotin or biotin-alkyne via a CuAAC or a DAinv reaction, respectively. Samples were separated by SDS-PAGE and analyzed by immunoblotting against biotin on a Western blot. (B) Control experiments were performed with lysates of HEK293T cells treated with the same monosaccharides for 48 h, which were also labeled with Tz-biotin or biotin-alkyne. Equal loading was confirmed with Ponceau S staining.

β-1,4-galactosyltransferase,[511–513] do not selectively mark *O*-GlcNAc. Antibodies for *O*-GlcNAc detect only a subset of *O*-GlcNAcylated proteins and hence are not generally applicable.[411] Even the chemical reporter Ac_4GlcNAz, which was shown here to be attached to probably intracellular plant proteins, has also been found in *N*-glycans of *A. thaliana*.[199] Consequently, a strategy allowing for the visualization of the *O*-GlcNAcylation of selected proteins would be useful. FLIM-FRET microscopy of plant leaves and roots has already been achieved,[514,515] which strengthened the idea to image protein-specific *O*-GlcNAcylation in *A. thaliana* roots using this technique. A possible obstacle would be the need to perform the bioorthogonal ligation reaction within the cells, which requires all reagents to pass cell walls and membranes. This problem might be solved by using enzymes digesting cell walls in combination with permeabilization strategies.[516] Another hurdle is the necessity of *A. thaliana* plants expressing fluorescently tagged proteins of interest. Thus, Arabidopsis stock centers were screened for seeds of plants stably expressing GFP-fusions of known *O*-GlcNAcylated proteins. However, among a few stocks expressing GFP-fusion proteins found only one was available. To generate such plants by oneself would necessitate the cloning of appropriate vectors, the transfection of *A. thaliana* plants, their growth, and selection until the second daughter generation in order to receive homozygote plants. This would have to be addressed in a separate project.

4.1.7. Visualizing the Sialyl Tn Antigen

More than 70 years ago it has first been reported that alterations in glycosylation are linked to oncogenic transformations.[517,518] Meanwhile, glycosylation has been shown to be associated with the hallmarks of cancer,[519] as glycans play roles in nearly all biological processes underlying this disease. These include cell signaling and communication, the dissociation and invasion of tumor cells, interactions of cells with the extracellular matrix, angiogenesis of tumor tissues, the modulation of the immune system, and metastasis.[520] Common alterations of glycosylation in cancer cells are increases in sialylation and fucosylation, truncations of *O*-glycans, and extended branching of both *N*- and *O*-glycans.[521–523] Whereas the incomplete synthesis of glycans results in truncated glycosides at early stages of cancer, the glycan neosynthesis takes place in more advanced carcinomas.[524–526] Examples for truncated glycans are the Tn antigen (*O*-linked GalNAc) and its sialylated form sialyl Tn (Neu5Acα2-6 GalNAcα-*O*-linked to hydroxyl groups of protein side chains) and for newly synthesized glycans sialyl Lewis a (Neu5Acα2-3Galβ1-3[Fucα1-4]GlcNAcβ~ attached to *N*- or *O*-glycans) and sialyl Lewis x (Neu5Acα2-3Galβ1-4[Fucα1-3]GlcNAcβ~ attached to *N*- or *O*-glycans, Figure 4.31). Sialyl Tn is rarely found in healthy tissues, but prevalently detected in many cancer types,[520] such as pancreas[527], stomach[524], colorectal[524], breast[525,528], bladder[529], and ovarian carcinomas[530]. Overexpression of sialyl Tn is associated with a decrease in cell-cell aggregation, an increase in the adhesion of cells to the extracellular matrix, and the migration and invasion of cancer cells.[531] The enzyme, which is responsible for the biosynthesis of sialyl Tn, is α-GalNAcα2-6-sialyltransferase 1 (ST6GalNAc1). It attaches Neu5Ac to *O*-linked GalNAc prematurely and thereby disrupts further elongations of *O*-glycans.[520,524,525,532]

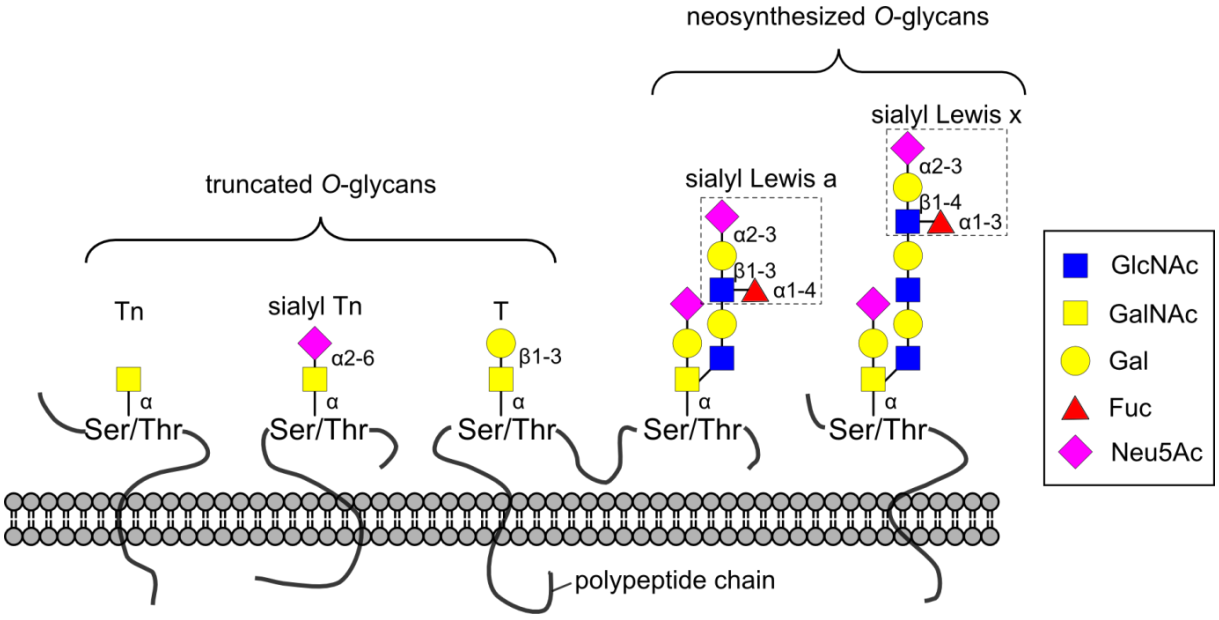

Figure 4.31: Examples of tumor-associated *O*-glycans. Inspired by [520].

Specific cell surface glycans are usually detected with antibodies and lectins, but both approaches do not allow for a perfect discrimination among different glycan structures. Aptamers are better suited for this purpose, since they can be designed for a certain glycan in a protein- and site-specific manner.[533] In addition, (imaging) mass spectrometry, microarrays, and proximity ligation assays are widely used to identify and visualize distinct glycans.[534,535] Moreover, metabolic glycoengineering has for instance been employed to enrich and identify proteins modified with the Tn antigen,[536] to image heparan sulfate and the Tn antigen on cells,[537] to visualize the fate of sialylated glycoconjugates,[538] or as therapeutic and diagnostic tool in cancer[539].

Within a cooperation project of the groups of Prof. Dr. Zumbusch, Prof. Dr. Wittmann (both University of Konstanz), and Prof. Dr. Reis (i3S Porto, Portugal), the presence of sialyl Tn on cell surfaces should be detected via the proximity of the *O*-glycan initiating GalNAc and the *O*-glycan terminating Neu5Ac. In cancer cells, *O*-glycans are truncated and thus GalNAc and Neu5Ac should be closer to one another than in healthy cells. Chemical reporters for both sugars should be selected in a way that they can be labeled with different but orthogonal ligation reactions. GalNAc was targeted with Ac_4GalNAz that can be fluorescently labeled via a SPAAC. Ac_4ManNCyoc was used as metabolic precursor analog for Neu5Ac and tagged with a fluorophore via a DAinv reaction. The proximity of both fluorophores should then be determined by measuring FRET. A human gastric cancer cell line (MKN45) overexpressing ST6GalNAc1, which has been shown to possess significantly increased amounts of sialyl Tn on its cell surface,[531] was used. To assure that FRET arises from the proximity of GalNAc and Neu5Ac in sialyl Tn, an empty vector transfected cell line MKN45 Mock [531] was employed. A MKN45 cell line overexpressing the sialyltransferase ST3Gal4 served as additional control. The expression of ST3Gal4 in gastrointestinal cancer cells has been reported to be correlated with increased cell surface levels of sialyl Lewis x.[540,541] Besides this, it interferes with the overall glycosylation of cancer cells, for example by reducing the extension of *O*-glycans and increasing the branching of *N*-glycans.[542,543] GalNAc and Neu5Ac in *O*-glycans modified with sialyl Lewis x are not as close as in sialyl Tn and thus less FRET should be observed.

Data underlying Figure 4.32, Figure 4.33, Figure 4.34, and Figure 4.35 were obtained at i3S Porto in collaboration with Dr. Stefan Mereiter (group of Prof. Dr. Reis). Firstly, possible cytotoxic effects of the chemical reporters Ac_4GalNAz and Ac_4ManNCyoc on the MKN45 cell lines Mock, ST6GalNAc1, and ST3Gal4 were assessed by resazurin tests. Resazurin is the main component of the commercial AlamarBlue solution.[544,545] DMSO was used as solvent control. As cellular viabilities decreased only slightly upon reporter treatment (Figure 4.32), the highest tested concentration (200 µM) was used in further experiments. Interestingly, viabilities of ST3Gal4 cells decreased stronger than those of ST6GalNAc1 or Mock cells from 50 µM Ac_4GalNAz and Ac_4ManNCyoc onwards, but not for DMSO.

In a next step, labeling parameters for the SPAAC and DAinv reaction were optimized. For this purpose, all three MKN45 cell lines were treated with Ac_4GalNAz and Ac_4ManNCyoc or DMSO for 48 h. Subsequently, metabolized and incorporated chemical reporters on cell membranes were labeled with different concentrations of Alexa Fluor 488-DIBO and Cy3-Tz for 30 min or 25 µM of each fluorophore for different periods of time. The labeling efficiency

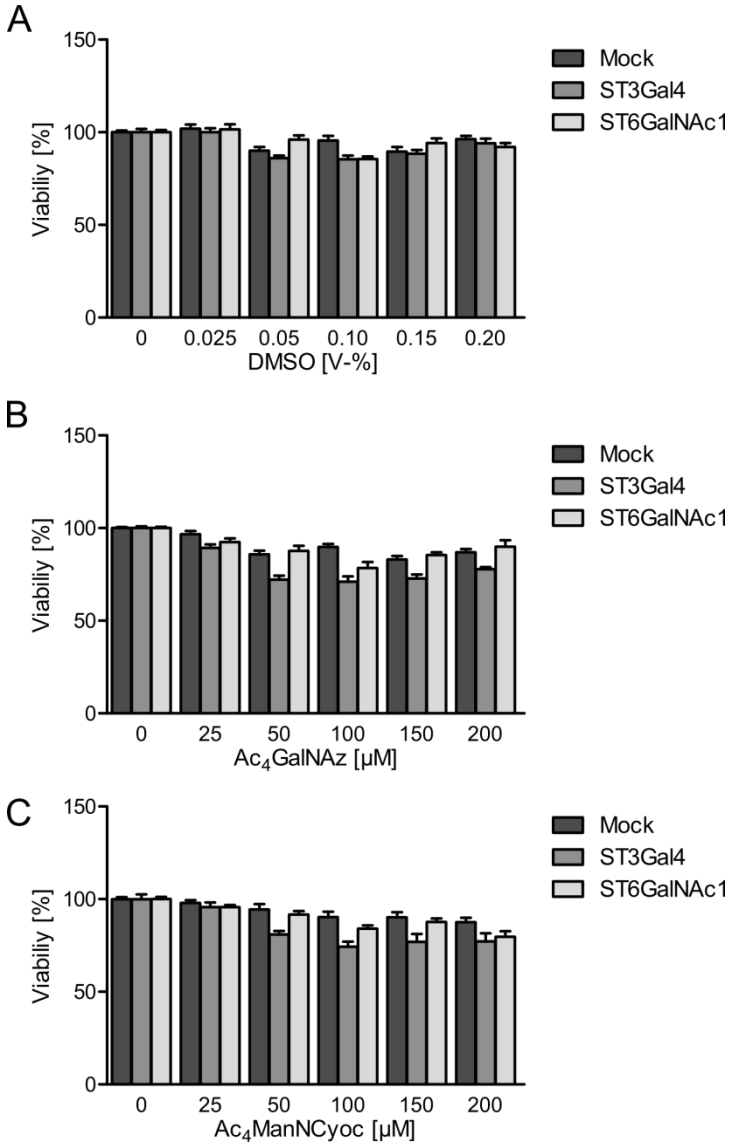

Figure 4.32: Effects of Ac_4GalNAz and Ac_4ManNCyoc on cellular viabilities of MKN45 cell lines. Viabilities of Mock, ST3Gal4, and ST6GalNAc1 cells treated with different concentrations of Ac_4GalNAz or Ac_4ManNCyoc for 48 h were assessed with resazurin tests. DMSO was used as solvent control. Columns correspond to mean values of three independent experiments performed in triplicates and error bars to SEMs.

was determined by confocal fluorescence microscopy. Representative images of ST6GalNAc1 cells are depicted in Figure 4.33. Fluorescence of Alexa Fluor 488 and Cy3 was detected on membranes of cells treated with both chemical reporters, but not on DMSO-treated cells. This leads to the conclusions that Ac_4GalNAz and Ac_4ManNCyoc were metabolized and incorporated in cell surface glycans and that both labeling reactions proceeded specifically. Highest fluorescence intensities were achieved with 25 µM Alexa Fluor 488-DIBO and Cy3-Tz and incubation times of 60 min. Nevertheless, 30 min were used in following studies, because these samples displayed far less in-cell fluorescence resulting from endocytosis of fluorescently labeled membrane structures than samples incubated for 60 min. Fluorescence intensities of Mock, ST6GalNAc1, and ST3Gal4 cells treated with

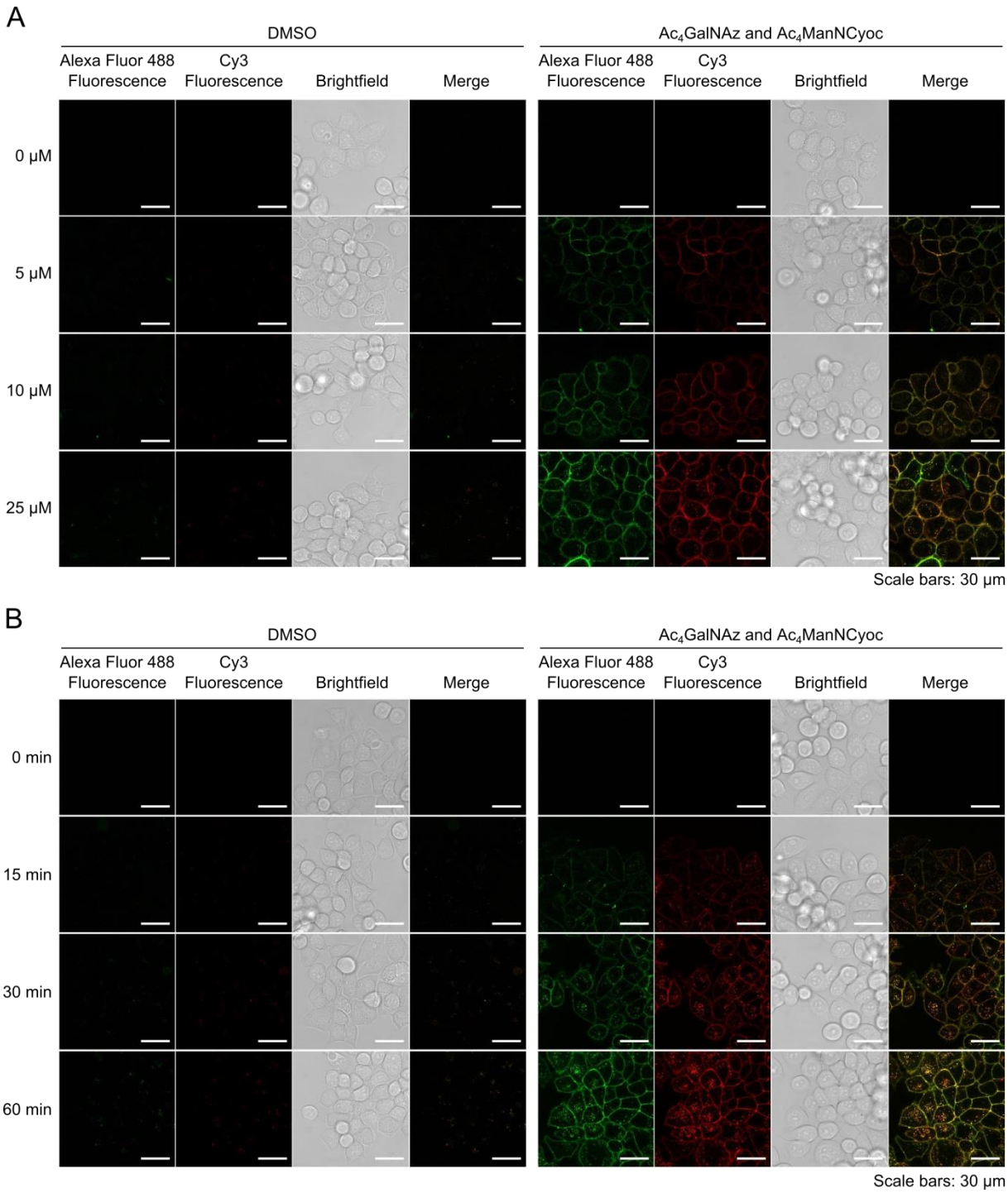

Figure 4.33: Optimization of dual labeling parameters. Representative confocal fluorescence and brightfield images of living ST6GalNAc1 cells treated with 200 µM Ac_4GalNAz and Ac_4ManNCyoc or 0.2 V-% DMSO for 48 h and subsequently labeled (A) with different concentrations of Alexa Fluor 488-DIBO and Cy3-Tz at 37 °C for 30 min or (B) with 25 µM Alexa Fluor 488-DIBO and Cy3-Tz at 37 °C for different times are displayed.

Ac_4GalNAz and Ac_4ManNCyoc were compared using optimized labeling parameters. Signals of ST3Gal4 cells were much stronger than those of Mock or ST6GalNAc1 cells (Figure 4.34). Thus, ST3Gal4 cells must have taken up more chemical reporters, metabolized or incorporated them more efficiently, or chemical handles of reporters present at cell surfaces

were better accessible for the ligation reactions. Higher cellular levels of chemical reporters in cells would explain the results from viability tests, which revealed smaller viabilities of ST3Gal4 cells than of the other two cell lines (Figure 4.32).

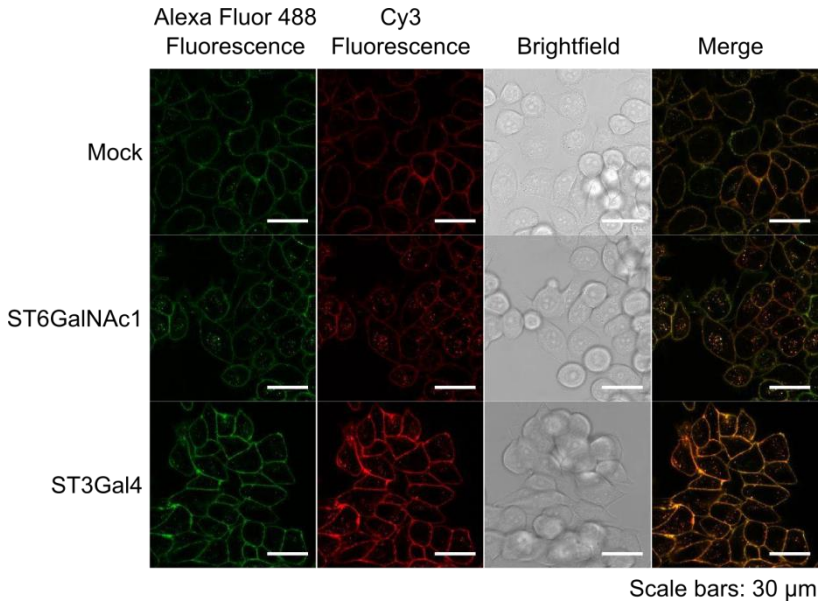

Figure 4.34: Comparison of fluorescence intensities of different cell lines. Mock, ST6GalNAc1, and ST3GalNAc4 cells were incubated with 200 µM Ac_4GalNAz and Ac_4ManNCyoc for 48 h and marked with 25 µM Alexa Fluor 488-DIBO and Cy3-Tz at 37 °C for 30 min. Representative confocal fluorescence and brightfield images are depicted.

To verify the overexpression of sialyl Tn in ST6GalNAc1 cells, they were treated with DMSO or Ac_4GalNAz and Ac_4ManNCyoc, dually labeled with Alexa Fluor 488-DIBO and Cy3-Tz, fixed, and immunostained with a primary anti-sialyl Tn and a secondary Alexa Fluor 647-tagged antibody. Fluorescences of Alexa Fluor 647, Alexa Fluor 488, or Cy3 were only detected on cell membranes, if anti-sialyl Tn antibodies, Ac_4GalNAz, or Ac_4ManNCyoc have been utilized, respectively (Figure 4.35). Treatment of cells with neuraminidase prior to immunostaining removed sialyl Tn and hence no fluorescence of Alexa Fluor 647 was present in these samples. This demonstrates that the antibody indeed binds to sialyl Tn located on cell surface glycoconjugates. Moreover, Mock cells treated with Ac_4GalNAz and Ac_4ManNCyoc, dually labeled via ligation reactions, and immunolabeled with antibodies showed fluorescence of Alexa Fluor 488 and Cy3, but not of Alexa Fluor 647. Consequently, Mock cells possessed far less sialyl Tn on cell surfaces than similarly treated ST6GalNAc1 cells, which proved that ST6GalNAc1 cells overexpress sialyl Tn and confirmed the suitability of Mock cells as control cell line for the planned FRET experiments.
In addition, the temporal course of the incorporation of Ac_4GalNAz and Ac_4ManNCyoc was studied. Mock, ST6GalNAc1, and ST3Gal4 cells were treated with both chemical reporters for different periods, dually labeled, and imaged on a confocal fluorescence microscope. As expected, cell membrane fluorescence intensities of both fluorophores increased with increasing incubation time (Figure 4.36A). The quantification of fluorescence intensities of Alexa Fluor 488, which reports on the incorporation of Ac_4GalNAz, and Cy3, which labels

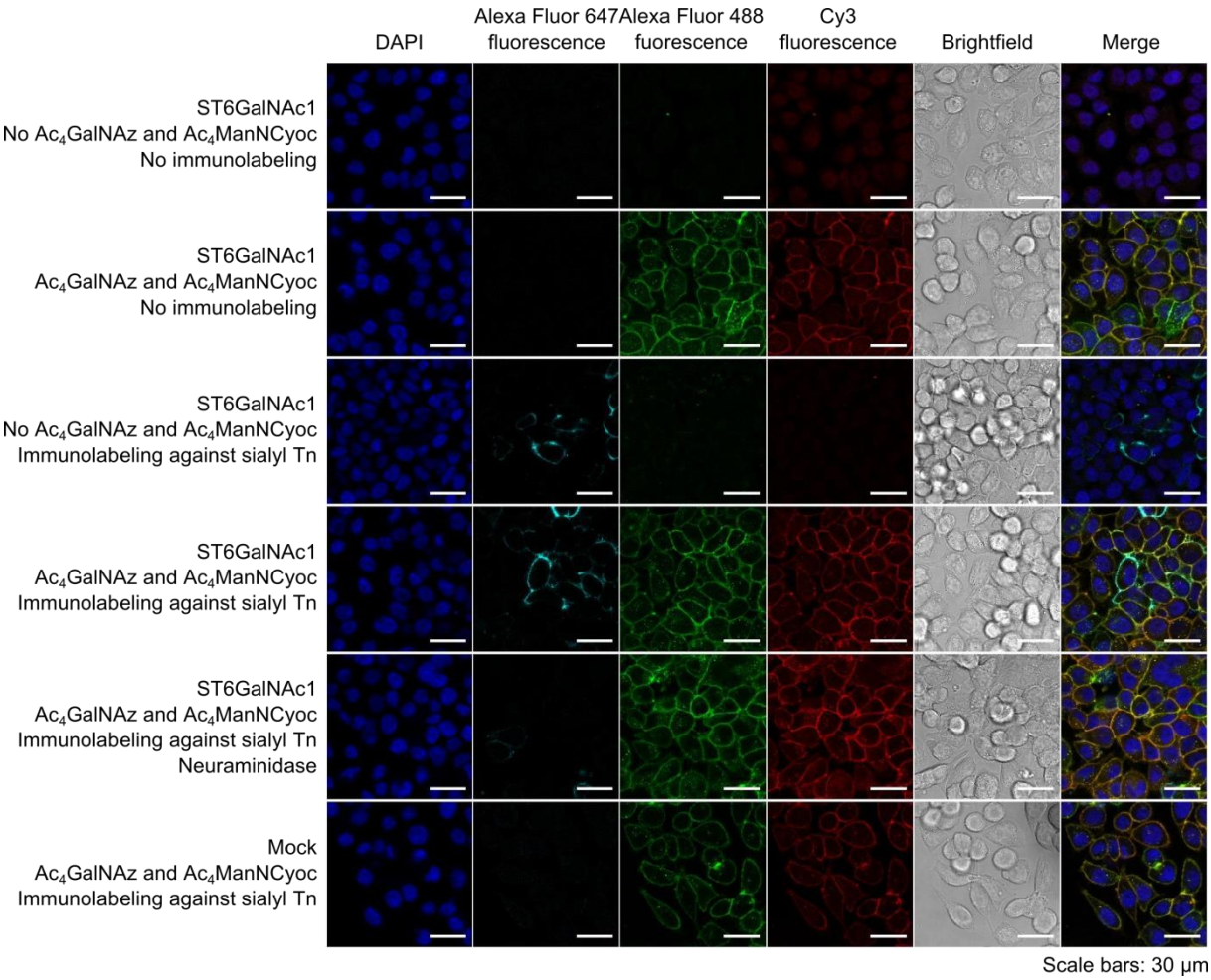

Figure 4.35: Demonstrating overexpression of sialyl Tn on ST6GalNAc1 cells. ST6GalNAc1 and Mock cells were treated with 200 µM Ac_4GalNAz and Ac_4ManNCyoc or 0.2 V-% DMSO for 48 h, labeled with 25 µM Alexa Fluor 488-DIBO and Cy3-Tz at 37 °C for 30 min, and fixed. Indicated samples were treated with 100 mUnits mL^{-1} neuraminidase in acetate buffer at 37 °C for 2 h. Immunolabeling was performed with a primary anti-sialyl Tn antibody and a secondary anti-mouse Alexa Fluor 647-tagged antibody. Nuclei of all samples were labeled with 4′,6-diamidino-2-phenylindole dihydrochloride (DAPI, 1:100 in PBS) for 5 min. Representative confocal fluorescence and brightfield images are shown.

metabolized Ac_4ManNCyoc, is shown in Figure 4.36B. Whereas fluorescence intensities of Alexa Fluor 488 increased until roughly 24 h and did not change considerably in the next 24 h, Cy3 intensities increased during the whole 48 h time course, although increases were less steep in the last 24 h. Hence, kinetics for the metabolism, incorporation, and removal of Ac_4GalNAz and Ac_4ManNCyoc are different. Since cells are not assumed to take up and incorporate all reporters present in the cell culture medium, incorporation of the artificial monosaccharide Ac_4GalNAz must have reached a saturation level after 24 h. For Ac_4ManNCyoc, no saturation was reached within 48 h. Again, higher fluorescence intensities were observable for ST3Gal4 cells in comparison with the other two MKN45 cell lines. This finding is in line with fluorescence microscopy data presented earlier (Figure 4.34).

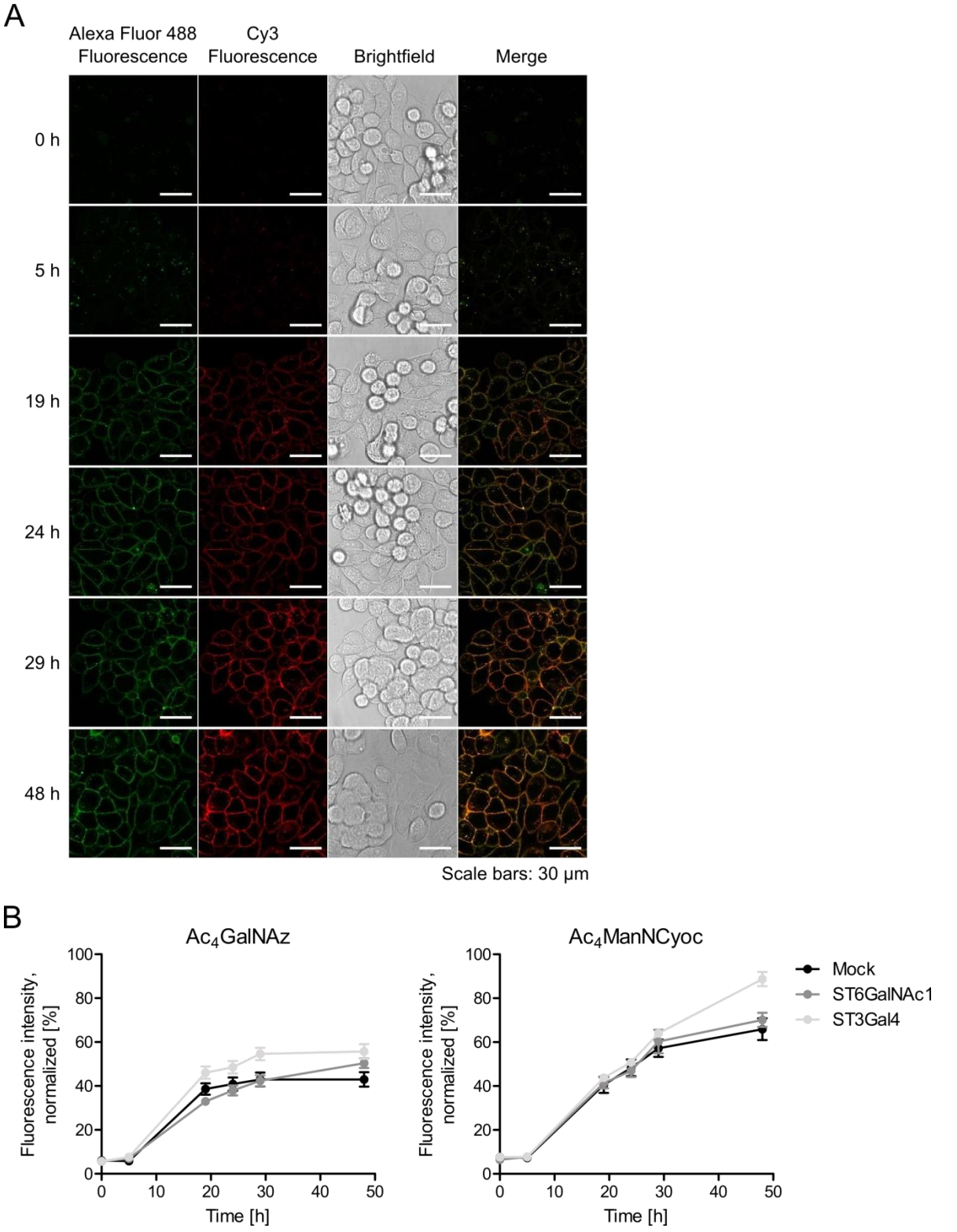

Figure 4.36: Time-dependent incorporation of Ac_4GalNAz and Ac_4ManNCyoc in membrane glycans. (A) Representative confocal fluorescence and brightfield images of living ST6GalNAc1 cells treated with 200 µM Ac_4GalNAz and Ac_4ManNCyoc for the indicated times and thereafter labeled with 25 µM Alexa Fluor 488-DIBO and Cy3-Tz at 37 °C for 30 min are presented. (B) Quantification of the time-dependent incorporation of Ac_4GalNAz and Ac_4ManNCyoc in membrane glycans. Normalized fluorescence intensities of Mock, ST6GalNAc1, and ST3Gal4 cells were plotted over time. Dots represent mean fluorescence intensities calculated from eleven images out of three independent experiments. Error bars are SEMs.

Finally, FLIM microscopy was performed to investigate whether FRET from fluorescently-tagged GalNAz to Neu5Cyoc occurs. Mock, ST6GalNAc1, and ST3Gal4 MKN45 cells were treated with both, one, or no chemical reporter for 48 h. Upon dual labeling, images of Alexa Fluor 488 fluorescence lifetimes were acquired. Nearly no fluorescence signals were detected for samples treated with no chemical reporter or only Ac_4ManNCyoc, but strong membrane fluorescence was observed for samples treated with Ac_4GalNAz or both sugars (Figure 4.37A+B). Fluorescence modulation and phase lifetimes of Alexa Fluor 488 decreased for all cell lines from approximately 3.7 ns and 3.2 ns (Ac_4GalNAz-treated cells) to roughly 3.0 ns and 2.4 ns (Ac_4GalNAz- and Ac_4ManNCyoc-treated cells), respectively. FRET efficiencies were calculated from averaged Alexa Fluor 488 fluorescence modulation lifetimes, phase lifetimes, and fluorescence intensities and are plotted in Figure 4.37C+D. Dissimilar FRET efficiencies for the same sample derived from fluorescence modulation and phase lifetimes are common, as they were calculated from different parameters and are only expected to be equal for monoexponential fluorescence decays.[292] Among the three cell lines, differences in FRET efficiencies determined from fluorescence lifetimes or intensities were not significant. As it was shown that ST6GalNAc1 cells possess much more sialyl Tn on their cell surface than Mock cells (Figure 4.35), the FLIM-FRET results revealed that the combination of chemical reporter strategies and FLIM-FRET microscopy was not appropriate to visualize the presence of this cancer epitope. FRET was detected to a similar extent in all cell lines. Several explanations for these findings can be considered: As all cell lines were gastric cancer cells and exhibit truncated *O*-glycans,[531,542,543] GalNAc and Neu5Ac derivatives in *O*-glycans could have been very close in all of them. In addition, detected FRET could have been of intramolecular and intermolecular origin. Since only averaged fluorescence lifetimes can be detected per pixel, a differentiation among subpopulations is not easily implementable. Moreover, also glycosphingolipids contain GalNAc and Neu5Ac in close proximity.[520] It is very likely that chemical reporters are also incorporated in these glycoconjugates. Hence, the background arising from intramolecular and intermolecular FRET between labeled GalNAc and Neu5Ac derivatives of other glycoproteins or glycosphingolipids could have been too high in order to detect signals belonging to sialyl Tn. Glycosphingolipids could be removed with endoglycoceramidases to assess FRET only arising from glycoproteins.[546] Additionally, *N*-glycans also containing Neu5Ac could be cleaved from proteins with PNGase F.[547,548] Furthermore, a non-cancer gastric cell line would be a more suitable control, as its *O*-glycans should not be truncated and thus GalNAc and Neu5Ac further apart from one another. These experiments are subject of further studies.

4.1.8. Conclusions

The aim of the first part of this thesis was the development of a novel method capable of imaging the glycosylation state of individual proteins inside living cells. The selected chemical reporter Ac_4GlcNCyoc was found to be enzymatically processed and at least to some extent incorporated as *O*-GlcNAc by OGT. OGA did not seem to be involved in the removal of incorporated Cyoc-derivatives. Using Ac_4GlcNCyoc, a FLIM-FRET-based approach for the visualization of protein-specific glycosylation inside living cells was

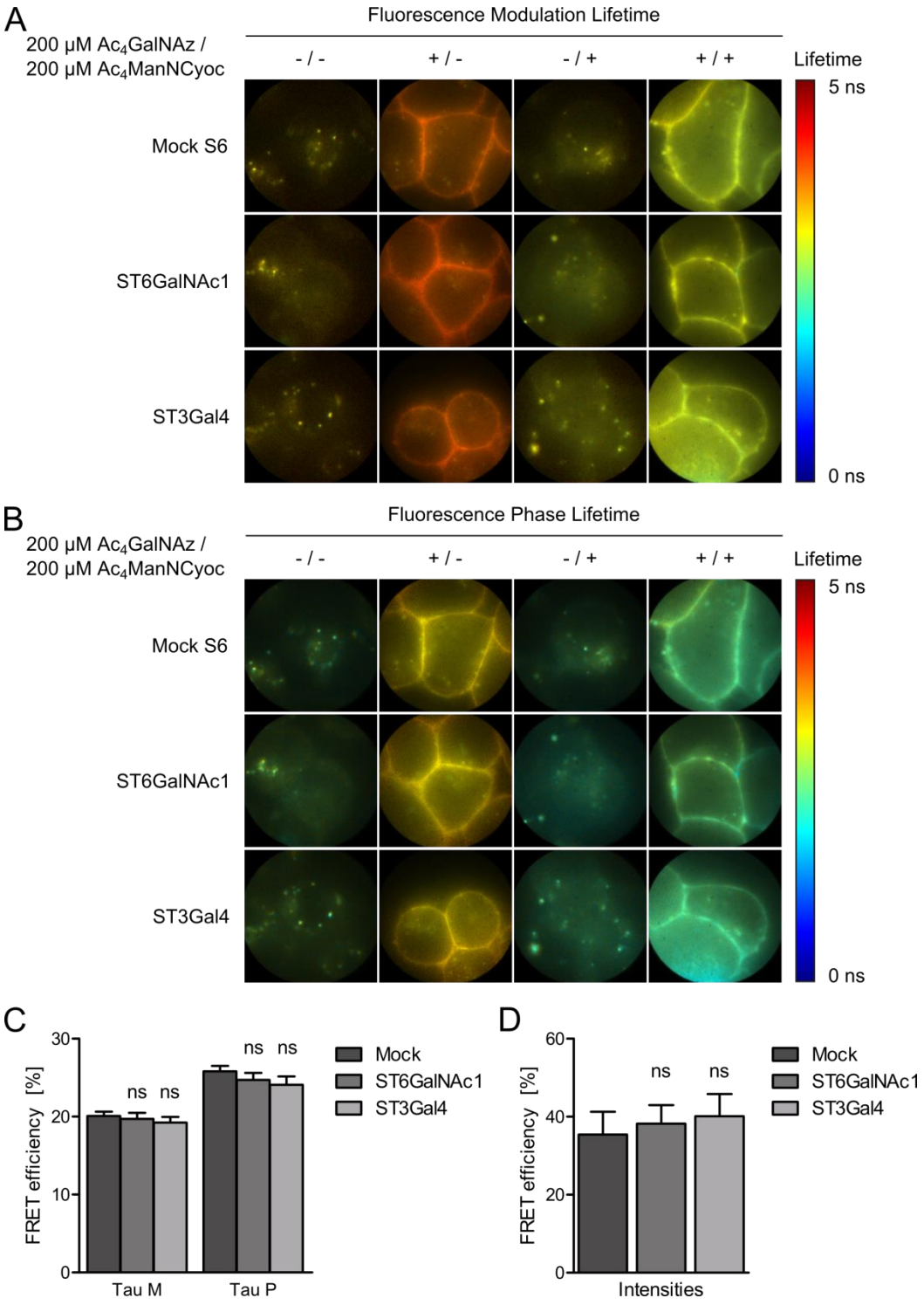

Figure 4.37: Detecting FRET from GalNAc-anchored Alexa Fluor 488 to Cy3-labeled sialic acids. (A+B) Representative intensity-weighted fluorescence modulation and phase lifetime images of living Mock, ST6GalNAc1, and ST3Gal4 cells treated with 200 µM Ac_4GalNAz and Ac_4ManNCyoc (+/+) and dually labeled with 25 µM Alexa Fluor 488-DIBO and Cy3-Tz at 37 °C for 30 min are depicted. Control samples received 0.2 V-% DMSO (-/-), Ac_4GalNAz and DMSO (+/-), or DMSO and Ac_4ManNCyoc (-/+). (C+D) FRET efficiencies were calculated (C) from fluorescence modulation (Tau M) and phase lifetimes (Tau P) or (D) from fluorescence intensities of Alexa Fluor 488 averaged over three independent experiments with 15 cells each. Columns correspond to mean values and error bars to SEMs. Statistical significance compared to Mock cells was assessed with (C) a two-way and (D) a one-way ANOVA followed by Bonferroni posttests. The degree of significance is ns $p>0.05$.

successfully developed. Its general applicability was demonstrated by imaging the glycosylation states of OGT, p53, Foxo1, and Akt1. For the latter protein, even a localization-dependent glycosylation pattern was detected, which can hardly be achieved using standard biochemical methods. The established approach thus is a valuable tool for studying intracellular protein glycosylation and allows experiments in living cells. However, it possesses some drawbacks, which emerged during attempts to examine the *O*-GlcNAcylation of selected proteins in detail. The EGFP-tag needs to be localized in close proximity to the glycosylation site of the protein of interest to enable the occurrence of efficient FRET. This was not the case for CAMK4-EGFP, whose modification with GlcNCyoc was proven upon immunoprecipitation, but could not be detected by FLIM microscopy. In addition, the method presented here is not suitable for the determination of a protein's modification, if only a small proportion of it becomes glycosylated. Hence, the modification of sparsely glycosylated α-synuclein with GlcNCyoc was not observed. Furthermore, Ac_4GlcNCyoc does not perfectly mimic native protein *O*-GlcNAcylation, as the dynamic *O*-GlcNAcylation at the N-terminal residues S23, T40, T41, and T112 of β-catenin could not be studied by FLIM-FRET microscopy.

Very recent work by the Chen group indicated that peracetylated unnatural monosaccharides are not completely deacetylated inside cells and attached to cysteine instead of serine and threonine residues.[549] Using mass spectrometry, they found that Ac_4GlcNAz, Ac_4GlcNAlk, and $Ac_3$6AzGlcNAc mainly and Ac_4GalNAz partially end up on cysteine residues. In contrast, the usage of deacetylated monosaccharides, as demonstrated for GalNAz, does not lead to artificial *S*-glycosylation. Although Chen and coworkers proposed that the *S*-glycosylation occurs non-enzymatic, data supporting this statement are missing. Whether Ac_4GlcNCyoc, which was not investigated in this report, might also be linked to cysteine residues, is an important question to be answered. Still, our experiments revealed Ac_4GlcNCyoc to be enzymatically attached to proteins and OGT to be involved into this process. Since the only known glycosylation type of all EGFP-fusion proteins studied is *O*-GlcNAcylation, it was assumed that this modification was imaged. To fully solve this issue, mass spectrometry analysis of proteins from Ac_4GlcNCyoc-treated cells would be required.

In *A. thaliana*, the incorporation of several chemical glycosylation reporters could be imaged by confocal fluorescence microscopy. Ac_4GlcNAz and to a lesser extent also Ac_4GalNAz were found to be attached to proteins, whereas Ac_4GlcNCyoc was not. Most likely, Ac_4GlcNCyoc is metabolized in a different way in plants than in mammalian cells and ends up in other glycoconjugates on cell membranes or cell walls.

The potential of metabolic glycoengineering as tool for investigating the presence of certain truncated *O*-glycans in cancer cells was explored. Although the proximity of GalNAc and Neu5Ac on cell membranes could be detected by FRET, measurements did not reveal any specificity for sialyl Tn. Nevertheless, the established dual labeling strategy with chemical glycosylation reporters in MKN45 cells turned out to be a valuable tool for the glycobiology in cancer research group.

4.2. Protein Acetylation

Having successfully developed an approach for protein-specific imaging of intracellular glycosylation/*O*-GlcNAcylation, a similar strategy was established for protein acetylation. In a first step, an appropriate chemical reporter was chosen and its applicability evaluated. Thereafter, FLIM-FRET microscopy was utilized to image protein-specific acetylation.

4.2.1. Evaluation of Na4P as Chemical Reporter for Protein Acetylation

Until now, four acetylation reporters have been developed, which were presented in chapter 2.2.2. All of them led to the modification of proteins with 4-pentynoyl or 4-pentenoyl groups that can be fluorescently labeled in a CuAAC or an oxidative Heck reaction, respectively.[157,200–202] Among the chemical reporters known, sodium 4-pentynoate (Na4P) has been shown to outperform the sugar derivative[201] and to be at least as useful as 4-pentenoyl-derivatives.[202] Thus, Na4P was assumed to be the most promising candidate for protein acetylation studies. It was prepared by treating 4-pentynoic acid with equimolar amounts of sodium hydroxide.

Firstly, HEK293T and HeLa S3 cells were treated with 10 mM Na4P for 8 h according to the protocol of Yang et al.[157] Control samples were treated with sodium acetate (NaOAc). Cells were lysed and the CuAAC performed with sulfo-Cy3-azide or TAMRA-azide using different CuAAC reaction mixtures. Proteins of some lysates were precipitated to remove excess dyes by washing. The fluorescence readout of Western blots of these lysates revealed that Na4P-treated samples did not display higher fluorescence intensities than corresponding NaOAc control samples (exemplary shown for HEK293T cells in Figure 4.38). Consequently, pentynoyl groups of Na4P were not attached to proteins or could not be labeled via the CuAAC. Still, these data demonstrated that surplus sulfo-Cy3-azide could be efficiently removed by precipitating proteins from lysates. Background fluorescence resulting from unspecific attachment of the fluorophore to proteins depended on the composition of the CuAAC reaction mixture. The first mixture utilizing $CuSO_4$, TBTA, and TCEP adopted from Yang et al. resulted in the highest fluorescence background. The second was a commercial kit supplemented with the fluorophore of choice. Barely any background was present in these samples, but it was too expensive to be used in further experiments. The third mixture was the one successfully applied to label GalNAz with Cy3-alkyne and led to only weak fluorescence background of precipitated samples. Hence, this CuAAC reaction mixture was used for further experiments. Sulfo-Cy3-azide was preferred over TAMRA-azide due to its better availability and reduced costs.

Biochemical experiments with Na4P-treated samples were performed with altered CuAAC reaction conditions and composition of CuAAC mixtures. However, no attempt resulted in higher fluorescence signals of Na4P-treated samples compared to control samples. This might be due to a very weak labeling of proteins with Na4P, which was already observed by others (Prof. Dr. Hang, Rockefeller University, New York, USA, personal communication). Probably the poor cellular permeability of Na4P could be the reason for the weak or non-existent fluorescence signals detected.

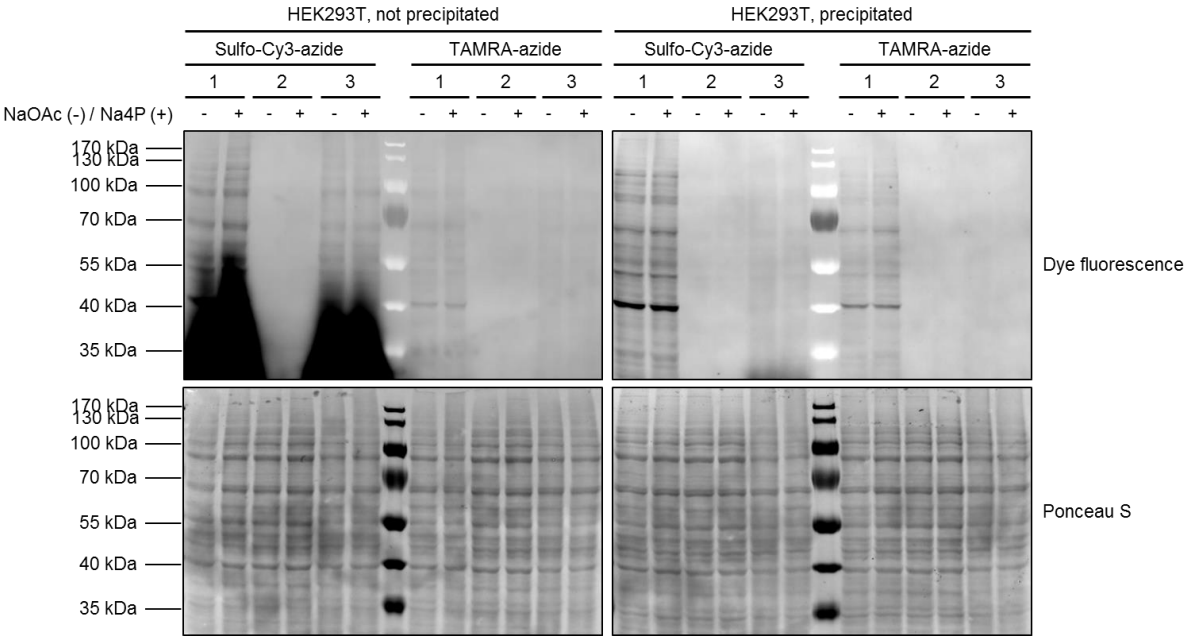

Figure 4.38: Attachment of Na4P's pentynoyl groups to proteins. Lysates of HEK293T cells treated with 10 mM NaOAc (-) or Na4P (+) for 8 h were labeled with sulfo-Cy3-azide or TAMRA-azide via a CuAAC, separated by SDS-PAGE, and analyzed on Western blots. Different CuAAC mixtures were tested (1: 1 mM $CuSO_4$, 100 µM TBTA, 1 mM TCEP, 100 µM dye-azide; 2: Click-iT Protein Reaction Buffer Kit with 40 µM dye-azide; 3: 500 µM $CuSO_4$, 500 µM THPTA, 5 mM sodium ascorbate, 50 µM dye-azide). Proteins of several samples were precipitated with methanol and chloroform to enable the removal of excess dyes by washing. Fluorescence of Cy3 and TAMRA was read out from Western blots to determine the modification of proteins with pentynoyl groups. Ponceau S staining served as loading control.

4.2.2. Synthesis of New Reporters for Protein Acetylation

Na4P is a salt and almost not cell permeable. Thus, esterification of 4-pentynoic acid might help the molecule to pass cellular membranes. Esters are assumed to be rapidly cleaved by non-specifically acting esterases in cells.[169] In order to develop possible alternative acetylation reporters, the methyl and acetoxymethyl esters of 4-pentynoic acid were synthesized. Methyl 4-pentynoate (M4P) was prepared according to a known procedure by treating 4-pentynoic acid with acetyl chloride in methanol (Figure 4.39A).[550] The synthesis of acetoxymethyl 4-pentynoate (AM4P) was based on a route reported for the synthesis of a malonylation reporter.[155] Thereto, 4-pentynoic acid was treated with *N*,*N*-diisopropylethylamine (DIPEA) and bromomethyl acetate (Figure 4.39B). The identity and purity of both products was proven by NMR spectroscopy.

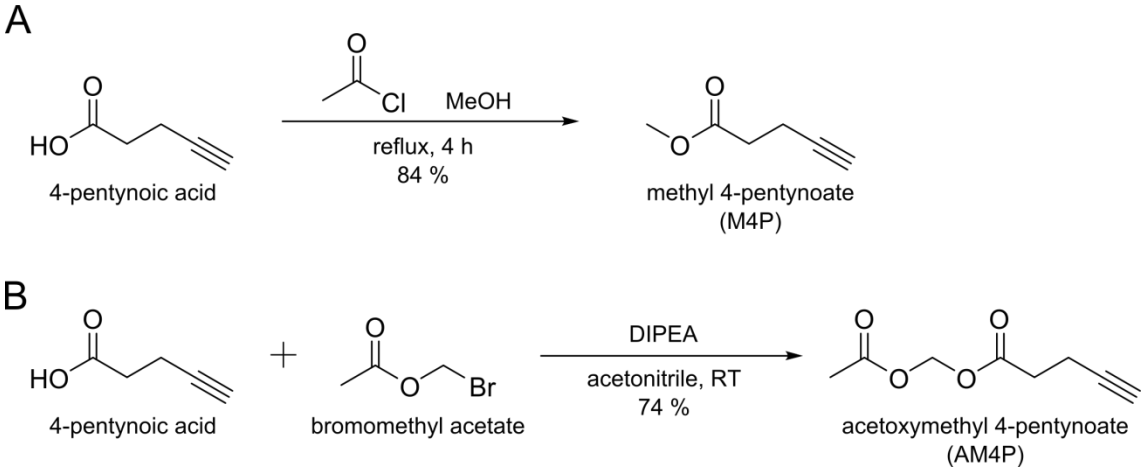

Figure 4.39: Synthetic routes to (A) M4P and (B) AM4P.

4.2.3. Biological Evaluation of Na4P, M4P, and AM4P

Before Na4P, M4P, or AM4P could be used in FLIM experiments, their incorporation in the cellular acetylome was studied. Many chemical reporters affect the integrity of cells. Thus, impacts of the three compounds on viabilities of HEK293T and HeLa S3 cells were assessed with resazurin assays. In addition, a mouse fibroblast cell line generated at New York University (NIH 3T3) was utilized, which has been reported to incorporate pentynoyl groups of Na4P strongest among several cell lines tested.[157] NaOAc served as control substance to account for effects arising from increased acetylation levels. Milli-Q (MQ) water and DMSO were used as solvent controls. NaOAc, Na4P, M4P, and both solvents did not affect cellular viabilities, but AM4P reduced them considerably (Figure 4.40). They dropped below 50 % for a concentration of 1 mM AM4P. As Na4P and AM4P only differ in the presence of the acetoxymethyl group, AM4P's toxicity must originate from the cleavage of the protecting group from AM4P by esterases, which most likely produces acetic acid and formaldehyde. Particularly the latter compound is cytotoxic,[551] which led to the conclusion that AM4P might not be a suitable acetylation reporter. Nevertheless, it was included in experiments presented in this chapter to investigate the attachment of its pentynoyl groups to proteins.
Next, CuAAC reaction conditions were further examined. To this end, a fluorescence assay based on the reaction of non-fluorescent 3-azido-7-hydroxycoumarin with an alkyne-tagged molecule to a fluorescent product was employed (Figure 4.41A).[552] Thereto, 50 µM NaOAc, Na4P, M4P, or AM4P, different CuAAC reaction mixtures, and 100 µM 3-azido-7-hydroxycoumarin were added to lysis buffer or lysates of HEK293T, HeLa S3, or NIH 3T3 cells. Whereas the first CuAAC mixture was prepared according to recommendations for an optimized CuAAC,[251] the second included four times more $CuSO_4$ and lacked aminoguanidine. The third reaction mixture was prepared according to Yang et al.[157] The progress of the CuAAC was monitored over time by measuring fluorescence intensities of the 1,2,3-triazole product. For Na4P, M4P, and AM4P, fluorescence increased strongest for CuAAC reaction mixture two (exemplarily shown for HEK293T cell lysates in Figure 4.41B), which was thus chosen for further experiments. Decreases in fluorescence intensities after approximately 50 min could be due to photobleaching of fluorophores. Among the chemical

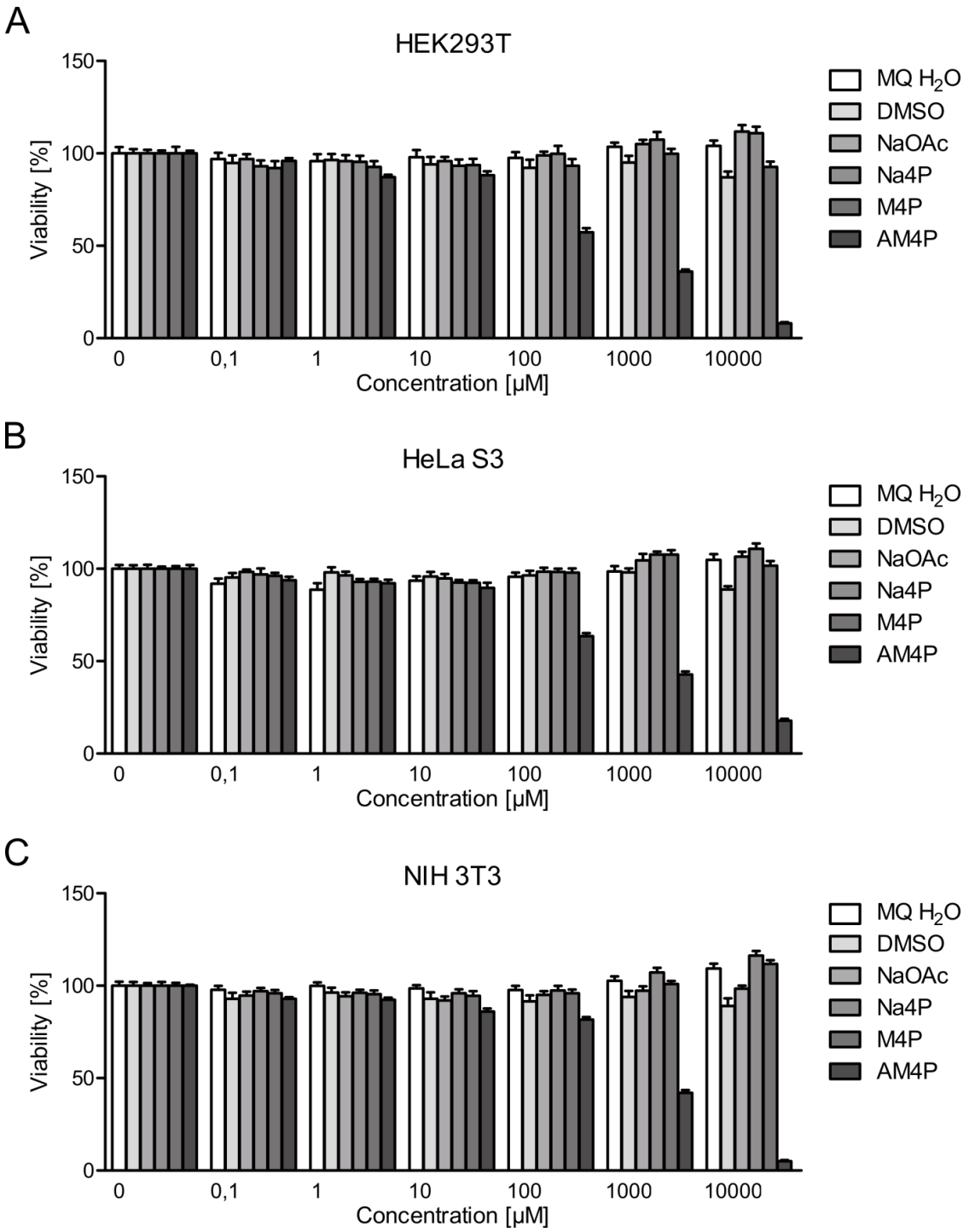

Figure 4.40: Investigation of possible cytotoxic effects of chemical acetylation reporters. Viabilities of HEK293T, HeLa S3, and NIH 3T3 cells treated with up to 10 mM NaOAc, Na4P, M4P, or AM4P for 8 h were assessed with AlamarBlue assays. 0 to 3 V-% MQ water or DMSO were used as solvent controls. Columns represent mean values from three independent experiments performed in quadruplicates. Error bars are SEMs.

reporters tested, Na4P performed best. For NaOAc, no increase of fluorescence intensities occurred over time, which states that 3-azido-7-hydroxycoumarin requires the reaction with alkynes to form the fluorescent product.

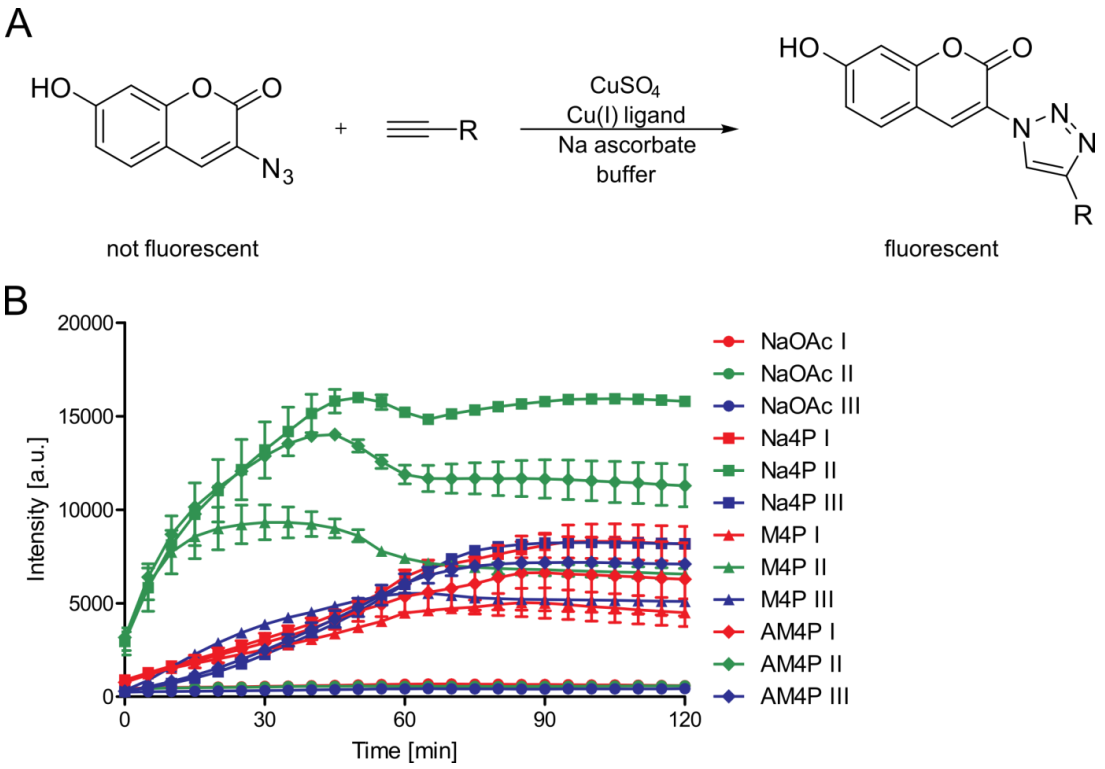

Figure 4.41: Optimizing CuAAC parameters by means of a fluorogenic plate assay. (A) The non-fluorescent 3-azido-7-hydroxycoumarin reacts with an alkyne in a CuAAC to a fluorescent product. (B) HEK293T cell lysates with a final protein concentration of 2 mg mL^{-1} were treated with 50 µM NaOAc, Na4P, M4P, or AM4P, 100 µM 3-azido-7-hydroxycoumarin, and different CuAAC reaction mixtures (I: 250 µM $CuSO_4$, 1.25 mM THPTA, 5 mM aminoguanidine, 5 mM sodium ascorbate; II: 1 mM $CuSO_4$, 1.25 mM THPTA, 5 mM sodium ascorbate; III: 1 mM $CuSO_4$, 100 µM TBTA, 1 mM TCEP) in wells of a 96-well plate. Fluorescence upon excitation of samples with light from a lamp passing a 360/40 nm bandpass filter was detected behind a 460/60 nm emission filter with the microplate reader Synergy HT. Samples were kept at 37 °C throughout the measurements. Dots are mean values of three independent experiments performed in technical quadruplicates and error bars are SEMs.

To test whether the new potential acetylation reporters result in better availability of 4-pentynoate in cells and thus higher incorporation rates, HEK293T, HeLa S3, and NIH 3T3 cells were treated with NaOAc, Na4P, M4P, or AM4P, lysed, and transferred pentynoyl groups were marked with sulfo-Cy3-azide. Fluorescence readouts of Western blots from these lysates unambiguously demonstrate strong signals for AM4P-treated, but no signals higher than those of NaOAc for Na4P- or M4P-treated samples (Figure 4.42). In accordance with above presented results, precipitation and washing of proteins upon CuAAC removed excess fluorophores. Amounts of proteins loaded were much lower in case of AM4P samples than for other samples, which can be attributed to the toxicity of AM4P. Similar to the Western blot experiments, confocal fluorescence microscopy of reporter-treated, fixed, permeabilized, and sulfo-Cy3-labeled HEK293T, HeLa S3, and NIH 3T3 was performed. As shown in Figure 4.43 for HEK293T cells, stronger Cy3 fluorescence than background fluorescence was detected solely for cells treated with 1 mM AM4P. Alongside with higher fluorescence intensities, the number of cells present in microscopy chambers reduced notably. Taken

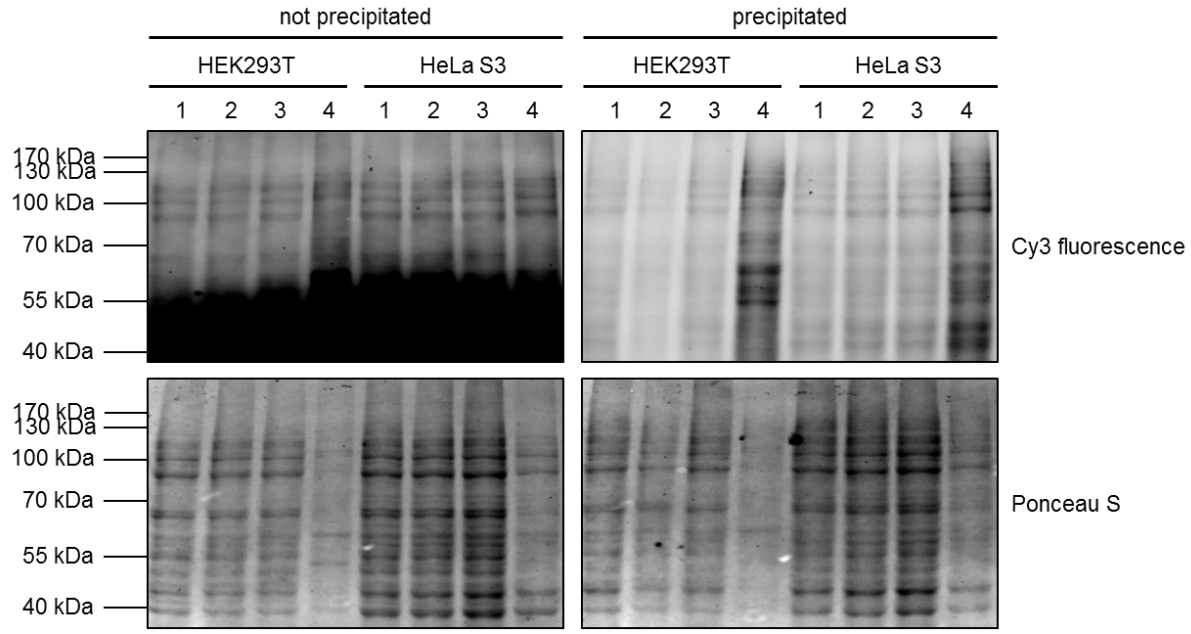

Figure 4.42: Attachment of pentynoyl groups of AM4P to proteins. Lysates of HEK293T and HeLa S3 cells treated with 5 mM NaOAc (1), Na4P (2), M4P (3), or AM4P (4) for 6 h were labeled with 100 µM sulfo-Cy3-azide via a CuAAC for 90 min. Cy3 fluorescence was read out from Western blots to assess the incorporation of the chemical reporters. Amounts of loaded proteins were defined with Ponceau S staining.

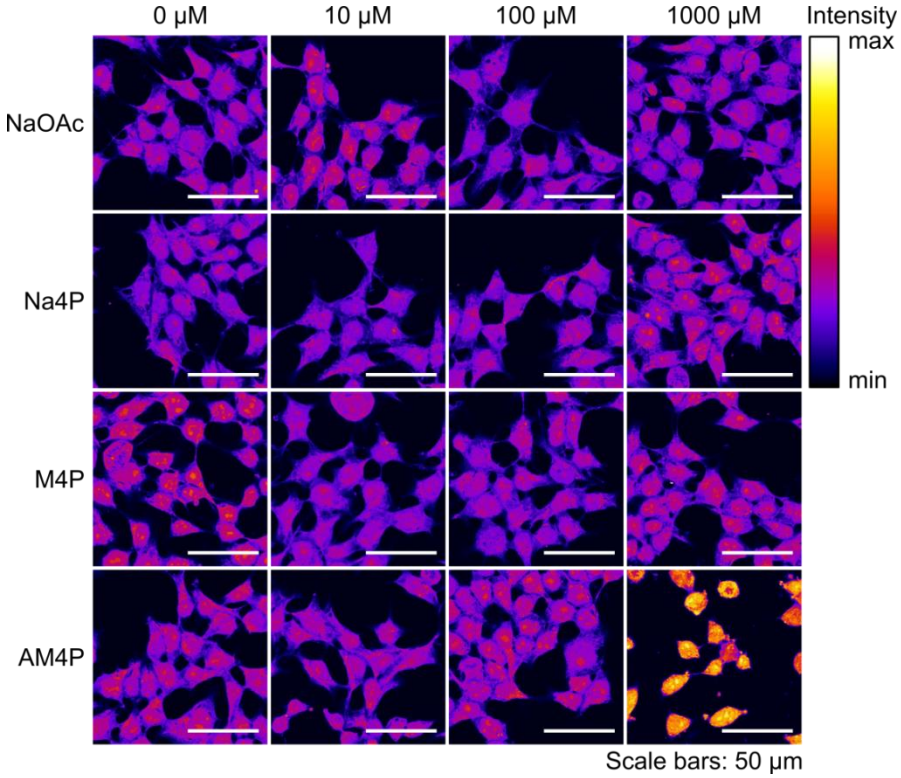

Figure 4.43: Detection of pentynoyl groups in cells by fluorescence microscopy. Representative confocal fluorescence microscopy images of HEK293T cells treated with up to 1 mM NaOAc, Na4P, M4P, or AM4P for 8 h, fixed, permeabilized, and labeled with 10 µM sulfo-Cy3-azide in a CuAAC for 60 min are depicted.

together, the microscopy and Western blot data revealed that AM4P entered cells and its alkyne moiety was attached to proteins, which could not be observed for Na4P and M4P. Consequently, AM4P was chosen for further studies at that moment.
For Western blot experiments, 100 µM sulfo-Cy3-azide were used and the reaction was allowed to proceed for 90 min. As both the concentration of the fluorophore and the

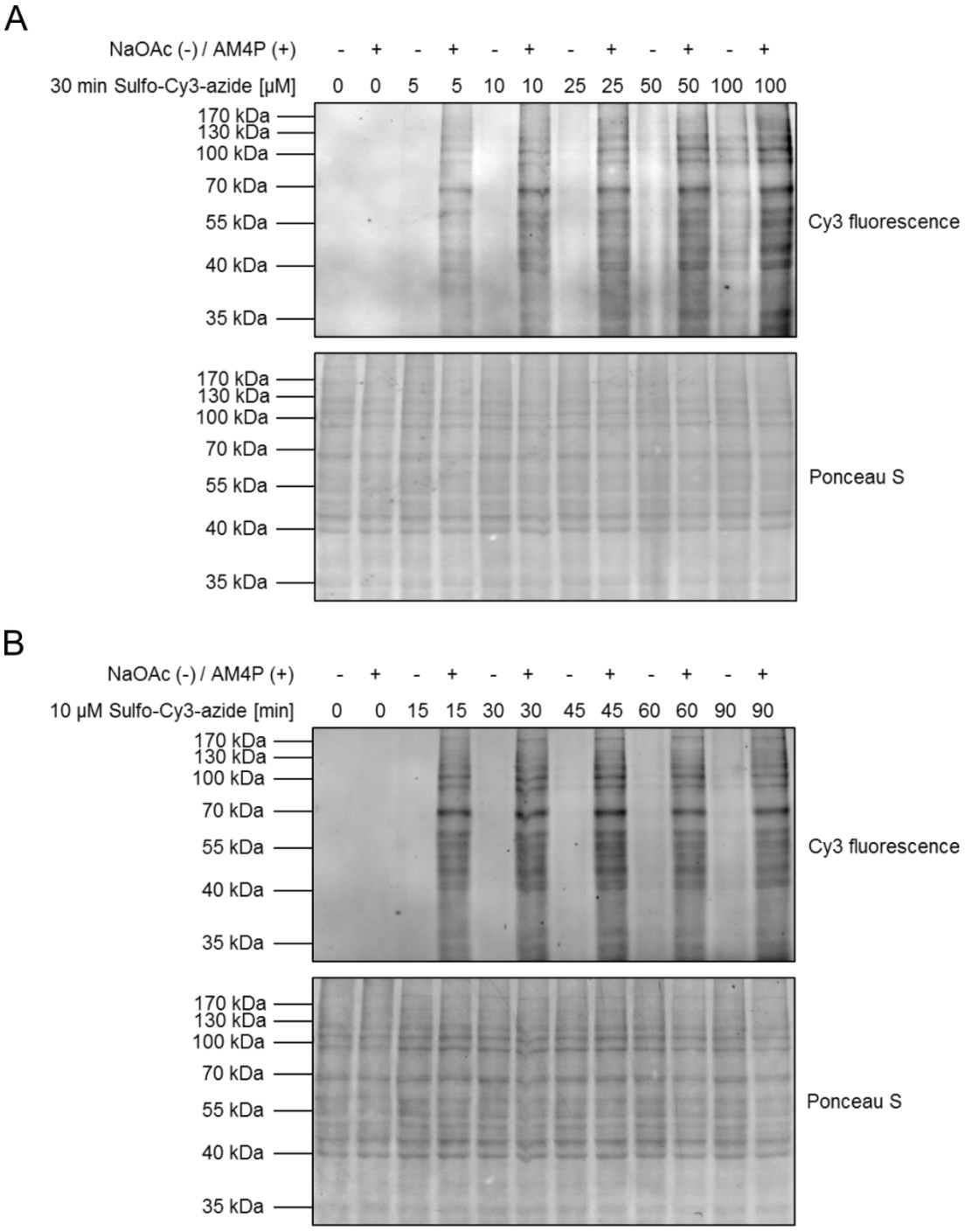

Figure 4.44: Optimizing CuAAC labeling parameters for lysate experiments. Fluorescence readouts of Western blots from lysates of HEK293T cells treated with 1 mM NaOAc or AM4P and labeled (A) with different concentrations of sulfo-Cy3-azide for 30 min or (B) with 10 µM sulfo-Cy3-azide for different durations are depicted. Equal loading of samples was assessed by staining of proteins with Ponceau S.

incubation time were relatively high and might increase unspecific attachments of sulfo-Cy3 to proteins resulting in background fluorescence, alterations of these parameters were studied. For this purpose, lysates of HEK293T cells treated with 1 mM NaOAc or AM4P were incubated with different concentrations of sulfo-Cy3-azide in the CuAAC mixture for 30 min. Fluorescence of Cy3 detected in AM4P-treated samples was sufficient from 10 µM onwards, but fluorescence detected for NaOAc-treated samples increase at higher concentrations (Figure 4.44A). Hence, 10 µM sulfo-Cy3-azide were used to assess the influence of the CuAAC reaction time on the fluorescence readout. As depicted in Figure 4.44B, Cy3 signals for AM4P-treated samples did not vary much for different incubation times. Background fluorescence of NaOAc samples increased slightly for longer reaction times. A duration of the CuAAC of 15 min was chosen for subsequent experiments.

CuAAC reaction parameters were adjusted for fluorescence microscopy studies in a similar manner. HEK293T cells treated with 1 mM NaOAc or AM4P were fixed, permeabilized, and incubated with the CuAAC mixture supplemented with different concentrations of sulfo-Cy3-azide for 30 min or 10 µM of the dye for different time spans. Cy3 fluorescence of AM4P-treated samples as well as unspecific background signals of NaOAc samples increased with increasing sulfo-Cy3-azide concentration and incubation time (Figure 4.45). A sulfo-Cy3-azide concentration of 10 µM and a CuAAC reaction time of 15 min were considered to be optimal, since ratios of fluorescence intensities detected for AM4P and NaOAc samples were highest for these cells.

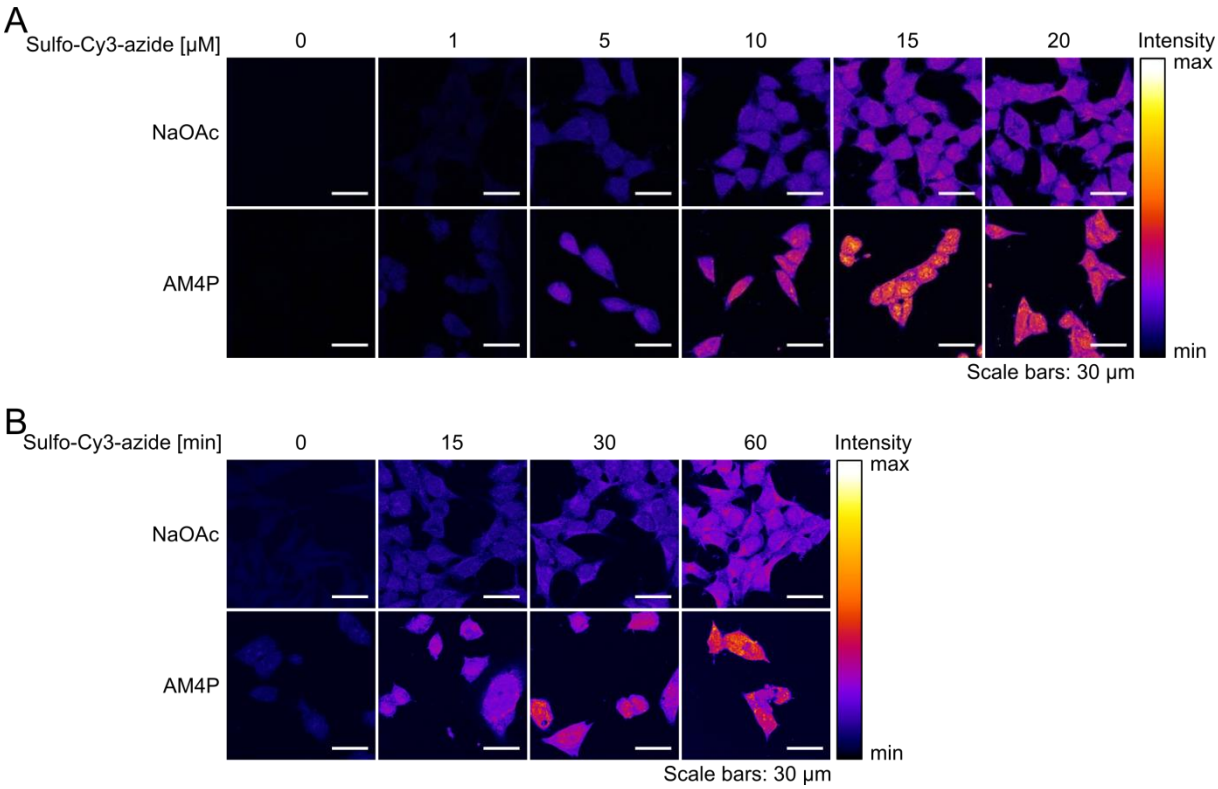

Figure 4.45: Optimizing CuAAC labeling parameters for microscopy. Representative confocal fluorescence images of HEK293T cells treated with 1 mM NaOAc or Na4P for 8 h, fixed, permeabilized, and labeled (A) with different concentrations of sulfo-Cy3-azide for 30 min or (B) with 10 µM sulfo-Cy3-azide for different periods of time are presented.

In a next step, it was investigated whether optimized CuAAC parameters allowed for the observation of the attachment of pentynoyl groups from Na4P and M4P to proteins, too. HEK293T, HeLa S3, and NIH 3T3 cells were treated with up to 10 mM Na4P, 10 mM M4P, or 1 mM AM4P for 8 h, lysed, and labeled with sulfo-Cy3-azide in a CuAAC. Indeed, Cy3 signals stronger than the fluorescence background of samples not treated with any chemical reporter were measured for Na4P, M4P, and AM4P (exemplarily displayed for HEK293T cells in Figure 4.46A). Signals increased with increasing reporter concentration and were much higher for M4P and AM4P than for Na4P. Furthermore, the time-dependent incorporation of the chemical reporters in HEK293T, HeLa S3, and NIH 3T3 cells was

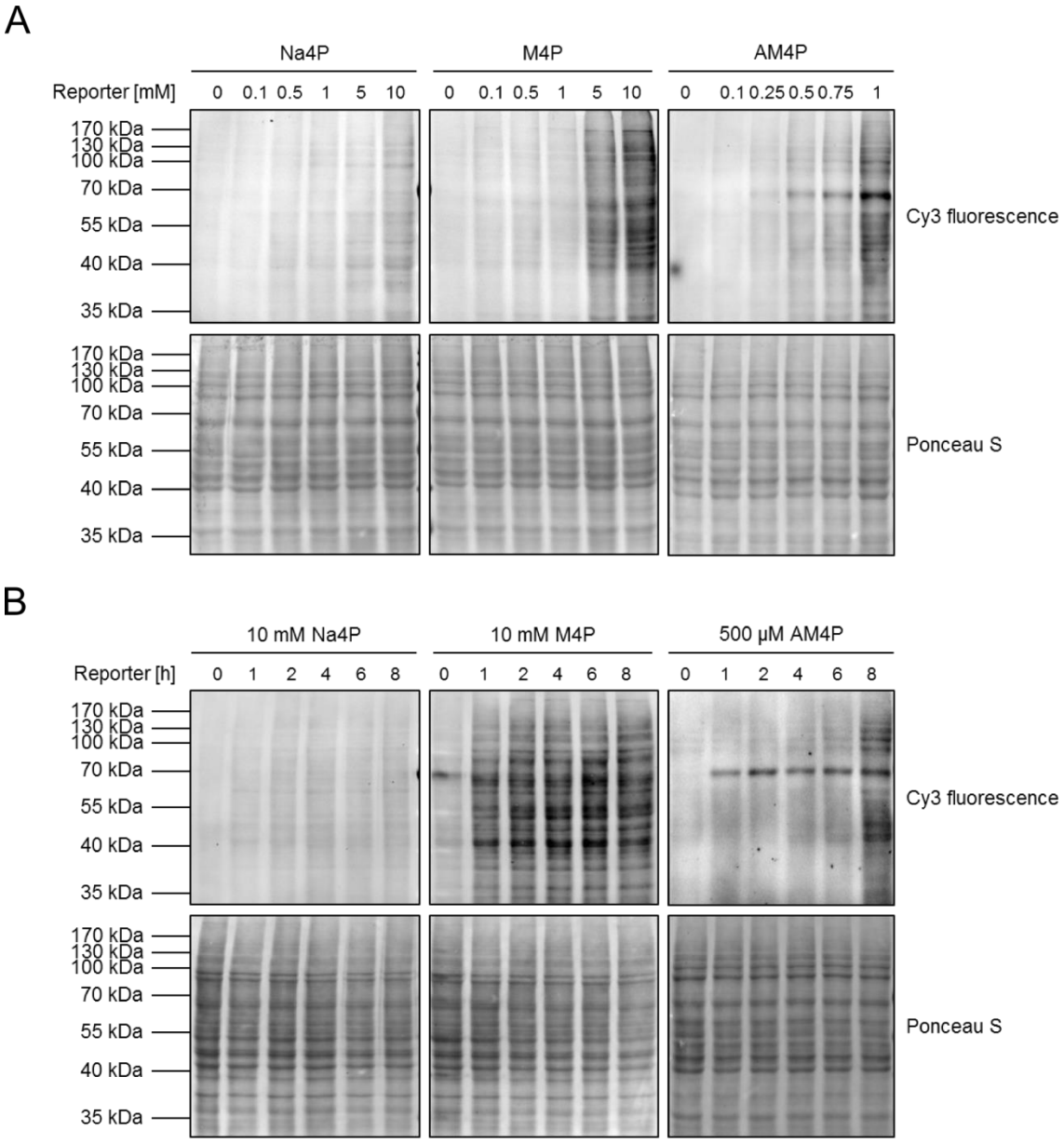

Figure 4.46: Concentration- and time-dependent incorporation of acetylation reporters. HEK293T cells were treated (A) with different concentrations of Na4P, M4P, or AM4P for 8 h or (B) with 10 mM Na4P, 10 mM M4P, or 500 µM AM4P for different periods of time. Cells were lysed and transferred 4-pentynoyl groups were marked with sulfo-Cy3-adzie in a CuAAC. Fluorescence of Cy3 was read out from Western blots. Ponceau S staining served as loading control.

examined. Concentrations of 10 mM were selected for Na4P and M4P, but due to its high cytotoxicity only 500 µM AM4P were utilized. Fluorescence readouts from Western blots of sulfo-Cy3-marked cell lysates revealed a time-dependence of sulfo-Cy3 fluorescence for AM4P, but not for Na4P and M4P (Figure 4.46B). Interestingly, a prominent fluorescent band was visible in AM4P samples at early time points, but strong signals from many proteins were only present after an incubation time of 8 h. As all three reporters are assumed to end up as 4-pentynoate in cells, which then is modified with CoA in order to be transferred to proteins by acetyltransferases, it was quite surprising that AM4P behaved differently. This might be caused by its cytotoxicity or different processing by cellular esterases in comparison to M4P. Since Na4P and M4P did not affect cellular viabilities, it was decided to keep the incubation time of 8 h in order to maximize Cy3 signals for AM4P.
Using optimal concentrations and incubation times of the chemical reporters, their effects on viabilities of HEK293T, HeLa S3, and NIH 3T3 cells were assessed by viability assays. Solely AM4P was cytotoxic and reduced cellular viabilities at 500 µM to approximately 40 % (Figure 4.47). A further decrease of the AM4P concentration was not reasonable, as this would reduce the attachment of its pentynoyl groups to proteins.

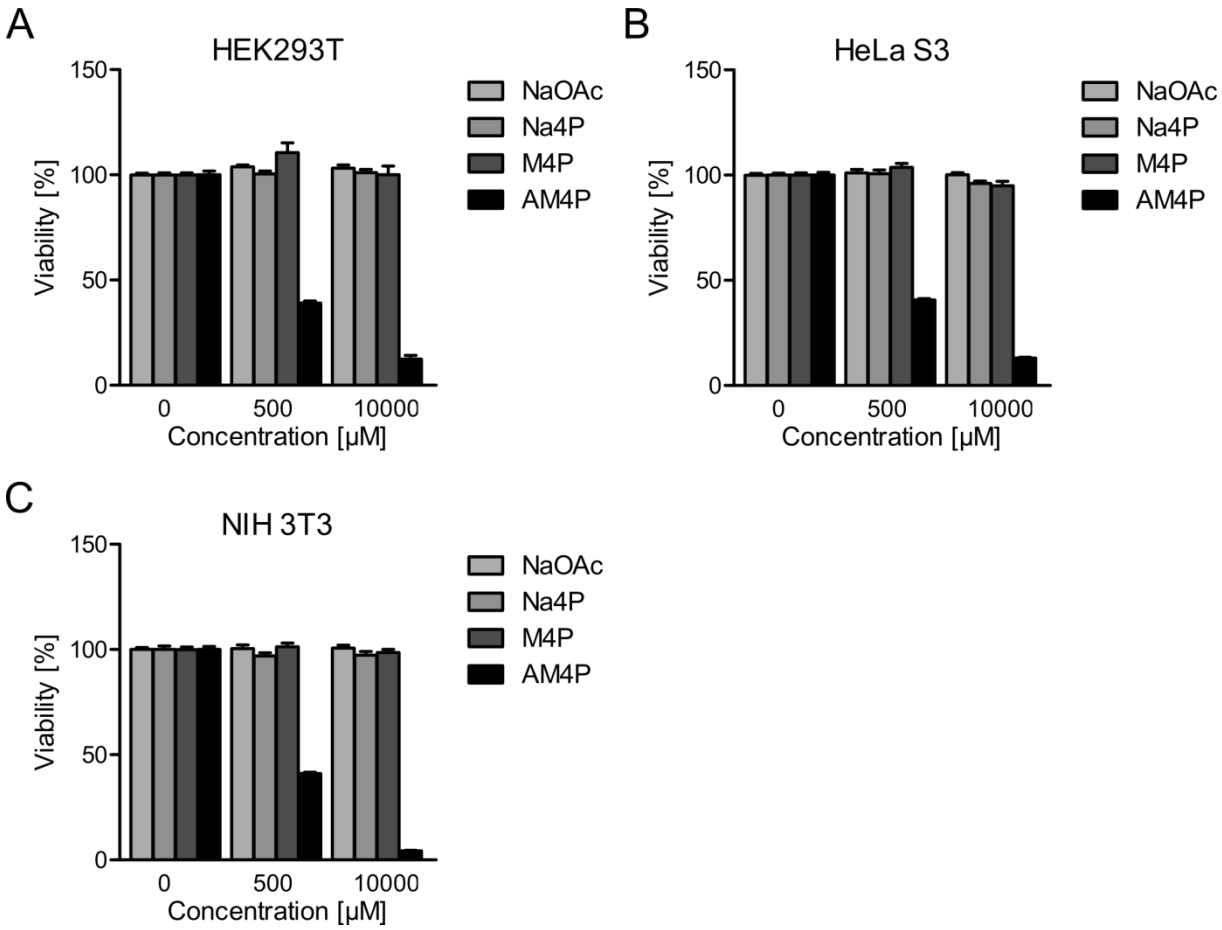

Figure 4.47: Comparison of cellular viabilities after treatment with acetylation reporters. Viabilities of HEK293T, HeLa S3, and NIH 3T3 cells treated with 0 µM, 500 µM, or 10 mM NaOAc, Na4P, M4P, or AM4P for 8 h were assessed with AlamarBlue assays. Columns represent mean values from three biologically independent experiments performed in technical quadruplicates. Error bars are SEMs.

To directly compare the incorporation efficiencies of pentynoyl groups from the three different reporters, Western blot and confocal fluorescence microscopy experiments were carried out at optimal concentrations and incubation times. Cy3 fluorescence detected on Western blots of HEK293T and HeLa S3 cells revealed labeling of proteins resulting from 500 µM AM4P, 10 mM Na4P, and 10 mM M4P (Figure 4.48). Among these three samples, signals of M4P were brightest. In contrast to HEK293T and HeLa S3 cells, lysates of NIH 3T3 cells showed strong Cy3 fluorescences of Na4P-treated samples. Fluorescence intensities of the Na4P-treated sample were even higher than that of the AM4P-treated one at 500 µM. Comparable results were achieved with confocal fluorescence microscopy (Figure 4.49). Quantification of single cell fluorescence intensities showed signals higher than the background of NaOAc samples for 500 µM AM4P and 10 mM M4P in HEK293T cells, for 10 mM M4P in HeLa S3 cells, and for 500 µM and 10 mM Na4P, 500 µM AM4P, and 10 mM M4P in NIH 3T3 cells. Thus, M4P was the only reporter applicable in all cell lines.
Fluorescence intensities of Cy3-tagged pentynoyl groups measured in NIH 3T3 cell lysates and fixed cells differed from those of the other cell lines. For Na4P-treated cells, the accumulation of Cy3 in cytoplasmic structures was observed by fluorescence microcopy. To elucidate in which cellular compartments Na4P accumulated, green fluorescent trackers for the endoplasmic reticulum, lysosomes, and mitochondria were utilized. They nicely stained the respective cellular organelle in living NIH 3T3 cells, but were not retained after fixation and permeabilization. Hence, colocalization with alkyne-tagged molecules, which can only be fluorescently labeled upon permeabilization of cells, could not be achieved. Still, the comparison of labeling patterns from tracker dyes and Cy3-labed 4-pentynoyl groups/

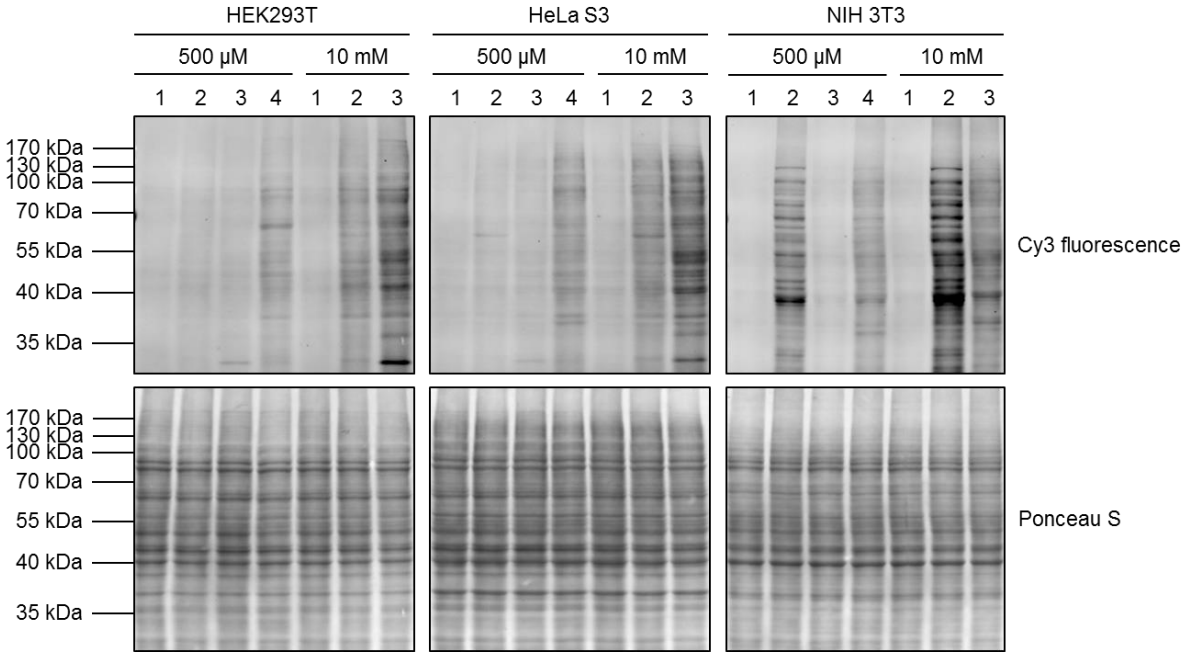

Figure 4.48: Direct comparison of acetylation reporters on Western blots. HEK293T, HeLa S3, and NIH 3T3 cells were incubated in presence of 500 µM or 10 mM NaOAc (1), Na4P (2), M4P (3), or AM4P (4) for 8 h, lysed, and tagged with sulfo-Cy3-azide. Fluorescence of Cy3 was read out from Western blots to determine the modification of proteins with pentynoyl groups. Equal loading of lysate samples was confirmed by Ponceau S staining.

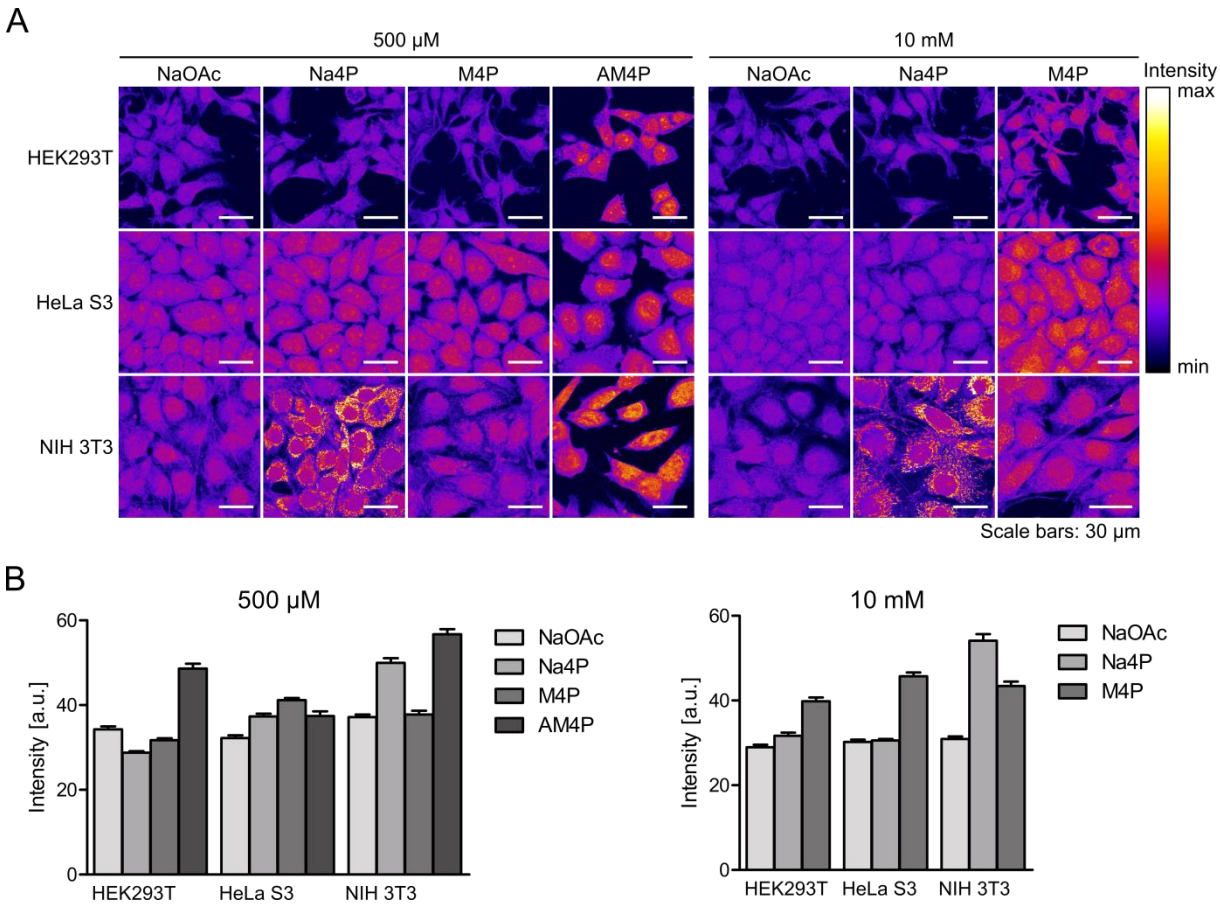

Figure 4.49: Direct comparison of Cy3-fluorescence arising from incorporated acetylation reporters by fluorescence microscopy. (A) Representative confocal fluorescence microscopy images of HEK293T, HeLa S3, and NIH 3T3 cells treated with 500 µM or 10 mM NaOAc, Na4P, M4P, or AM4P for 8 h, fixed, permeabilized, and reacted with sulfo-Cy3-azide in a CuAAC are depicted. (B) Fluorescence intensities of single cells were quantified for five cells per image from two independent experiments with four images taken each. Columns are mean values and error bars SEMs.

4-pentynoate suggested these structures to be mitochondria (Figure 4.50). As non-enzymatic protein acetylation of lysine ε-amino groups occurs in mitochondria frequently,[98,99] it is very likely that this was also the case for modifications of proteins with pentynoyl groups from Na4P. The reason why this reporter and not M4P or AM4P accumulated in mitochondria is not yet clear. To enable colocalization studies, GFP-fusion proteins solely localized in mitochondria could be employed. Based on their changed processing of chemical acetylation reporters, NIH 3T3 cells were no longer used in acetylation studies.

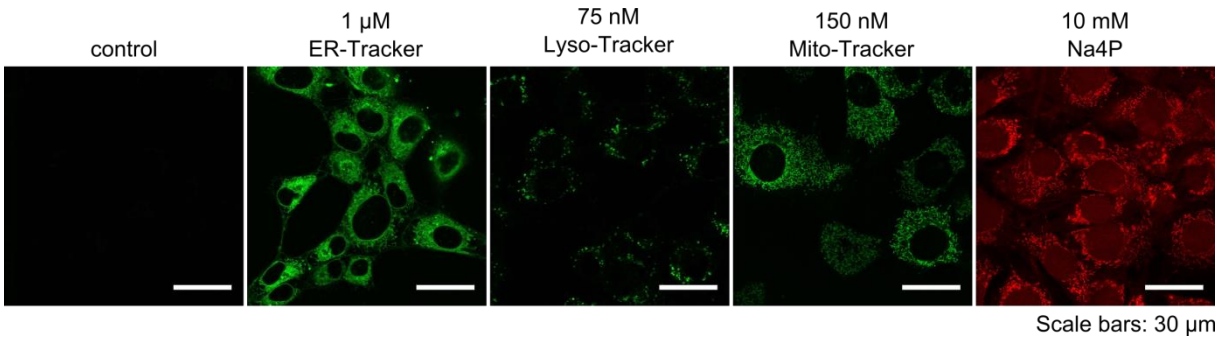

Figure 4.50: Accumulation of Na4P in mitochondria of NIH 3T3 cells. Confocal fluorescence microscopy images of differently treated NIH 3T3 cells are displayed. Control cells were not treated at all. Trackers were added at the indicated concentrations to cells for 5 min (Lyso-Tracker) or 30 min (ER- and Mito-Tracker). Cells presented in the last image on the right side were treated with 10 mM Na4P for 8 h. Only these cells were fixed, permeabilized, and labeled with sulfo-Cy3-azide via a CuAAC.

A suitable chemical acetylation reporter needs to behave similarly to native protein acetylation precursors. To test if this is the case for Na4P, M4P, and AM4P, cellular acetylation levels were varied by using chemical inhibitors. A commercial deacetylation inhibition cocktail known to effectively inhibit histone deacetylases and sirtuins as well as curcumin, which inhibits histone acetyltransferases,[553,554] were used. These inhibitors should elevate and reduce cellular acetylation levels, respectively. HEK293T and HeLa S3 cells were treated with the inhibitors and NaOAc, Na4P, M4P, or AM4P, lysed, and labeled with sulfo-Cy3-azide. Control cells did not receive any inhibitor, but were also treated with one of the chemical reporters. Immunoblotting of these samples against acetyllysine proved that deacetylase inhibitors increased cellular acetylation levels (Figure 4.51). A clear effect resulting from the treatment with curcumin could not be observed. Curcumin concentrations and pre-incubation times were altered in subsequent experiments, but this did not result in reduced acetyllysine levels. If Na4P, M4P, and AM4P would end up in the cellular acetylome, their incorporation levels should be affected by deacetylase inhibitors. Indeed, fluorescence of Cy3-tagged pentynoyl groups of Na4P-treated samples increased in presence of deacetylase inhibitors in HEK293T and HeLa S3 cells. Moreover, curcumin decreased the incorporation of this reporter. It is possible that alkyne-moieties of Na4P were not transferred by all acetyltransferases and mainly by those, which are targeted by curcumin. The overall acetylation levels, as assessed with a pan anti-acetyllysine antibody, might not have been reduced enough to detect it. Cy3 signals of M4P- and AM4P-treated cells did not change in presence of any inhibitor. Since M4P and AM4P are expected to lose their protecting groups inside cells, Na4P, M4P, and AM4P should theoretically behave similarly. As this was not the case, it needed to be concluded that non-specifically acting esterases do not remove the methyl and acetoxymethyl groups completely and/or M4P and AM4P are processed by other enzymes and are attached in a different way to proteins than the pentynoyl groups of Na4P. This result is surprising and questions the usage of methyl and acetoxymethyl groups to facilitate the diffusion of chemical reporters in cells. It has been shown by mass spectrometry and biochemical experiments that Na4P is metabolized and incorporated as native acetyl-CoA.[157] Additionally, it appeared to be better suited than M4P and AM4P in experiments presented in this thesis, although it was incorporated to a less extent.

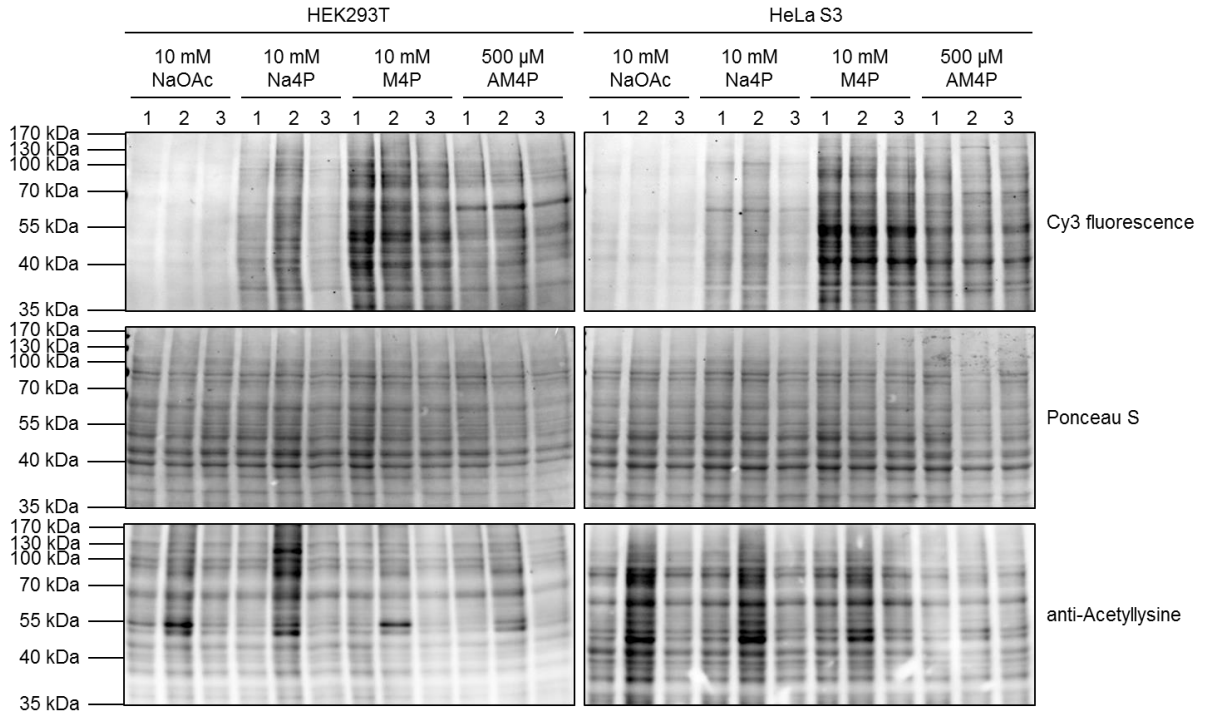

Figure 4.51: Altering cellular acetylation levels with chemical inhibitors. HEK293T and HeLa S3 cells were pretreated with 1:100 deacetylase inhibitor cocktail for 24 h (2) or with 60 µM curcumin for 30 min (3), incubated with indicated reporters for 8 h, lysed, and labeled with sulfo-Cy3-azide. Control cells were not pretreated (1). Fluorescence of Cy3 was detected on Western blots. The functionality of the inhibitors was demonstrated by immunoblotting against acetyllysine. Ponceau S served as loading control.

4.2.4. Protein-Specific Imaging of Protein Acetylation

The approach for protein-specific imaging of intracellular acetylation should be based on the detection of FRET, which occurs only if the EGFP-tag of the protein of interest is present in close proximity to the acetylation-site anchored acceptor fluorophore. A prerequisite for the functionality of this strategy is that EGFP itself is not modified with the chemical reporter of choice. Since initial immunoprecipitation experiments were performed before the acetylation inhibition studies, all reporters were tested. HEK293T cells were transfected with expression vectors encoding EGFP or EGFP-histone 2B (H2B), treated with NaOAc, Na4P, M4P, or AM4P, and lysed. EGFP and EGFP-H2B were isolated by immunoprecipitation from cell lysates and labeled with sulfo-Cy3-azide in a CuAAC. Stronger Cy3 fluorescence bands compared to the one of the control NaOAc were found for EGFP, if cells were treated with M4P and AM4P, and for EGFP-H2B in case of Na4P, M4P, and AM4P (when considering lower amounts of proteins present in the AM4P sample, Figure 4.52). H2B is known to be acetylated at the N-terminal lysine residues K6, K12, K13, K16, K17, K21, K24, and K86.[555–557] Using an anti-acetyllysine antibody, acetylation of EGFP-H2B but not EGFP could be attested. As Cy3 signals of M4P and AM4P resulting from the modification of proteins with pentynoyl groups were also present for EGFP, it must be concluded that these two reporters are not suitable. In contrast, Na4P resulted in the labeling of only EGFP-H2B. These data are in line with above mentioned experiments showing the response of Na4P, but not of M4P and AM4P, to alterations of acetylation levels by inhibitors (Figure 4.51). Thus,

Na4P was used as chemical reporter for the development of the imaging approach for protein-specific acetylation.

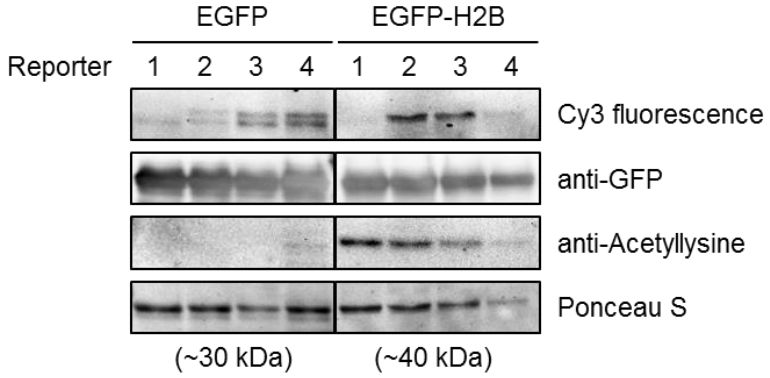

Figure 4.52: Immunoprecipitations of EGFP and EGFP-H2B. HEK293T cells transiently expressing EGFP or EGFP-H2B were treated with 10 mM NaOAc (1), 10 mM Na4P (2), 10 mM M4P (3), or 500 µM AM4P (4) for 8 h and lysed. EGFP and EGFP-H2B were immunoprecipitated from lysates. Transferred pentynoyl groups were marked with sulfo-Cy3-azide in a CuAAC. Cy3 fluorescence was detected on Western blots to determine the modification state of EGFP and EGFP-H2B. Immunoblotting against acetyllysine revealed the modification of H2B with acetyl groups. Ponceau S staining and anti-GFP antibodies were used as loading controls.

Next, immunoprecipitates of further 37 EGFP-fusion proteins were prepared using Na4P as chemical reporter and NaOAc as control substance. Abbreviations for proteins not mentioned so far are the following: α-actinin 1 and 4 (ACTN1 and ACTN4), transcription factor Sp1 (SP1), Myc proto-oncogene protein (c-Myc), serine/threonine-protein phosphatase PP1-β catalytic subunit (PP1β), cytokeratin 8 (KRT8), α-enolase (ENO1), glucose-6-phosphate isomerase (GPI), glyceraldehyde-3-phosphate dehydrogenase (GAPDH), phosphoglycerate kinase 1 (PGK1), poly [ADP-ribose] polymerase 1 (PARP1), histone deacetylase 1 (HDAC1), heat shock protein 70 kDa (HSP70), nucleophosmin (NPM), heat shock protein 105 kDa (HSPH1), heat shock cognate protein 71 kDa (HSPA8), transitional endoplasmic reticulum ATPase (VCP), microtubule-associated protein RP/EB family member 1 (EB1), and phosphatidylinositol 3,4,5-trisphosphate 3-phosphatase and dual-specificity protein phosphatase (PTEN). If the Cy3 fluorescence intensity read out from Western blots at the size of the immunoprecipitated EGFP-fusion protein was higher for the Na4P- than for the NaOAc-treated sample, the modification of this protein with the pentynoyl group was assumed. This was the case for the twelve proteins p53-EGFP, Foxo1-EGFP, EGFP-SP1, EGFP-SNAC and SNAC-EGFP, EGFP-PARP1 and PARP1-EGFP, EGFP-H2B, EGFP-NPM, EGFP-nucleolin, EB1-EGFP, and EGFP-PTEN (Figure 4.53). Out of them, PARP1, H2B, NPM, and nucleolin have already been identified by Yang et al. to be modified with Na4P.[157] In addition, they have reported the modification of CAMK4, ENO1, GPI, GAPDH, PGK1, HDAC1, HSP70, HSPA8, moesin, and VCP with Na4P. Discrepancies in Na4P-modified proteins detected might be due to the different methods used for their identification. Yang et al. enriched alkyne-tagged proteins before performing mass spectrometry. Hence, they could determine the modification of proteins modified to very low extents. Here, EGFP-tagged

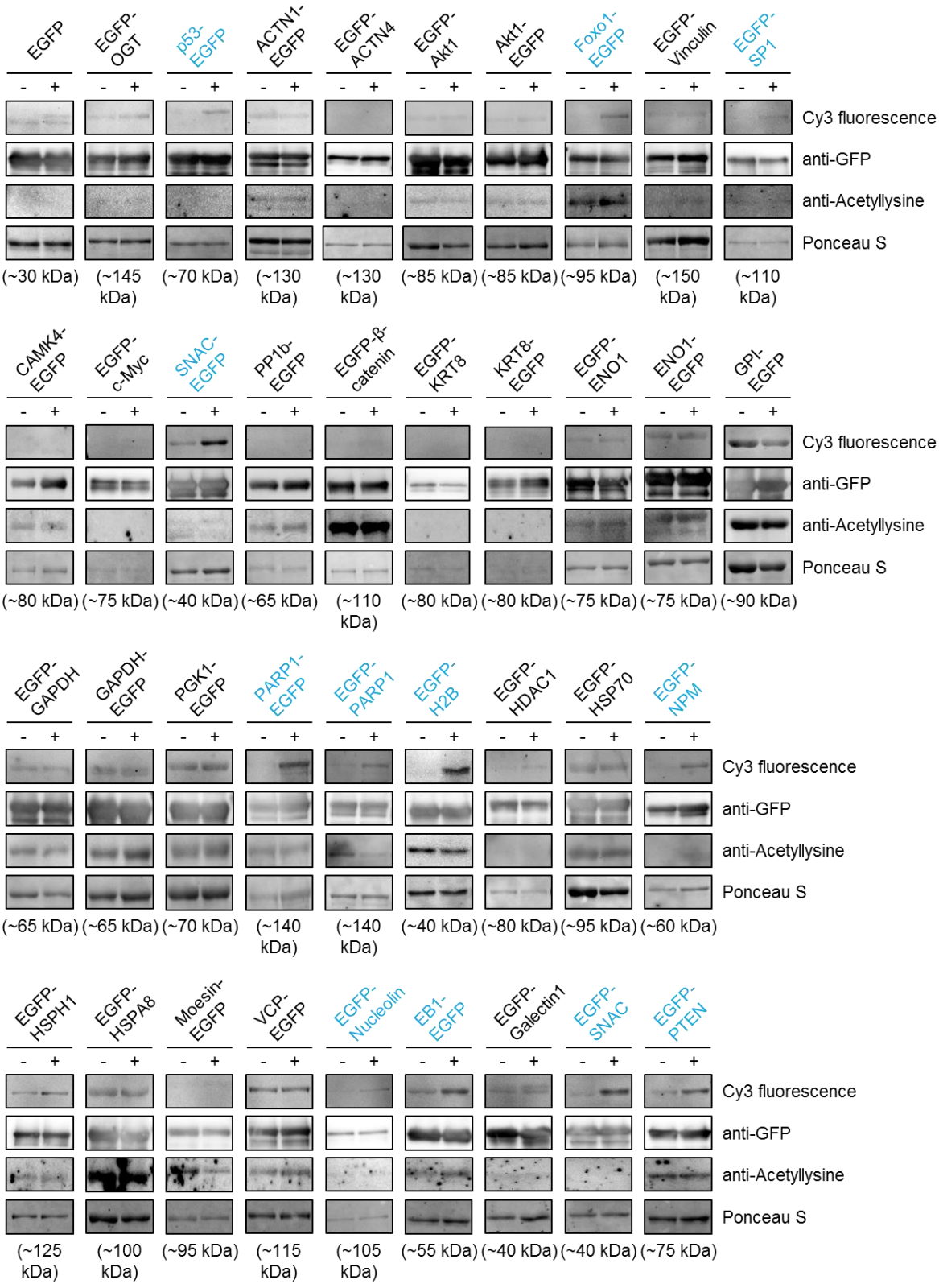

Figure 4.53: Assessing the modification of 37 EGFP-fusion proteins with Na4P. HEK293T cells expressing EGFP or various EGFP-fusion proteins were treated with 10 mM NaOAc (-) or Na4P (+) for 8 h and lysed. EGFP and EGFP-fusion proteins were immunoprecipitated and labeled with sulfo-Cy3-azide. The Na4P modification state of each protein was determined by investigating the fluorescence of Cy3 detected on Western blots. Proteins modified with Na4P are highlighted in blue. Antibodies against GFP and acetyllysine were used. Ponceau S staining served as loading control.

Table 4.2: Summary of localizations, sizes, acetylation sites, and functions of EGFP-fusion proteins whose acetylation states were investigated within this thesis by FLIM-FRET microscopy. The localization can be nuclear (N), cytoplasmic (C), or membranous (M). Proteins are either N-terminally (NT) or C-terminally (CT) tagged with EGFP. Information on localizations and functions were obtained from the UniProt knowledge database.[558]

Protein	Localization	Number of amino acids	Acetylation sites	EGFP tag	Function
Human p53	N	393	K120[559], K305[560], K320[561], (K370, K372, K373, K381, K382)[81]	CT	Tumor suppressor; induces growth arrest or apoptosis
Human SNAC	N, C, M	140	NT[562]	NT or CT	Induces fibrillization of microtubule-associated protein tau; reduces neuronal responsiveness
Human PARP1	N	1014	NT[563], (K97, K105, K131, K600, K621)[557], (K498, K505, K508, K521, K524)[564]	NT or CT	Involved in base excision repair pathway; catalyzes poly(ADP-ribosyl)ation
Human H2B	N	126	(K6, K12, K13, K16, K17, K21)[556], K24[557], K86[555]	NT	Core component of nucleosome
Human NPM	N	294	NT[565], (K32, K150, K267, K273)[557], (K154, K212)[83], (K229, K230, K250, K257, K292)[566]	NT	Involved in ribosome biogenesis, centrosome duplication, protein chaperoning, histone assembly, cell proliferation, and regulation of tumor suppressors
Human nucleolin	N	710	(K9, K102, K116, K124, K377, K398, K403, K513, K572, K577, K646)[557] (K15, K16, K96, K109, K348, K427, K444, K467, K477, K521)[567], K88[568]	NT	Major nucleolar protein; induces chromatin decondensation
Human EB1	C	268	(K66, K86, K100, K112, K212)[569], K220[570]	CT	Regulates dynamics of the microtubule cytoskeleton
Human PTEN	N, C	403	NT[563], (K125, K128)[571], K163[572], K402[573]	NT	Tumor suppressor; protein and lipid phosphatase

proteins were immunoprecipitated regardless of their modification state. This method is too insensitive to allow for the detection of the modification of a subpopulation of proteins. Besides, it needs to be mentioned that different proteins were found to be acetylated with a pan acetyllysine antibody and modified with Na4P on Western blots of immunoprecipitates.

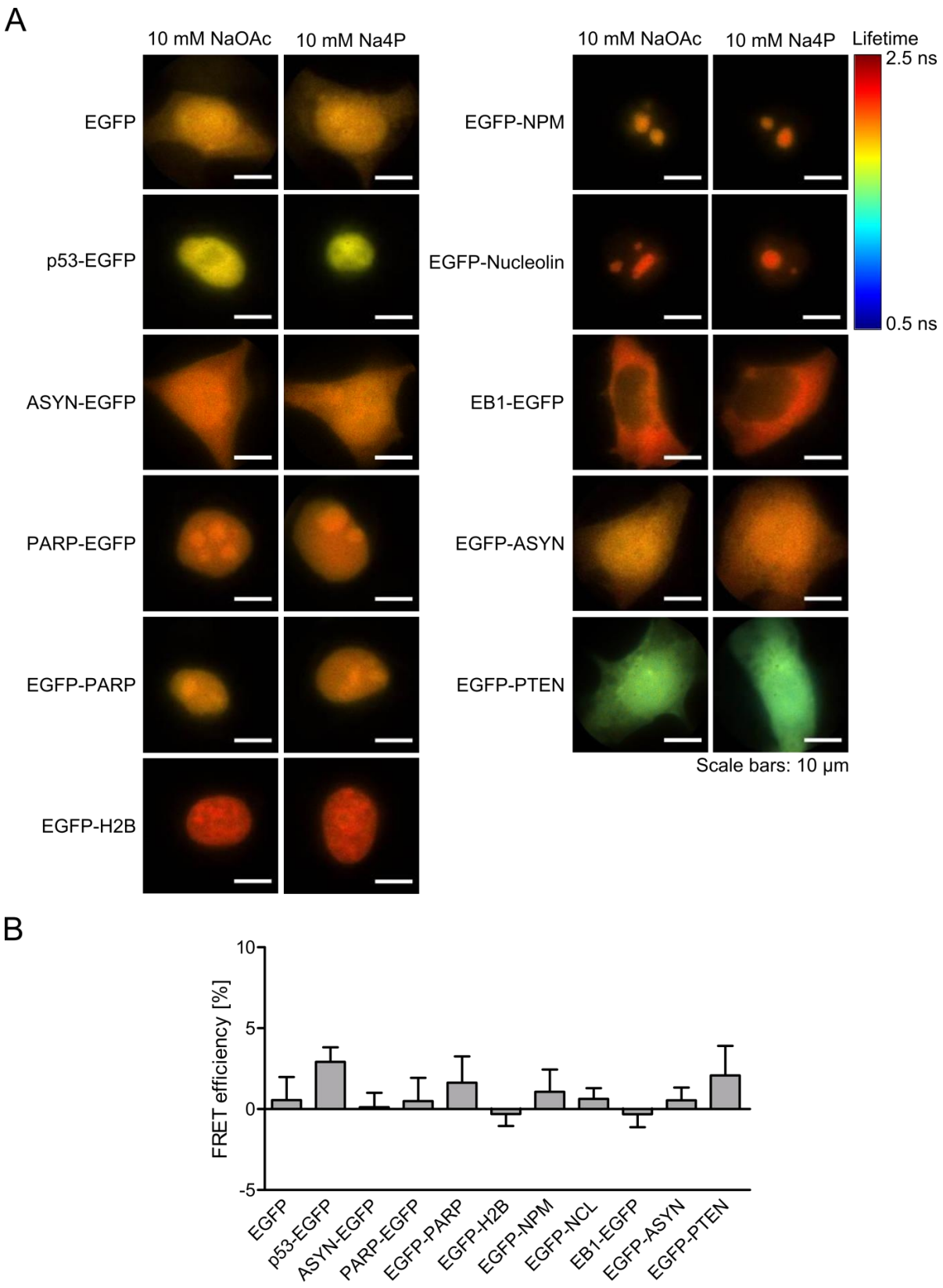

Figure 4.54: FLIM-FRET experiments with 10 mM Na4P. HEK293T cells expressing EGFP or various EGFP-fusion proteins were treated with 10 mM NaOAc or Na4P, fixed, permeabilized, and labeled in a CuAAC with sulfo-Cy3-azide. (A) Representative fluorescence modulation lifetime images are depicted. (B) Fluorescence lifetimes were averaged over three independent experiments with ten cells measured each and used to calculate apparent FRET efficiencies. Columns correspond to mean FRET efficiencies and error bars to SEMs.

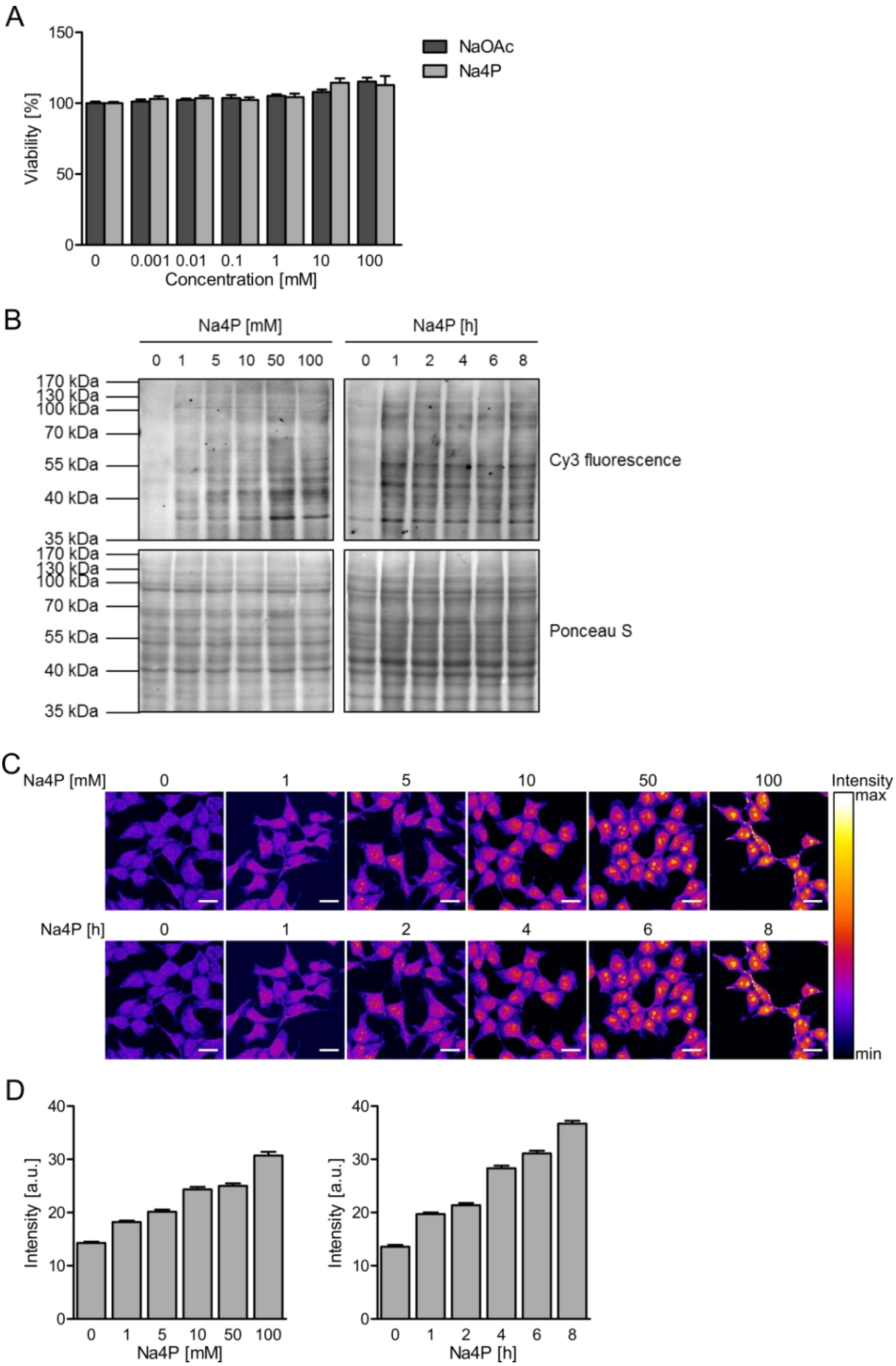
A
150
100
50
0
Viability [%]
NaOAc
Na4P
0
0.001
0.01
0.1
1
10
100
Concentration [mM]
B
Na4P [mM]
Na4P [h]
0 1 5 10 50 100
0 1 2 4 6 8
170 kDa
130 kDa
100 kDa
70 kDa
55 kDa
40 kDa
35 kDa
Cy3 fluorescence
Ponceau S
C
Na4P [mM]
Na4P [h]
0 1 5 10 50 100
0 1 2 4 6 8
Intensity
max
min
D
Intensity [a.u.]
Na4P [mM]
Na4P [h]

Figure 4.55: Increasing the Na4P concentration to 100 mM. (A) Viabilities of HEK293T cells treated with up to 100 mM NaOAc or Na4P were assessed with AlamarBlue tests. Columns represent mean viability values of three experiments each carried out in quadruplicates. Error bars are SEMs. (B) Cy3 fluorescence was read out from Western blots of lysates from HEK293T cells treated with different concentrations of Na4P for 8 h (left) or 100 mM Na4P for different durations (right), lysed and labeled with sulfo-Cy3-azide. (C) Representative confocal fluorescence microscopy images of HEK293T cells treated with different concentrations of Na4P for 8 h (upper row) or 100 mM Na4P for different periods of times (lower row) and marked with sulfo-Cy3-azide are presented. (D) Fluorescence intensities were quantified for five cells per image from two independent experiments with four images taken each. Columns represent mean fluorescence intensities. Error bars are SEMs.

This hints at Na4P not being metabolized and accepted in the same way as the native substrate acetyl-CoA or questions the specificity of the acetyllysine antibody. Since many acetyltransferases and deacetylases exist, it might be possible that only a subset of them uses pentynoyl-CoA as substrate.

The EGFP-fusions of the proteins p53, SNAC, PARP1, H2B, NPM, nucleolin, EB1, and PTEN were used for FLIM experiments. Information on sizes, cellular localizations, functions, and acetylation sites of these proteins are presented in Table 4.2. All of them have been shown to be acetylated. Acetylation sites of p53-EGFP, EGFP-H2B, EGFP-NPM, and EGFP-nucleolin are particularly close to the position of the EGFP-tag. Thus, these proteins are promising candidates for the detection of FRET. FLIM-FRET experiments with Na4P were performed together with Eliana Landwehr in the framework of her bachelor's thesis.[574] Representative fluorescence lifetime images of HEK293T cells expressing the above mentioned EGFP-fusion proteins or EGFP are presented in Figure 4.54A. Different EGFP-fusion proteins exhibited different fluorescence lifetimes in NaOAc-treated samples. As explained in the chapters on glycosylation, fluorescence lifetimes need not be equal, since they are affected by local parameters including viscosity, oxygen and ion concentrations temperature, and pH value.[293,345] Moreover, background FRET resulting from a close proximity of the EGFP-fusion protein and unspecifically incorporated Cy3 alters fluorescence lifetimes, but also occurs in Na4P-treated samples. All Na4P-treated cells showed no reduced fluorescence lifetimes compared to NaOAc-treated cells. Consistent with this observation, calculated FRET efficiencies for EGFP and all EGFP-fusion proteins tested were below 3 % (Figure 4.54B). This corresponds to fluorescence lifetime changes of approximately 60 ps, which is below the resolution limit of the FLIM microscope. Hence, no conclusion on the modification state of these proteins can be drawn from these imaging experiments.

As all tested EGFP-fusion proteins were shown to be modified with Na4P via immunoprecipitations, cellular concentrations of Na4P and thus also of Cy3 must have been too low for the detection of meaningful FRET. Na4P is hardly cell permeable and presumably only a small portion of it enters cells. Consequently, the concentration of this chemical reporter was increased to 100 mM. Viability tests with HEK293T cells revealed that 100 mM Na4P added to the cell culture medium were not cytotoxic (Figure 4.55A). Furthermore, Western blot and confocal fluorescence microscopy experiments showed increased Cy3 fluorescence intensities if 100 mM Na4P instead of 10 mM Na4P were used (Figure 4.55B-D). However, Cy3 intensities detected by fluorescence microscopy increased only by roughly 25 %.

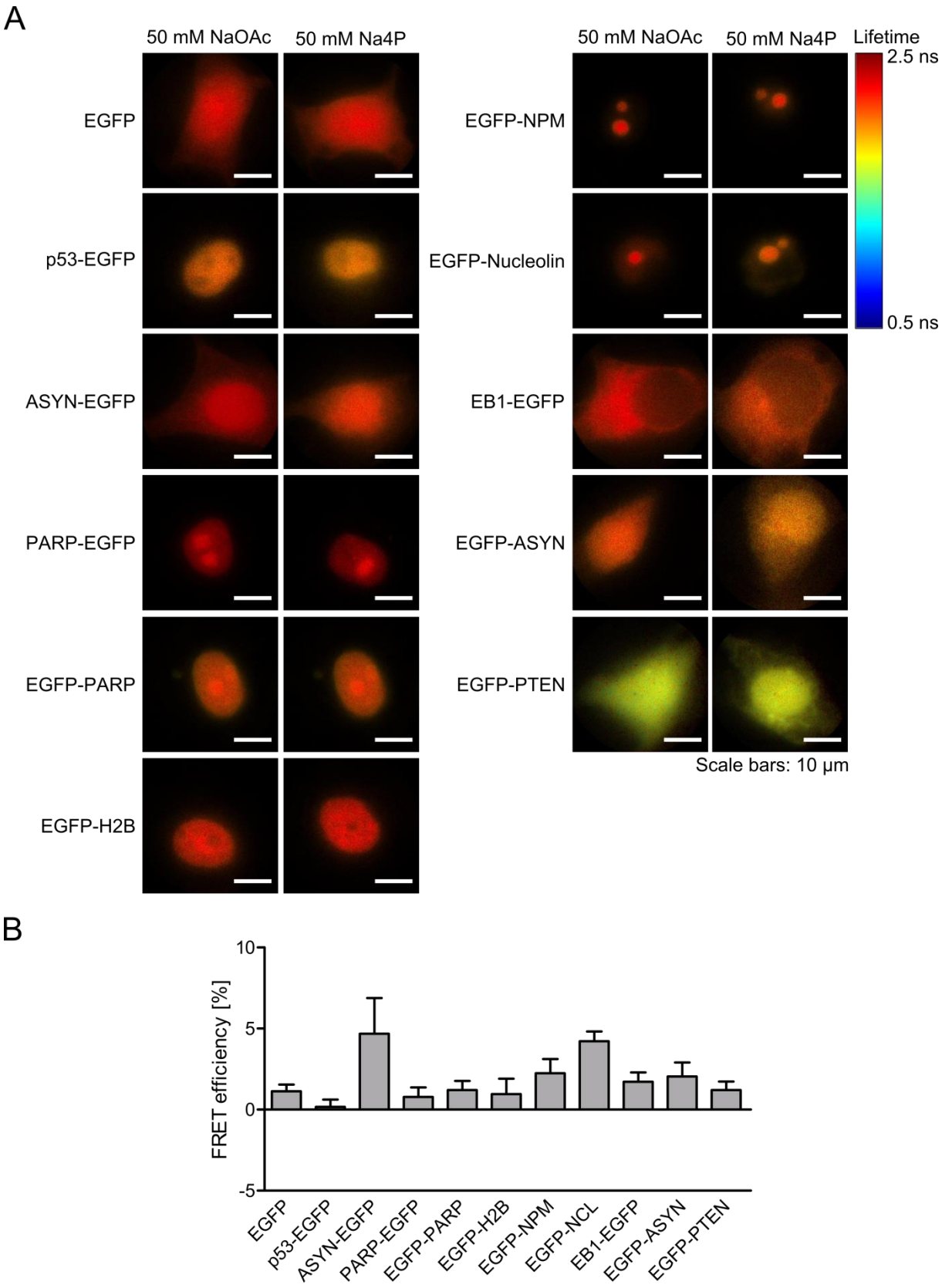

Figure 4.56: FLIM-FRET experiments with 50 mM Na4P. (A) Representative fluorescence modulation lifetime images of HEK293T cells expressing EGFP or various EGFP-fusion proteins treated with 50 mM NaOAc or Na4P, fixed, permeabilized, and marked with sulfo-Cy3-azide are displayed. (B) FRET efficiencies were calculated from fluorescence lifetimes averaged over ten cells. Columns represent mean FRET efficiencies and error bars SEMs.

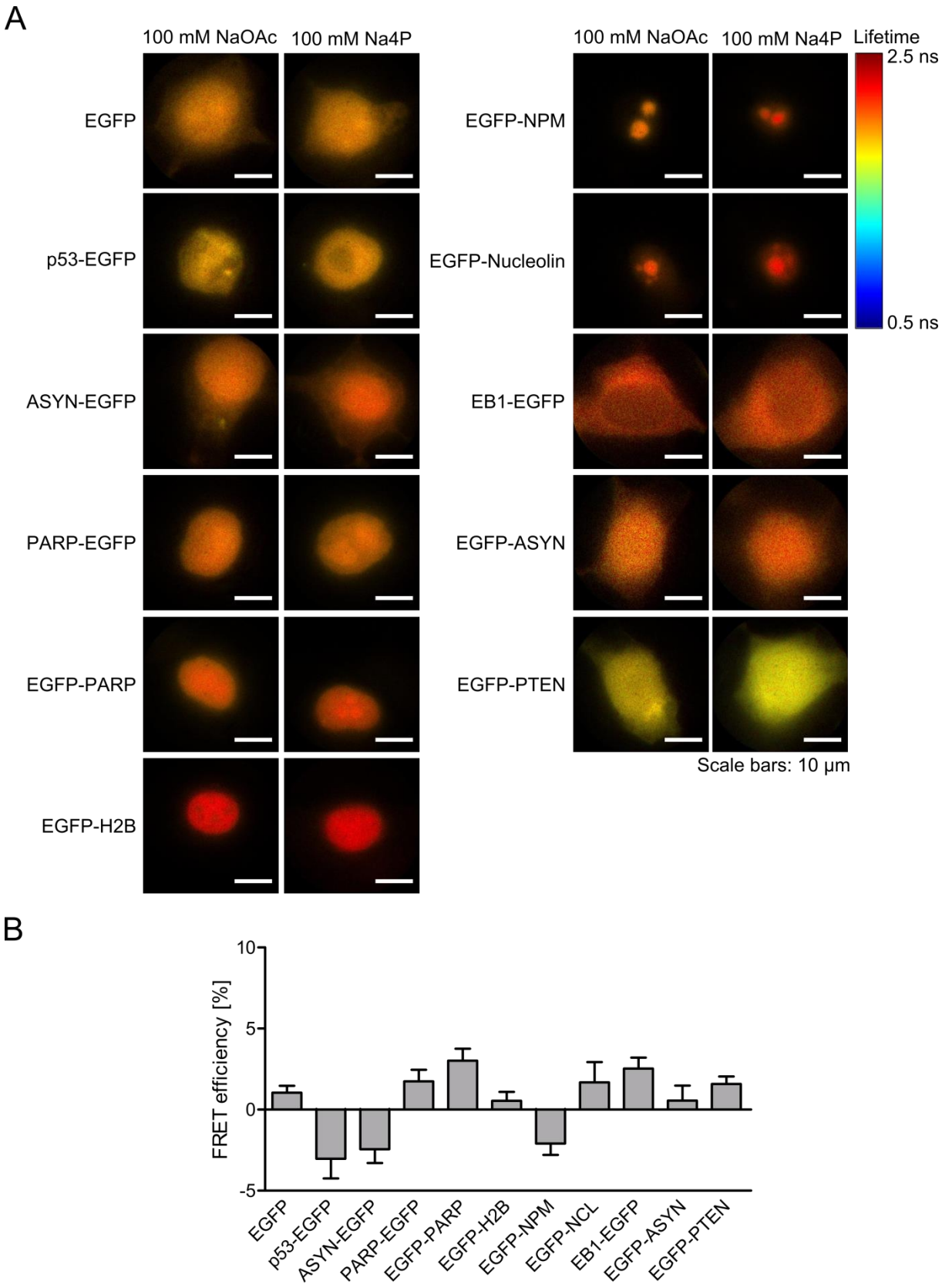

Figure 4.57: FLIM-FRET experiments with 100 mM Na4P. (A) Representative fluorescence modulation lifetime images of HEK293T cells expressing EGFP or EGFP-fusion proteins treated with 100 mM NaOAc or Na4P, fixed, permeabilized, and labeled in a CuAAC with sulfo-Cy3-azide are shown. (B) Quantification of calculated FRET efficiencies. Columns correspond to mean FRET efficiencies derived from fluorescence lifetimes averaged over ten cells per condition. Error bars are SEMs.

Nevertheless, FLIM experiments were repeated with EGFP and the same EGFP-fusion proteins using NaOAc and Na4P concentrations of 50 mM and 100 mM. Again, no reductions of fluorescence lifetimes were measureable and consequently no reasonable FRET efficiencies were obtained from calculations (Figure 4.56 and Figure 4.57). To further increase the concentration of Na4P would neither be useful nor meaningful. The amount of sulfo-Cy3-azide used was not assumed to be the bottleneck, since higher concentrations of sulfo-Cy3-azide (up to 100 µM) did not result in increased Cy3 signals of AM4P-treated samples detected on Western blots and by confocal fluorescence microscopy (Figure 4.44 and Figure 4.45). Moreover, Cy3 fluorescence intensities of M4P and AM4P were always higher.
To exclude any technical problems at the FLIM microscope as reasons for the failed FLIM-FRET experiments, FRET of the 50 mM and 100 mM samples was measured by acceptor photobleaching. Obtained FRET efficiencies for NaOAc and NA4P samples were below 1 % (Figure 4.58). These data substantiate the FLIM results.

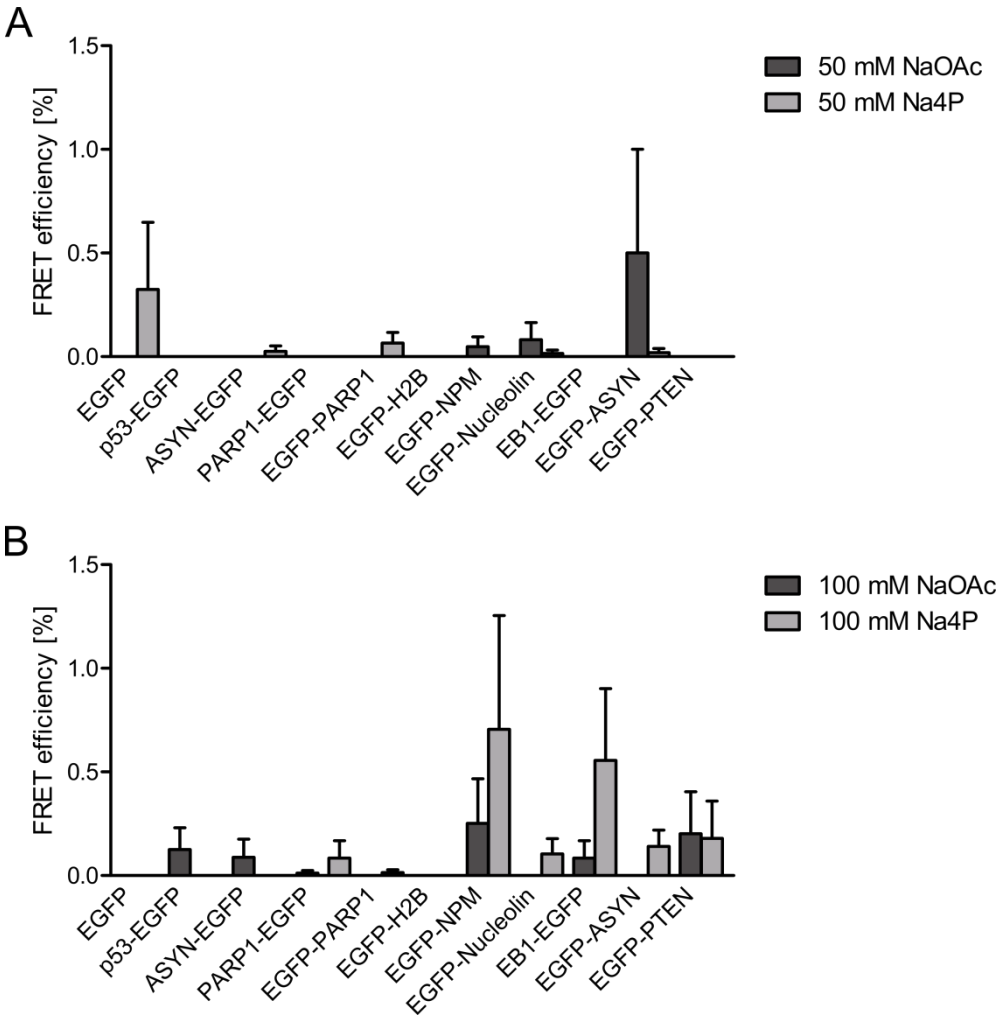

Figure 4.58: Acceptor photobleaching substantiates FLIM data. HEK293T cells expressing EGFP or different EGFP-fusion proteins were treated with (A) 50 mM or (B) 100 mM NaOAc or Na4P for 8 h, fixed, permeabilized, and the CuAAC with sulfo-Cy3-azide was performed. FRET from EGFP to the acetylation site-anchored Cy3 was determined by acceptor photobleaching. Columns belong to mean values of five measurements and error bars to SEMs.

4.2.5. Conclusions

Na4P was chosen as chemical reporter for protein acetylation studies. Since its incorporation in the cellular proteome could not be detected initially, the two putative acetylation reporters M4P and AM4P were synthesized. Optimization of the CuAAC conditions enabled in cell imaging of acetylation by confocal fluorescence microscopy based on acetylation reporters for the first time. However, biochemical experiments demonstrated differences in the attachment of pentynoyl-groups from Na4P, M4P, and AM4P. This questions the use of methyl and acetoxymethyl moieties as protecting groups for chemical reporters and the widely accepted activity of non-specifically acting esterases in cells. Only Na4P allowed mapping of alterations of the proteome's acetylation level and thus was selected for further studies aiming on protein-specific imaging of acetylation inside single cells. This should be achieved by combining the chemical reporter strategy with EGFP-tagged fusion proteins and FLIM-FRET microscopy. Beforehand, the modification states of EGFP itself and 37 EGFP-fusion proteins were assessed by immunoprecipitation, which enabled the identification of twelve alkynylated proteins. Although various conditions and many EGFP-fusion proteins were tested, protein-specific acetylation could not be detected in cells by FLIM. A possible explanation of this finding is that the EGFP-tag and the acetylation site-anchored acceptor fluorophore on proteins of interest were too far apart from each other to enable FRET. Yet, this is very unlikely, since ten different EGFP-fusion proteins were studied. As malfunctions of the FLIM microscope could be excluded, it was concluded that the inability to obtain efficient FRET originated from too few acceptor fluorophores present per donor fluorophore. However, the concentration of Na4P could not be increased above 100 mM and the amount of sulfo-Cy3-azide applied did not seem to be the bottleneck. Thus, the establishment of an imaging approach for protein-specific acetylation requires new cell permeable chemical acetylation reporters that are better accepted by cellular acetyltransferases and deacetylases.

4.3. Protein Methylation

Next to protein-specific imaging of glycosylation and acetylation, a similar FLIM-FRET-based approach should be established for protein methylation. Results presented in this chapter have been included in a manuscript submitted for publication.

4.3.1. Evaluation of ProSeAM as Chemical Reporter for Protein Methylation

As discussed in section 2.2.3, many chemical methylation reporters have been developed. Among them, ProSeAM is the most promising reporter known.[220,222] At the beginning of this project, ProSeAM was synthesized by Raphael René Steimbach within his master's thesis.[205] It was isolated as epimeric mixture by medium pressure liquid chromatography. ProSeAM's spectroscopic data were in agreement with literature values.[220,222]

To prove the functionality of synthesized ProSeAM, the concentration-dependent attachment of propargyl groups originating from this reporter to proteins was studied in a similar manner as it has been done by Bothwell et al.[220] For this purpose, HEK293T and HeLa S3 cell lysates were treated with up to 100 µM ProSeAM and transferred propargyl residues were labeled with sulfo-Cy3-azide in a CuAAC. For the CuAAC, optimal reaction conditions, as determined in chapter 4.2.3, were used. Proteins were precipitated, washed, separated by SDS-PAGE, and transferred to a membrane. Fluorescence from blots was read out to estimate the degree of Cy3-marked propargyl residues incorporated in the proteome. As shown in Figure 4.59A, fluorescence of sulfo-Cy3 increased with increasing concentrations of ProSeAM added to cell lysates in both HEK293T and HeLa S3 cells. These data were in line with findings from Bothwell et al.[220] and thus verified the functionality of ProSeAM. Interestingly, ProSeAM concentrations as low as 5 µM allowed the detection of its incorporation.

Next, the temporal course of ProSeAM processing was investigated. For the treatment of HEK293T and HeLa S3 cells for different durations with ProSeAM, a concentration of 50 µM was chosen, as this resulted in considerable sulfo-Cy3 signals and was also utilized by Bothwell et al.[220] The fluorescence readouts of Western blots demonstrated a very fast turnover of ProSeAM (Figure 4.59B), since even "0 min" samples, to which ProSeAM was added simultaneously with the CuAAC reaction mixture, displayed Cy3-labeled proteins. The incorporation of propargyl residues reached a maximum level for an incubation time of 60 min. This value corresponds to the half-life time of ProSeAM under physiological conditions.[220] Thus, it can be speculated that amounts of incorporated Cy3-labeled propargyl residues did not further increase due to the decomposition of ProSeAM. Strong Cy3 fluorescence was detected from 10 min onwards and thus this incubation time was used in following lysate experiments.

It has already been shown that ProSeAM is accepted as methylation substrate by various methyl transferases.[220,222] To verify this, cell lysates of HEK293T and HeLa S3 cells were pretreated with SAH, which competitively inhibits methyltransferases, and the SAH hydrolase inhibitor adenosine-2',3'-dialdehyde (Adox).[575] Subsequently, ProSeAM was added to lysates and the CuAAC was performed. Cy3 fluorescence intensities detected on Western blots of all inhibitor-pretreated samples were much lower compared to lysates that were not

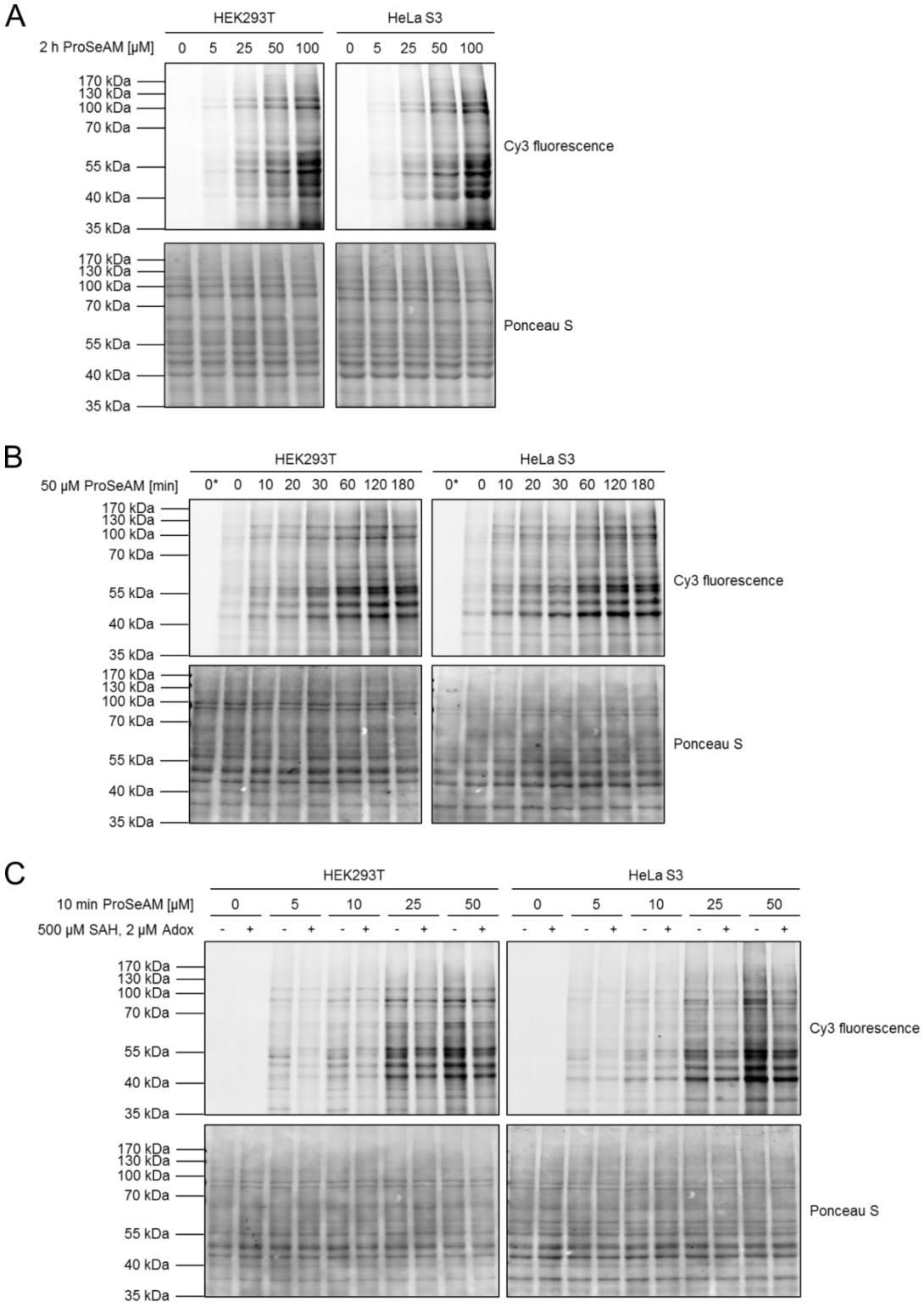

Figure 4.59: ProSeAM processing in cell lysates. Western blots of HEK293T and HeLa S3 cell lysates treated with (A) various concentrations of ProSeAM for 2 h or (B) 50 µM ProSeAM for different times (0* min: samples were not treated with ProSeAM. 0 min: ProSeAM was added to cell lysates and CuAAC was performed immediately) are displayed. (C) Western blots of lysates from cells pretreated with 500 µM SAH and 2 µM Adox at 37 °C for 15 min and then treated with different concentrations of ProSeAM for 10 min are shown. Fluorescence of sulfo-Cy3 attached to transferred propargyl residues via a CuAAC was read out. Ponceau S staining of proteins confirms equal loading of lysate samples. Data presented in (A) were acquired by R. R. Steimbach,[205] but processed by myself.

exposed to any inhibitor (Figure 4.59C). Cy3 signals of samples treated with inhibitors still exhibited detectable fluorescence. However, this is expected, since the inhibitors cannot completely block methyltransferase activities. Results of the inhibitor experiments stated that ProSeAM serves as substrate for methyl transferases and were in accordance with findings from others.[220]

4.3.2. Delivery of ProSeAM in Mammalian Cells

Published experiments with SAM analogs have been carried out in cell lysates or buffers. To be able to perform FLIM-FRET experiments later on, ProSeAM needed to be introduced inside cells. To test whether ProSeAM diffuses into cells, HEK293T and HeLa S3 cells were treated with 100 µM ProSeAM for 2 h. Thereafter, cells were fixed and permeabilized to allow for the CuAAC with sulfo-Cy3-azide. Confocal fluorescence microscopy of ProSeAM-treated HEK293T cells showed weak sulfo-Cy3 fluorescence, but no fluorescence intensities higher than those of the control samples were found in ProSeAM-treated HeLa S3 cells (Figure 4.60A). Thus, it was concluded that ProSeAM is barely cell permeable, which is in accordance with earlier findings from others.[207]

Several methods exist to introduce probes in cells, as summarized in chapter 2.2.4. Among them, electroporation was chosen for ProSeAM, since it results in a fast and homogenously delivery of probes in cells, has no long-term cytotoxic effects, and can be applied to adherent cells. HEK293T and HeLa S3 cells were electroporated in presence of 100 µM ProSeAM in buffer with different pulse duration and were fixed and permeabilized 2 h later. Ensuing the CuAAC with sulfo-Cy3-azide, confocal fluorescence microscopy was performed. Cellular fluorescence intensities resulting from Cy3-labeled propargyl residues increased with prolonged pulse durations (Figure 4.60B). They were maximal for 250 µs long pulses in HEK293T and for pulse durations of 500 µs in HeLa S3 cells. As a consequence, 500 µs were chosen for subsequent electroporation experiments.

As seen in fluorescence microscopy images of HEK293T and HeLa S3 cells, Cy3 signals were not evenly distributed throughout cells. Higher fluorescence intensities were detected in the nucleus and nuclear compartments. To examine whether nuclear structures were nucleoli, HEK293T and HeLa S3 cells were transiently transfected with an expression vector encoding EGFP-nucleolin. In addition, cells were electroporated to deliver ProSeAM in cells, whose propargyl groups were then marked with sulfo-Cy3-azide. Fluorescence microscopy revealed that accumulated Cy3 signals colocalized with EGFP-nucleolin (Figure 4.61). The data presented here are in line with reports from others stating the nuclear localization of many methylated proteins.[576] As ProSeAM functions as universal substrate for methylation, it is also utilized by DNA and RNA methyltransferases.[222,224] Nucleoli comprise ribosomal DNA and RNA, proteins, and preribosomal particles,[577] which all have been reported to be methylated. Hence, increased Cy3 fluorescence detected in nucleoli most likely arises from propargylated proteins, DNA, and RNA.

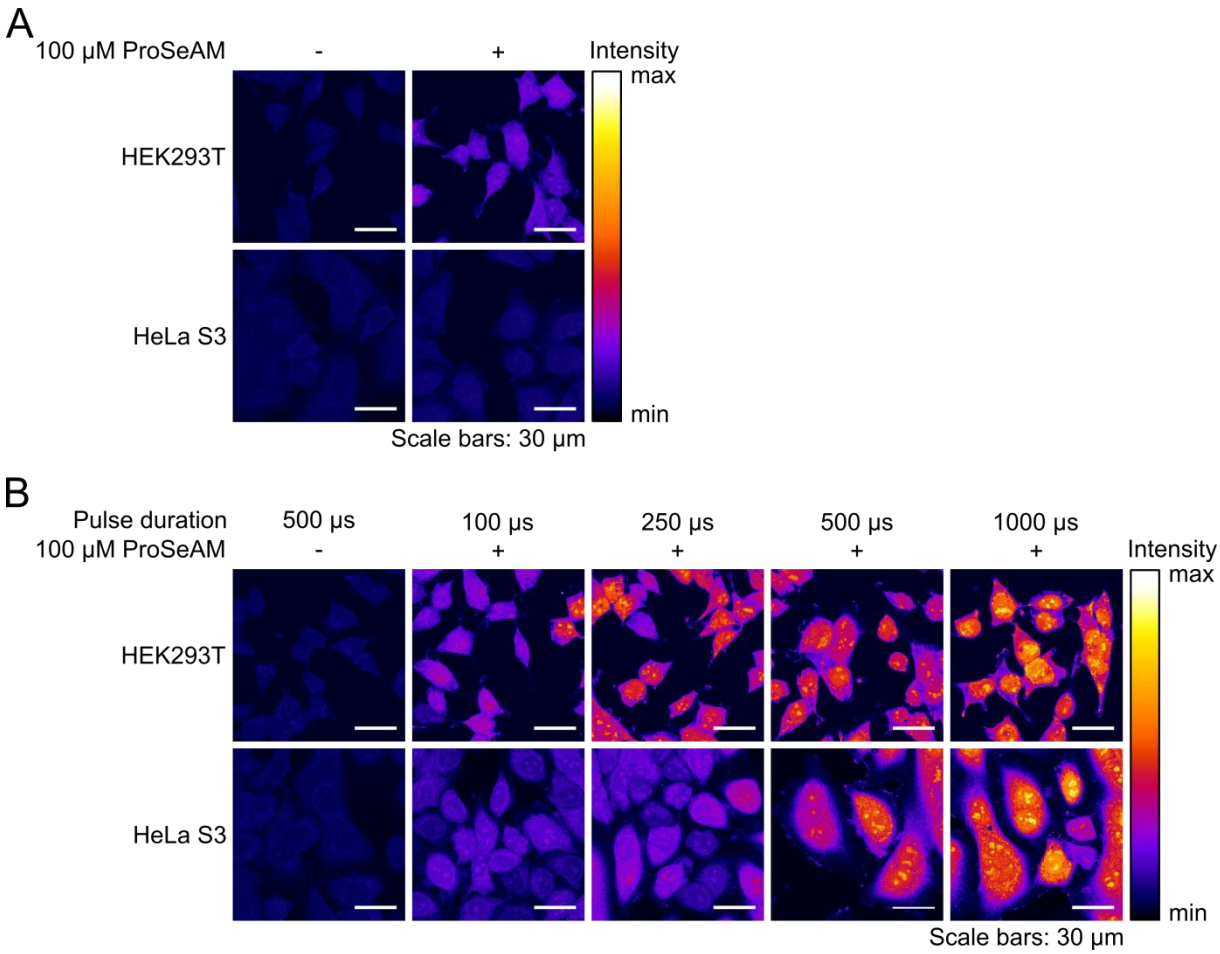

Figure 4.60: Delivery of ProSeAM in cells. HEK293T and HeLa S3 cells were incubated for 2 h after (A) treatment with 100 µM ProSeAM (+) or solvent control (-) or (B) electroporation in presence of 100 µM ProSeAM (+) or solvent control (-) with different pulse durations. Cells were fixed, permeabilized and transferred propargyl residues labeled via a CuAAC with sulfo-Cy3-azide. Representative confocal fluorescence images are depicted. Images in (A) and (B) were prepared with the same intensity scale bars. Data underlying this figure were acquired by R. R. Steimbach,[205] but processed and analyzed by myself.

In a next step, the concentration- and time-dependent turnover of ProSeAM was assessed. To this end, HEK293T and HeLa S3 cells were electroporated in presence of up to 50 µM ProSeAM and incubated for 2 h. Upon CuAAC, fluorescence microscopy was performed. Comparable to Western blot results, fluorescence intensities of Cy3 increased with increasing concentration of ProSeAM (Figure 4.62A). A quantification of single cell fluorescence intensities revealed that 25 µM ProSeAM are necessary to obtain Cy3 signals brighter than the background detected in control cells (Figure 4.62B). Since Cy3 intensities were much higher for cells electroporated in buffer containing 50 µM ProSeAM, this concentration was used for time dependent experiments. After electroporation, HEK293T and HeLa S3 cells were incubated for different durations before they were fixed, permeabilized, and marked with sulfo-Cy3-azide. Even cells fixed directly after electroporation possessed fluorescence intensities four to five times higher than cells electroporated in buffer without ProSeAM (Figure 4.62C+D). Cy3 signals were maximal for an incubation time of 20 min, which was used for FLIM-FRET experiments. These findings were largely consistent with time-dependent studies in cell lysates (Figure 4.59B).

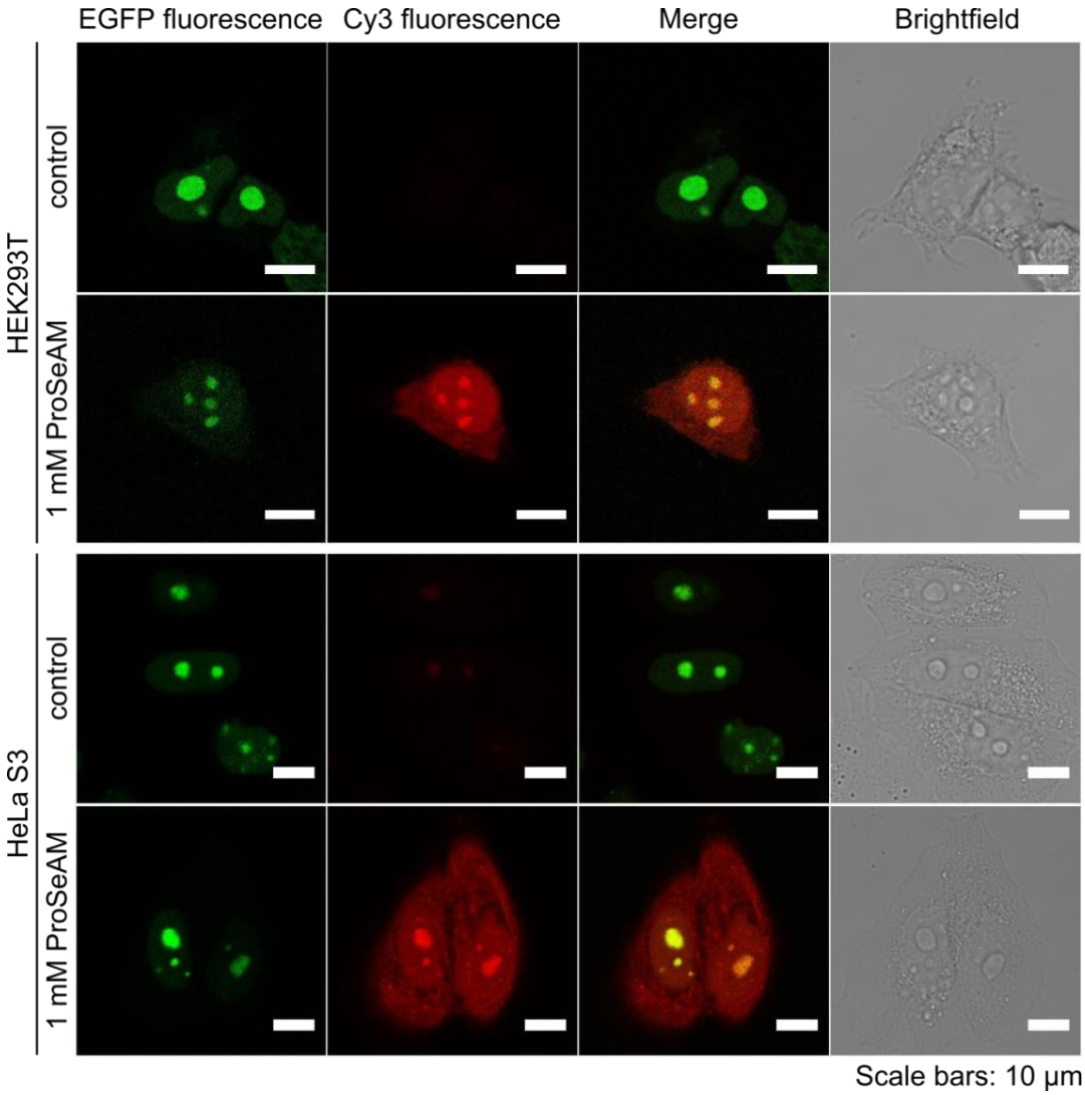

Figure 4.61: Colocalization of ProSeAM with nucleolin. Representative confocal fluorescence and brightfield images of HEK293T and HeLa S3 cells expressing EGFP-Nucleolin, electroporated in presence of a solvent control or ProSeAM, and labeled with sulfo-Cy3-azide upon fixation and permeabilization are presented.

To assess whether ProSeAM affects the integrity of HEK293T and HeLa S3 cells, viability tests were performed. Cells were not electroporated, electroporated in buffer, or electroporated in buffer with 50 µM ProSeAM and incubated for 2 h or 24 h. Viabilities of HEK293T and HeLa S3 cells were considerably reduced by electroporation (Figure 4.63), which is caused by the electroporation procedure. Electrodes need to be pressed onto the surface of the microscopy chamber, which kills adjacent cells. Nevertheless, viabilities of cells electroporated in buffer and those electroporated in buffer with 50 µM ProSeAM did not differ strongly for both incubation times and cell lines tested. Thus, it can be concluded that ProSeAM has neither short- nor long-term effects on cellular viabilities at a concentration of 50 µM.

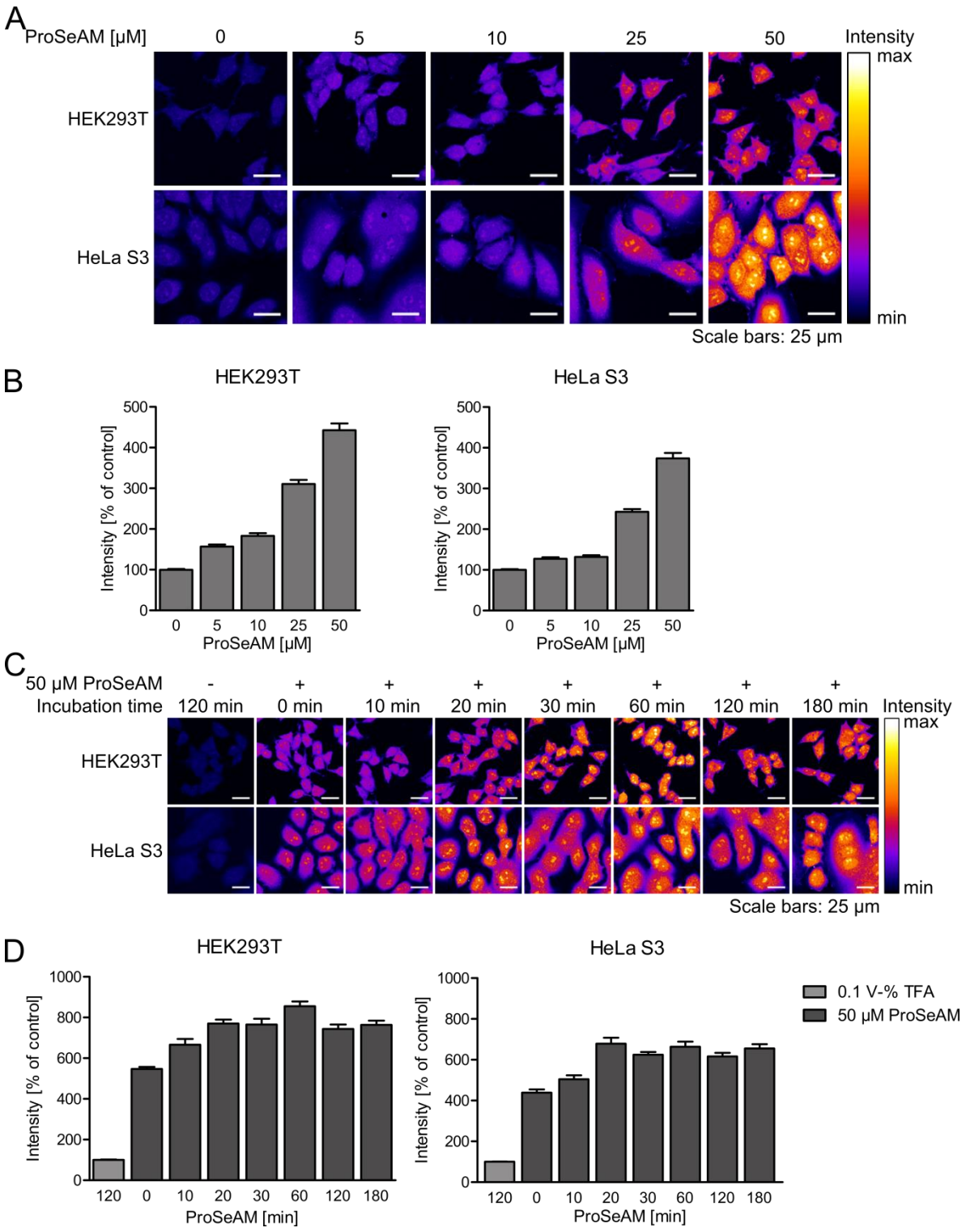

Figure 4.62: Concentration- and time-dependent processing of ProSeAM in human cells. HEK293T and HeLa S3 cells were electroporated in presence of (A+B) 0 µM to 50 µM ProSeAM and then incubated for 2 h or (C+D) 50 µM ProSeAM and then incubated for different periods of time. Cells were fixed, permeabilized, and transferred propargyl residues labeled with sulfo-Cy3-azide via a CuAAC. (A+C) Representative confocal fluorescence images are displayed. (B+D) Fluorescence intensities were quantified for 40 cells out of 2 independent experiments. Columns represent mean values and error bars SEMs. Data underlying this figure were acquired by R. R. Steimbach,[205] but processed and analyzed by myself.

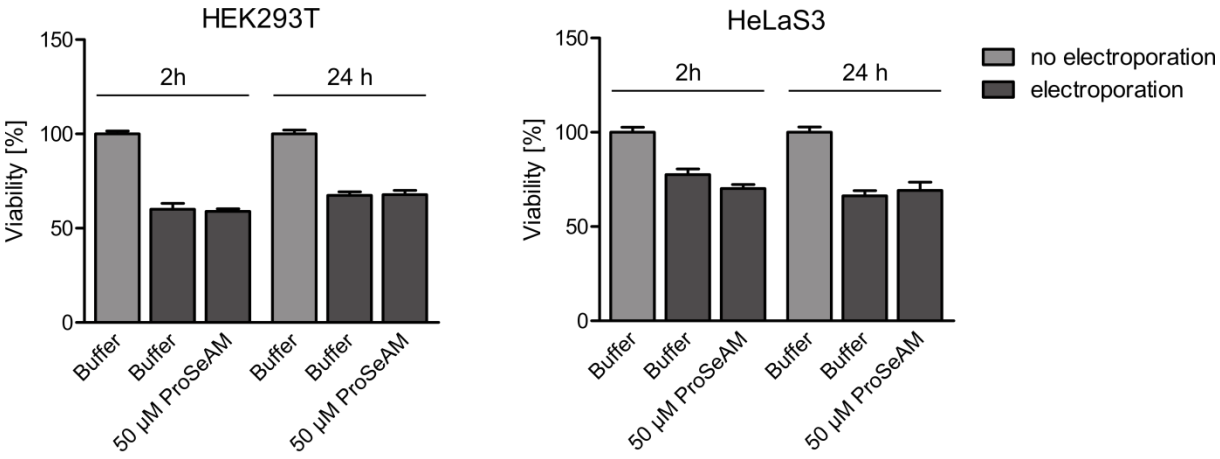

Figure 4.63: Assessing cytotoxic effects of ProSeAM. Cellular viabilities of HEK293T or HeLa S3 cells electroporated in buffer or buffer containing different concentrations of ProSeAM and incubated for 2 h or 24 h were determined with resazurin tests. Control samples were not electroporated. Columns correspond to mean values of triplicates from quadruplicates. Error bars are SEMs.

4.3.3. Protein-Specific Imaging of Protein Methylation

After finding a way to deliver ProSeAM efficiently in cells, a FLIM-FRET microscopy-based approach for the protein-specific imaging of methylation similar to the glycosylation and acetylation experiments was established. For this study, thirteen EGFP-fusion proteins were investigated, which comprised p53-EGFP, EGFP-Akt1, Akt1-EGFP, GAPDH-EGFP, EGFP-H2B, EB1-EGFP, Foxo1-EGFP, histone 3 (H3)-EGFP, histone 4 (H4)-EGFP, EGFP-HSP70, EGFP-HSPA8, VCP-EGFP, and EGFP-nucleolin. Information on localizations, sizes, methylation sites, and functions of these proteins is presented in Table 4.3. All proteins except EB1 have been shown to be methylated. The proteins p53, Akt1, H2B, H3, and H4 have already been reported to be modified with ProSeAM.[220,222] In addition, EGFP was used as control, as it should not be modified with ProSeAM.

To assess which EGFP-fusion proteins become modified with propargyl groups from ProSeAM, lysates of HEK293T cells expressing one of the fusion proteins or EGFP were treated with 10 µM ProSeAM or 1 V-% trifluoracetic acid (TFA) as solvent control for 10 min. Immunoprecipitation was performed with an anti-GFP antibody. Subsequently, transferred propargyl residues were labeled in a CuAAC with sulfo-Cy3-azide. Upon SDS-PAGE and Western blotting, fluorescence of sulfo-Cy3 was read out to determine the modification of each protein of interest with ProSeAM. If the Cy3 fluorescence of the ProSeAM-treated sample was much stronger than that of the solvent control sample, the protein was considered to be modified with the chemical methylation reporter. In this way, p53-EGFP, EGFP-Akt1, Akt1-EGFP, GAPDH-EGFP, Foxo1-EGFP, and H4-EGFP were found to be modified with ProSeAM's propargyl groups (Figure 4.64). EGFP itself was not detected to be propargylated. Thus, it can indeed serve as control for FLIM experiments. Discrepancies in comparison with data from Bothwell et al., who have additionally recognized propargyl groups on H2B and H3 but not on GAPDH and Foxo1 by mass spectrometry,[220] might be due to the different CuAAC reaction mixture and analysis technique used. They have enriched modified proteins before performing mass analysis that

Table 4.3: Summary of localizations, sizes, methylation sites, and functions of EGFP-fusion proteins, whose methylation states were examined within this thesis. The localization can be nuclear (N) or cytoplasmic (C). Proteins are either N-terminally (NT) or C-terminally (CT) tagged with EGFP. Information on localizations and functions were obtained from the UniProt knowledge database.[558]

Protein	Localization	Number of amino acids	Methylation sites	EGFP tag	Function
Human p53	N	393	(K370, K372, K382)[578], K373[579]	CT	Tumor suppressor; induces growth arrest or apoptosis
Mouse or human Akt1	N, C	480	K14[580]	NT or CT	Regulates metabolism, proliferation, cell survival, growth, and angiogenesis
Human GAPDH	C	335	(K5, K66, K194, K215, K227, K260, K263, K334)[581]	CT	Glyceraldehyde-3-phosphate dehydrogenase and nitrosylase activity; roles in glycolysis and nuclear functions
Human H2B	N	126	(K47, K58, K109)[556], (R80, K86, R87, R93)[555]	NT	Core component of nucleosome
Human EB1	C	268	-	CT	Regulates dynamics of the microtubule cytoskeleton
Mouse Foxo1	N, C	652	(R248, R250)[582], K270[583]	CT	Transcription factor, which regulates metabolic homeostasis; main target of insulin signaling
Human H3	N	136	R3[584], (K5, K10, K19, K24, K28, K37, K57, K65, K80, K123)[585], R9[586], R18[587], K38[588]	CT	Core component of nucleosome
Human H4	N	103	R4[589], K21[590], K32[585]	CT	Core component of nucleosome
Human HSP70	C	641	R469[591], K561[592]	NT	Molecular chaperone
Human HSPA8	C	646	(R469, K561)[593]	NT	Molecular chaperone
Human VCP	C	806	K315[594]	CT	Formation of the transitional ER; fragmentation of Golgi stacks during mitosis
Human Nucleolin	N	710	(R656, R660, R666, R670, R673)[595], R694[593]	NT	Major nucleolar protein; induces chromatin decondensation

enables the detection of the modification of a subpopulation of proteins. This is scarcely possible with the immunoprecipitation strategy used here, as no enrichment step occurred and all EGFP-tagged proteins including modified and unmodified ones were studied together.

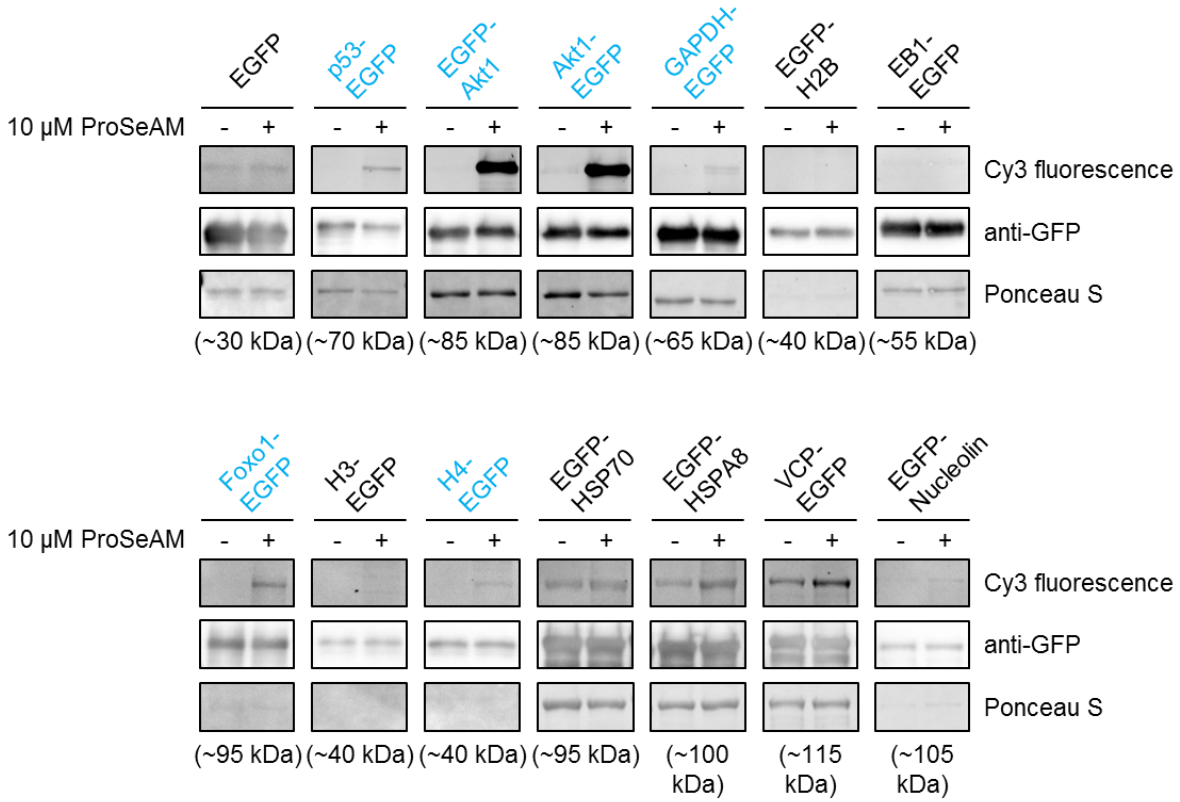

Figure 4.64: Investigating the modification of EGFP-tagged proteins with propargyl residues by immunoprecipitations. Lysates of HEK293T cells expressing certain EGFP-fusion proteins were treated with 10 µM ProSeAM (+) or solvent control (-) for 10 min. EGFP-fusion proteins were isolated by immunoprecipitation and marked with sulfo-Cy3-azide via a CuAAC. Fluorescence readout of Cy3 from Western blots indicates the modification of several proteins with propargyl residues (marked in blue). Equal loading was confirmed by immunoblotting against GFP and staining with Ponceau S.

In a next step, the proteins' methylation was visualized in single cells. For initial experiments, EGFP and the EGFP-fusion proteins of p53, Akt1, and H2B were chosen. HEK293T cells were seeded in microscopy chambers, transiently transfected with the respective expression vectors, and electroporated in buffer containing TFA as solvent control (0 µM), 25 µM, 50 µM, or 100 µM ProSeAM. After an incubation time of 20 min, cells were fixed, permeabilized, and alkyne-moieties were marked with sulfo-Cy3-azide in a CuAAC. Fluorescence lifetimes of EGFP and EGFP attached to different proteins were measured. Given that FRET from the EGFP-fusion proteins to propargyl-linked Cy3 on its amino acids takes place, fluorescence lifetimes of ProSeAM-treated samples are expected to be lower than those of control samples. As seen from representative fluorescence lifetime images and calculated FRET efficiencies (Figure 4.65), no notable decrease in fluorescence lifetimes and therefore no meaningful increase in FRET efficiencies occurred. FRET efficiencies ranged from approximately -5 % to 5 %, which corresponds to fluorescence lifetimes of -100 ps to

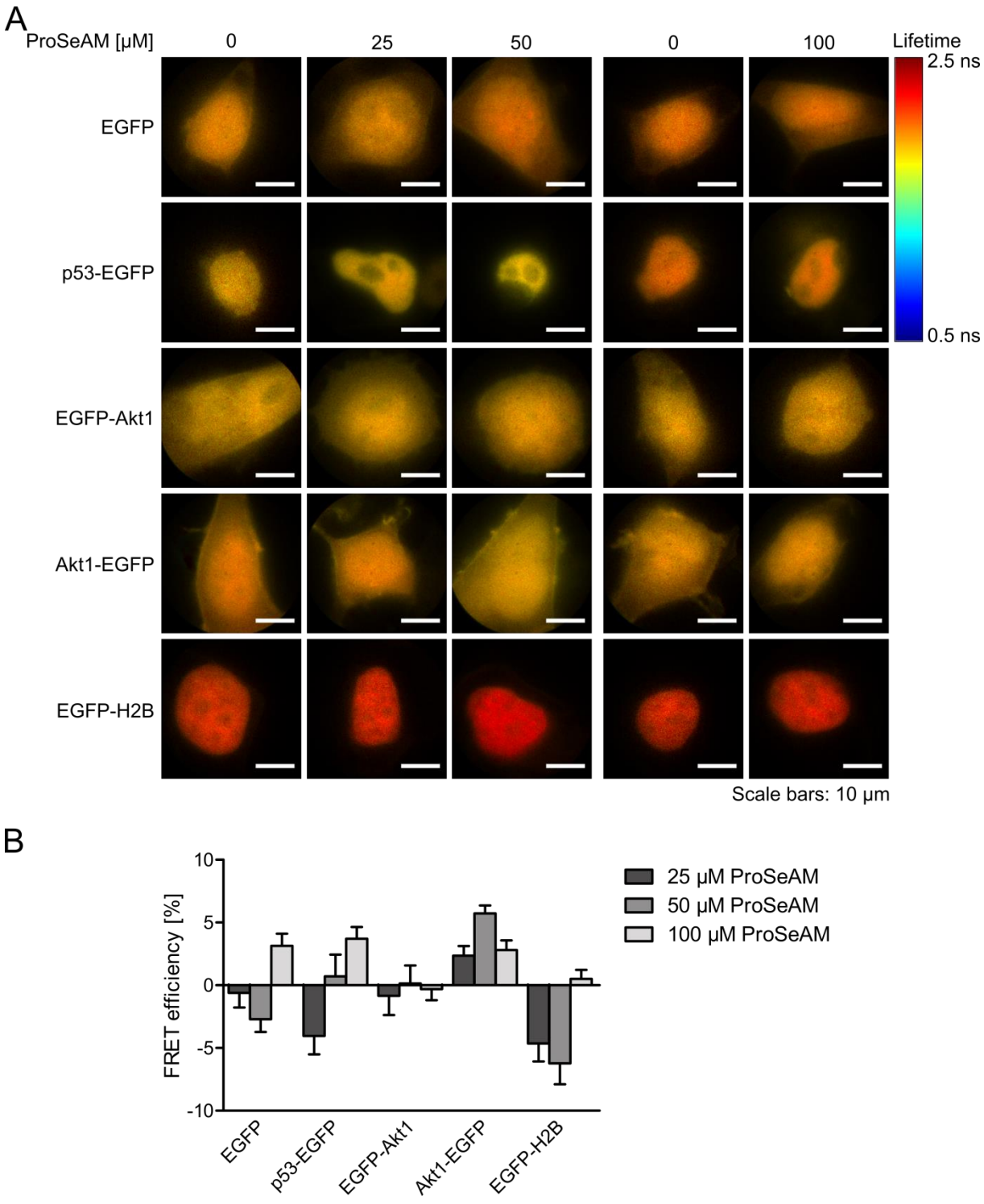

Figure 4.65: FLIM-FRET experiments in HEK293T cells with low ProSeAM concentrations. (A) Representative fluorescence lifetime images of HEK293T cells expressing EGFP-fusion proteins and electroporated in buffer containing 0 µM, 25 µM, 50 µM, or 100 µM ProSeAM are shown. Transferred propargyl residues were labeled in fixed and permeabilized cells via a CuAAC with sulfo-Cy3-azide. (B) FRET efficiencies for each EGFP-fusion protein were calculated from fluorescence lifetimes averaged over ten cells per condition. Columns belong to mean values and error bars to SEMs.

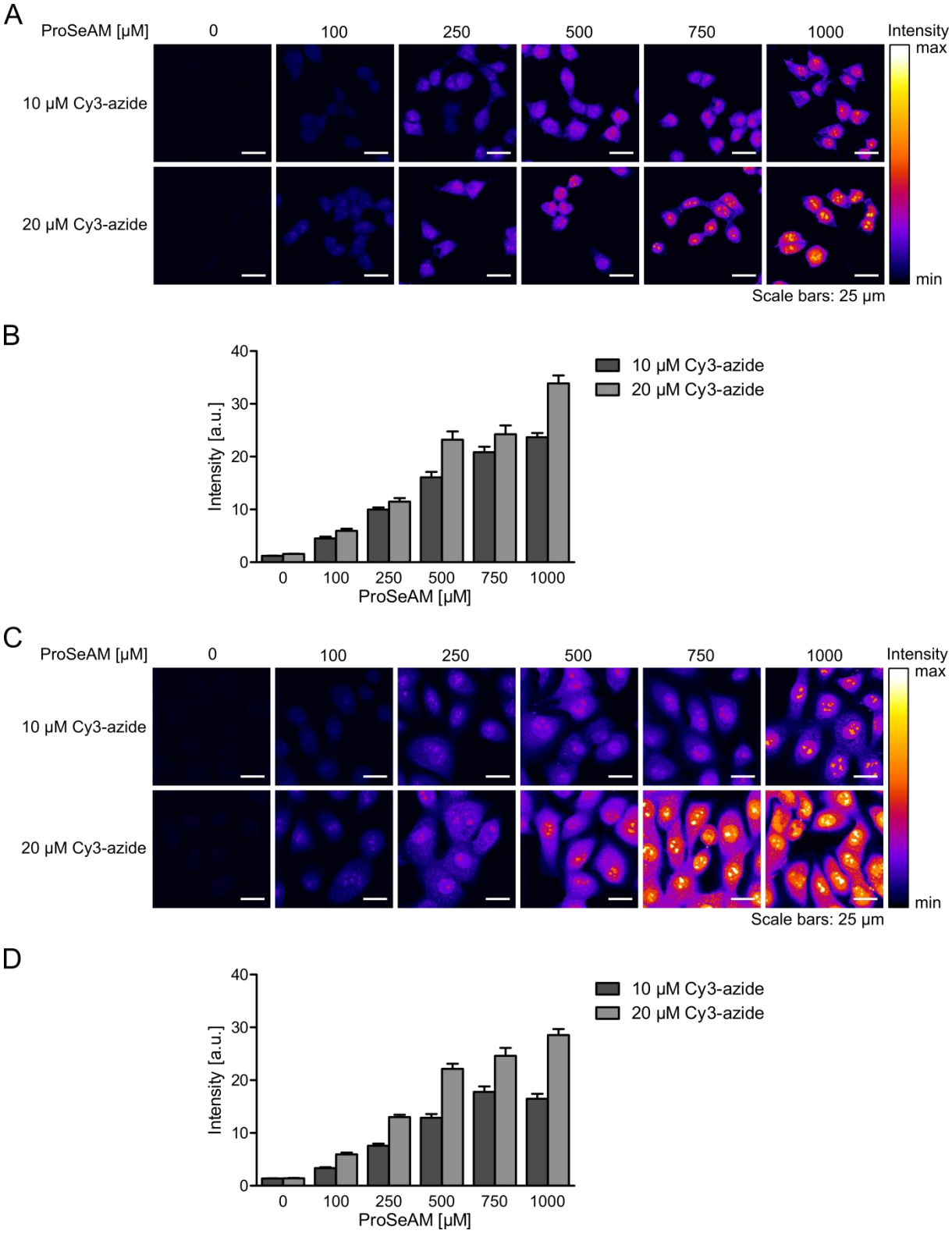

Figure 4.66: Increasing cellular Cy3 fluorescence intensities with higher concentrations of ProSeAM. Confocal fluorescence microscopy of (A+B) HEK293T and (C+D) HeLa S3 cells electroporated in presence of 0 to 1000 µM ProSeAM, subsequently incubated at 37 °C for 20 min, and labeled with sulfo-Cy3-azide was performed. (A+C) Representative confocal fluorescence images are depicted. (B+D) Fluorescence intensities were quantified for 30 different cells out of two independent experiments. Columns correspond to mean values and error bars to SEMs.

100 ps. Such differences are below the detection limit of the FLIM microscope employed. Knowing from immunoprecipitation results that p53 and Akt1 carry Cy3-labeled propargyl residues, the inability to measure FRET must originate from too few Cy3 fluorophores attached to proteins. In FLIM microscopy, fluorescence lifetimes are averaged over each pixel exhibiting fluorescence of many EGFP-fusion proteins. Hence, efficient FRET can only be detected, if a large proportion of EGFP-fusion proteins transfer their absorbed excitation energy to acceptor fluorophores. Consequently, concentrations of ProSeAM were increased from 100 µM to 1 mM. This resulted in five times higher Cy3 fluorescence intensities in HEK293T and HeLa S3 cells, which were measured by confocal fluorescence microscopy (Figure 4.66). Increasing the sulfo-Cy3-azide concentration from 10 µM to 20 µM led to a further elevation of fluorescence intensities by factors of 1.4 in HEK293T and 1.7 in HeLa S3 cells. Moreover, higher ProSeAM concentrations did not affect cellular viabilities (Figure 4.67).

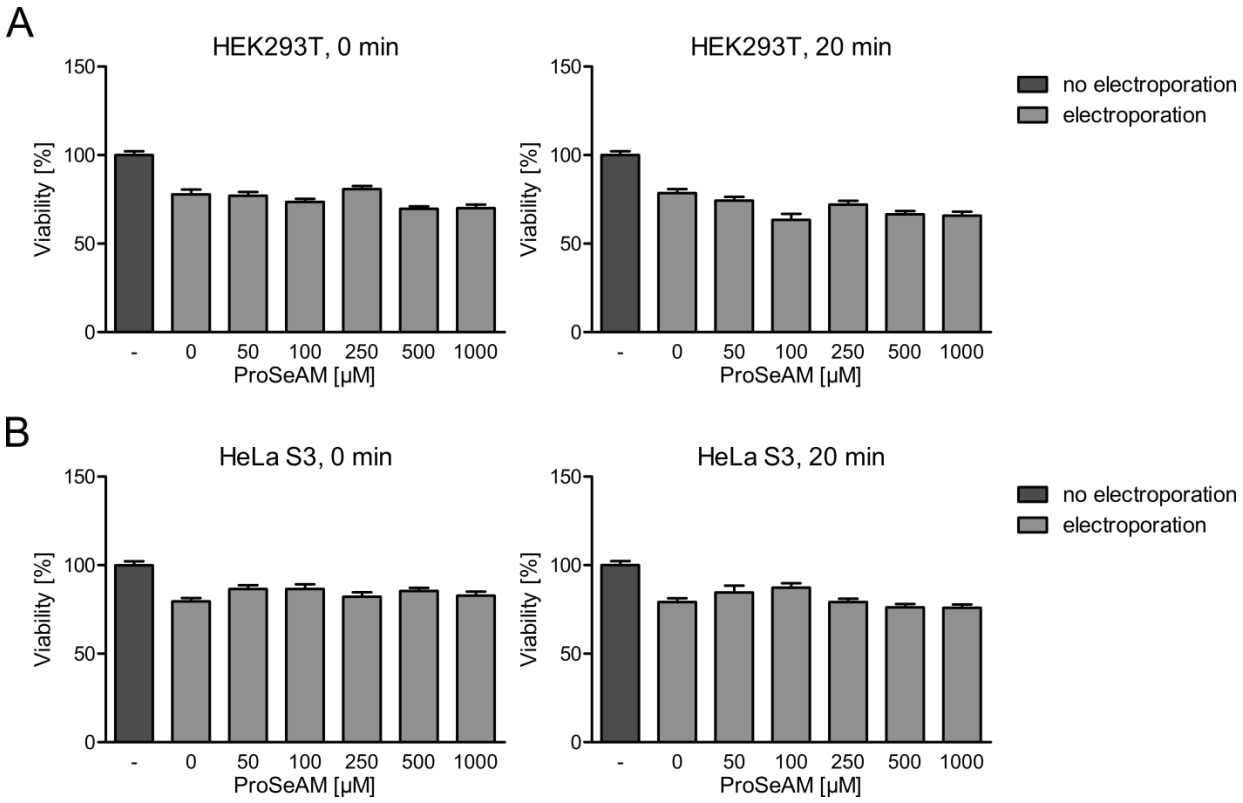

Figure 4.67: Assessing the cytotoxicity of higher concentrations of ProSeAM. Viabilities of HEK293T or HeLa S3 cells electroporated in buffer or buffer containing different concentrations of ProSeAM and subsequently incubated for 0 or 20 min were assessed with ATP assays. Control samples were not electroporated. Columns represent mean values of triplicates performed in technical quadruplicates. Error bars are SEMs.

FLIM experiments were repeated with 250 µM, 500 µM, and 1 mM ProSeAM and a sulfo-Cy3-azide concentration of 20 µM using EGFP and the fusion proteins p53-EGFP, EGFP-Akt1, Akt1-EGFP, GAPDH-EGFP, EGFP-H2B, and EB1-EGFP. Decreases in fluorescence lifetimes with increasing ProSeAM concentrations were detected for all proteins assessed (Figure 4.68). For p53-EGFP, EGFP-Akt1, and Akt1-EGFP, these were larger than for the

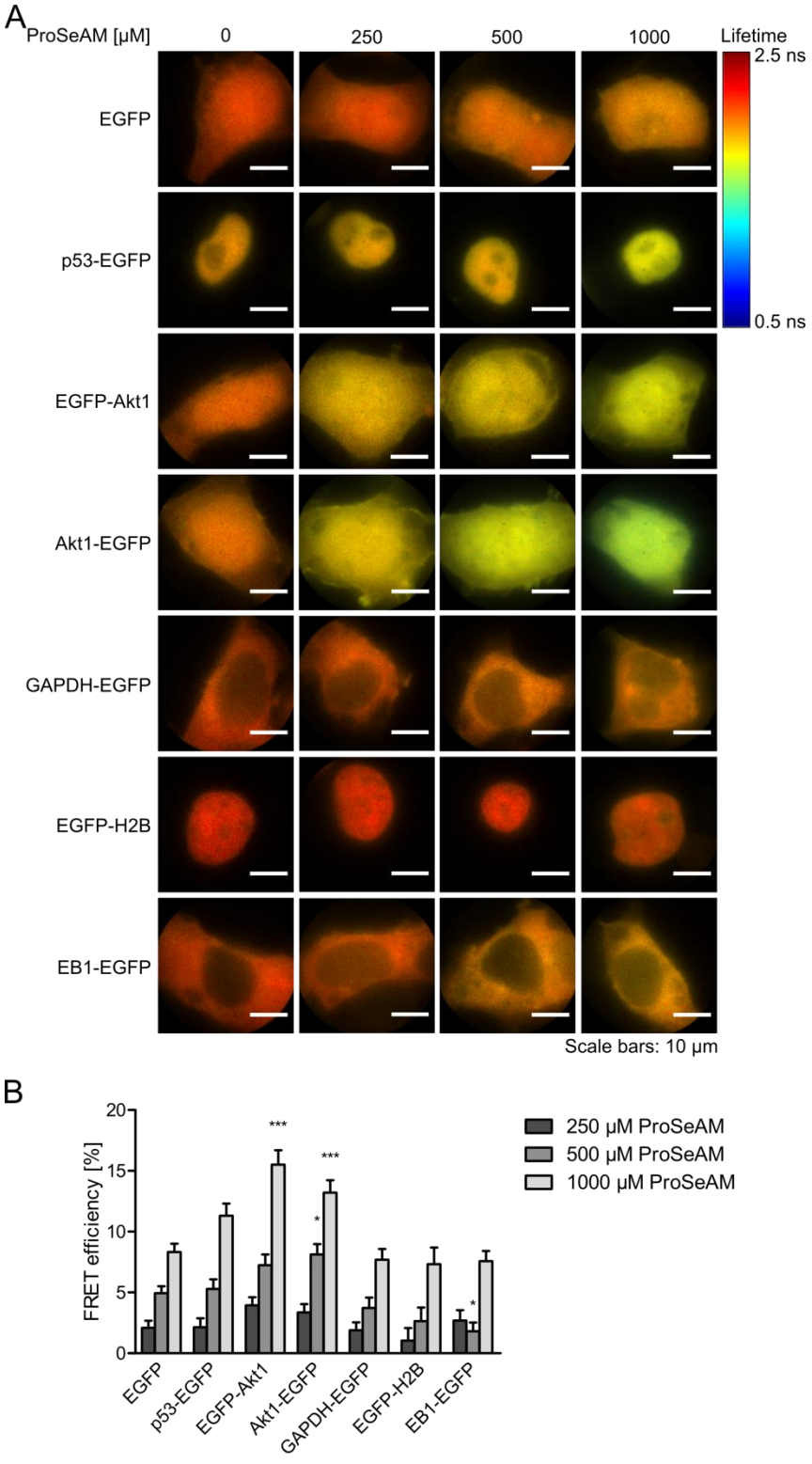

Figure 4.68: Imaging protein-specific methylation in HEK293T cells. (A) Representative fluorescence lifetime images of HEK293T cells expressing different EGFP-fusion proteins, electroporated in buffer containing 0 µM to 1000 µM ProSeAM, and labeled with sulfo-Cy3-azide via a CuAAC are presented. (B) FRET efficiencies for each EGFP-fusion protein and each concentration were calculated from fluorescence lifetimes averaged over three biological replicates with ten cells each and compared to those of EGFP with a two-way ANOVA and a Bonferroni posttest. Columns represent mean values and error bars SEMs. All columns not labeled own FRET efficiencies not significantly different with respect to those of EGFP. Degrees of significance are: ns $p>0.05$, * $p<0.05$, and *** $p<0.001$.

control protein EGFP. Since EGFP was not modified with ProSeAM's propargyl groups, reductions in its fluorescence lifetime might be caused by background FRET (unspecific intermolecular FRET to Cy3-labeled molecules in vicinity or free sulfo-Cy3-azide). Calculated FRET efficiencies for EGFP-Akt1 and Akt1-EGFP were significantly larger than those of EGFP. Thus, it can be concluded that the methylation state of Akt1 could be visualized inside HEK293T cells. Fluorescence lifetimes of EGFP-Akt1 and Akt1-EGFP did not vary within single cells stating that the localization of Akt1 does not alter its methylation and *vice versa*. Akt1 has been reported to be methylated at lysine 14.[580] Nevertheless, no differences between N- and C-terminally EGFP-tagged Akt1 were observed. This led to the conclusion that both termini of the protein have roughly the same distance to lysine 14 in Akt1's tertiary protein structure or that a further, so far unknown, methylation site of Akt1 exists. FRET efficiencies of p53-EGFP and GAPDH-EGFP were not significantly larger than those of EGFP, although the modification of these two proteins with propargyl groups has been proven (Figure 4.64). Reasons therefore could be that only small fractions of the proteins were modified or that methylation sites were spatially too far away from C-terminal EGFP to allow for efficient FRET.

For FLIM experiments with the proteins Foxo1-EGFP, H3-EGFP, H4-EGFP, EGFP-HSP70, EGFP-HSPA8, VCP-EGFP, and EGFP-nucleolin, 1 mM ProSeAM was used, since this resulted in highest FRET efficiencies and significant differences compared to EGFP. Representative fluorescence lifetime images and related FRET efficiencies are shown in Figure 4.69. Significantly higher FRET efficiencies were found for Foxo1-EGFP and H4-EGFP. It needs to be mentioned, that fluorescence lifetimes of EGFP were always constant over whole cells, although more sulfo-Cy3 fluorophores are attached to propargylated structures in the nucleus. Hence, the FLIM-FRET measurements presented here were not affected by the heterogeneous distribution of acceptor fluorophores in cells. Moreover, the non-propargylated proteins EGFP-H2B and H3-EGFP, which strongly interact with DNA that is most likely also modified with groups originating from ProSeAM, did not exhibit FRET efficiencies greater than EGFP. The same was true for EGFP-nucleolin, which colocalizes with the highest Cy3 fluorescence signals in cells. These negative controls indicate that FRET observed was most likely of intramolecular nature and not due to nearby sulfo-Cy3.

To test, whether the protein-specific imaging approach is also applicable to another cell line, similar FLIM measurements were performed with HeLa S3 cells using expression vectors for EGFP and various EGFP-fusion proteins. Strong decreases of fluorescence lifetimes along with significantly larger FRET efficiencies compared to EGFP were obtained for p53-EGFP, EGFP-Akt1, Akt1-EGFP, Foxo1-EGFP, and H4-EGFP (Figure 4.70). Thus, it was inferred that the established approach can be transferred to other cell lines provided that these cells can be transfected with plasmids encoding the desired EGFP-fusion proteins. Results were in line with the HEK293T experiments with the exception that p53 could be shown to be propargylated in HeLa S3 cells, but not in HEK293T cells. Although the FRET efficiency of p53-EGFP was higher in HEK293T cells treated with 1 mM ProSeAM than the one of EGFP, FRET efficiencies did not differ significantly. This resulted most likely from a larger fraction of p53 proteins propargylated in HeLa S3 than in HEK293T cells or differences in cellular levels of ProSeAM and native SAM.

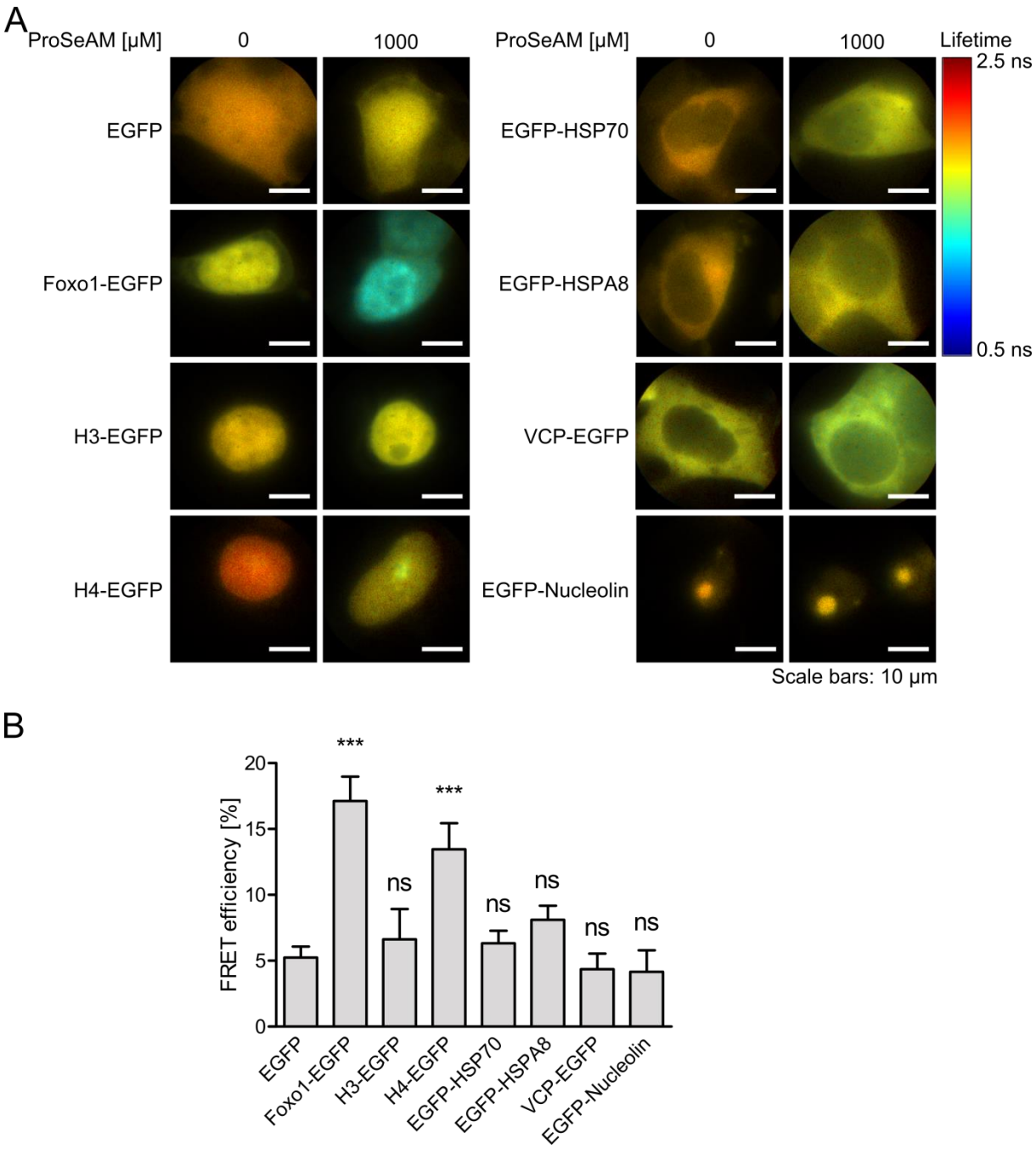

Figure 4.69: Visualizing protein-specific methylation of Foxo1 and H4 in HEK293T cells. (A) Representative fluorescence lifetime images of HEK293T cells expressing different EGFP-fusion proteins, having been electroporated in buffer containing 0 µM or 1000 µM ProSeAM, and labeled with sulfo-Cy3-azide via a CuAAC are shown. (B) FRET efficiencies calculated for each EGFP-fusion protein and each concentration from fluorescence lifetimes averaged over three biological replicates with ten cells each are displayed. Statistical significance compared to EGFP was tested with a one-way ANOVA and Dunnett's multiple comparison posttest. Columns are mean values and error bars SEMs. Degrees of significance are: ns $p>0.05$, ** $p<0.01$, and *** $p<0.001$.

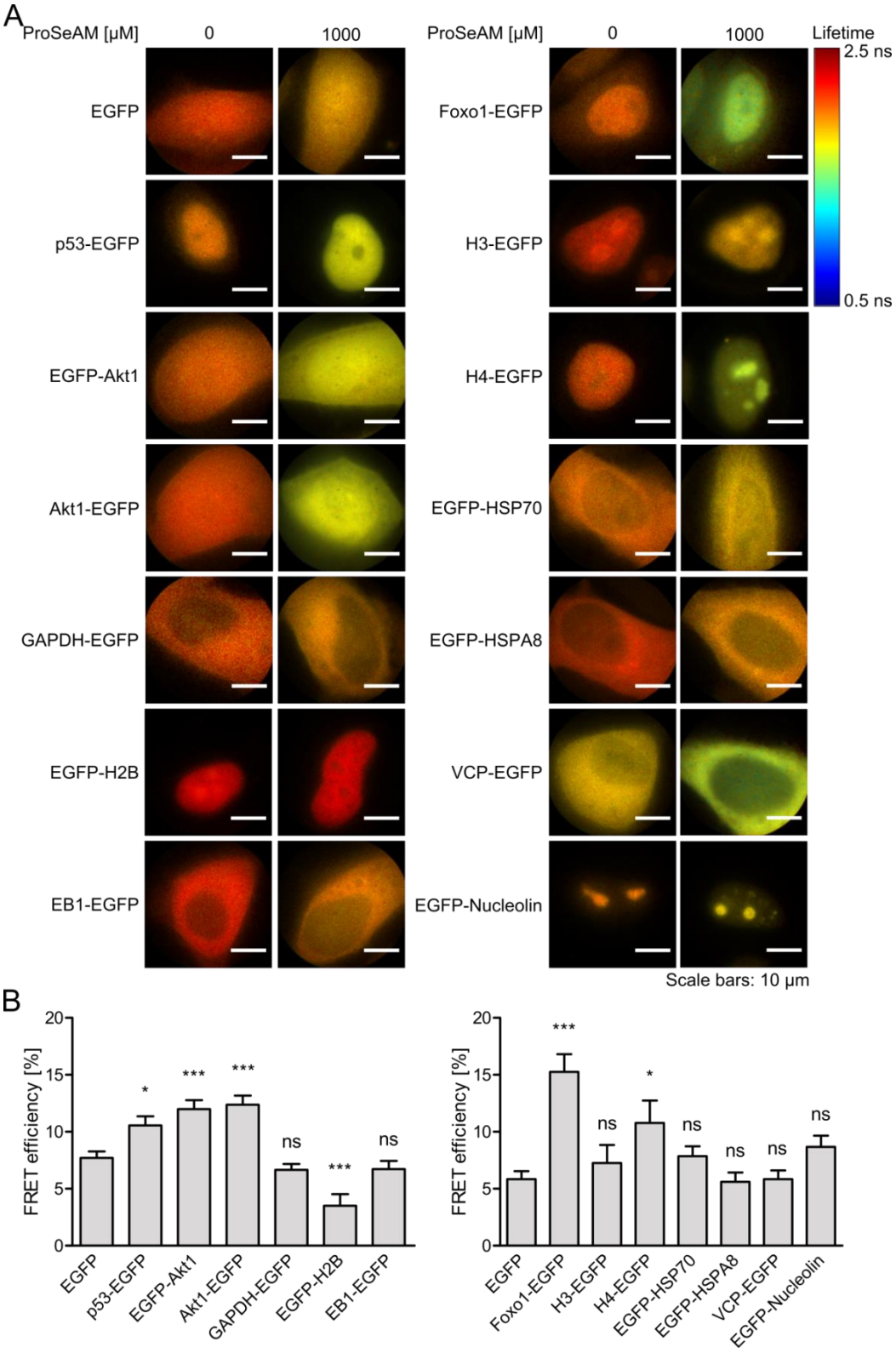

Figure 4.70: Imaging methylation of p53, Akt1, Foxo1, and H4 in single HeLa S3 cells. (A) Representative fluorescence modulation lifetime images of HeLa S3 cells transiently expressing EGFP or -fusion proteins, electroporated in buffer containing 0 µM or 1000 µM ProSeAM, and labeled with sulfo-Cy3-azide are depicted. (B) FRET efficiencies for EGFP and EGFP-fusion proteins were calculated from fluorescence lifetimes averaged over three independent experiments with ten cells each and compared to those of EGFP with one-way ANOVAs and Dunnett's multiple comparison posttests. Columns belong to mean values and error bars to SEMs. Degrees of significance are: not significant (ns) $p>0.05$, * $p<0.05$, and *** $p<0.001$.

Having successfully established an approach for protein-specific imaging of methylation that could be applied in different cell lines and with various EGFP-fusion proteins, it was aimed to study the dependence of a protein's behavior on its methylation. Such differences can hardly be resolved using mass spectrometry or biochemical methods and hence necessitates suitable imaging techniques. The transcription factor Foxo1 was chosen, which shuttles between the nucleus and cytoplasm. In its enzymatically active form, Foxo1 is present in the nucleus of cells, where it is involved in many cellular and physiological processes including metabolism, proliferation, cell cycle regulation, and apoptosis.[427] As a result of insulin treatment,

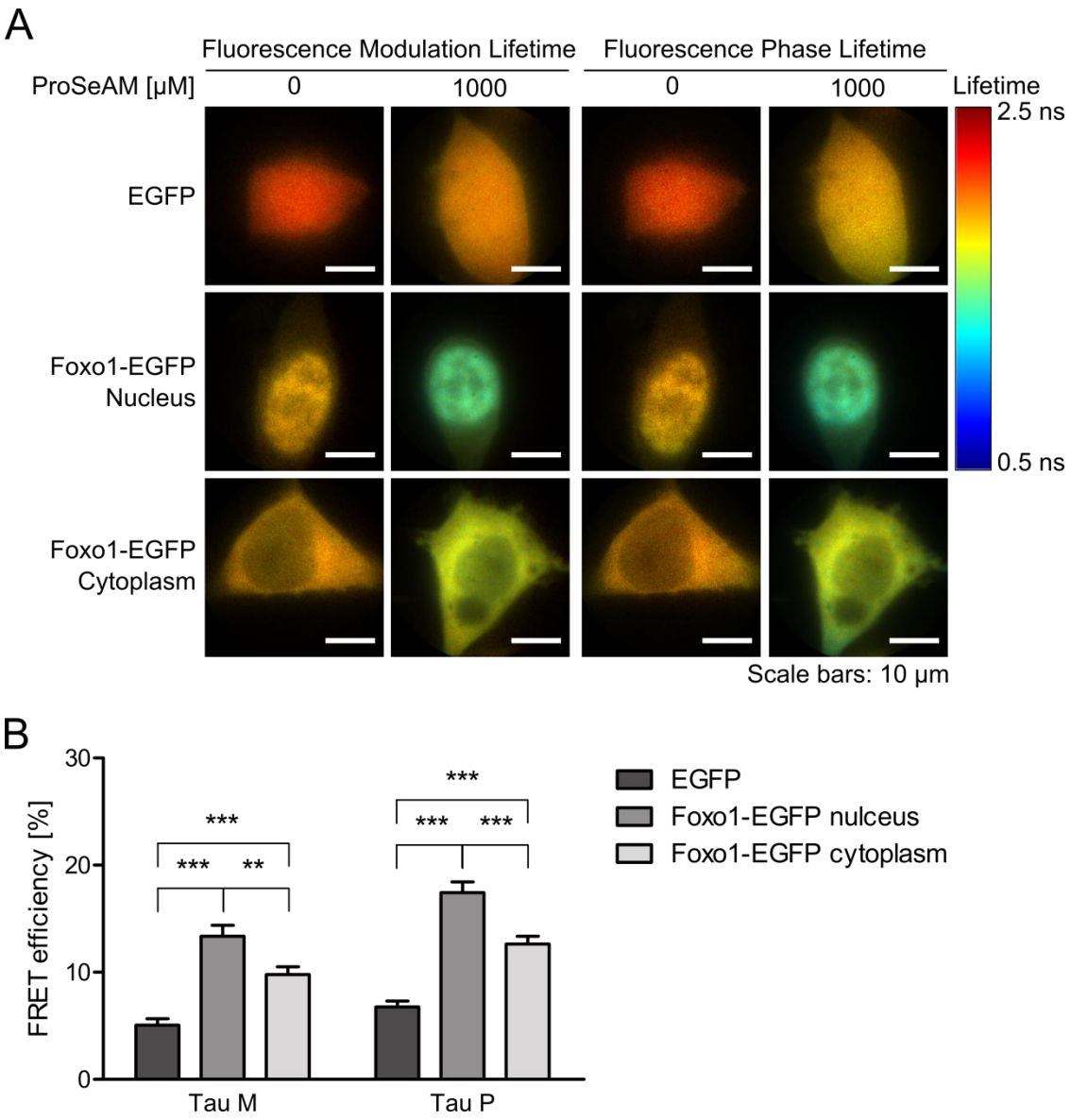

Figure 4.71: Dependence of Foxo1's methylation state on its cellular localization. (A) Representative fluorescence modulation and phase lifetime images of HEK293T cells expressing EGFP or Foxo1-EGFP and electroporated in buffer containing 0 µM or 1000 µM ProSeAM are depicted. (B) FRET efficiencies of EGFP and each EGFP-fusion protein were calculated from fluorescence modulation (Tau M) and phase (Tau P) lifetimes averaged over twelve (EGFP), nine (Foxo1-EGFP cytoplasm), or six (Foxo1-EGFP nucleus) biological replicates with ten cells each and were compared with two-way ANOVAs and Bonferroni posttests. Columns correspond to mean values and error bars to SEMs. Degrees of significance are: ** $p<0.01$ and *** $p<0.001$.

the key target of the insulin signaling cascade Foxo1 becomes phosphorylated at serine 253 by Akt1. This leads to its export from the nucleus to the cytoplasm and ensuing degradation by the ubiquitin-proteasome pathway. If Foxo1 is methylated at ε-amino groups of the arginine residues 248 and 250, it stays in the nucleus and cannot be phosphorylated.[582] Based on these discoveries, localization-dependent FRET efficiencies might be detectable for Foxo1-EGFP. To this end, HEK293T cells expressing Foxo1-EGFP were similarly treated as explained above, but cells with Foxo1-EGFP localized in the nucleus and cytoplasm were measured separately. Representative fluorescence lifetime images and calculated FRET efficiencies are presented in Figure 4.71. Fluorescence lifetimes of nuclear Foxo1-EGFP were smaller and FRET efficiencies significantly larger than those of cytoplasmic Foxo1-EGFP. These data are in accordance with literature[582] and led to the conclusion that the local methylation pattern of Foxo1 could indeed be deciphered using this imaging approach.

4.3.4. Conclusions

In summary, the methylation reporter ProSeAM was successfully delivered in HEK293T and HeLa S3 cells by electroporation. In cell imaging of protein methylation after the CuAAC of transferred propargyl residues with sulfo-Cy3-azide was accomplished by confocal fluorescence microscopy for the first time. The combination of this chemical reporter strategy and FLIM-FRET microscopy allowed for the visualization of protein-specific methylation inside single cells. Imaging of the methylation state of twelve different EGFP-fusion proteins in two distinct cell lines validated the general applicability of this approach. The huge potential of this method was demonstrated by directly resolving the localization-dependent methylation pattern of the transcription factor Foxo1.
All imaging experiments presented here were carried out in fixed cells. To allow for protein-specific imaging in living cells, new chemical reporters with a chemical handle capable of reacting in a DAinv reaction with tetrazines, such as a cyclopropene, would need to be synthesized.

5. Outlook

This thesis describes the successful realization of novel strategies for in cell imaging of protein-specific glycosylation and methylation and their application to investigations of the modification states of various proteins with high spatial resolution. Both approaches could be used to assess the modification of further EGFP-fusion proteins and to decipher their localization-dependencies, first examples of which were presented. In addition, the modification of individual proteins could be followed upon an external stimulus, such as insulin, by fixing cells and labeling chemical handles of monosaccharides after different times. Imaging of temporal changes of single cells would be possible with respect to the microscope employed, but most likely only the incorporation and not the removal of the respective reporters could be observed. Once a fluorophore is attached to the reporter, it is improbable that it will still be recognized by glycosidases or demethylases.

For the chemical reporter Ac_4GlcNCyoc, it should be verified by mass spectrometry that it is bound to hydroxy groups of serine and threonine residues and is not attached to cysteines, as proposed by Chen and coworkers for peracetylated GalNAc and GlcNAc derivatives.[549]

Besides this, new *O*-GlcNAc reporters with smaller chemical handles than Ac_4GlcNCyoc, but also capable of being labeled in a DAinv reaction, could be synthesized and used for protein-specific imaging.

Although visualizing β-catenin's N-terminal *O*-GlcNAcylation in cells was not successful, the created single, double, triple, and quadruple *O*-GlcNAc point mutants of EGFP-β-catenin could be used to assess the influence of the *O*-GlcNAcylation of each residue and also their combined effects on the localization of the protein by fluorescence microscopy. Until now, changes of β-catenin's localization have just been shown for the mutant S23A.[490] The created set of point mutants is perfectly suited to investigate the N-terminal *O*-GlcNAcylation of β-catenin in more detail.

If seeds of *A. thaliana* mutants expressing GFP-fusions of proteins known to be *O*-GlcNAcylated in roots would be available or would have been created, the protein's glycosylation state could be visualized by FLIM-FRET microscopy upon treatment of seedlings with Ac_4GlcNAz followed by fixation, permeabilization, and CuAAC. This could give further insights into the functional importance of protein *O*-GlcNAcylation in plants, which is not fully understood to date.[507]

Metabolic glycoengineering appeared as interesting tool for studying protein glycosylation in cancer. Even though the proximity of GalNAc and Neu5Ac in sialyl Tn could not be imaged specifically, the usage of non-cancer gastric control cells might allow to distinguish between cancer and non-cancer cells based on the truncation of *O*-glycans. Apart from this, MGE could be employed to study the kinetics of the incorporation of various modified monosaccharides in different cancer cell lines. Moreover, experiments on the exchange of cell surface glycans among cells, which were started in Porto but not included in this thesis, could

be further pursued. This field is extremely interesting, as little is known on the occurrence and mechanisms of this process so far. Initial experiments were promising, since they showed differences in glycan exchange rates among different cancer cells.

To enable the visualization of protein-specific acetylation, new chemical reporters that are better cell permeable and better accepted by cellular enzymes than Na4P need to be synthesized. An ideal acetylation reporter would carry a chemical handle that can react with a tetrazine-tagged fluorophore in a DAinv reaction. This would enable investigations inside living cells. Alternatively, the poorly cell permeable Na4P could be mechanically or chemically delivered in cells using electroporation, microinjection, cell squeezing, Triton X-100 permeabilization, or peptide carriers.

Similarly, new chemical methylation reporters bearing alkenes on the sulfonium or selenium center that could be labeled via a DAinv reaction could be synthesized. Since ProSeAM is also a substrate of DNA and RNA methyltransferases,[222,224] it could be used to study the methylation of nucleic acids isolated from cells. When combining the usage of ProSeAM with fluorescently-marked DNA or RNA, the modification of selected nucleic acids with propargyl groups could be imaged in cells by FLIM-FRET microscopy.

Furthermore, strategies similar to those for imaging protein glycosylation and methylation could be developed for other PTMs. Especially interesting would be the recently identified lysine modifications malonylation, crotonylation, propionylation, and butyrylation.[103–105] Chemical reporters have already been synthesized for these PTMs,[155–157] but little is known about their biological functions and possible localization- and time-dependent modification patterns of targeted proteins. Having protein-specific imaging approaches for these PTMs at hands would allow shedding light on their biological impacts.

Finally, the strategies for protein-specific imaging themselves could be expanded. The need of modification sites to be in close proximity to the N- or C-terminus to ensure a small enough distance to EGFP for FRET measurements could be overcome by placing the donor fluorophore next to the modification site of interest. To this end, unnatural amino acids could be introduced in the amino acid sequence of selected proteins and marked with donor fluorophores via bioorthogonal ligation reactions or the probe incorporation mediated by enzymes (PRIME) strategy.[275,596]

6. Materials and Methods

6.1. Materials

6.1.1. Organisms

Eukaryotic cells

Table 6.1: Eukaryotic cell lines used within this thesis.

Cell line	Description	Origin
CHO	Chinese hamster ovary cells	Group of Prof. Dr. Zumbusch, University of Konstanz (used by Dr. Christelle Rosazza)
HEK293T	Human embryonic kidney cells	Group of Prof. Dr. Brunner, University of Konstanz
HeLa	Derived from cervical cancer cells taken from Henrietta Lacks	Group of Prof. Dr. Scheffner, University of Konstanz
HeLa S3	Derived from cervical cancer cells taken from Henrietta Lacks	Group of Prof. Dr. Zumbusch, University of Konstanz (used by Dr. Christian Jüngst)
HeLa EGFP	Derived from cervical cancer cells taken from Henrietta Lacks, stably expressing EGFP under a tetracycline promotor	Group of Prof. Dr. Mayer, University of Konstanz, created by Dr. Julia Häfner via the Flp-In T-Rex system
HeLa EGFP-Kif18A	Derived from cervical cancer cells taken from Henrietta Lacks, stably expressing EGFP-Kif18A under a tetracycline promotor	Group of Prof. Dr. Mayer, University of Konstanz, created by Dr. Julia Häfner via the Flp-In T-Rex system
H1299	Human non-small cell lung carcinoma cells	Group of Prof. Dr. Scheffner, University of Konstanz
MKN45 Mock	Human gastric cancer cell line stably expressing a control vector	Group of Prof. Dr. Reis, University of Porto, Portugal
MKN45 ST6GalNAc1	Human gastric cancer cell line stably overexpressing ST6GalNAc1	Group of Prof. Dr. Reis, University of Porto, Portugal
MKN45 ST3Gal4	Human gastric cancer cell line stably overexpressing ST3Gal4	Group of Prof. Dr. Reis, University of Porto, Portugal
NIH 3T3	Mouse embryonic fibroblast cells	Group of Prof. Dr. Leist, University of Konstanz

Prokaryotic cells

Table 6.2: Bacteria utilized within this thesis.

Cell line	Description	Origin
E. coli Nova Blue	endA1, hsdR17 (rk12- mk12+), supE44, thi-1, recA1, gyrA96, relA1, lac [F´proA+B+ lacIqZ_M15::Tn10 (TetR)]	Novagen

Plants

Table 6.3: Plants employed within this thesis.

Plant	Description	Origin
Arabidopsis thaliana Col(0)	Wild-type plant from Columbia	Group of PD Dr. Funck, University of Konstanz

6.1.2. Media

Table 6.4: Summary of media components used.

Component	Manufacturer	Catalog number
Agar	Roth	S210.3
Ampicillin	Roth	K029.2
BME vitamins	Sigma-Aldrich	B6891
Carbenicillin	Roth	6344.2
Chloramphenicol	Roth	3886.2
D-(+)-glucose solution	Sigma-Aldrich	G8769
Dublecco's modified eagle medium (DMEM) high glucose	Thermo Fisher Scientific	41965039
DMEM high glucose with pyruvate	Thermo Fisher Scientific	41966052
DMEM high glucose, no glutamine, no phenol red	Thermo Fisher Scientific	31053028
Fetal bovine serum (FBS)	Biochrom	S0615
Fetal calve serum (FCS), tetracycline free	Group of Prof. Dr. Mayer, University of Konstanz	
Geneticin (G418)	Thermo Fisher Scientific	10131-035
Hygromycin B	Calbiochem	400053
Kanamycin sulfate	Genaxxon	M3129
L-glutamine	Thermo Fisher Scientific	25030123
Lysogeny broth (LB)-agar	Roth	X965
LB-medium	Roth	X964
Minimum essential medium (MEM)	Thermo Fisher Scientific	10370021
MS medium	Duchefa Biochemie	M0221.0050
MS vitamin solution, 1000x	Sigma-Aldrich	M3900
Opti-MEM	Thermo Fisher Scientific	31985062
Penicillin-Streptomycin (10,000 units mL^{-1} penicillin and 10,000 µg mL^{-1} streptomycin)	Thermo Fisher Scientific	15140-122
Roswell Park Memorial Institute cell culture medium (RPMI) 1640 GlutaMAX with 25 mM 2-[4-(2-Hydroxyethyl)piperazin-1-yl]ethanesulfonic acid (HEPES)	Thermo Fisher Scientific	72400-021
RPMI 1640, no HEPES, no phenol red	Thermo Fisher Scientific	11835-063
Sucrose	Roth	4621.2
Synth-a-Freeze Cryopreservation Medium	Thermo Fisher Scientific	A1254201
Tryptose phosphate	Sigma-Aldrich	T8782

Table 6.5: Composition of different media.

Organism/Medium	Medium composition
CHO cells	MEM, 8 V-% FBS, 3.5 g L^{-1} D-(+)-glucose, 2.95 g L^{-1} tryptose phosphate, 1x BME vitamins, 2 mM L-glutamine, 1 V-% penicillin-streptomycin
HEK293T, HeLa, HeLa S3, and NIH 3T3 cells	DMEM high glucose with pyruvate, 10 V-% FBS, 1 V-% penicillin-streptomycin
HeLa EGFP and HeLa EGFP-Kif18A cells	DMEM high glucose with pyruvate, 10 V-% FCS (tetracycline free), 1 V-% penicillin-streptomycin, hygromycin B
H1299 cells	DMEM high glucose, 10 V-% FBS, 1 V-% penicillin-streptomycin
MKN45 cells	RPMI 1640 GlutaMAX, 10 V-% FBS, 1 V-% penicillin-streptomycin, 0.5 mg mL^{-1} geneticin
Freezing medium for mammalian cells	Corresponding DMEM, 20 V-% FBS, 10 V-% DMSO or Synth-a-Freeze Cryopreservation Medium
Microscopy media for mammalian cells	DMEM high glucose without glutamine or phenol red, 10 mM HEPES *or* RPMI 1640 GlutaMAX without phenol red, 10 V-% FBS, 1 V-% penicillin-streptomycin, 0.5 mg mL^{-1} geneticin, 10 mM HEPES
E. coli liquid LB medium	Liquid LB medium: 20 g L^{-1} of LB-medium (10 g L^{-1} tryptone, 5 g L^{-1} yeast extract, 5 g L^{-1} NaCl, pH 7.0)
E. coli freezing medium	50 V-% liquid LB medium, 50 V-% glycerol
E. coli LB agar plates	35 g L^{-1} of LB-agar (10 g L^{-1} tryptone, 5 g L^{-1} yeast extract, 5 g L^{-1} NaCl, 15 g L^{-1} agar-agar, pH 7.0)
E. coli additives	100 µg mL^{-1} ampicillin, 50 µg mL^{-1} carbenicillin, 50 µg mL^{-1} kanamycin, 30 µg mL^{-1} chloramphenicol, or 7 w-% sucrose
A. thaliana liquid medium	1x MS medium (4.3 g L^{-1}), 1 w-% sucrose, 1x MS vitamins
A. thaliana agar plates	0.8 w-% agar, 1x MS medium, 1 w-% sucrose, 1x MS vitamins

6.1.3. Buffers and Solutions

Commercially available buffers and solutions

Buffer G (Thermo Fisher Scientific, #BG5), Cre recombinase reaction buffer (group of Prof. Dr. Hauck, University of Konstanz and New England Biolabs (NEB)), Cut smart buffer (NEB, supplied with corresponding restriction enzymes), DPBS (Thermo Fisher Scientific, #14190094), Fast digest buffer (Thermo Fisher Scientific, #B64), NEBuffer 2 (NEB, #B7002S), TE buffer (supplied with DNA isolation kits).

Self-made buffers and solutions

Table 6.6: Composition of self-made buffers and solutions.

Buffer/Solution	Composition
10x PBS	26.7 mM KCl, 14.7 mM KH_2PO_4, 1.38 M NaCl, 80.6 mM Na_2HPO_4 x 7 H_2O
2x HEPES buffered saline (HBS)	280 mM NaCl, 50 mM HEPES, 1.48 mM Na_2HPO_4 x 7 H_2O
4% paraformaldehyde (PFA)	4 w-% PFA in MQ water, pH 7.4
4x SDS sample buffer	100 mM Tris pH 6.8, 30 V-% glycerol, 0.21 M SDS, 2.84 M ß-mercaptoethanol, 0.29 mM bromophenol blue

50x TAE	2 M Tris, 50 mM ethylenediamine-*N*,*N*,*N*',*N*'-tetraacetic acid (EDTA) pH 8.0, 0.0571 V-% acetic acid
6x GEBS	746 µM bromophenol blue, 18.4 mM *N*-lauroylsarcosine, 50 mM EDTA, 20 V-% glycerol
Acetate buffer	0.2 M CH_3COOH/CH_3COONa pH 5.0 in MQ water
Birnboim-Doly buffer 1	50 mM Tris pH8, 10 mM EDTA, 100 µg mL^{-1} RNAse A
Birnboim-Doly buffer 2	200 mM NaOH, 1 % SDS
Birnboim-Doly buffer 3	3 M potassium acetate, pH 5.5
Blotto	2 w-% bovine serum albumin (BSA), 0.05 w-% NaAz in PBS-T
$CaCl_2$ solution	2.5 M $CaCl_2$ in MQ water, sterile filtered
Dilution buffer for CuAAC	1x PBS with 300 mM NaCl, 1x protease inhibitors, 0.5 V-% Triton X-100
Dilution buffer for IP	10 mM Tris pH 7.5, 150 mM NaCl, 0.5 mM EDTA
GelRed destaining solution	0.1 M NaCl
GelRed staining solution	0.1 M NaCl with 0.03 V-% GelRed
Lower buffer	370 mM Tris-HCl pH 8.8, 0.1 w-% SDS
Lysis buffer used in acetylation and methylation experiments	1x PBS with 300 mM NaCl, 1x protease inhibitors, 1 V-% Triton X-100, 10 U mL^{-1} DNAse I
Lysis buffer used in glycosylation experiments	0.5 V-% Triton X-100, 25 mM Tris pH 7.4, 300 mM NaCl, 5 mM EDTA, 20 mM β-glycerophosphate, 20 mM NaF, 0.3 mM Na_3VO_4, 10 U mL^{-1} DNAse I, 1x protease inhibitors EDTA was omitted, if CuAAC was performed afterwards.
PBS-T	0.5 V-% Tween-20 in 1x PBS
SDS-PAGE running buffer	25 mM Tris pH 8.3, 192 mM glycerol, 3.45 mM SDS
Triton buffer	1 V-% Triton X-100, 50 mM HEPES pH 7.4, 150 mM NaCl, 10 V-% glycerol, 1.5 mM $MgCl_2$, 1 mM ethylene glycol-bis(β-aminoethyl ether)-*N*,*N*,*N'*,*N'*-tetraacetic acid (EGTA), 10 mM $Na_4P_2O_7$, 100 mM NaF, 1 mM Na_3VO_4, 1x protease inhibitors
Upper buffer	125 mM Tris-HCl pH 6.8, 0.1 w-% SDS
Western Blot running buffer	25 mM Tris pH 8.3, 192 mM glycerol, 20 V-% methanol
ZAP buffer	10 mM K_2HPO_4/KH_2PO_4 pH 7.4, 1 mM $MgCl_2$, 250 mM sucrose

6.1.4. Chemicals

3-azido-7-hydroxycoumarin (Roth, 7811), 4-pentynoic acid (Sigma-Aldrich, #232211), $Ac_4$5SGlcNAc (synthesized by the group of Prof. Dr. Vocadlo, Simon Fraser University, British Columbia, Canada), Ac_4GalNAz (Jena Bioscience, #CLK-1086), Ac_4GalNCyoc (synthesized by Dr. Anne-Katrin Späte, group of Prof. Dr. Wittmann, University of Konstanz), Ac_4GlcNAc (Sigma-Aldrich, #859990), Ac_4GlcNAz (Jena Bioscience, #CLK-1085), Ac_4GlcNCyoc (synthesized by Dr. Anne-Katrin Späte, group of Prof. Dr. Wittmann, University of Konstanz), Ac_4ManNAz (Jena Bioscience, #CLK-1084), Ac_4ManNCyoc (synthesized by Dr. Anne-Katrin Späte and later by Monica Boldt, group of Prof. Dr. Wittmann, University of Konstanz), acetyl chloride (Sigma-Aldrich, #00990), acetylene-PEG_4-biotin (Jena Bioscience, #CLK-TA105), acrylamide (Rotiphorese Gel 30, Roth, #3029),

adenosine periodate oxidized (Sigma-Aldrich, #A7154), agarose (Genaxxon, #M3044), AlamarBlue (Thermo Fisher Scientific, #DAL1100), Alexa Fluor 488-DIBO (Thermo Fisher Scientific, #C10405), AM4P (synthesized by myself), aminoguanidine hypochlorite (Sigma-Aldrich, #396494), ammoniumchloride (Roth, #5470.1), ammonium peroxodisulfate (Roth, #9592.2), biotin-alkyne (Jena Bioscience, #CLK-TA105), biotin-Tz (synthesized by the group of Prof. Dr. Wittmann, University of Konstanz), bromomethylacetate (Alfa Aesar, #H56755), bromophenyl blue (Roth, #P3862.1), BSA (Sigma-Aldrich, #A7030), CellTiter-Glo Luminescent Cell Viability Assay (promega, #G7571), chloroform for spectroscopy (Merck, #1.02447), chloroquine (Sigma-Aldrich, #C6628), coumarin 6 (Sigma-Aldrich, #442631), curcumin (Biomol, #AG-CN2-0059), $CuSO_4$ (Merck, #2787.1000), Cy3-Tz (Jena Bioscience, #CLK-014-05), Cy3-Tz (synthesized by Holger Bußkamp, group of Prof. Dr. Marx, University of Konstanz), DAPI (Sigma-Aldrich, #32670), deacetylases inhibitor cocktail (Santa Cruz Biotechnology, #sc-362323), DIPEA (Sigma-Aldrich, #496219), DMSO (Sigma-Aldrich, #D8418), dNTP-Set (Genaxxon, #M3015), enhanced chemiluminescence (ECL) substrates (Bio-Rad, #1705061), EDTA (Roth, #CN06.1), ER-Tracker (Thermo Fisher Scientific, #E34251), ethanol p.a. (Roth, #9065.3), GelRed (Genaxxon, #M3199), Gen ladder 1kb (Genaxxon, #M3328), GenaxxoFect (Genaxxon, #M3053), GFP-Trap_A (ChromoTek, #gta-20), glycerol (VWR, #24386.298 and Sigma, #G2025), HEPES solution 1 M (Sigma-Aldrich, #H0887 and Thermo Fisher Scientific, #15630-056), immersion oil (Leica, #11513859), iodine (Roth, 7935.1), isopropanol p.a. (Sigma-Aldrich, #3353.9), Lipofectamine™ 2000 Transfection Reagent (Thermo Fisher Scientific, #11668019), Lyso-Tracker (Thermo Fisher Scientific, #L7526), M4P (synthesized by myself), methanol p.a. (Honeywell Riedel-de Haën, #322B), milk powder (Roth, #T145.3), Mito-Tracker (Thermo Fisher Scientific, #M7514), Na_2SO_4 (Merck, #1.06649.100), Na4P (prepared by myself), nocodazole (Sigma-Aldrich, #M1404), OSMI-1 (synthesized by myself), PFA (Merck, #1.04005), poly-L-lysine (Sigma-Aldrich, #P4707), Ponceau S (Sigma-Aldrich, #P7170), ProSeAM (synthesized by Raphael Steimbach, group of Prof. Dr. Zumbusch, University of Konstanz), protease inhibitors EDTA-free (Sigma-Aldrich, #4693159001), protein A/G PLUS-Agarose (Santa Cruz Biotechnology, #sc-2003), protein ladder (Thermo Fisher Scientific, #26617), PUGNAc (*O*-(2-acetamido-2-deoxy-D-glucopyranosylidenamino) *N*-phenylcarbamate, Sigma-Aldrich, #A7229), resazurin sodium salt (Sigma-Aldrich, #R7017), rhodamine 6G (Radiant Dyes Laser & Accessories, #79), sand (Thermo Fisher Scientific, #S|0320|63), SDS (Roth, #2326.2), silica gel 60 (Roth, #P091.2), sodium acetate (Sigma-Aldrich, #S5636), sodium ascorbate (Sigma-Aldrich, #11140), sodium hypochlorite solution (Roth, #9062.3), sulfo-Cy3-alkyne (Jena Bioscience, #CLK-TA117.1), sulfo-Cy3-azide (Lumiprobe, #B1330), TAMRA-Az (Jena Bioscience, #CLK-FA008), TAMRA-Tz (Jena Bioscience, #CLK-017-05), TBTA (Sigma-Aldrich, #678937), TCEP (Sigma-Aldrich, #75259), tetramethylethylenediamine (TEMED, Roth, #2367.3), tetracycline hydrochloride (Genaxxon, #M3148), THPTA (Sigma-Aldrich, #762342), thymidine (Sigma-Aldrich, #T1895), Triton X-100 (Roth, #3051.3), Tween 20 (Roth, #9127.1).

6.1.5. Enzymes

AccI (NEB, #R0161S), accutase (Thermo Fisher Scientific, #A1110501), Cre recombinase (group of Prof. Dr. Hauck, University of Konstanz and NEB, #M0298S), DNAseI (Thermo Fisher Scientific, #90083), DpnI (group of Prof. Dr. Hauck, University of Konstanz), NarI (NEB, #R0191S), neuraminidase from *C. perfringens* type VI (Sigma-Aldrich, #N3001), PaeI (Thermo Fisher Scientific, #FD0604), Pfu polymerase (group of Prof. Dr. Hauck, University of Konstanz), PNGase F (Promega #V4831), PvuII (Thermo Fisher Scientific, #FD0634), RNAse A (Genaxxon, #S5218.0050), SacI (Thermo Fisher Scientific and NEB, #R3156S), SacII (NEB, #R0157S), SfoI (NEB, #R0606S), T4 polymerase (group of Prof. Dr. Hauck, University of Konstanz and NEB, #M0203S), Taq polymerase (group of Prof. Dr. Hauck, University of Konstanz and NEB, #M0267S), TrypLE Express Enzyme (Thermo Fisher Scientific, #12604013).

6.1.6. Plasmids

Table 6.7: Plasmids used within this thesis.

Abbreviation used in this thesis	Lab code	Origin
E.v.	1	Group of Prof. Dr. Hauck (#311), University of Konstanz
EGFP	2	Group of Prof. Dr. Hauck (#321), University of Konstanz
EGFP NT for Cre	3	Group of Prof. Dr. Hauck (#367), University of Konstanz
EGFP CT for Cre	5	Group of Prof. Dr. Hauck (#353), University of Konstanz
pDNR-Dual	6	Group of Prof. Dr. Hauck (#326), University of Konstanz
EGFP-OGT	11	Group of Prof. Dr. Hauck (#2015), University of Konstanz
OGA	12	Harvard Medical School (HMS) #HsCD00338122
p53-EGFP	20	Arthur Fischbach, group of Prof. Dr. Bürkle, University of Konstanz
ACTN1-EGFP	30	Group of Prof. Dr. Hauck (#276), University of Konstanz
EGFP-ACTN4	35	Group of Prof. Dr. Hauck (#3047), University of Konstanz
IR-EGFP	40	Addgene plasmid #22286, Joseph Bass[597]
EGFP-Akt1	42	Addgene plasmid #39531, Julian Downward[598]
Akt1-EGFP	43	Harvard Medical School (HMS) #HsCD00026041[599]
Foxo1-EGFP	44	Addgene plasmid #17551, Domenico Accili[436]
EGFP-Vinculin	51	Group of Prof. Dr. Hauck (#2045), University of Konstanz
EGFP-SP1	53	Addgene plasmid #39325, Beatrice Yue[600]
CAMK4-EGFP	54	Harvard Medical School (HMS) #HsCD00026148[599]
EGFP-c-Myc	55	Addgene plasmid #37608, Peter Howley[601]
SNAC-EGFP	56	Group of Prof. Dr. Leist, University of Konstanz
PP1β-EGFP	57	Addgene plasmid #44223, Angus Lamond and Laura Trinkle-Mulcahy[602]
pcDNA3.0-β-catenin	60	Addgene plasmid #16828, Eric Fearon[603]
pDNR-Dual-β-catenin WT	61	Cloned with Pia Widder

pDNR-Dual-β-catenin S23A	62	Cloned with Pia Widder
pDNR-Dual-β-catenin T40A	63	Cloned with Pia Widder
pDNR-Dual-β-catenin T41A	64	Cloned with Pia Widder and Laura Scheinost
pDNR-Dual-β-catenin T112A	65	Cloned with Pia Widder and Laura Scheinost
pDNR-Dual-β-catenin T40AT41A	66	Cloned with Pia Widder
pDNR-Dual-β-catenin S23AT40AT41A	67	Cloned with Laura Scheinost
pDNR-Dual-β-catenin T40AT41AT112A	68	Cloned with Laura Scheinost
pDNR-Dual-β-catenin Δ4	69	Cloned with Pia Widder and Laura Scheinost
EGFP-β-catenin WT	70	Cloned with Pia Widder and Laura Scheinost
EGFP-β-catenin S23A	71	Cloned with Pia Widder
EGFP-β-catenin T40A	72	Cloned with Pia Widder
EGFP-β-catenin T41A	73	Cloned with Pia Widder
EGFP-β-catenin T112A	74	Cloned with Laura Scheinost
EGFP-β-catenin T40AT41A	75	Cloned with Laura Scheinost
EGFP-β-catenin S23AT40AT41A	76	Cloned with Laura Scheinost
EGFP-β-catenin T40AT41AT112A	77	Cloned with Pia Widder
EGFP-β-catenin Δ4	78	Cloned with Pia Widder
pDNR-Dual-KRT8 for NT	80	Harvard Medical School (HMS) #HsCD00000322[604]
pDNR-Dual-KRT8 for CT	81	Harvard Medical School (HMS) #HsCD00002939[604]
pDNR-Dual-ENO1 for NT	82	Harvard Medical School (HMS) #HsCD00003308
pDNR-Dual-ENO1 for CT	83	Harvard Medical School (HMS) #HsCD00003307
pDNR-Dual-GPI for CT	84	Harvard Medical School (HMS) #HsCD00003345[604]
pDNR-Dual-GAPDH for NT	85	Harvard Medical School (HMS) #HsCD00004784[604]
pDNR-Dual-GAPDH for CT	86	Harvard Medical School (HMS) #HsCD00004782
pDNR-Dual-PGK1 for CT	87	Harvard Medical School (HMS) #HsCD00005982[599,604]
EGFP-KRT8	88	Cloned by myself
KRT8-EGFP	89	Cloned by myself
EGFP-ENO1	90	Cloned by myself
ENO1-EGFP	91	Cloned by myself
GPI-EGFP	92	Cloned by myself
EGFP-GAPDH	93	Cloned by myself
GAPDH-EGFP	94	Cloned by myself
PGK1-EGFP	95	Cloned by myself
PARP-EGFP	110	Sascha Beneke, Group of Prof. Dr. Dietrich, University of Konstanz
EGFP-PARP	111	Sascha Beneke, Group of Prof. Dr. Dietrich, University of Konstanz
EGFP-H2B	113	Bioimaging Center, University of Konstanz

H3-EGFP	115	Bioimaging Center, University of Konstanz (#272)
H4-EGFP	116	Bioimaging Center, University of Konstanz (#273)
EGFP-HDAC1	120	Addgene plasmid #11054, Ramesh Shivdasani[605]
EGFP-HSP70	121	Addgene plasmid #15215, Lois Greene[606]
EGFP-NPM	123	Addgene plasmid #17578, Xin Wang[607]
EGFP-HSPH1	124	Addgene plasmid #19480, Harm Kampinga[608]
EGFP-HSPA8	125	Addgene plasmid #19487, Harm Kampinga[608]
Moesin-EGFP	126	Addgene plasmid #20671, Stephen Shaw[609]
VCP-EGFP	127	Addgene plasmid #23971, Nico Dantuma[610]
EGFP-Nucleolin	128	Addgene plasmid #28176, Michael Kastan[611]
EB1-EGFP	129	Addgene plasmid #39299, Tim Mitchison & Jennifer Tirnauer
EGFP-Galectin1	131	Addgene plasmid #56434, Michael Davidson
EGFP-SNAC	139	Addgene plasmid #40822, David Rubinsztein[612]
EGFP-PTEN	140	Addgene plasmid #13039, Alonzo Ross[613]

Information on the vector backbone, insert species, and antibiotic resistance can be found in the plasmid collection file of the group of Prof. Dr. Zumbusch. Plasmids are stored as *Escherichia coli* (*E. coli*) stocks at -80 °C and as DNA mid-size preparations in TE buffer at 4 °C.

6.1.7. Oligonucleotides

Table 6.8: Oligonucleotides employed within this thesis.

Oligonucleotide	**Lab code**	**Sequence**
β-catenin Lic forward	2895	CCCCACTAACCCGTTACAGGTCAGTATCAAACCAGGC
β-catenin Lic reverse	2896	ACTCCTCCCCCGCCATGGCTACTCAAGCTG
β-catenin S23A forward	2907	CCAGACAGAAAAGCAGCTGTTGCTCACTGGCAGCAACAGTCTTACC
β-catenin S23A reverse	2908	GGTAAGACTGTTGCTGCCAGTGAGCAACAGCTGCTTTTCTGTCTGG
β-catenin T40A forward	2909	GGAATCCATTCTGGCGCCGCTACCACAGCTCCTTCTCTGAGTGG
β-catenin T40A reverse	2910	CCACTCAGAGAAGGAGCTGTGGTAGCGGCGCCAGAATGGATTCC
β-catenin T41A forward	2911	GGAATCCATTCTGGCGCCACTGCCACAGCTCCTTCTCTGAGTGG
β-catenin T41A reverse	2912	CCACTCAGAGAAGGAGCTGTGGCAGTGGCGCCAGAATGGATTCC
β-catenin T40AT41A forward	2913	GGAATCCATTCTGGTGCCGCGGCCACAGCTCCTTCTCTGAGTGG
β-catenin T40AT41A reverse	2914	CCACTCAGAGAAGGAGCTGTGGCCGCGGCACCAGAATGGATTCC

β-catenin T112A forward	2915	CCTGAGACATTAGATGAGGGAATGCAGATCCC ATCTGCACAGTTTGATGCTGCTCATCCC
β-catenin T112A reverse	2916	GGGATGAGCAGCATCAAACTGTGCAGATGGG ATCTGCATTCCCTCATCTAATGTCTCAGG

Oligonucleotides are stored in the oligonucleotide collection of the group of Prof. Dr. Hauck at the University of Konstanz at -20 °C. Lab code numbers refer to numbers of the group of Prof. Dr. Hauck.

6.1.8. Antibodies

Table 6.9: Primary and secondary antibodies utilized within this thesis.

Abbreviation used in this thesis	**Description**	**Manufacturer**	**Catalog number**	**Dilution**
anti-acetyllysine	Primary monoclonal mouse-anti-acetyllysine antibody (IgG)	Thermo Fisher Scientific	MA1-2021	1:1000
anti-biotin	Primary monoclonal mouse-anti-biotin antibody (IgG1)	Abnova	MAB3274	1:2000
anti-GFP	Primary monoclonal mouse-anti-GFP antibody (IgG2a, JL-8)	clontech	632380	1:2000
anti-GFP	Primary monoclonal rabbit-anti-GFP antibody	Group of Prof. Dr. Hauck, University of Konstanz		For immuno-precipitations
anti-mouse	Secondary polyclonal goat-anti-mouse antibody, peroxidase conjugated	Dianova	115-035-003	1:3000
anti-mouse Alexa Fluor 647	Secondary polyclonal goat-anti-mouse antibody, labelled with Alexa Fluor 647	Jackson ImmunoResearch Laboratories	115-605-068	1:200
anti-OGA	Primary polyclonal rabbit-anti- OGA antibody	Sigma-Aldrich	HPA036141	1:300
anti-*O*-GlcNAc	Primary monoclonal mouse-anti-*O*-GlcNAc antibody (IgG1, RL2)	Thermo Fisher Scientific	MA1-072	1:1000
anti-OGT	Primary polyclonal rabbit-anti- OGT antibody	Sigma-Aldrich	HPA030751	1:300
anti-rabbit	Secondary polyclonal goat-anti-rabbit antibody, peroxidase conjugated	Sigma-Aldrich	A0545	1:3000
anti-sialyl Tn	Primary antibody from hybridoma supernatant	Group of Prof. Dr. Reis, University of Porto	B72.3	1:5

anti-α-tubulin	Primary mouse-anti-α-tubulin antibody	Group of Prof. Dr. Mayer, University of Konstanz	AA4.3	1:200

6.1.9. Kits

Click-iT Cell Reaction Buffer Kit (Thermo Fisher Scientific, #C10269), Click-iT Protein Reaction Buffer Kit (Thermo Fisher Scientific, #C10276), NucleoBond Xtra Midi (Macherey-Nagel, #740410), Plasmid DNA Purification Mini Prep Kit (Genaxxon, # S5369), QIAprep Spin Miniprep Kit (Qiagen, # 27106), QIAquick Gel Extraction Kit (Qiagen, #28706).

6.1.10. Equipment

BioPhotometer (eppendorf), camping stove (Camping Gaz), centrifuges 5424 R, 5430, 5417R, and 5418 (Eppendorf), ChemiDocTMTouch Imaging System (Bio-Rad), CO_2 incubator for cell culture (Binder), confocal microscope TCS SP5 (Leica Microsystems CMS), contact thermometer (Heidolph), counting chamber (Neubauer), electronic balances (Sartorius and Kern), electroporator ElectroCell S20 (βtech), freeze dryer (Christ), freezer -80 °C (Thermo Scientific), gel imaging system GelDocXR (Bio-Rad), incubator for *E. coli* (Memmert), magnetic stirrer with heating plate (Heidolph), mass spectrometer (micrOTOF, Bruker), microscope DMIL LED (Leica Microsystems CMS) with fluorescence lamp pE-300^{white} (CoolLED), microwave (Sharp and Severin), microwave reactor (Biotage), mini Trans-Blot Cell for Western Blotting (Bio-Rad), mini-PROTEAN tetra vertical electrophoresis cell for SDS-PAGE (Bio-Rad), NanoDrop 1000 (PeqLab), overhead shaker (A. Hartenstein), polymerase chain reaction (PCR) cycler peqSTAR (PeqLab), pellet pestles (Thermo Fisher Scientific), PerfectBlue Gel System Mini for agarose electrophoresis (Peqlab), pH meter (Phoenix Instruments), plate reader (BioTek), rocking shaker (stuart), rotatory evaporator Laborota 4000 (Heidolph), sealing unit (Raypack), shaker Polymax1040 (Heidolph), shaking incubator for *E. coli* (Edmund Bühler), small centrifuge MiniStar (VWR), sonifier 250 (Branson), spectrophotometer ND-1000 (PeqLab), sterile bench (Heraeus and Hera), thermomixer (Eppendorf), Typhoon FLA 9500 imager (GE Healthcare Life Sciences), ultrasonic bath (Bandelin Sonorex), UV/VIS spectrophotometer (Agilent), vortex MS2 (Ika) and vortex (Phoenix instrument), water bath (Benchmark), water bath, shaking (Thermo Fisher Scientific), wide-field frequency domain FLIM setup (diode laser LDM488.20.A350 (Omicron), DMI 6000B inverted microscope (Leica Microsystems CMS), multi-mode fiber with a numeric aperture (NA) of 0.25 (Thorlabs), PIMAX4:1024i RF CCD camera coupled to a GenIII intensifier (Princeton Instruments), Tempcontrol 37-2 digital (Pecon)).

6.1.11. Consumables

10 cm dishes for agar plates (Sarstedt), 1.5 mL reaction tubes (Stein Labortechnik), cover glass with thickness #1.5 (VWR), gas cartridges (Camping Gaz), glass equipment (Schott, VWR Brand), inoculation loop (VWR), microscopy chambers 8-well ibiTreat µ-Slides (ibidi), microscopy chambers µ-Slide VI0.4 uncoated (ibidi), nail polish (dm), nitrocellulose membrane 0.2 µm (Bio-Rad), parafilm (Pechiney Plastic Packing Chicago), pasteur pipettes

(WU Mainz), PCR tubes (Genaxxon), pipette tips (VWR, neoLab), sterile plastic labware (10 cm dishes, 25 cm² and 75 cm² tissue culture flasks, 6-well plates, 24-well plates, 96-well plates, serological pipettes, 15 mL and 50 mL tubes, cryo tubes; all from Corning), swabs (VWR), thick blot filter paper (Bio-Rad or Thermo Fisher Scientific), thin layer chromatography plate (Merck and Macherey-Nagel), tube with assembled ventilation cap (Greiner and Sarstedt), welding foil (Raypack).

6.1.12. Software

ChemBioDraw Ultra (version 14, PerkinElmer Inc.), Clone Manager (version 8, Scientific and Educational Software), EndNote X7 (version X7.7.1, Thomson Reuters), Gen5 (version 1.11.5, BioTek), GraphPad Prism (version 5.0, GraphPad Software, Inc.), Image Lab (version 5.2.1, Bio-Rad Laboratories), ImageJ (version 1.48v, National Institutes of Health), Inkscape (version 0.48, Inkscape Community), Leica LAS (version 4.4.0 build 454, Leica Microsystems CMS), Leica LAS AF (version 2.7.3 build 9723, Leica Microsystems CMS), Leica LAS AF Lite (version 2.6.3 build 8173, Leica Microsystems CMS), Lightfield (V5.2.0, Princeton Instruments), MATLAB (version R2013b, The MathWorks, Inc.), Mestrenova (version 10, Mestrelab Research S.L.), Microsoft Office 2010 (Microsoft Corporation), SimFCS (version 3.0, Laboratory for Fluorescence Dynamics, University of California), Zotero (version 4, George Mason University).

6.2. Biochemical Methods for Mammalian Cells

6.2.1. Cell Culture

Mammalian cells were grown in 10 cm cell culture Petri dishes or cell culture flasks in the appropriate cell culture medium at 37 °C and 5 % CO_2. All experimental steps using living cells were performed under a sterile bench. Cells were passaged all three to five days at 80 % to 90 % confluence. To this end, old medium was aspirated, cells were washed once with 7 mL to 10 mL DPBS, and detached by the addition of 1 mL to 2 mL trypsin solution. HEK293T cells detach at room temperature rapidly, whereas all other cell lines desire incubation at 37 °C for 5 min to 20 min. Subsequently, 5 mL to 9 mL fresh cell culture medium were added to collect cells. If residual trypsin needed to be eliminated, cells were pelleted by centrifugation at 600 g for 3 min or at 290 g for 5 min, the supernatant was removed, and cells were resuspended in fresh cell culture medium. For MKN45 cells, a washing step with DPBS and a second centrifugation step were included before adding the fresh medium. A Neubauer chamber was used for the determination of the cell concentration. The desired amount of cells was transferred into a new Petri dish or cell culture flask.

6.2.2. Transient Transfection of Mammalian Cells

HEK293T cells were transiently transfected by calcium phosphate co-precipitation using a total amount of 1-4 µg plasmid DNA per 10 cm culture dish as described previously.[614] The day prior transfection, one to two million cells were seeded per 10 cm cell culture dish or 200,000 cells per 6-well. For transfection, 500 µL MQ water were mixed with plasmid DNA, 500 µL 2x HBS buffer, and 50 µL 2.5 M $CaCl_2$ solution while vortexing. The transfection

mixture was incubated at room temperature for 15 min. Subsequently, cells were treated with 1 µL of 25 mM chloroquine and 100 µL of the transfection mixture per mL of present cell culture medium. Cells were incubated at 37 °C and 5 % CO_2 for 6 h to 8 h. They were washed once with DPBS and covered with fresh cell culture medium. Optimal expression of proteins encoded by the transfected plasmids was achieved 36 h to 48 h after transfection.
HeLa S3 and NIH 3T3 cells were transfected by using either the commercially available GenaxxoFect kit or the Lipofectamine 2000 Transfection Reagent. For GenaxxoFect transfection, 2 µL to 6 µL GenaxxoFect Reagent were diluted in the supplied Dilution Buffer to a final volume of 120 µL. 1 µg of plasmid DNA to be introduced in cells was added to 120 µL Dilution Buffer. Both solutions were combined by pipetting and incubated at room temperature for 20 min. Meanwhile, cells were washed once with DPBS, detached with accutase, and counted. A suspension of 600,000 cells in 1250 µL cell culture medium was added to the GenaxxoFect-DNA mixture and pipetted up and down. This mixture was placed in a well of a 6-well plate. For Lipofectamine-mediated transfection, 1 µL Lipofectamine 2000 Transfection Reagent were diluted in 50 µL Opti-MEM medium. 0.25 µg to 2 µg plasmid DNA was added to 50 µL Opti-MEM medium. Both solutions were vortexed separately and incubated at room temperature for 3 min. They were combined by pipetting and incubated at room temperature for further 15 min. This complex was transferred to cells seeded in a well of an 8-well µ-slide the day before transfection (20,000 in 200 µL cell culture medium). For both transfection methods, protein expression was sufficient after one to two days.

6.2.3. Cell Lysis

Cells growing in 10 cm dishes (6-well plates) were washed once with DPBS and detached by addition of 1 mL (200 µL) trypsin as mentioned in section 6.2.1. 5 mL (800 µL) DPBS were added, cells were transferred into a 15 mL falcon (1.5 mL reaction tube), and were centrifuged at 600 g for 3 min. The supernatant was aspirated and the cell pellet was resuspended in 1 mL DPBS. Cells were transferred into a 1.5 mL reaction tube and pelleted by centrifugation. The supernatant was aspirated, the cell pellet was resuspended in 1 mL DPBS, and tubes were centrifuged once more. The supernatant was completely removed, 350 µL to 600 µL lysis buffer (35 µL to 50 µL) were added, and samples were mixed by pipetting up and down. Reaction tubes with samples were incubated on ice for 30 min and centrifuged at 4 °C and 18,000 g for 30 min. The supernatant, i.e. the lysate, was transferred into a new 1.5 mL reaction tube. Lysates were further processed or stored at -80 °C.
In glycosylation experiments, lysis buffer was usually supplemented with 100 µM PUGNAc to inhibit the activity of OGA.
In acetylation and methylation experiments, HEK293T cells were detached by pipetting their medium up and down. Cells were collected, transferred into a 15 mL falcon and further handled as mentioned above.

6.2.4. Immunoprecipitation

HEK293T cells were grown in 10 cm dishes, transfected with the desired plasmids encoding EGFP-fusion proteins, and treated with chemical reporters. Cells were lysed with 400 µL lysis

buffer. For immunoprecipitation of EGFP-fusion proteins, two different protocols were applied. The first one (A) was used at the beginning of glycosylation studies. The second procedure (B) was utilized for some glycosylation and throughout all acetylation and methylation experiments. Whereas (A) needs less expensive materials, (B) is less time-consuming and yields larger amounts of EGFP-fusion proteins. All work was conducted on ice or at 4 °C.

(A) 350 µL cell lysate were transferred into a 1.5 mL reaction tube and diluted with 350 µL ice-cold dilution buffer. 3 µg anti-GFP antibodies were added per sample. The tube was incubated with overhead rotation for 4 h. 25 µL Protein A/G PLUS-Agarose were added per sample and samples were overhead rotated for further 60 min. EGFP-fusion proteins bound to antibodies at agarose beads were pelleted by centrifugation at 8600 g for 2 min. The supernatant was aspirated down to approximately 50 µL. 500 µL Triton buffer were added per sample followed by centrifugation and aspiration. This step was repeated once, whereby the volume in the reaction tube was reduced to 30 µL during the last aspiration step. Immunoprecipitates were labeled via a CuAAC or a DAinv reaction as described in sections 6.2.10 and 6.2.11.

(B) Per sample, 500 µL ice-cold dilution buffer (for immunoprecipitations) and 10 µL GFP-Trap_A bead slurry were added in a 1.5 mL reaction tube. Tubes were centrifuged at 3000 g for 2 min and supernatants aspirated down to approximately 50 µL. To wash pelleted beads, 500 µL dilution buffer were added per tube, tubes were centrifuged, and supernatants were aspirated. This washing step was repeated once more. 200-350 µL lysate were added per tube and filled up to a total volume of 1 mL with dilution buffer to reduce the Triton X-100 concentration below 0.2 V-%. Samples were incubated with overhead rotation for 60 min. Beads were pelleted by centrifugation at 3500 g for 2 min. Supernatants were aspirated down to approximately 50 µL. Pellets were slightly green due to isolated EGFP-fusion proteins. 500 µL dilution buffer were added per tube, tubes were centrifuged and supernatants aspirated. This washing step was performed once more. The final volume in tubes was 30 µL. Immunoprecipitates were labeled via a CuAAC or a DAinv reaction as described in chapters 6.2.10 and 6.2.11. In some glycosylation and all acetylation and methylation experiments, beads were washed between the labeling reaction and the denaturation of proteins. To this end, 500 µL dilution buffer supplemented with 0.5 V-% Triton X-100 were added per sample, tubes were centrifuged at 3500 g for 2 min, and supernatants were aspirated down to approximately 50 µL. This washing step was repeated two more times.

6.2.5. SDS-PAGE and Western Blotting

If cell lysates had been frozen at -20 °C, they were thawed at room temperature and kept at 98 °C for 10 min. 10 w-% acrylamide SDS gels were prepared using the Mini-PROTEAN tetra cell equipment. The following solutions were mixed to give two separating and collecting gels:

Separating gel:	7.2 mL MQ water
	4.5 mL lower buffer
	6.0 mL acrylamide
	180 µL 10 w-% ammonium peroxodisulfate
	18 µL TEMED
Collecting gel:	3.58 mL MQ water
	625 µL upper buffer
	670 µL acrylamide
	70 µL ammonium peroxodisulfate
	5 µL TEMED

After pouring the separating gel, the not yet solidified gel was covered with isopropanol. The alcohol was removed prior to pouring the collecting gel. Typically, combs with 15 teeth were used. Gels were transferred into the electrophoresis chamber filled with SDS-PAGE running buffer. The protein ladder and lysates were pipetted into gel bags. SDS-PAGE was performed at 30 mA or 50 mA for approximately 60 min until bromophenol blue and excess fluorescence dyes left the gel.
A nitrocellulose membrane was placed on filter papers. The gel was transferred on top of this membrane and covered with another filter paper. This "sandwich" was caged in a gel holder cassette and installed in the electrophoresis chamber filled with ice-cold Western Blot running buffer. An ice pack and a stirring bar were added. Blotting was performed at 120 V for 60 min under constant stirring. Afterwards, membranes were laid in PBS-T buffer.
For sulfo-Cy3 or TAMRA fluorescence readout, membranes were placed overhead onto the "Fluor Stage" of the Typhoon FLA 9500 Fluorescence Imager. Fluorophores were excited at 532 nm and fluorescence was read out using a 575 nm longpass filters. The pixel size was set to 50 µm or 100 µm.
For immunoblotting, membranes were covered with 5 w-% milk powder in PBS-T and shaken for 60 min. Two quick washing steps with PBS-T removed residual milk. Membranes were sealed with the desired primary antibody in welding foil and incubated at 4 °C overnight or at room temperature for 2 h under constant shaking. Most primary antibody solutions were recycled and stored at 4 °C. Membranes were washed three times with PBS-T for 10 min each. The secondary antibody was diluted in 5 w-% milk powder in PBS-T. Approximately 25 mL of this solution were added to each membrane. Membranes were subsequently incubated at room temperature for 60 min. Secondary antibody solutions were not reused. Membranes were washed three times with PBS-T for 10 min each. ECL substrates were combined and pipetted on top of membranes. Chemiluminescence was read out using the ChemiDocTMTouch Imaging System.
Equal loading was assessed by incubation of membranes in Ponceau S solution for some minutes. To remove excess Ponceau S, membranes were quickly washed with PBS-T or MQ water. Color images were taken with the ChemiDocTMTouch Imaging System.
All images were processed and analyzed using the software Image Lab, ImageJ, Inkscape, and Microsoft Office 2010.

6.2.6. Cell Seeding for Microscopy

Microscopy chambers (8-well ibiTreat µ-Slides) were coated with 20 V-% Poly-L-lysine solution in MQ water at 37 °C for 60 min or at 4 °C overnight. The coating solution was removed and wells were rinsed with DPBS. Cells growing in 10 cm dishes were detached with trypsin and collected with new cell culture medium as explained in section 6.2.1. Between 20,000 and 50,000 cells were seeded per well of microscopy chambers in 200 µL cell culture medium. The exact cell number depended on the cell's size and growth rate. Cells were incubated at 37 °C and 5 % CO_2.

6.2.7. Metabolic Labeling of Mammalian Cells for Protein Glycosylation

Desired amounts of HEK293T, HeLa S3, H1299, or MKN45 cells were seeded in 10 cm dishes, 6-well plates, or microscopy dishes. 100 mM stock solutions of glycosylation reporters were prepared in DMSO and stored at 4 °C for several weeks or at -20 °C for long periods of time. Glycosylation reporters were diluted to the desired concentrations in prewarmed cell culture medium and vortexed briefly. In case of Cyoc-derivatives, reporters did not dissolve in DMEM culture media rapidly. Therefore, solutions were incubated at 37 °C for up to 3 h and vortexed from time to time. Reporter solutions were added to culture medium on cells 6 h to 20 h after seeding them. Labeling with glycosylation reporters was performed at 37 °C and 5 % CO_2 for one to three days.

6.2.8. Metabolic Labeling of Mammalian Cells for Protein Acetylation

Chemical reporters for monitoring protein acetylation diffused into mammalian cells. For their application, HEK293T, HeLa S3, or NIH 3T3 cells were seeded in 10 cm dishes, 6-well plates, or microscopy dishes in prewarmed cell culture medium. The next day, chemical reporters were diluted to the desired concentration in prewarmed cell culture medium from 1 M stocks (in MQ water or DPBS (NaOAc or Na4P) or DMSO (M4P and AM4P) stored at -20 °C) and added to cells. Labeling with acetylation reporters was performed at 37 °C and 5 % CO_2 for 8 h, if not indicated differently.
A 1 M Na4P solution was prepared by mixing equimolar amounts of 2.5 M 4-pentynoic acid and 2 M NaOH (both in MQ water). The pH value was adjusted to 7 by dropwise addition of 1 M HCl or 1 M NaOH. Finally, MQ water was added to receive a 1 M Na4P solution, which was passed through a 0.2 µm sterile filter.

6.2.9. Metabolic Labeling of Mammalian Cells for Protein Methylation

The chemical reporter for protein methylation, ProSeAM, was introduced in mammalian cells by electroporation. To this end, HEK293T or HeLa S3 cells were seeded in 8-well microscopy dishes according to chapter 6.2.6. Cell culture medium was supplemented with 25 µM Adox to reduce intracellular methylation levels. The next day, cells were washed once with DPBS. A 100 mM ProSeAM solution stored at -80 °C was thawed on ice and, if necessary, diluted to 10 mM in 0.1 V-% aqueous TFA solution. It was added to the desired concentration into ZAP buffer. 150 µL of this solution were pipetted on cells. ZAP buffer without ProSeAM but supplemented with a similar volume of 0.1 V-% TFA was used as

solvent control. Electroporation was performed with the ElectroCell S20 electroporator using electrodes of stainless steel with a distance of 4 mm. They fitted the 8-well µ-slides twice. Electroporation was performed with 10 pulses with a length of 500 µs every 1000 µs, if not indicated differently. The voltage was kept at 160 V resulting in an electrical field strength of 400 V cm^{-1}. After electroporation, cells were incubated at room temperature for 5 min, washed twice with DPBS, covered with prewarmed cell culture medium, and incubated for a desired duration at 37 °C and 5 % CO_2.

6.2.10. DAinv Reaction

In Cell Lysates

Cell lysates were normally treated with 10 µM sulfo-Cy3-Tz or TAMRA-Tz, vortexed briefly, and incubated at room temperature while shaking in a thermomixer at 400 rpm for 90 min. For β-elimination experiments, the DAinv reaction was performed with 150 µM biotin-Tz. Afterwards, cell lysates were treated with 4x SDS sample buffer to yield a 1x concentration and denatured at 98 °C for 10 min. Samples were stored until SDS-PAGE at -20 °C.

In Cells

For live cell labeling, cells were washed once with DPBS. 25 µM TAMRA-Tz were added in complete cell culture medium to cells. They were incubated at 37 °C and 5 % CO_2 for 60 min. Cells were washed twice with DPBS and covered with phenol red free DMEM supplemented with 10 mM HEPES. Microscopy was performed within the next 2 h.

For labeling of fixed samples, cells needed to be firstly fixed with PFA and permeabilized with Triton X-100 prior to the DAinv reaction. To this end, cells were washed twice with DPBS and fixed with 4 w-% PFA in DPBS. Afterwards, cells were washed with DPBS and with 50 mM NH_4Cl in DPBS for 2 min to quench remaining PFA. After another DPBS washing step, cells were permeabilized with 0.5 V-% Triton X-100 in DPBS for 15 min. Cells were washed once with DPBS, treated with 3 w-% BSA in DPBS for 2 min, and washed with DPBS. 25 µM sulfo-Cy3-Tz or TAMRA-Tz in DPBS were added to cells and these were incubated at room temperature in the dark for 60 min. Cells were washed with DPBS, 3 w-% BSA in DPBS, and DPBS. They were covered with DPBS and stored at 4 °C in the dark. Microscopy was performed within the next day.

6.2.11. CuAAC

In Cell Lysates

For glycosylation experiments, a CuAAC reaction mixture containing 10 mM $CuSO_4$, 10 mM THPTA, 100 mM Na-ascorbate, and 1 mM sulfo-Cy3-alkyne in MQ water was freshly prepared from stock solutions in MQ water. 1.25 µL of this mixture were added to 25 µL cell lysate in a 1.5 mL reaction tube that was vortexed and then incubated at room temperature under constant shaking for 30 min. 4x SDS sample buffer was added to a 1x concentration. The lysate was denatured at 98 °C for 10 min. Samples were stored until SDS-PAGE at -20 °C.

For acetylation and methylation experiments, cell lysates were diluted to a protein concentration of approximately 1 mg ml^{-1} in dilution buffer. A CuAAC reaction mixture

typically containing 5 mM $CuSO_4$, 6.25 mM THPTA, 25 mM Na-ascorbate, and 50 µM Cy3-Az in MQ water was freshly prepared from stock solutions in MQ water. Compounds were added one after the other to ensure proper reaction conditions. 20 µL of this reaction mixture were added to 80 µL diluted lysate, vortexed, and usually incubated at 37 °C for 15 min. Proteins were mostly precipitated after the CuAAC. To this end, 600 µL ice-cold methanol, 150 µL ice-cold chloroform, and 400 µL MQ water were added to each labeled lysate. Reaction tubes were inverted several times and centrifuged at 18,000 g and 4 °C for 5 min. Aqueous phases were removed, while precipitated proteins remained at the interphase. 450 µL ice-cold methanol were added and tubes were inverted several times. Proteins were pelleted by centrifugation at 18,000 g for 5 min. Supernatants were removed and proteins were washed with 450 µL ice-cold methanol. Tubes were centrifuged once more and supernatants were removed. Protein pellets were dried overnight in open tubes covered with a thin tissue. The next day, proteins were taken up in 30 µL 1x SDS sample buffer per pellet, vortexed for 30 s, and denatured at 98 °C for 10 min. Samples were stored until SDS-PAGE at -20 °C.

In Cells

Before performing the CuAAC, cells were fixed and permeabilized. Thereto, cells were washed twice with DPBS and fixed with 4 w-% PFA in DPBS for 20 min. Afterwards, they were washed with DPBS and with 50 mM NH_4Cl in DPBS for 2 min. Following another DPBS washing step, cells were permeabilized with 0.5 V-% Triton X-100 in DPBS for 15 min. Cells were washed once with DPBS, treated with 3 w-% BSA in DPBS for 2 min, and washed with DPBS. A CuAAC reaction mixture containing 1 mM $CuSO_4$, 1.25 mM THPTA, 5 mM Na-ascorbate, and 10 µM Cy3-Az in DPBS was freshly prepared from stock solutions in MQ water. The compounds were added one after the other to ensure proper reaction conditions. Cells were incubated with this mixture at 37 °C in the dark for 15 min followed by two DPBS washing steps. Finally, they were covered with DPBS and stored at 4 °C in the dark. Microscopy was performed within a day.

6.2.12. Dual Labeling of Membrane Glycans via SPAAC and DAinv Reactions

Labeling of artificial membrane glycans installed via MGE can only be performed with living cells. Otherwise, huge background labeling arises.

Living MKN45 cells previously seeded in 8-well µ-slides and treated with Ac_4GalNAz and/or Ac_4ManNCyoc were washed once with DPBS. A solution of 0 µM to 25 µM Alexa Fluor 488-DIBO and Cy3-Tz in RPMI cell culture medium was prepared from 10 mM DMSO stock solutions of the fluorophores. 150 µL of this medium were added per well of an 8-well microscopy µ-slide. Labeling was performed at 37 °C for 30 min, if not indicated differently. Afterwards, cells were washed twice with DPBS to remove residual fluorophores. They were covered with RPMI microscopy medium and incubated at 37 °C until microscopy was performed.

6.2.13. Immunocytochemistry

Immunocytochemistry of membrane glycans can only be performed with fixed cells, as membrane glycans get internalized with the antibody in living cells during the incubation time. Consequently, it was performed after dual labeling of membrane glycans.
Cells were washed once with DPBS and fixed with 4 w-% PFA in DPBS for 20 min. They were washed twice with DPBS and incubated with the primary anti-sialyl Tn antibody in DPBS (1:5) at 4 °C overnight. Cells were washed thrice with DPBS and incubated with the secondary antibody anti-mouse Alexa Fluor 647 in DPBS (1:200) at 37 °C for 30 min. They were washed once with DPBS. DNA was labelled with DAPI in DPBS (1:100) at room temperature for 5 min. Subsequently, cells were washed twice with DPBS, covered with DPBS, and stored at 4 °C until microscopy was performed.

6.2.14. Viability Tests

Resazurin Cell Viability Assay
7500 to 15,000 HEK293T, HeLa S3, or NIH 3T3 cells were seeded in 66 µL complete cell culture medium per well of a 96-well plate and were grown at 37 °C and 5 % CO_2. 8 h to 24 h later, they were treated with 34 µL of chemical reporters for protein glycosylation, acetylation, inhibitors, or solvent controls in complete cell culture medium for defined periods of time (dependent on the compound). Blank wells were filled with 100 µL cell culture medium. Afterwards, 50 µL of a 30 V-% AlamarBlue solution in complete cell culture medium were added per well. Plates were incubated at 37 °C and 5 % CO_2 for 60 min. During this time, resazurin, which is contained in AlamarBlue, is converted to red–fluorescent resorufin via a reduction reaction only occurring in metabolic active cells. Fluorescence of resorufin was read out with the Synergy HT and the Gen5 software. Samples were measured at 25 °C, excited using a 530/25 bandpass filter, and fluorescence was detected after a 590/30 bandpass emission filter. Experiments were performed three times in quadruplicates.
For glycosylation experiments with MKN45 cells, 8000 cells were seeded in 50 µL cell culture medium per well of a 96-well plate and grown at 37 °C and 5 % CO_2. Blank wells were filled with 100 µL cell culture medium. The next day, 50 µL of Ac_4GalNAz or Ac_4ManNCyoc (stock solutions 100 mM in DMSO) solutions in cell culture medium were added per well. DMSO was used as solvent control. 48 h later, 50 µL of 120 µM resazurin in cell culture medium were added per well. Plates were incubated at 37 °C and 5 % CO_2 for 60 min. The fluorescence readout was performed as described above. Experiments were performed three times in triplicates.
For methylation experiments, HEK293T and HeLa S3 cells were seeded in duplicates in 8-well µ-slides and electroporated in presence of 50 µM ProSeAM as explained in sections 6.2.6 and 6.2.9, respectively. As controls, cells were covered with ZAP buffer and not electroporated or covered with ZAP buffer and electroporated. After a defined incubation time at 37 °C and 5 % CO_2, a resazurin solution in complete cell culture medium was added to a final concentration of 40 µM per well. Cells were incubated at 37 °C and 5 % CO_2 for 60 min and two times 100 µL per well were transferred into a well of a 96-well plate. Fluorescence was read out as mentioned above. These viability tests were performed three times in duplicates of duplicates.

Luminescent Cell Viability Assay

To assess the effect of TAMRA-Tz on cellular viabilities, a resazurin assay could not be used, as the compound of interest is itself fluorescent. Thus, the CellTiter-Glo luminescent cell viability assay was performed according to the manufacture's protocol. 15,000 HEK293T cells were seeded in 66 µL cell culture medium per well of a 96 well plate and grown at 37 °C and 5 % CO_2. Blank wells were filled with 100 µL cell culture medium. The next day, 34 µL cell culture medium containing TAMRA-Tz at desired concentrations (stock solution was 5 mM in DMSO) or DMSO as solvent control were added per well. After a 30 min incubation period at 37 °C, plates were placed at room temperature in the dark for 30 min. 100 µL of the assay's substrate dissolved in the provided buffer were added per well to induce cell lysis. Plates were placed on an orbital shaker at 200 rpm and room temperature for 2 min. To correct for potentially occurring bioluminescent resonance energy transfer from luciferin to TAMRA during the readout, control samples were treated with TAMRA-Tz or DMSO at desired concentrations after cell lysis. Plates were shaken further 4 min. Within the next 10 min, luminescence was read out using the Synergy HT. No emission filter was used. Experiments were performed three times in quadruplicates.

In methylation experiments, the incubation time of the resazurin test would have been too long after electroporating cells in ZAP buffer with up to 1 mM ProSeAM and incubating them for only 0 min or 20 min. Hence, viabilities were quantified with the CellTiter-Glo luminescent cell viability assay. 150 µL of the assay's substrate solution were added to 150 µL cell culture medium in an 8-well of the µ-slide. Slides were placed on an orbital shaker for 2 min to induce cell lysis and incubated at room temperature further 10 min. Two times 100 µL were transferred into a 96-well plate per well of an 8-well µ-slide. Luminescence was read out as described above. Experiments were performed three times in technical duplicates of duplicates.

6.3. Biochemical Methods for *E. coli*

Most standard methods for *E. coli* were performed according to protocols from the script of the "Advanced Laboratory Course" offered by Prof. Dr. Hauck at the University of Konstanz in 2016.

6.3.1. Cultivation of *E. coli*

E. coli were grown on LB agar plates or in liquid LB medium containing appropriate antibiotics at 37 °C. All *E. coli* work was performed nearby the flame of a camping stove.

6.3.2. Transformation of Competent *E. coli*

Competent *E. coli* Nova Blue were thawed on ice. Maximal 10 µL plasmid DNA in MQ water were added to 100 µL *E. coli* suspension in a 1.5 mL reaction tube, mixed, and incubated on ice for 30 min. Bacteria were heat-treated in a water bath at 42 °C for 75 sec and quickly placed back on ice. 1 mL LB medium without antibiotics and bacteria was added into a tube with assembled ventilation cap and incubated for phenotypic expression at 37 °C under constant shaking at 220 rpm for 60 min. The mixture was transferred into a 1.5 mL reaction

tube and centrifuged to pellet bacteria at 3000 g for 3 min. The supernatant was discarded. Bacteria were resuspended in the remaining medium, pipetted onto an agar plate with the desired antibiotic(s), and distributed with a Dirgalski spatula. The agar plate was incubated at 37 °C for 14 h to 24 h.

6.3.3. Plasmid Preparation

Plasmid DNA was purified in different quantities and qualities using three procedures. Mini and Midi preparation yield purer DNA than a preparation related to a procedure published by Birnboim and Doly[615], but require costly spin columns. Mini and Birnboim-Doly preparations give 5 µg to 20 µg and Midi preparation approximately 100 µg to 500 µg plasmid DNA.

Mini Preparation

Mini preparations were performed with the Plasmid DNA Purification Mini Prep Kit from Genaxxon according to the manufacture's procedure. *E. coli* were grown on agar plates with the desired antibiotic(s) at 37 °C overnight. One to two inoculation loops full of bacteria were collected and resuspended by pipetting in 250 µL Resuspension Buffer in a 1.5 mL reaction tube. 250 µL Lysis Buffer were added and the tube was inverted ten times. 350 µL Neutralization Buffer were added and the tube was inverted ten more times. It was centrifuged at 4 °C and 18,000 g for 10 min. The remaining supernatant was applied on a DNA Purification Mini Spin Column. This column was centrifuged at 15,000 g for 1 min. The flow through was removed. DNA was washed by addition of 600 µL Wash Buffer and centrifugation at 15,000 g for 30 s. The flow through was discarded and the washing step repeated once more. After removal of the flow through, the column was centrifuged at 18,000 g for 2 min to remove residual buffers. For the elution of DNA, it was placed in a new 1.5 mL reaction tube. 50 µL MQ water preheated to 70 °C were added onto the column's membrane. After incubation at room temperature for 2 min, plasmid DNA was obtained by centrifugation at 15,000 g for 2 min. The concentration of DNA was determined by measuring the absorption at 260 nm with a spectrophotometer.

Midi Preparation

Midi preparations were performed with the NucleoBond Xtra Midi kit from Macherey-Nagel according to the manufacture's procedure. A starting culture was prepared by inoculation of 3 mL LB medium containing the proper antibiotic with a single colony from *E. coli* growing on an agar plate. This culture was incubated at 37 °C and 300 rpm for 8 h. The starting culture was added to 200 mL LB medium containing the appropriate antibiotic and grown at 37 °C and 300 rpm overnight. If an optical density, which was determined by measuring the absorption at 600 nm, reached a value of 4, bacteria were pelleted by centrifugation at 4 °C and 6000 g for 20 min. They were resuspended in 8 mL Resuspension Buffer containing RNase A. 8 mL Lysis Buffer were added, the tube was inverted five times, and then incubated at room temperature for 5 min. 8 mL Neutralization buffer were added to the lysate, the tube was inverted until the blue color disappeared, and centrifuged at 4 °C and 18,500 g for 20 min. A NucleoBond Xtra Column was equilibrated with 11 mL Equilibration Buffer. The

supernatant of the suspension was added onto this column. The filtrate was discarded and the column filter washed with 5 mL Equilibration Buffer. The filter was removed with a tweezer and the column was washed with 8 mL Wash Buffer. Plasmid DNA was eluted by addition of 5 mL Elution Buffer preheated to 50 °C. The filtrate was treated with 3.5 mL isopropanol to precipitate DNA and thoroughly vortexed. Centrifugation was performed at 4 °C and 6000 g for 60 min. The supernatant was discarded. The DNA pellet was washed with 2 mL 70 V-% ethanol and centrifuged at 4 °C and 6000 g for 35 min. After removing ethanol, the DNA pellet was dried at room temperature for 60 min and dissolved in 400 µL TE buffer at 4 °C overnight. The concentration of isolated DNA was determined by measuring the absorption at 260 nm with a spectrophotometer. It was adjusted to 1 µg μL^{-1} in TE buffer.

Birnboim-Doly Preparation

E. coli were grown on agar plates with the desired antibiotic(s) at 37 °C overnight. One to two inoculation loops full of bacteria were collected and resuspended by pipetting in 300 µL Birnboim-Doly buffer 1 in a 1.5 mL reaction tube. 300 µL Birnboim-Doly buffer 2 were added and the tube was inverted ten times. 300 µL Birnboim-Doly buffer 3 were added, the tube was inverted ten more times, and centrifuged at 4 °C and 18,000 g for 10 min. 800 µL of the supernatant were transferred into a new 1.5 mL reaction tube, treated with 560 µL isopropanol, and inverted three times. After centrifugation at 18,000 g for 15 min, the supernatant was removed. The pellet was washed with 500 µL 70 V-% ethanol. The tube was centrifuged at 18,000 g for 5 min and the supernatant was discarded. Following another centrifugation step at 18,000 g for 2 min, the DNA pellet was dried at room for 60 min. DNA was solved in 40 µL MQ water for 5 min. The DNA concentration was defined by measuring the absorption at 260 nm with a spectrophotometer.

6.3.4. Restriction Digest of Plasmid DNA

1 µg to 2 µg isolated plasmid DNA, 0.2 µL of the desired restriction enzyme, and 1 µL of the appropriate 10x digestion buffer (Table 6.10) were combined in a PCR-tube and filled up to a total volume of 10 µL with MQ water. This mixture was incubated for 2 h at 37 °C. For overnight digestion at 37 °C, 2 µg to 4 µg plasmid DNA, 0.1 µL restriction enzyme, and 2 µL digestion buffer were mixed. MQ water was added to a final volume of 20 µL. The success of digestion was assessed by agarose gel electrophoresis.

Table 6.10: Appropriate digestion buffers used for different restriction enzymes.

Restriction enzyme	Digestion buffer
Acc I	Cut smart buffer
Nar I	Cut smart buffer
Pae I (Sph I)	Fast digestion buffer
Pvu II	Buffer G
Sac I	Fast digestion buffer
Sac II	Cut smart buffer
Sfo I	Cut smart buffer

6.3.5. Hot-Start Gradient PCR

The PCR reaction mixture (1 µL DNA template with 20 ng μL^{-1}, 4 µL 10x Pfu buffer, 1 µL 10 µM forward primer, 1 µL 10 µM reverse primer, 1 µL 10 mM dNTPs, and 32 µL MQ water) and an enzyme mixture (1 µL Pfu polymerase, 1 µL 10x Pfu buffer, and 8 µL MQ water) were separately prepared. The PCR was performed according to the following program: The PCR reaction mixture was placed in the PCR machine. Its lid was preheated to 110 °C followed by a denaturation step at 95 °C for 30 s. The enzyme mixture was added during a short pause. Then, 25 cycles of denaturation at 94 °C for 20 s, hybridization at 62 °C to 55 °C for 20 s (varied between samples), and an elongation at 72 °C for 290 s occurred. A final elongation step at 72 °C for 5 min ensured completion of the reaction. The sample was cooled to 8 °C until further processing.

6.3.6. Ligation Independent Cloning (LIC)

A PCR with the desired plasmid and primers designed for cloning in a vector containing the LIC sequence (e.g. pDNR-Dual-LIC) was performed. The amount of PCR product required for LIC was assessed according to:

$$amount\ of\ substance\ (pmol\ \mu L^{-1}) = \frac{concentration\ of\ PCR\ product\ (pg\ \mu L^{-1})}{660\ x\ product\ size\ (bp)}$$

The desired amount of PCR product (~0.3 pmol) was treated with 1 µL T4 polymerase, 1 µL 10x NEBuffer 2, 1 µL 100 mM dCTP, 2 µL 100 mM dithiothreitol, and filled up with MQ water to a final volume of 40 µL. This reaction mixture was incubated at 22 °C for 30 min and subsequently heat-inactivated at 75 °C for 20 min. 6 µL thereof were mixed with 2 µL T4 polymerase pre-treated pDNR-Dual vector (~50 ng) as well as 1 µL NEBuffer 2 and incubated for 10 min at room temperature. 1 µL 100 mM EDTA solution was added and the sample was incubated at room temperature for 10 min. The same protocol was repeated with a vector-only control and a PCR product only control. All samples were used for transformations in *E. coli* Nova Blue.

6.3.7. Site Directed Mutagenesis of Plasmid DNA

To generate plasmids with point mutations of the β-catenin DNA sequence in pDNR-Dual, DpnI-mediated site-specific mutagenesis was performed. Primers complementary for at least 15 basepairs upstream and downstream of the mutation site and ending with a 3'-GC clamp were designed (Table 6.8). These primers inserted or deleted a restriction site of an enzyme. Primers were ordered from Thermo Fisher Scientific, solved in TE buffer, and stored at -20 °C. Plasmids of point mutants were generated by PCR using the pDNR-Dual-β-catenin WT plasmid as template. The PCR reaction mixture contained 1 µL template DNA (20 ng μL^{-1}), 5 µL 10x Pfu buffer, 0.5 µL 25 µM forward primer, 0.5 µL 25 µM reverse primer, 1 µL 10 mM dNTPs, 1 µL Pfu polymerase, and 41 µL MQ water. For PCR, the PCR reactor lid was heated to 110 °C. 20 cycles of denaturation at 95 °C for 30 s, hybridization at 55 °C to 70 °C (varied between samples) for 60 s, and elongation at 72 °C for 15 min

followed. Finally, an elongation at 72 °C for 20 min was performed and samples were stored at 8 °C until further usage. Successful amplification was checked by agarose gel electrophoresis. If a strong band at the desired size was visible, remaining template DNA in the PCR sample was degraded by addition of 2 µL DpnI and incubation at 37 °C for 2 h. 10 µL of the remaining PCR sample were transformed into *E. coli* Nova Blue, plated on LB agar plates with ampicillin, and incubated overnight at 37 °C. The following day, several single clones were streaked on new agar plates, which were incubated for 20 h. Plasmid DNA was isolated via Birnboim-Doly preparation and digested with the appropriate restriction enzymes. Sizes of DNA fragments were analyzed by agarose gel electrophoresis. Expected sizes are summarized in Table 6.11. Clones, whose DNA displayed correct fragments, were grown on LB agar plates with ampicillin overnight. The next day, plasmids were isolated with the Genaxxon kit. Success of the site directed mutagenesis was confirmed by sequencing. The triple mutants S23AT40AT41A and T40AT41AT112A were created from T40AT41A. The quadruple mutant S23AT40AT41AT112A was created from S23AT40AT41A.

Table 6.11: Sizes of DNA fragments from β-catenin mutants treated with selected restriction enzymes.

β-catenin mutant	Restriction enzyme	Size of fragments [basepairs]
WT	PvuII	144, 353, 542, 786, 896, 4349
S23A		144, 353, 542, 786, 896, 1200, 3149
WT	SfoI	Circular
T40A		7233
WT	SfoI	Circular
T41A		7233
WT	PaeI	1954, 5279
T40AT41A		7233
WT	SacII	7233
T112A		2531, 4702

6.3.8. Cre-LoxP Recombination

Cre recombination allows for the insertion of a gene from a donor vector into an acceptor vector. The insert from the donor vector is flanked by two LoxP sites recognized by the Cre recombinase. The insertion into the acceptor vector takes place at its single LoxP site.[616] In this thesis, the donor vector was always pDNR-Dual and the acceptor vector either pEGFP-C1-loxP for the generation of N-terminal EGFP-fusion plasmids or pLPS-3'EGFP for the generation of C-terminal EGFP-fusion plasmids.

For Cre mediated recombination of plasmids, 1 µL 10x Cre recombinase reaction buffer, 6 µL MQ water, 1 µL (100 ng) donor vector, 1 µL (100 ng) acceptor vector, and 1 µL Cre recombinase were combined in a PCR tube, mixed, and incubated at 37 °C for 45 min. Afterwards, Cre recombinase was inactivated by heat-treatment at 70 °C for 10 min. Subsequently, the sample was cooled to room temperature and was used for transformation of competent *E. coli* Nova Blue. Transformed *E. coli* were first grown at 37 °C on LB agar plates containing chloramphenicol and sucrose for 24 h. This ensures the presence of only

such bacteria, which carry the plasmid with the correct insertion of the donor into the acceptor vector. The next day, single clones were transferred to LB agar plates with kanamycin and grown overnight. Plasmid DNA of bacteria growing on this selection medium were isolated via a Birnboim-Doly plasmid preparation, digested with suitable restriction enzymes, and analyzed by agarose gel electrophoresis. Bacteria from samples showing the correct DNA fragments were grown on LB agar plates with chloramphenicol and sucrose. The next day, plasmid DNAs were isolated with the Genaxxon Mini preparation kit and were sent for sequencing.

6.3.9. Agarose Gel Electrophoresis

An 1 w-% agarose gel was prepared in the slide of a PerfectBlue Gel Mini System containing suitable combs. Combs with 24 teeth were chosen for analytical agarose electrophoresis and such with 8 teeth for preparative ones required for DNA purification. The gel was covered with 1x TAE buffer. DNA samples were mixed with 6x GEBS buffer to yield a 1x concentration. Gene ladder and DNA samples were pipetted into wells of the gel. If 24 teeth combs were used, 3 µL of gene ladder and 10 µL of DNA samples were suitable volumes. Analytical gels were run at 90 V and preparative ones at 50 V until the bromophenol blue band reached 2/3 of the gel. The used part of the agarose gel was cut out with a scalpel and transferred into the GelRed staining solution for 20 min. Excess GelRed was removed by placing the gel in a destaining solution for 2 min. Fluorescence of GelRed was read out using the ChemiDocTMTouch Imaging System. Images were processed and analyzed using the software Image Lab, ImageJ, and/or Inkscape.

6.3.10. Isolation of DNA from an Agarose Gel

Desired bands of an agarose gel were cut out with a scalpel and transferred into a 2 mL reaction tube. Extraction of DNA was performed with the QIAquick Gel Extraction Kit according to the manufacture's procedure. To this end, 1 µL QG buffer was added per mg of agarose gel to the tube. The sample was incubated at 50 °C until the gel dissolved completely. Vortexing the tube every 2 min to 3 min accelerated dissolving. The solution was transferred onto a QIAprep spin column and centrifuged at room temperature and 18,000 g for 1 min. The flow through was discarded. 750 µL PE buffer were added to the column to wash bound DNA. The column was centrifuged for 1 min and the flow through was discarded. Residual PE buffer was removed by centrifugation for 2 min. The column was placed in a fresh 1.5 mL reaction tube and 50 µL elution buffer or MQ water were added to elute DNA. After 1 min, the tube was centrifuged at 18,000 g for 1 min to yield isolated DNA. The concentration of DNA was determined by measuring the absorption at 260 nm with a spectrophotometer.

6.3.11. Sequencing of Plasmid DNA

DNA sequencing was performed by LGC Genomics. A FlexiRun required 40 µL plasmid DNA with a concentration of 100 ng μL^{-1}. Primers were chosen from standard primers provided at LGC genomics as summarized in Table 6.12. All EGFP-β-catenin fusion plasmids were additionally sequenced backwards with the primer CCCACTAACCCGTTACAGG. Sequencing data were evaluated using the software Clone Manager.

Table 6.12: Primers utilized for sequencing of plasmids.

Primer	Sequence	Plasmids
M13-21F	TGTAAAACGACGGCCAGT	60 – 69, 80 – 87
CMV-F	CGCAAATGGGCGGTAGGCGTG	12, 43, 44, 54, 55, 88 – 95
EGFP-C1-F	GAAGCGCGATCACATGGTC	42, 70 – 78, 88, 90, 93, 120, 121, 123 – 125, 128, 130, 131, 139, 140
EGFP-N1-R	ACTTGTGGCCGTTTACGTC	43, 44, 54, 55, 89, 91, 92, 94, 95, 115, 116, 126, 127, 129

6.4. Biochemical Methods for *A. thaliana*

6.4.1. Seeding *A. thaliana*

About 100 *A. thaliana* seeds were transferred into a 1.5 mL reaction tube. 1 mL 70 % ethanol was added for their sterilization. The reaction tube was incubated in a thermomixer at room temperature and 1400 rpm for 5 min. After seeds settled to the bottom of the tube, the supernatant was removed and 1 mL of a solution containing 1.2 % sodium hypochlorite and 0.1 % Triton X-100 in MQ water was added for bleaching seeds. The tube was incubated in a thermomixer at room temperature and 1400 rpm for 20 min. Work was continued under a sterile bench. The supernatant was removed and seeds were washed two times with MQ water. 200 µL of a 0.1 w-% agar solution in MQ water were added. The tube was incubated in the dark at 4 °C for 48 h. Thereafter, seeds in the agar solution were taken up in a 1 mL pipette tip and placed on an agar plate. Plates were incubated at 23 °C and short day conditions (8 h light/16 h dark cycle with light intensities of 10 to 100 µmol photons m^{-2} s^{-1}).

6.4.2. Treatment of *A. thaliana* with Chemical Reporters

Chemical reporters were diluted to the desired concentration in liquid MS medium and transferred into wells of a 24-well plate (1 mL per well). Four days old *A. thaliana* seedlings growing on an agar plate were pulled out of the agar with a tweezer and transferred into wells of the 24-well plate. Three seedlings were placed into the same well. The 24-well plate was closed, its margin was covered with parafilm, and it was incubated at 23 °C and short day conditions (8 h light/16 h dark cycle with light intensities of 10 to 100 µmol photons m^{-2} s^{-1}).

6.4.3. Lysis of *A. thaliana*

A. thaliana seedlings treated with chemical reporters for 48 h were washed twice with 1 mL liquid MS medium. Twelve seedlings treated with the same reporter were positioned on a glass plate. Roots were separated from seedlings, covered with some drops of liquid MS medium to prevent them from drying out, and transferred into a 1.5 mL reaction tube. Excess medium was removed. The rest of the seedlings, which was mainly made up by the leaves, was also collected and transferred into another reaction tube. 50 µL or 20 µL lysis buffer were added to leave and root samples, respectively. They were crushed with a special drill with pellet pestles for 1 min. Subsequently, samples were placed on ice for 30 min and centrifuged at 4 °C and 18,000 g for 30 min. The supernatant was transferred into a new 1.5 mL reaction tube and stored at -80 °C.

6.4.4. DAinv Reaction

In Lysates

Plant lysates were thawed on ice. Protein concentrations were determined by measuring the absorption at 280 nm with a spectrophotometer and were adjusted to the same value by addition of lysis buffer. Biotin-Tz was added to a final concentration of 150 µM to lysates in 1.5 mL reaction tubes. Samples were mixed by vortexing and were incubated at 25 °C and 400 rpm for 90 min. 4x SDS sample buffer was added to yield a 1x concentration. Samples were denatured at 98 °C for 10 min and stored until SDS-PAGE at -20 °C.

In Seedlings

A. thaliana seedlings having been treated with Ac_4GlcNAc or Ac_4GlcNCyoc in 24-well plates were washed with liquid MS medium three times. 4 w-% PFA in DPBS was added to fix seedlings at 4 °C for 30 min. Thereafter, seedlings were washed with liquid MS medium three times. 1 mL staining solution containing 1 µM or 10 µM TAMRA-Tz in liquid MS medium was added per well. Incubation took place at room temperature in the dark for 60 min. Seedlings were washed three more times with liquid MS medium and stored at 4 °C until their preparation for microscopy.

6.4.5. CuAAC

In Lysates

Plant lysates were thawed on ice. Protein concentrations were determined by measuring the absorption at 280 nm with a spectrophotometer and adjusted to the same value by addition of lysis buffer. A CuAAC reaction mixture containing 10 mM $CuSO_4$, 10 mM THPTA, 100 mM Na-ascorbate, and 3 mM biotin-alkyne in MQ water was freshly prepared from stock solutions in MQ water. Compounds were added one after the other to ensure proper reaction conditions. 1 µL of this mixture was added per 19 µL of *A. thaliana* lysate in a 1.5 mL reaction tube. Samples were mixed by vortexing and incubated at 25 °C and 400 rpm for 30 min. 4x SDS sample buffer was added to yield a 1x concentration. Samples were heat-denatured at 98 °C for 10 min and stored until SDS-PAGE at -20 °C.

In Seedlings

A. thaliana seedlings having been treated with Ac_4GlcNAc, Ac_4GlcNAz, or Ac_4GalNAz in 24-well plates were washed with liquid MS medium three times. 4 w-% PFA in DPBS was added to fix seedlings at 4 °C for 30 min. Thereafter, seedlings were washed with liquid MS medium three times. Different CuAAC reaction mixtures were prepared in liquid MS medium from stock solutions in MQ water as listed in Table 6.13. A fourth CuAAC reaction mixture was prepared from the Click-iT Cell Reaction Buffer Kit by combining 2.772 mL MQ water with 308 µL 10x buffer, 70 µL $CuSO_4$ solution, 350 µL additive, and 3.5 µL sulfo-Cy3-alkyne. 1 mL of different CuAAC reaction mixtures in liquid MS medium was added per well. Incubation occurred at room temperature in the dark for 60 min. Seedlings were washed three more times with liquid MS medium and stored at 4 °C until their preparation for microscopy.

Table 6.13: Composition of different CuAAC reaction mixtures.

Compound	**1**	**2**	**3**
$CuSO_4$	1 mM	0.5 mM	1 mM
THPTA	-	0.5 mM	1 mM
Amminoguanidine	-	-	5 mM
Na ascorbate	1 mM	5 mM	5 mM
Sulfo-Cy3-alkyne	1 µM	1 µM	1 µM

6.4.6. Seedling Preparation for Microscopy

Seedlings treated with glycosylation reporters and labeled via a CuAAC or DAinv reaction were placed on a glass slide, wetted with some drops of liquid MS medium, and covered with a cover glass. Confocal fluorescence microscopy was performed as described in chapter 6.6.1. Afterwards, samples were sealed with nail polish, which was applied at the interface of the cover slip and the glass slide. They were stored at room temperature in the dark.

6.5. Chemical Synthesis

6.5.1. OSMI-1

(R)-2-(2-formylphenyl)-*N*-(furan-2-ylmethyl)-2-((2-oxo-1,2-dihydroquinoline)-6-sulfonamido)-*N*-(thiophe-2-ylmethyl)acetamide (OSMI-1) was synthesized in four steps according to a procedure published by Ortiz-Meoz et al. (Figure 6.1).[413] $\boldsymbol{R_f}$ = 0.12 (CH_2Cl_2/(90 % MeOH + 10 % NH_4OH), 95:5); **^{1}H NMR** and **^{13}C NMR** spectra were in accordance with literature.[413] **HRMS** (ESI-TOF) calculated for $C_{28}H_{25}N_3O_6S_2$ [*M* + Na]$^+$ *m/z*: 563.1258; found 564.1222.

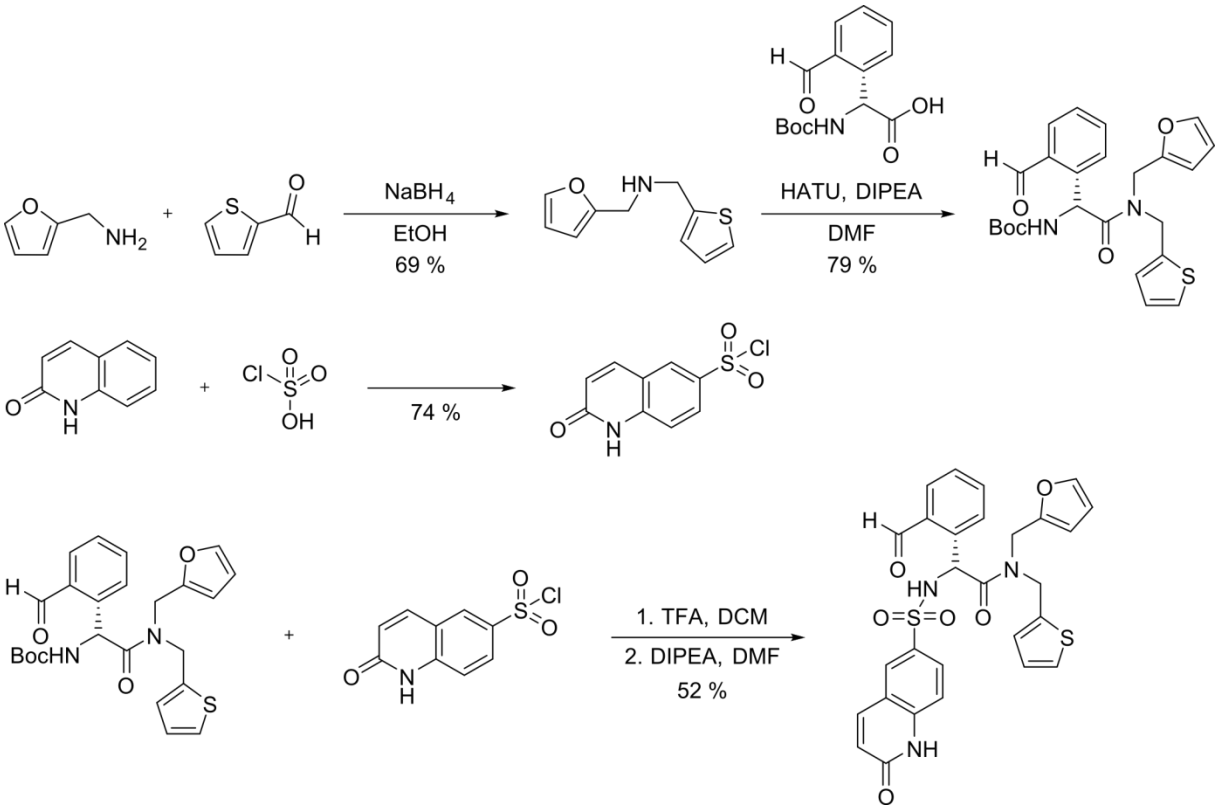

Figure 6.1: Synthesis route to OSMI-1.

6.5.2. M4P

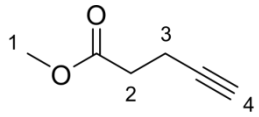

Chemical Formula: $C_6H_8O_2$
Molecular Weight: 112.13

Figure 6.2: Chemical structure of M4P and assignment of ^{1}H NMR signals.

M4P was synthesized according to a known procedure with slight variations.[550] 4-Pentynoic acid (1 g, 10.2 mmol) was dissolved in 20 mL dry methanol under nitrogen atmosphere and constant stirring. Acetyl chloride (2 mL, 28 mmol) was added dropwise over 15 min. The solution was heated to reflux for 4 h. Completion of the reaction was monitored by thin-layer chromatography (TLC). Afterwards, the mixture was cooled to room temperature. A saturated $NaHCO_3$ solution was added to 20 mL deionized water to reach a pH value of 8 to 9. The reaction mixture was slowly added to the water under constant stirring and the pH value was kept between 7 and 9 by addition of $NaHCO_3$. The aqueous phase was extracted with diethylether (3 x 40 mL). Organic phases were combined, washed once with brine, and dried over sodium sulfate. Solvents were evaporated under reduced pressure. Methyl 4-pentynoate was obtained as clear, fruity-smelling liquid with a yield of 84 % (1.03 g, 8.6 mmol). $\boldsymbol{R_f}$ = 0.5 (CH_2Cl_2); **^{1}H NMR** (400 MHz, $CDCl_3$) δ = 3.70 (s, 3H, 1), 2.58 – 2.53 (m, 2 H, 2/3), 2.53 – 2.47 (m, 2H, 2/3), 1.97 (t, J = 2.5 Hz, 1H, 4) ppm; **^{13}C NMR** (101 MHz, $CDCl_3$) δ = 172.3, 82.6, 69.1, 51.9, 33.3, 14.5 ppm. Analytical data were in accordance with literature.[550]

6.5.3. AM4P

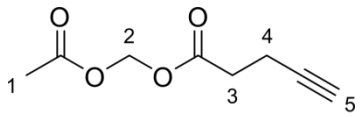

Chemical Formula: $C_8H_{10}O_4$
Molecular Weight: 170.16

Figure 6.3: Chemical structure of AM4P and assignment of ^{1}H NMR signals.

AM4P was synthesized from 4-pentynoic acid by following a procedure reported for the synthesis of diacetoxymethyl-2-propargylmalonate.[155] 4-Pentynoic acid (1 g, 10.2 mmol) was dissolved in 10 mL dry acetonitrile under nitrogen atmosphere and constant stirring. DIPEA (2.2 mL, 12.7 mmol) and bromomethylacetate (1.1 mL, 11.2 mmol) were added dropwise to the reaction mixture. This solution was stirred overnight at room temperature. Completion of the reaction was monitored by TLC and the solvent was evaporated under reduced pressure. The resulting yellow oil was purified by silica column chromatography (petrol ether/ethyl acetate 10:1) to give acetoxymethyl 4-pentynoate as yellowish oil (1.29 g, 7.6 mmol, 74 %). $\boldsymbol{R_f}$ = 0.18 (petrol ether/ethyl acetate 10:1); **^{1}H NMR** (400 MHz, $CDCl_3$) δ = 5.76 (s, 2H, 2), 2.64 – 2.57 (m, 2H, 3), 2.55 – 2.49 (m, 2H, 4), 2.11 (s, 3H, 1), 1.98 (t, J = 2.6 Hz, 1 H, 5) ppm; **^{13}C NMR** (101 MHz, $CDCl_3$) δ = 170.7, 196.7, 82.1, 79.4, 69.4, 33.2, 20.8, 14.2 ppm. **HRMS** (ESI-TOF) calculated for $C_8H_{10}O_4$ $[M + Na]^+$ *m/z*: 193.0471; found 193.0467.

6.6. Microscopy

6.6.1. Confocal Fluorescence Microscopy

Confocal fluorescence microscopy was performed on a TCS SP5 laser scanning microscope using an oil immersion objective (63x 1.4 NA HCX PL APO CS, Leica Microsystems CMS) and the LAS AF software. The temperature within the microscope box was usually kept at room temperature for experiments with fixed cells, but was increased to 37 °C for live cell experiments. EGFP was excited at 488 nm (argon laser, 10 %). Its fluorescence was detected with a photomultiplier tube (PMT) between 500 nm and 550 nm. Cy3 and TAMRA were excited at 561 nm (diode pumped solid state (DPSS) laser, 10 %). Their fluorescence was detected with a PMT between 570 nm and 625 nm. Transmission images were acquired with a transmitted light detector. Images were generally taken using the following parameters: scanning speed: 100 lines s^{-1}, pixel size: 68.8 nm x 68.8 nm, image size: 70.3 µm x 70.3 µm (1024 pixels x 1024 pixels), line average: 4, bit depth: 8 bit. PMT gain and smart offset were adjusted per experiment individually. Images were processed using the software LAS AF Lite, ImageJ, and Inkscape. Average intensities of cells were obtained from LAS AF Lite by drawing polygons around individual cells.

For microscopy of *A. thaliana* seedlings, an air objective (40x 0.85 NA HCX PL APO CS, Leica Microsystems CMS) was used.

For experiments carried out at i3s Porto, a TCS SP5 laser scanning microscope (Leica Microsystems CMS) was employed as well. Parameters and settings were the same as

mentioned above except the following: The temperature in the box was kept at room temperature for all measurements. DAPI was excited at 405 nm (diode laser, 20 %) and its fluorescence was detected with a PMT between 420 nm and 500 nm. Alexa Fluor 488 was excited at 488 nm (argon laser, 20 %) and its fluorescence was acquired with a PMT between 500 nm and 550 nm. Cy3 was excited at 561 nm (DPSS laser, 20 %) and its fluorescence was detected with a PMT between 570 nm and 625 nm. Alexa Fluor 647 was excited at 633 nm (helium neon laser, 5 %) and its fluorescence was acquired with a HyD between 645 nm and 700 nm.

6.6.2. Acceptor Photobleaching

Acceptor photobleaching experiments were performed on a TCS SP5 laser scanning microscope using the LAS AF FRET acceptor photobleaching wizard. Images of donor and acceptor fluorescence were taken before and after bleaching the acceptor using wavelengths of 488 nm (10 %, detection between 500 nm and 550 nm) and 561 nm (10 %, detection between 570 nm and 625 nm) and the following settings: scanning speed: 200 lines s^{-1}, pixel size: 68.7 nm x 68.7 nm, image size: 70.3 µm x 70.3 µm (1024 pixels x 1024 pixels), line average: 2, bit depth: 8 bit. Bleaching of the acceptor (Cy3) was performed to decrease its fluorescence intensity by at least 80 %. Care was taken to not decrease the donor fluorescence intensity while bleaching the acceptor. To this end, two bleaching steps with 25 % and one step with 100 % of the DPSS laser intensity were used in glycosylation and acetylation experiments, respectively. The bleaching area was kept constant to a circle with a diameter of 7 µm (glycosylation experiments) or a square with an edge length of 7 µm (acetylation experiments).
Donor fluorescence intensities before and after bleaching the acceptor were used to calculate apparent FRET efficiency according to equation 2.12. Images were processed using the software LAS AF Lite, ImageJ, and Inkscape. FRET images were generated with the FRETcalc ImageJ plugin.[617]

6.6.3. Wide-field Frequency Domain FLIM

For FLIM microscopy, a home-built wide field frequency domain FLIM setup was utilized. It was first realized by Dr. Annette S. Indlekofer[320], then rebuilt twice by myself, and recently modified by Tobias Löffler.
The setup is schematically drawn in Figure 6.4. A diode laser at 488 nm (LDM488.20.A350, Omicron) modulated at 70 MHz is used as excitation source. Behind the laser, a clean-up filter (ZET488/10, Chroma) is integrated. The laser intensity is adjusted via neutral density filters. Its beam diameter is enlarged to 3 mm using a telescope composed of two lenses (LA1805-A, f = 30 mm and LA1134-A, f = 60 mm, Thorlabs) and coupled via a collimator (FC220FC-A, f = 10.90 mm, NA = 0.25, Thorlabs) into a shaken multi-mode fiber (UM22-600, diameter = 600 µm, NA = 0.22, Thorlabs) to illuminate the sample homogenously. Following another collimator (FC220FC-A, f = 10.90 mm, NA = 0.25, Thorlabs) and two lenses (LA1422-A, f = 40 mm and LA1509-A, f = 100 mm, Thorlabs), the beam is passed in an inverted microscope (DMI 6000B, Leica Microsystems CMS) and is deflected onto a sample via a dichroic mirror (QuadLine zt440/488/560/635rpc, Chroma) and an oil immersion

objective (HC PL APO 100x 1.40 NA Oil CS2, Leica Microsystems CMS). For maintaining biological samples for live cell imaging at 37 °C, the microscope can be equipped with a heating stage connected to a temperature controller (Tempcontrol 37-2 digital, Pecon).
Fluorescence of EGFP is gathered in epi direction via the objective and separated from the excitation laser light by the dichroic mirror. An intermediate image is generated by the tube lens (f = 200 mm) behind the microscope and widened 4.25 fold by two photo objectives (f = 20 mm, Sigma and f = 85 mm, Walimex Pro) to match the size of the detector chip. Two bandpass filters (525/50 BrightLine HC, Semrock and 515/30 ET, Chroma) are located between these objectives. Instead of the bandpass 525/50, a 488 nm longpass filter can be integrated (EdgeBasic Langpass 488, Semrock). The PIMAX4:1024i RF CCD camera (Princeton Instruments) coupled to a GenIII intensifier (Princeton Instruments) is used as detector.
The Omicron laser controller software was used to adjust the laser power. The LightField software was utilized to run the CCD camera and to control the laser's modulation. The following settings were chosen: output frequency: 70 MHz, intensifier gain: 90x, pixel number: 512 x 512 (pixel size: 70 nm x 70 nm). Image acquisition parameters were: frames to save: 12, exposures per frame: 10, modulation duration: 100 ms, modulation phase: alternating phase order (0 °, 131 °, 262 °, 196 °, 327 °, 65 °, 295 °, 33 °, 164 °, 98 °, 229 °, 0 °). This special recording order of the 12 phase steps was shown to suppress photobleaching induced artifacts most efficiently.[618]

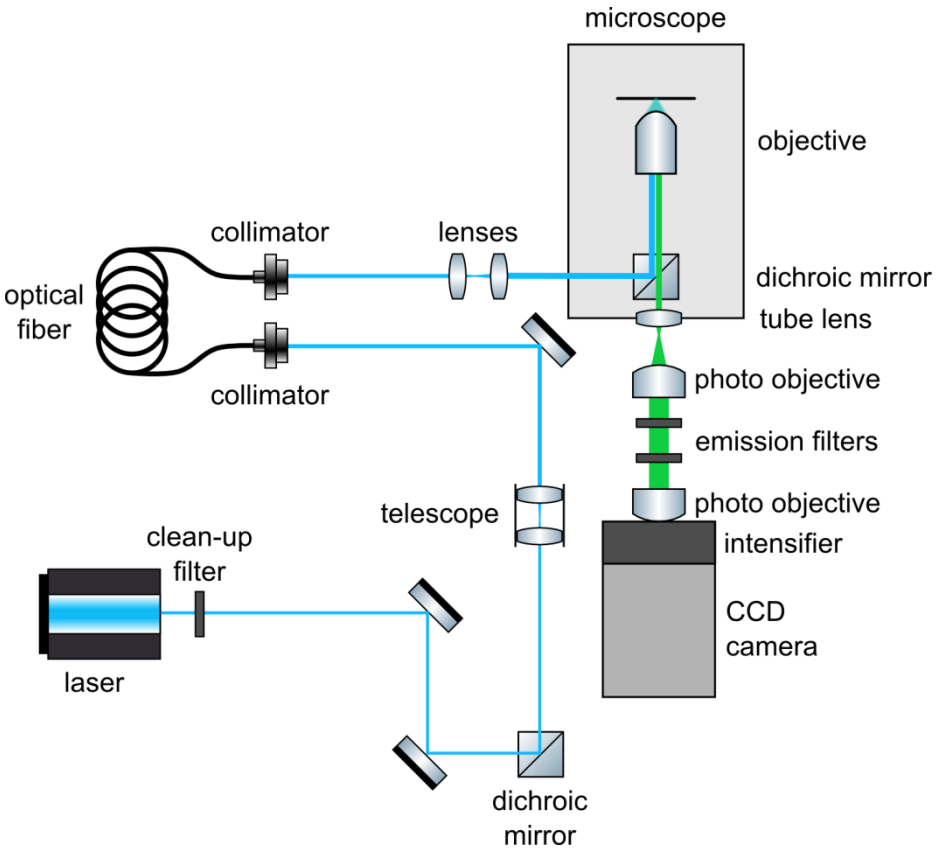

Figure 6.4: Schematic structure of the wide-field frequency domain FLIM setup. Reprinted (adapted) with permission from Doll et al.[355] Copyright (2018) Elsevier Inc.

To calibrate the setup, two fluorophore solutions with known fluorescence lifetimes were measured. Solutions of 10 µM or 100 µM coumarin 6 in ethanol have a known fluorescence lifetime of 2.5 ns and a 10 µM rhodamine 6G solution in MQ water one of ~3.9 ns.[619,620] Laser powers of 5 µW and 100 µW were used for their excitation, respectively. 30 µL of each solution were filled in chambers of a µ-slide VI 0.4 (ibidi). Three images were acquired per fluorophore. The SimFCS software was used to assess the correctness of lifetimes. To this end, the fluorescence modulation and phase lifetimes of coumarin 6 were set to 2.5 ns. If rhodamine 6G fluorescence lifetimes were between 3.8 ns and 4.0 ns, experiments were started. Otherwise, the incoupling of the laser light into the multimode fiber was optimized and the collimator as well as the two lenses behind the fiber adjusted. Cells were measured with laser powers between 50 µW and 150 µW. The laser power was kept constant throughout measurement series. For optimal comparability of data, cells displaying roughly the same fluorescence intensities were chosen.
Raw images generated by LightField were background-corrected and sorted according to the phase steps by the software. After exporting them as tiff file, MATLAB macros were used for calculation of fluorescence modulation and phase lifetime images. These macros were developed by Dr. Waldemar Schrimpf (group of Prof. Dr. Lamb, Ludwig-Maximilians-Universität, Munich, Germany).[621] An additional correction of the irising effect was implemented by Dr. Annette S. Indlekofer.[320] Images were intensity-weighted and an intensity threshold of 10 % of the maximum intensity was chosen. Additionally, a 2 x 2 moving average filter was applied.
Next to the fluorescence modulation and phase lifetime images, MATLAB macros were used to calculate average fluorescence modulation and phase lifetimes τ of each image. These were averaged and the SEM δ was calculated over all cells measured at a certain condition. Apparent FRET efficiencies $E_{FRETapp}$ were derived from average fluorescence lifetimes of cells treated with a chemical reporter and those treated with the corresponding control compound according to:

$$E_{FRETapp} = \left(1 - \frac{\tau_{Reporter}}{\tau_{Control}}\right) \cdot 100\ \% \tag{6.1}$$

SEMs of apparent FRET efficiencies were derived via a Gaussian propagation of errors:

$$\delta_{E_{FRETapp}} = \sqrt{\left(\frac{\tau_{Reporter}}{{\tau_{Control}}^2} \cdot 100\ \% \cdot \delta_{Control}\right)^2 + \left(\frac{1}{\tau_{Control}} 100\ \% \cdot \delta_{Reporter}\right)^2} \tag{6.2}$$

6.7. Statistics

Statistical evaluation of data was performed with the GraphPad Prism software. The confidence interval was set to 95 % for all statistical calculations. Degrees of significance were defined as ns $p>0.05$, * $p<0.05$, ** $p<0.01$, and *** $p<0.001$. Statistical tests and posttests performed with individual data sets are indicated in the corresponding figure legend.

7. Publications

F. Doll, R. R. Steimbach, A. Zumbusch, "Direct Imaging of Protein-Specific Methylation in Mammalian Cells", **2018**, *submitted*.

Parts of this manuscript are included in chapter 4.3.

F. Doll, J. Hassenrück, V. Wittmann, A. Zumbusch, "Intracellular Imaging of Protein-Specific Glycosylation", *Methods Enzymol.* **2018**, *598*, 283-319.

Parts of this publication are included in chapters 4.1.1, 4.1.2, 6.2, and 6.6.3.

F. Doll, A. Buntz, A.-K.-Späte, V.F. Schart, A. Timper, W. Schrimpf, C.R. Hauck, A. Zumbusch, V. Wittmann, "Visualization of Protein-Specific Glycosylation inside Living Cells", *Angew. Chem. Int. Ed. Engl.* **2016**, *55*, 2262-2266; *Angew. Chem.* **2016**, *128*, 2303-2308.

Parts of this publication are included in chapters 4.1.1 and 4.1.2.

8. Conference Contributions

2018/08	EMBO Workshop Chemical Biology 2018 in Heidelberg (Germany) **Talk** entitled "In cell imaging of protein-specific methylation"
2017/09	International Symposium on Bioorganic Chemistry (ISBOC-11) in Konstanz (Germany) **Poster** entitled "FLIM-FRET Microscopy for Visualizing Protein-Specific Glycosylation inside Living Cells"
2017/06	67th Lindau Nobel Laureate Meeting in Lindau (Germany) **Talk** in the masterclass of Prof. Dr. Aaron Ciechanova entitled "In Cell Imaging of Protein-Specific Post-Translational Modifications"
2017/04	Focus on Microscopy 2017 in Bordeaux (France) **Poster** entitled "FLIM-FRET Microscopy for in Cell Imaging of Protein Post-Translational Modifications"
2016/10	Symposium of the SFB 969 "Two Days of Proteostasis" in Konstanz (Germany) **Poster** entitled "FLIM-FRET microscopy as a tool for studying protein-specific glycosylation inside living cells"
2016/07	Conference of the section Biochemie of the Gesellschaft Deutscher Chemiker "Shaping the Molecules of Life: Chemical Biology of Nucleic Acid and Protein Modifications" in Frankfurt a. M. (Germany) **Talk** entitled "Imaging the Glycosylation of Designated Proteins Inside Living Cells"
2016/04	International discussion meeting on Förster Resonance Energy Transfer in Life Science "FRET II" in Göttingen (Germany) **Poster** entitled "Using FLIM-FRET microscopy to study protein-specific glycosylation inside living cells"
2015/10	Konstanz Symposium Chemical Biology in Konstanz (Germany) **Talk** entitled "Visualizing Protein-Specific Glycosylation Inside Living Cells"
2015/09	23rd International Symposium on Glycoconjugates of the International Glycoconjugate Organization in Split (Croatia) **Talk** entitled "Visualizing Protein-Specific Glycosylation Inside Living Cells", abstract published in: *Glycoconj. J.* **2015**, *32*, 199.

9. List of Abbreviations

A. thaliana	*Arabidopsis thaliana*
$Ac_3$6AzGlcNAc	Triacetylated 6-azido-*N*-acetylglucosamine
Ac_4GalNAz	Tetraacetylated *N*-azidoacetylgalactosamine
Ac_4GalNCyoc	Tetraacetylated methylcyclopropene-tagged *N*-acetylgalactosamine
Ac_4GlcNAc	Tetraacetylated *N*-acetylglucosamine
Ac_4GlcNAz	Tetraacetylated *N*-azidoacetylglucosamine
Ac_4GlcNCp	Tetraacetylated cyclopropene-tagged *N*-acetylglucosamine
Ac_4GlcNCyoc	Tetraacetylated methylcyclopropene-tagged *N*-acetylglucosamine
Ac_4ManNAz	Tetraacetylated *N*-azidoacetylmannosamine
Ac_4ManNCyoc	Tetraacetylated methylcyclopropene-tagged *N*-acetylmannosamine
ACTN1	α-actinin 1
ACTN4	α-actinin 4
Adox	Adenosine-2′,3′-dialdehyde
Akt1	RAC-α serine/threonine-protein kinase
Alk	Alkyne
AM4P	Acetoxymethyl 4-pentynoate
ANOVA	Analysis of variances
ATP	Adenosine triphosphate
Az	Azide
BARAC	Biarylazacyclooctynone
BCN	Bicyclo[6.1.0]non-4-yne
BSA	Bovine serum albumin
BTTAA	2-(4-((Bis((1-(tert-butyl)-1H-1,2,3-triazol-4-yl)methyl)amino)methyl)-1H-1,2,3-triazol-1-yl)acetic acid
BTTES	2-(4-((Bis((1-(tert-butyl)-1H-1,2,3-triazol-4-yl)methyl)amino)methyl)-1H-1,2,3-triazol-1-yl)ethyl hydrogen sulfate
CAMK4	Calcium/calmodulin-dependent protein kinase type IV
CCD	Charge-coupled device
CHO	Chinese hamster ovary cells
CMP	Cytidine monophosphate
c-Myc	Myc proto-oncogene protein
CoA	Coenzyme A
CuAAC	Cu(I)-catalyzed azide-alkyne-cycloaddition
Cy	Cyanine
DAinv	Inverse-electron-demand Diels-Alder
DAPI	4′,6-Diamidino-2-phenylindole dihydrochloride
DIBO	Dibenzocyclooctye

DIPEA	*N*,*N*-diisopropylethylamine
DMEM	Dublecco's modified eagle medium
DMSO	Dimethyl sulfoxide
DNA	Deoxyribonucleic acid
DPBS	Dulbecco's phosphate buffered saline
DPSS	Diode pumped solid state
E. coli	*Escherichia coli*
EB1	Microtubule-associated protein RP/EB family member 1
ECL	Enhanced chemiluminescence
EDTA	Ethylenediamine-*N*,*N*,*N*',*N*'-tetraacetic acid
EGFP	Enhanced green fluorescent protein
EGTA	Ethylene glycol-bis(β-aminoethyl ether)-*N*,*N*,*N*',*N*'-tetraacetic acid
ENO1	α-enolase
E.v.	Empty vector
FBS/FCS	Fetal bovine/calf serum
FLIM	Fluorescence lifetime imaging
Foxo1	Forkhead box protein O1
FRET	Förster resonance energy transfer
Fuc	Fucose
GalNAc	*N*-acetylgalactosamine
GAPDH	Glyceraldehyde-3-phosphate dehydrogenase
GFP	Green fluorescent protein
GlcNAc	*N*-acetylglucosamine
GPI	Glucose-6-phosphate isomerase
GSK-3β	Glycogen synthase kinase-3β
H1299	Human non-small cell lung carcinoma cell line
H2B	Histone 2B
H3	Histone 3
H4	Histone 4
HBS	HEPES buffered saline
HDAC1	Histone deacetylase 1
HEK	Human embryonic kidney cell line
HeLa	Cervical cancer cells taken from Henrietta Lacks
HEPES	2-[4-(2-Hydroxyethyl)piperazin-1-yl]ethanesulfonic acid
HOMO	Highest occupied molecular orbital
HSP70	Heat shock protein 70 kDa
HSPA8	Heat shock cognate protein 71 kDa
HSPH1	Heat shock protein 105 kDa
Kdo	3-Deoxy-D-manno-oct-2-ulosonic acid
KRT8	Cytokeratin 8
LB	Lysogeny broth
LIC	Ligation independent cloning
LUHMES	Lund human mesencephalic
LUMO	Lowest unoccupied molecular orbital

M4P	Methyl 4-pentynoate
ManNAc	*N*-acetylmannosamine
MEM	Minimum essential medium
MGE	Metabolic glycoengineering
MKN45	Human gastric cancer cell line
MOE	Metabolic oligosaccharide engineering
MQ	Milli-Q
MS	Murashige and Skoog
NA	Numeric aperture
Na4P	Sodium 4-pentynoate
NEB	New England Biolabs
NIH 3T3	Mouse fibroblast cell line generated at New York University
NPM	Nucleophosmin
Ns	Not significant
OCT	Cyclooctyne
OGA	*O*-GlcNAcase
O-GlcNAc	*O*-linked *N*-acetylglucosamine
OGT	*O*-GlcNAc transferase
OSMI-1	(R)-2-(2-formylphenyl)-*N*-(furan-2-ylmethyl)-2-((2-oxo-1,2-dihydro quinoline)-6-sulfonamido)-*N*-(thiophen-2-ylmethyl)acetamide
p300	Histone acetyltransferase p300
p53	Tumor protein p53
PARP1	Poly [ADP-ribose] polymerase 1
PBS	Phosphate buffered saline
PCR	Polymerase chain reaction
PFA	Paraformaldehyde
PGK1	Phosphoglycerate kinase 1
PMT	Photomultiplier tube
PP1β	Serine/threonine-protein phosphatase PP1 β catalytic subunit
PRIME	Probe incorporation mediated by enzymes
ProSeAM	(2S)-4-((((2S,3S,4R,5R)-5-(6-amino-9H-purin-9-yl)-3,4-dihydroxy tetrahydrofuran-2-yl)methyl)(prop-2-yn-1-yl)selenonio)-2-ammoniobutanoate
PTEN	Phosphatidylinositol 3,4,5-trisphosphate 3-phosphatase and dual-specificity protein phosphatase
PTM	Post-translational modification
PUGNAc	*O*-(2-Acetamido-2-deoxy-D-glucopyranosylidenamino) *N*-phenylcarbamate
RNA	Ribonucleic acid
RPMI	Roswell Park Memorial Institute cell culture medium
SAH	*S*-Adenosyl-L-homocysteine
SAM	*S*-Adenosyl-L-methionine
SDS-PAGE	Sodium dodecylsulfate-polyacrylamide gelelectrophoresis
SEM	Standard error of the mean

SNAC	α-Synuclein
SP1	Transcription factor Sp1
SPAAC	Strain-promoted azide-alkyne cycloaddition
ST3Gal4	CMP-*N*-acetylneuraminate-β-galactosamide-α-2,3-sialyltransferase 4
ST6GalNAc1	α-*N*-acetylgalactosaminide α-2,6-sialyltransferase 1
TAMRA	Tetramethylrhodamine
TBTA	Tris((1-benzyl-1H-1,2,3-triazol-4-yl)methyl)amine
TCEP	Tris(2-carboxyethyl)phosphine
TCSPC	Time-correlated single photon counting
TEMED	Tetramethylethylenediamine
TFA	Trifluoracetic acid
THPTA	Tris(3-hydroxypropyltriazolylmethyl)amine
TLC	Thin-layer chromatography
Tz	Tetrazine
UDP	Uridine diphosphate
V-%	Volume percentage
VCP	Transitional endoplasmic reticulum ATPase
WT	Wild type

10. References

[1] F. Crick, *Nature* **1970**, *227*, 561–563.
[2] International Human Genome Sequencing Consortium, *Nature* **2004**, *431*, 931–945.
[3] G. A. Petsko, *Genome Biol.* **2001**, *2*, comment1003.1-comment1003.2.
[4] The C. elegans Sequencing Consortium, *Science* **1998**, *282*, 2012–2018.
[5] The French-Italian Public Consortium for Grapevine Genome Characterization, O. Jaillon, J.-M. Aury, B. Noel, A. Policriti, C. Clepet, A. Casagrande, N. Choisne, S. Aubourg, N. Vitulo, et al., *Nature* **2007**, *449*, 463–467.
[6] M. Pertea, S. L. Salzberg, *Genome Biol.* **2010**, *11*, 206.
[7] C. T. Walsh, S. Garneau-Tsodikova, J. Gatto G. J., *Angew. Chem. Int. Ed Engl.* **2005**, *44*, 7342–7372.
[8] D. L. Black, *Annu. Rev. Biochem.* **2003**, *72*, 291–336.
[9] C. T. Walsh, *Posttranslational Modification of Proteins. Expanding Nature's Inventory.*, Roberts & Company Publishers, Greenwood Village, CO, **2005**.
[10] G. A. Khoury, R. C. Baliban, C. A. Floudas, *Sci. Rep.* **2011**, *1*, 90.
[11] Y. Zhao, O. N. Jensen, *Proteomics* **2009**, *9*, 4632–4641.
[12] H. Mohabatkar, P. Rabiei, M. Alamdaran, *Curr. Top. Med. Chem.* **2017**, *17*, 2381–2392.
[13] R. Hooke, *Micrographia : Or, Some Physiological Descriptions of Minute Bodies Made by Magnifying Glasses. With Observations and Inquiries Thereupon*, J. Martyn And J. Allestry, Royal Society, London, **1665**.
[14] H. Gest, *Notes Rec. R. Soc.* **2004**, *58*, 187–201.
[15] M. J. Sanderson, I. Smith, I. Parker, M. D. Bootman, *Cold Spring Harb. Protoc.* **2014**, *2014*, pdb.top071795.
[16] K. Li, "A History of Microscopy – Harvard Science Review" **2017**, https://harvardsciencereview.com/2017/12/15/a-history-of-microscopy/, accessed 24.5.2018, 7:22:04 PM.
[17] O. Shimomura, F. H. Johnson, Y. Saiga, *J. Cell. Comp. Physiol.* **1962**, *59*, 223–239.
[18] D. M. Chudakov, M. V. Matz, S. Lukyanov, K. A. Lukyanov, *Physiol. Rev.* **2010**, *90*, 1103–1163.
[19] M. Grammel, H. C. Hang, *Nat. Chem. Biol.* **2013**, *9*, 475–484.
[20] W. Lin, L. Gao, X. Chen, *Curr. Opin. Chem. Biol.* **2015**, *28*, 156–163.
[21] D. I. Udenwobele, R.-C. Su, S. V. Good, T. B. Ball, S. Varma Shrivastav, A. Shrivastav, *Front. Immunol.* **2017**, *8*, 751.
[22] P. Cohen, *Nat. Cell Biol.* **2002**, *4*, E127–E130.
[23] K. N. Chuh, M. R. Pratt, *Curr. Opin. Chem. Biol.* **2015**, *24*, 27–37.
[24] T. M. Karve, A. K. Cheema, T. M. Karve, A. K. Cheema, *J. Amino Acids* **2011**, *2011*, e207691.
[25] Y. L. Deribe, T. Pawson, I. Dikic, *Nat. Struct. Mol. Biol.* **2010**, *17*, 666–672.
[26] A. Hirano, Y.-H. Fu, L. J. Ptáček, *Nat. Struct. Mol. Biol.* **2016**, *23*, 1053–1060.
[27] K. N. Chuh, A. R. Batt, M. R. Pratt, *Cell Chem. Biol.* **2016**, *23*, 86–107.
[28] S. Hardivillé, G. W. Hart, *Cell Metab.* **2014**, *20*, 208–213.

[29] N. E. Zachara, N. O'Donnell, W. D. Cheung, J. J. Mercer, J. D. Marth, G. W. Hart, *J. Biol. Chem.* **2004**, *279*, 30133–30142.
[30] T. Lefebvre, V. Dehennaut, C. Guinez, S. Olivier, L. Drougat, A.-M. Mir, M. Mortuaire, A.-S. Vercoutter-Edouart, J.-C. Michalski, *Biochim. Biophys. Acta* **2010**, *1800*, 67–79.
[31] M. Chaibva, S. Jawahery, A. W. Pilkington, J. R. Arndt, O. Sarver, S. Valentine, S. Matysiak, J. Legleiter, *Biophys. J.* **2016**, *111*, 349–362.
[32] J. Y. Kim-Muller, Y. J. R. Kim, J. Fan, S. Zhao, A. S. Banks, M. Prentki, D. Accili, *J. Biol. Chem.* **2016**, *291*, 10162–10172.
[33] H. Wei, R. Mundade, K. C. Lange, T. Lu, *Cell Cycle* **2014**, *13*, 32–41.
[34] E. L. Greer, Y. Shi, *Nat. Rev. Genet.* **2012**, *13*, 343–357.
[35] S. O.-V. Stichelen, V. Dehennaut, A. Buzy, J.-L. Zachayus, C. Guinez, A.-M. Mir, I. E. Yazidi-Belkoura, M.-C. Copin, D. Boureme, D. Loyaux, et al., *FASEB J.* **2014**, *28*, 3325–3338.
[36] X. Shi, I. Kachirskaia, H. Yamaguchi, L. E. West, H. Wen, E. W. Wang, S. Dutta, E. Appella, O. Gozani, *Mol. Cell* **2007**, *27*, 636–646.
[37] R. Apweiler, H. Hermjakob, N. Sharon, *Biochim. Biophys. Acta* **1999**, *1473*, 4–8.
[38] A. Varki, R. D. Cummings, J. D. Esko, H. H. Freeze, P. Stanley, C. R. Bertozzi, G. W. Hart, M. E. Etzler, Eds. , *Essentials of Glycobiology*, Cold Spring Harbor Laboratory Press, Cold Spring Harbor (NY), **2009**.
[39] F. Schwarz, M. Aebi, *Curr. Opin. Struct. Biol.* **2011**, *21*, 576–582.
[40] R. S. Haltiwanger, L. Wells, H. H. Freeze, P. Stanley, in *Essent. Glycobiol.* (Eds.: A. Varki, R.D. Cummings, J.D. Esko, P. Stanley, G.W. Hart, M. Aebi, A.G. Darvill, T. Kinoshita, N.H. Packer, J.H. Prestegard, et al.), Cold Spring Harbor Laboratory Press, Cold Spring Harbor (NY), **2015**.
[41] K. Ohtsubo, J. D. Marth, *Cell* **2006**, *126*, 855–867.
[42] P. M. Rudd, T. Elliott, P. Cresswell, I. A. Wilson, R. A. Dwek, *Science* **2001**, *291*, 2370–2376.
[43] C.-R. Torres, G. W. Hart, *J. Biol. Chem.* **1984**, *259*, 3308–3317.
[44] G. D. Holt, G. W. Hart, *J. Biol. Chem.* **1986**, *261*, 8049–8057.
[45] G. W. Hart, *Annu. Rev. Biochem.* **1997**, *66*, 315–335.
[46] L. K. Kreppel, M. A. Blomberg, G. W. Hart, *J. Biol. Chem.* **1997**, *272*, 9308–9315.
[47] G. W. Hart, M. P. Housley, C. Slawson, *Nature* **2007**, *446*, 1017–1022.
[48] B. Shen, W. Zhang, Z. Shi, F. Tian, Y. Deng, C. Sun, G. Wang, W. Qin, X. Qian, *Talanta* **2017**, *169*, 195–202.
[49] B. D. Lazarus, D. C. Love, J. A. Hanover, *Glycobiology* **2006**, *16*, 415–421.
[50] R. Shafi, S. P. Iyer, L. G. Ellies, N. O'Donnell, K. W. Marek, D. Chui, G. W. Hart, J. D. Marth, *Proc. Natl. Acad. Sci. U. S. A.* **2000**, *97*, 5735–5739.
[51] S. Varshney, P. Stanley, *Biochem. Soc. Trans.* **2017**, *45*, 401–408.
[52] D. L. Dong, G. W. Hart, *J. Biol. Chem.* **1994**, *269*, 19321–19330.
[53] D. J. Vocadlo, G. J. Davies, *Curr. Opin. Chem. Biol.* **2008**, *12*, 539–555.
[54] G. W. Hart, C. Slawson, G. Ramirez-Correa, O. Lagerlof, *Annu. Rev. Biochem.* **2011**, *80*, 825–58.
[55] N. Zachara, Y. Akimoto, G. W. Hart, in *Essent. Glycobiol.* (Eds.: A. Varki, R.D. Cummings, J.D. Esko, P. Stanley, G.W. Hart, M. Aebi, A.G. Darvill, T. Kinoshita, N.H. Packer, J.H. Prestegard, et al.), Cold Spring Harbor Laboratory Press, Cold Spring Harbor (NY), **2015**.
[56] H. J. Tarbet, L. Dolat, T. J. Smith, B. M. Condon, E. T. O. Iii, R. H. Valdivia, M. Boyce, *eLife* **2018**, *7*, e31807.
[57] E. T. Powers, *Nat. Chem. Biol.* **2015**, *11*, 307–308.

[58] N. E. Zachara, G. W. Hart, *Biochim. Biophys. Acta* **2006**, *1761*, 599–617.
[59] P. S. Banerjee, O. Lagerlöf, G. W. Hart, *Mol. Aspects Med.* **2016**, *51*, 1–15.
[60] P.-H. Chen, J.-T. Chi, M. Boyce, *Glycobiology* **2018**, *28*, 556–564.
[61] Z. Li, W. Yi, *Glycoconj. J.* **2013**, *31*, 185–191.
[62] J. Zhong, M. Martinez, S. Sengupta, A. Lee, X. Wu, R. Chaerkady, A. Chatterjee, R. N. O'Meally, R. N. Cole, A. Pandey, et al., *Proteomics* **2015**, *15*, 591–607.
[63] A. C. Leney, D. El Atmioui, W. Wu, H. Ovaa, A. J. R. Heck, *Proc. Natl. Acad. Sci. U. S. A.* **2017**, *14*, E7255–E7261.
[64] Q. Zeidan, G. W. Hart, *J. Cell Sci.* **2010**, *123*, 13–22.
[65] W. H. Yang, J. E. Kim, H. W. Nam, J. W. Ju, H. S. Kim, Y. S. Kim, J. W. Cho, *Nat. Cell Biol.* **2006**, *8*, 1074–1083.
[66] K. Sakabe, G. W. Hart, *J. Biol. Chem.* **2010**, *285*, 34460–34468.
[67] N. Fülöp, R. B. Marchase, J. C. Chatham, *Cardiovasc. Res.* **2007**, *73*, 288–297.
[68] I. Brockhausen, H. Schachter, P. Stanley, in *Essent. Glycobiol.* (Eds.: A. Varki, R.D. Cummings, J.D. Esko, H.H. Freeze, P. Stanley, C.R. Bertozzi, G.W. Hart, M.E. Etzler), Cold Spring Harbor Laboratory Press, Cold Spring Harbor (NY), **2009**.
[69] T. Angata, A. Varki, *Chem. Rev.* **2002**, *102*, 439–470.
[70] A. Varki, R. L. Schnaar, R. Schauer, in *Essent. Glycobiol.* (Eds.: A. Varki, R.D. Cummings, J.D. Esko, P. Stanley, G.W. Hart, M. Aebi, A.G. Darvill, T. Kinoshita, N.H. Packer, J.H. Prestegard, et al.), Cold Spring Harbor Laboratory Press, Cold Spring Harbor (NY), **2015**.
[71] R. Schauer, *Curr. Opin. Struct. Biol.* **2009**, *19*, 507–514.
[72] M. Boyce, I. S. Carrico, A. S. Ganguli, S.-H. Yu, M. J. Hangauer, S. C. Hubbard, J. J. Kohler, C. R. Bertozzi, *Proc. Natl. Acad. Sci. U. S. A.* **2011**, *108*, 3141–3146.
[73] S. J. Luchansky, K. J. Yarema, S. Takahashi, C. R. Bertozzi, *J. Biol. Chem.* **2003**, *278*, 8035–8042.
[74] S. Hinderlich, M. Berger, M. Schwarzkopf, K. Effertz, W. Reutter, *Eur. J. Biochem.* **2000**, *267*, 3301–3308.
[75] S. Goon, C. R. Bertozzi, *J. Carbohydr. Chem.* **2002**, *21*, 943–977.
[76] F. Lipmann, N. O. Kaplan, *Fed. Proc.* **1946**, *5*, 145.
[77] F. Lipmann, N. O. Kaplan, *J. Biol. Chem.* **1947**, *167*, 869.
[78] C. Choudhary, B. T. Weinert, Y. Nishida, E. Verdin, M. Mann, *Nat. Rev. Mol. Cell Biol.* **2014**, *15*, 536–550.
[79] D. M. Phillips, *Biochem. J.* **1963**, *87*, 258–263.
[80] S. W. L'Hernault, J. L. Rosenbaum, *J. Cell Biol.* **1983**, *97*, 258–263.
[81] W. Gu, R. G. Roeder, *Cell* **1997**, *90*, 595–606.
[82] L.-F. Chen, W. Fischle, E. Verdin, W. C. Greene, *Science* **2001**, *293*, 1653–1657.
[83] S. C. Kim, R. Sprung, Y. Chen, Y. Xu, H. Ball, J. Pei, T. Cheng, Y. Kho, H. Xiao, L. Xiao, et al., *Mol. Cell* **2006**, *23*, 607–618.
[84] A. Drazic, L. M. Myklebust, R. Ree, T. Arnesen, *Biochim. Biophys. Acta* **2016**, *1864*, 1372–1401.
[85] A. O. Helbig, S. Gauci, R. Raijmakers, B. van Breukelen, M. Slijper, S. Mohammed, A. J. R. Heck, *Mol. Cell. Proteomics* **2010**, *9*, 928–939.
[86] P. V. Damme, R. Evjenth, H. Foyn, K. Demeyer, P.-J. D. Bock, J. R. Lillehaug, J. Vandekerckhove, T. Arnesen, K. Gevaert, *Mol. Cell. Proteomics* **2011**, *10*, M110.004580.
[87] H. Aksnes, K. Hole, T. Arnesen, *Int. Rev. Cell Mol. Biol.* **2015**, *316*, 267–305.
[88] G.-W. Kim, X.-J. Yang, *Trends Biochem. Sci.* **2011**, *36*, 211–220.
[89] P. Filippakopoulos, S. Knapp, *FEBS Lett.* **2012**, *586*, 2692–2704.
[90] V. G. Allfrey, R. Faulkner, A. E. Mirsky, *Proc. Natl. Acad. Sci. U. S. A.* **1964**, *51*, 786–794.

[91] M. D. Shahbazian, M. Grunstein, *Annu. Rev. Biochem.* **2007**, *76*, 75–100.
[92] M. Shogren-Knaak, H. Ishii, J.-M. Sun, M. J. Pazin, J. R. Davie, C. L. Peterson, *Science* **2006**, *311*, 844–847.
[93] R. Zhang, J. Erler, J. Langowski, *Biophys. J.* **2017**, *112*, 450–459.
[94] M. A. McBrian, I. S. Behbahan, R. Ferrari, T. Su, T.-W. Huang, K. Li, C. S. Hong, H. R. Christofk, M. Vogelauer, D. B. Seligson, et al., *Mol. Cell* **2013**, *49*, 310–321.
[95] F. Gay, D. Calvo, M.-C. Lo, J. Ceron, M. Maduro, R. Lin, Y. Shi, *Genes Dev.* **2003**, *17*, 717–722.
[96] S. T. Bond, K. F. Howlett, G. M. Kowalski, S. Mason, T. Connor, A. Cooper, V. Streltsov, C. R. Bruce, K. R. Walder, S. L. McGee, *FASEB J.* **2017**, *31*, 2592–2602.
[97] M. Haberland, R. L. Montgomery, E. N. Olson, *Nat. Rev. Genet.* **2009**, *10*, 32–42.
[98] W. K. Paik, D. Pearson, H. W. Lee, S. Kim, *Biochim. Biophys. Acta* **1970**, *213*, 513–522.
[99] G. R. Wagner, R. M. Payne, *J. Biol. Chem.* **2013**, *288*, 29036–29045.
[100] B. T. Weinert, V. Iesmantavicius, T. Moustafa, C. Schölz, S. A. Wagner, C. Magnes, R. Zechner, C. Choudhary, *Mol. Syst. Biol.* **2014**, *10*, 716.
[101] A. M. James, K. Hoogewijs, A. Logan, A. R. Hall, S. Ding, I. M. Fearnley, M. P. Murphy, *Cell Rep.* **2017**, *18*, 2105–2112.
[102] J. R. Wiśniewski, A. Zougman, M. Mann, *Nucleic Acids Res.* **2008**, *36*, 570–577.
[103] Y. Chen, R. Sprung, Y. Tang, H. Ball, B. Sangras, S. C. Kim, J. R. Falck, J. Peng, W. Gu, Y. Zhao, *Mol. Cell. Proteomics* **2007**, *6*, 812–819.
[104] E. Montellier, S. Rousseaux, Y. Zhao, S. Khochbin, *BioEssays* **2012**, *34*, 187–193.
[105] C. Peng, Z. Lu, Z. Xie, Z. Cheng, Y. Chen, M. Tan, H. Luo, Y. Zhang, W. He, K. Yang, et al., *Mol. Cell. Proteomics* **2011**, *10*, M111.012658.
[106] Z. Zhang, M. Tan, Z. Xie, L. Dai, Y. Chen, Y. Zhao, *Nat. Chem. Biol.* **2011**, *7*, 58–63.
[107] M. Tan, C. Peng, K. A. Anderson, P. Chhoy, Z. Xie, L. Dai, J. Park, Y. Chen, H. Huang, Y. Zhang, et al., *Cell Metab.* **2014**, *19*, 605–617.
[108] P. K. Chiang, R. K. Gordon, J. Tal, G. C. Zeng, B. P. Doctor, K. Pardhasaradhi, P. P. McCann, *FASEB J.* **1996**, *10*, 471–480.
[109] G. L. Cantoni, *J. Am. Chem. Soc.* **1952**, *74*, 2942–2943.
[110] H. L. Schubert, R. M. Blumenthal, X. Cheng, *Trends Biochem. Sci.* **2003**, *28*, 329–335.
[111] C. R. Vinci, S. G. Clarke, *J. Biol. Chem.* **2010**, *285*, 20526–20531.
[112] C. Dalhoff, E. Weinhold, in *Modif. Nucleosides*, Wiley-Blackwell, **2008**, pp. 223–247.
[113] S. C. Lu, *Int. J. Biochem. Cell Biol.* **2000**, *32*, 391–395.
[114] L. Zhang, X. Ding, J. Cui, H. Xu, J. Chen, Y.-N. Gong, L. Hu, Y. Zhou, J. Ge, Q. Lu, et al., *Nature* **2012**, *481*, 204–208.
[115] P. V. D. Werf, D. E. Koshland, *J. Biol. Chem.* **1977**, *252*, 2793–2795.
[116] A. Stock, S. Clarke, C. Clarke, J. Stock, *FEBS Lett.* **1987**, *220*, 8–14.
[117] W. Fischle, D. Schwarzer, *ACS Chem. Biol.* **2016**, *11*, 689–705.
[118] J. C. Fisk, L. K. Read, *Eukaryot. Cell* **2011**, *10*, 1013–1022.
[119] P. Byvoet, G. R. Shepherd, J. M. Hardin, B. J. Noland, *Arch. Biochem. Biophys.* **1972**, *148*, 558–567.
[120] L. J. Walport, R. J. Hopkinson, C. J. Schofield, *Curr. Opin. Chem. Biol.* **2012**, *16*, 525–534.
[121] Z. Wu, J. Connolly, K. K. Biggar, *FEBS J.* **2017**, *284*, 2732–2744.
[122] B. Chang, Y. Chen, Y. Zhao, R. K. Bruick, *Science* **2007**, *318*, 444–447.
[123] L. J. Walport, R. J. Hopkinson, R. Chowdhury, R. Schiller, W. Ge, A. Kawamura, C. J. Schofield, *Nat. Commun.* **2016**, *7*, 11974.

[124] G. L. Cuthbert, S. Daujat, A. W. Snowden, H. Erdjument-Bromage, T. Hagiwara, M. Yamada, R. Schneider, P. D. Gregory, P. Tempst, A. J. Bannister, et al., *Cell* **2004**, *118*, 545–553.
[125] Y. Wang, J. Wysocka, J. Sayegh, Y.-H. Lee, J. R. Perlin, L. Leonelli, L. S. Sonbuchner, C. H. McDonald, R. G. Cook, Y. Dou, et al., *Science* **2004**, *306*, 279–283.
[126] W. K. Paik, D. C. Paik, S. Kim, *Trends Biochem. Sci.* **2007**, *32*, 146–152.
[127] P. A. C. Cloos, J. Christensen, K. Agger, K. Helin, *Genes Dev.* **2008**, *22*, 1115–1140.
[128] M. T. Bedford, S. Richard, *Mol. Cell* **2005**, *18*, 263–272.
[129] S. Lanouette, V. Mongeon, D. Figeys, J. Couture, *Mol. Syst. Biol.* **2014**, *10*, 724.
[130] D. Levy, A. J. Kuo, Y. Chang, U. Schaefer, C. Kitson, P. Cheung, A. Espejo, B. M. Zee, C. L. Liu, S. Tangsombatvisit, et al., *Nat. Immunol.* **2011**, *12*, 29–36.
[131] G. S. Ivanov, T. Ivanova, J. Kurash, A. Ivanov, S. Chuikov, F. Gizatullin, E. M. Herrera-Medina, F. Rauscher, D. Reinberg, N. A. Barlev, *Mol. Cell. Biol.* **2007**, *27*, 6756–6769.
[132] S. Doll, A. L. Burlingame, *ACS Chem. Biol.* **2015**, *10*, 63–71.
[133] Y. Merbl, M. W. Kirschner, *Wiley Interdiscip. Rev. Syst. Biol. Med.* **2010**, *3*, 347–356.
[134] K. T. Pilobello, L. K. Mahal, *Methods Mol. Biol.* **2007**, *385*, 193–203.
[135] J. Hirabayashi, *Glycoconj. J.* **2004**, *21*, 35–40.
[136] W. Pradidarcheep, W. T. Labruyère, N. F. Dabhoiwala, W. H. Lamers, *J. Histochem. Cytochem.* **2008**, *56*, 1099–1111.
[137] H. Ohba, R. Bakalova, *Cancer Chemother. Pharmacol.* **2003**, *51*, 451–458.
[138] L. L. Kiessling, N. L. Pohl, *Chem. Biol.* **1996**, *3*, 71–77.
[139] P. V. Chang, C. R. Bertozzi, *Chem. Commun.* **2012**, *48*, 8864–8879.
[140] D. S. Cornett, M. L. Reyzer, P. Chaurand, R. M. Caprioli, *Nat. Methods* **2007**, *4*, 828–833.
[141] S. G. Boxer, M. L. Kraft, P. K. Weber, *Annu. Rev. Biophys.* **2009**, *38*, 53–74.
[142] C. Besanceney-Webler, H. Jiang, T. Zheng, L. Feng, D. Soriano del Amo, W. Wang, L. M. Klivansky, F. L. Marlow, Y. Liu, P. Wu, *Angew. Chem. Int. Ed Engl.* **2011**, *50*, 8051–8056.
[143] R. Xie, L. Dong, Y. Du, Y. Zhu, R. Hua, C. Zhang, X. Chen, *Proc. Natl. Acad. Sci. U. S. A.* **2016**, *113*, 5173–5178.
[144] D. H. Dube, J. A. Prescher, C. N. Quang, C. R. Bertozzi, *Proc. Natl. Acad. Sci. U. S. A.* **2006**, *103*, 4819–4824.
[145] P. Agarwal, B. J. Beahm, P. Shieh, C. R. Bertozzi, *Angew. Chem. Int. Ed Engl.* **2015**, *54*, 11504–11510.
[146] S. T. Laughlin, C. R. Bertozzi, *ACS Chem. Biol.* **2009**, *4*, 1068–1072.
[147] A. Buntz, S. Wallrodt, E. Gwosch, M. Schmalz, S. Beneke, E. Ferrando-May, A. Marx, A. Zumbusch, *Angew. Chem. Int. Ed Engl.* **2016**, *55*, 11256–11260.
[148] S. Hong, T. Chen, Y. Zhu, A. Li, Y. Huang, X. Chen, *Angew. Chem. Int. Ed Engl.* **2014**, *53*, 5827–5831.
[149] Z. X. Chen, D. W. Paley, L. Wei, A. L. Weisman, R. A. Friesner, C. Nuckolls, W. Min, *J. Am. Chem. Soc.* **2014**, *136*, 8027–8033.
[150] L. Wei, F. Hu, Y. Shen, Z. Chen, Y. Yu, C. C. Lin, M. C. Wang, W. Min, *Nat. Methods* **2014**, *11*, 410–412.
[151] M. D. Duncan, J. Reintjes, T. J. Manuccia, *Opt. Lett.* **1982**, *7*, 350–352.
[152] A. Zumbusch, G. R. Holtom, X. S. Xie, *Phys. Rev. Lett.* **1999**, *82*, 4142–4145.
[153] C. W. Freudiger, W. Min, B. G. Saar, S. Lu, G. R. Holtom, C. He, J. C. Tsai, J. X. Kang, X. S. Xie, *Science* **2008**, *322*, 1857–1861.
[154] R. Wang, K. Islam, Y. Liu, W. Zheng, H. Tang, N. Lailler, G. Blum, H. Deng, M. Luo, *J. Am. Chem. Soc.* **2013**, *135*, 1048–1056.

[155] X. Bao, Q. Zhao, T. Yang, Y. M. E. Fung, X. D. Li, *Angew. Chem. Int. Ed Engl.* **2013**, *52*, 4883–4886.
[156] J. Bos, T. W. Muir, *J. Am. Chem. Soc.* **2018**, *140*, 4757–4760.
[157] Y.-Y. Yang, J. M. Ascano, H. C. Hang, *J. Am. Chem. Soc.* **2010**, *132*, 3640–3641.
[158] H. C. Hang, M. E. Linder, *Chem. Rev.* **2011**, *111*, 6341–6358.
[159] X. Gao, R. N. Hannoush, *J. Am. Chem. Soc.* **2014**, *136*, 4544–4550.
[160] R. N. Hannoush, J. Sun, *Nat. Chem. Biol.* **2010**, *6*, 498–506.
[161] H. C. Hang, J. P. Wilson, G. Charron, *Acc. Chem. Res.* **2011**, *44*, 699–708.
[162] S. Wallrodt, A. Buntz, Y. Wang, A. Zumbusch, A. Marx, *Angew. Chem. Int. Ed Engl.* **2016**, *55*, 7660–7664.
[163] Y. Wang, D. Rösner, M. Grzywa, A. Marx, *Angew Chem Int Ed* **2014**, *53*, 8159–8162.
[164] M. Grammel, P. Luong, K. Orth, H. C. Hang, *J. Am. Chem. Soc.* **2011**, *133*, 17103–17105.
[165] S. E. Lee, L. M. Elphick, A. A. Anderson, L. Bonnac, E. S. Child, D. J. Mann, V. Gouverneur, *Bioorg. Med. Chem. Lett.* **2009**, *19*, 3804–3807.
[166] J. Du, M. A. Meledeo, Z. Wang, H. S. Khanna, V. D. Paruchuri, K. J. Yarema, *Glycobiology* **2009**, *19*, 1382–1401.
[167] E. Saxon, C. R. Bertozzi, *Science* **2000**, *287*, 2007–2010.
[168] J. H. Lee, T. J. Baker, L. K. Mahal, J. Zabner, C. R. Bertozzi, D. F. Wiemer, M. J. Welsh, *J. Biol. Chem.* **1999**, *274*, 21878–21884.
[169] A. K. Sarkar, T. A. Fritz, W. H. Taylor, J. D. Esko, *Proc. Natl. Acad. Sci. U. S. A.* **1995**, *92*, 3323–3327.
[170] H. Kayser, R. Zeitler, C. Kannicht, D. Grunow, R. Nuck, W. Reutter, *J. Biol. Chem.* **1992**, *267*, 16934–16938.
[171] O. T. Keppler, P. Stehling, M. Herrmann, H. Kayser, D. Grunow, W. Reutter, M. Pawlita, *J. Biol. Chem.* **1995**, *270*, 1308–1314.
[172] O. T. Keppler, R. Horstkorte, M. Pawlita, C. Schmidt, W. Reutter, *Glycobiology* **2001**, *11*, 11R-18R.
[173] L. K. Mahal, K. J. Yarema, C. R. Bertozzi, *Science* **1997**, *276*, 1125–1128.
[174] K. J. Yarema, C. R. Bertozzi, *Genome Biol.* **2001**, *2*, reviews0004.1-reviews0004.10.
[175] E. Saxon, S. J. Luchansky, H. C. Hang, C. Yu, S. C. Lee, C. R. Bertozzi, *J. Am. Chem. Soc.* **2002**, *124*, 14893–14902.
[176] P. V. Chang, X. Chen, C. Smyrniotis, A. Xenakis, T. Hu, C. R. Bertozzi, P. Wu, *Angew. Chem. Int. Ed Engl.* **2009**, *48*, 4030–4033.
[177] L. A. Bateman, B. W. Zaro, K. N. Chuh, M. R. Pratt, *Chem. Commun.* **2013**, *49*, 4328–4330.
[178] A. Niederwieser, A.-K. Späte, L. D. Nguyen, C. Jüngst, W. Reutter, V. Wittmann, *Angew. Chem. Int. Ed Engl.* **2013**, *52*, 4265–4268.
[179] A.-K. Späte, V. F. Schart, S. Schöllkopf, A. Niederwieser, V. Wittmann, *Chem. Eur. J.* **2014**, *20*, 16502–16508.
[180] D. M. Patterson, K. A. Jones, J. A. Prescher, *Mol. Biosyst.* **2014**, *10*, 1693–1697.
[181] A.-K. Späte, H. Bußkamp, A. Niederwieser, V. F. Schart, A. Marx, V. Wittmann, *Bioconjug. Chem.* **2014**, *25*, 147–154.
[182] A.-K. Späte, V. F. Schart, J. Häfner, A. Niederwieser, T. U. Mayer, V. Wittmann, *Beilstein J. Org. Chem.* **2014**, *10*, 2235–2242.
[183] A.-K. Späte, J. E. G. A. Dold, E. Batroff, V. F. Schart, D. E. Wieland, O. R. Baudendistel, V. Wittmann, *ChemBioChem* **2016**, *17*, 1374–1383.
[184] X. Ning, R. P. Temming, J. Dommerholt, J. Guo, D. B. Ania, M. F. Debets, M. A. Wolfert, G.-J. Boons, F. L. van Delft, *Angew. Chem. Int. Ed Engl.* **2010**, *49*, 3065–3068.

[185] K. A. Andersen, M. R. Aronoff, N. A. McGrath, R. T. Raines, *J. Am. Chem. Soc.* **2015**, *137*, 2412–2415.
[186] P. R. Wratil, R. Horstkorte, W. Reutter, *Angew. Chem. Int. Ed Engl.* **2016**, *55*, 9482–9512.
[187] D. J. Vocadlo, H. C. Hang, E.-J. Kim, J. A. Hanover, C. R. Bertozzi, *Proc. Natl. Acad. Sci. U. S. A.* **2003**, *100*, 9116–9121.
[188] H. C. Hang, C. Yu, D. L. Kato, C. R. Bertozzi, *Proc. Natl. Acad. Sci. U. S. A.* **2003**, *100*, 14846–14851.
[189] B. W. Zaro, Y. Y. Yang, H. C. Hang, M. R. Pratt, *Proc. Natl. Acad. Sci. U. S. A.* **2011**, *108*, 8146–8151.
[190] K. N. Chuh, B. W. Zaro, F. Piller, V. Piller, M. R. Pratt, *J. Am. Chem. Soc.* **2014**, *136*, 12283–12295.
[191] K. N. Chuh, A. R. Batt, B. W. Zaro, N. Darabedian, N. P. Marotta, C. K. Brennan, A. Amirhekmat, M. R. Pratt, *J. Am. Chem. Soc.* **2017**, *139*, 7872–7885.
[192] J. Li, J. Wang, L. Wen, H. Zhu, S. Li, K. Huang, K. Jiang, X. Li, C. Ma, J. Qu, et al., *ACS Chem. Biol.* **2016**, *11*, 3002–3006.
[193] S. Pouilly, V. Bourgeaux, F. Piller, V. Piller, *ACS Chem. Biol.* **2012**, *7*, 753–760.
[194] B. W. Zaro, A. R. Batt, K. N. Chuh, M. X. Navarro, M. R. Pratt, *ACS Chem. Biol.* **2016**, *12*, 787–794.
[195] N. Darabedian, J. Gao, K. N. Chuh, C. M. Woo, M. R. Pratt, *J. Am. Chem. Soc.* **2018**, *140*, 7092–7100.
[196] Y. Zhu, X. Chen, *ChemBioChem* **2017**, *18*, 1286–1296.
[197] J. Hoogenboom, N. Berghuis, D. Cramer, R. Geurts, H. Zuilhof, T. Wennekes, *BMC Plant Biol.* **2016**, *16*, 220.
[198] M. Sawa, T.-L. Hsu, T. Itoh, M. Sugiyama, S. R. Hanson, P. K. Vogt, C.-H. Wong, *Proc. Natl. Acad. Sci. U. S. A.* **2006**, *103*, 12371–12376.
[199] Y. Zhu, J. Wu, X. Chen, *Angew. Chem. Int. Ed Engl.* **2016**, *55*, 9301–9305.
[200] L. A. Bateman, B. W. Zaro, S. M. Miller, M. R. Pratt, *J. Am. Chem. Soc.* **2013**, *135*, 14568–14573.
[201] B. W. Zaro, K. N. Chuh, M. R. Pratt, *ACS Chem. Biol.* **2014**, *9*, 1991–1996.
[202] M. E. Ourailidou, P. Dockerty, M. Witte, G. J. Poelarends, F. J. Dekker, *Org. Biomol. Chem.* **2015**, *13*, 3648–3653.
[203] T. D. Huber, B. R. Johnson, J. Zhang, J. S. Thorson, *Curr. Opin. Biotechnol.* **2016**, *42*, 189–197.
[204] J. Deen, C. Vranken, V. Leen, R. K. Neely, K. P. F. Janssen, J. Hofkens, *Angew. Chem. Int. Ed Engl.* **2017**, *56*, 5182–5200.
[205] R. R. Steimbach, Developing an Approach for Imaging Protein Methylation Inside Cells, Master's thesis, University of Konstanz, **2017**.
[206] M. Pignot, C. Siethoff, M. Linscheid, E. Weinhold, *Angew. Chem. Int. Ed Engl.* **1998**, *37*, 2888–2891.
[207] J. Zhang, Y. G. Zheng, *ACS Chem. Biol.* **2016**, *11*, 583–597.
[208] L. R. Comstock, S. R. Rajski, *Nucleic Acids Res.* **2005**, *33*, 1644–1652.
[209] G. Pljevaljcic, M. Pignot, E. Weinhold, *J. Am. Chem. Soc.* **2003**, *125*, 3486–3492.
[210] T. Osborne, R. L. Weller Roska, S. R. Rajski, P. R. Thompson, *J. Am. Chem. Soc.* **2008**, *130*, 4574–4575.
[211] F. Schlenk, J. L. Dainko, *Biochim. Biophys. Acta* **1975**, *385*, 312–323.
[212] C. Dalhoff, G. Lukinavicius, S. Klimasăuskas, E. Weinhold, *Nat. Chem. Biol.* **2006**, *2*, 31–32.
[213] C. Dalhoff, G. Lukinavicius, S. Klimasauskas, E. Weinhold, *Nat. Protoc.* **2006**, *1*, 1879–1886.

[214] W. Peters, S. Willnow, M. Duisken, H. Kleine, T. Macherey, K. E. Duncan, D. W. Litchfield, B. Lüscher, E. Weinhold, *Angew. Chem. Int. Ed Engl.* **2010**, *49*, 5170–5173.
[215] K. Islam, Y. Chen, H. Wu, I. R. Bothwell, G. J. Blum, H. Zeng, A. Dong, W. Zheng, J. Min, H. Deng, et al., *Proc. Natl. Acad. Sci. U. S. A.* **2013**, *110*, 16778–16783.
[216] O. Binda, M. Boyce, J. S. Rush, K. K. Palaniappan, C. R. Bertozzi, O. Gozani, *ChemBioChem* **2011**, *12*, 330–334.
[217] B. W. K. Lee, H. G. Sun, T. Zang, B. J. Kim, J. F. Alfaro, Z. S. Zhou, *J. Am. Chem. Soc.* **2010**, *132*, 3642–3643.
[218] G. Blum, K. Islam, M. Luo, *Curr. Protoc. Chem. Biol.* **2013**, *5*, 45–66.
[219] S. Singh, J. Zhang, T. D. Huber, M. Sunkara, K. Hurley, R. D. Goff, G. Wang, W. Zhang, C. Liu, J. Rohr, et al., *Angew. Chem. Int. Ed Engl.* **2014**, *53*, 3965–3969.
[220] I. R. Bothwell, K. Islam, Y. Chen, W. Zheng, G. Blum, H. Deng, M. Luo, *J. Am. Chem. Soc.* **2012**, *134*, 14905–14912.
[221] J. L. Hoffman, *Biochemistry (Mosc.)* **1986**, *25*, 4444–4449.
[222] S. Willnow, M. Martin, B. Lüscher, E. Weinhold, *ChemBioChem* **2012**, *13*, 1167–1173.
[223] D. F. Iwig, A. T. Grippe, T. A. McIntyre, S. J. Booker, *Biochemistry (Mosc.)* **2004**, *43*, 13510–13524.
[224] M. Tomkuvienė, B. Clouet-d'Orval, I. Černiauskas, E. Weinhold, S. Klimašauskas, *Nucleic Acids Res.* **2012**, *40*, 6765–6773.
[225] S. Willnow, Enzymatic Alkyne-Functionalization for Labeling and Identification of Protein Methyltransferase Substrates, PhD thesis, RWTH Aachen, **2012**.
[226] M. Martin, Analoga Des S-Adenosyl-L-Methionins Zur Gezielten Markierung von Nukleinsäuren Und Proteinen Durch Methyltransferasen, PhD thesis, RWTH Aachen, **2013**.
[227] Y. Zhang, Y. Pan, W. Liu, Y. J. Zhou, K. Wang, L. Wang, M. Sohail, M. Ye, H. Zou, Z. K. Zhao, *Chem. Commun. (Camb)* **2016**, *52*, 6689–6692.
[228] K. Hartstock, B. S. Nilges, A. Ovcharenko, N. V. Cornelissen, N. Püllen, A.-M. Lawrence-Dörner, S. A. Leidel, A. Rentmeister, *Angew. Chem. Int. Ed Engl.* **2018**, *57*, 6342–6346.
[229] C. Chen, S. W. Smye, M. P. Robinson, J. A. Evans, *Med. Biol. Eng. Comput.* **2006**, *44*, 5–14.
[230] S. M. Hacker, A. Buntz, A. Zumbusch, A. Marx, *ACS Chem. Biol.* **2015**, *10*, 2544–2552.
[231] Y. Zhang, L.-C. Yu, *Bioessays* **2008**, *30*, 606–610.
[232] D. Koley, A. J. Bard, *Proc. Natl. Acad. Sci. U. S. A.* **2010**, *107*, 16783–16787.
[233] M. C. Morris, J. Depollier, J. Mery, F. Heitz, G. Divita, *Nat. Biotechnol.* **2001**, *19*, 1173–1176.
[234] A. Sharei, N. Cho, S. Mao, E. Jackson, R. Poceviciute, A. Adamo, J. Zoldan, R. Langer, K. F. Jensen, *J. Vis. Exp.* **2013**, e50980.
[235] Y. Sun, S. Hong, R. Xie, R. Huang, R. Lei, B. Cheng, D. Sun, Y. Du, C. M. Nycholat, J. C. Paulson, et al., *J. Am. Chem. Soc.* **2018**, *140*, 3592–3602.
[236] Y. Du, R. Xie, Y. Sun, X. Fan, X. Chen, in *Methods Enzymol.* (Ed.: B. Imperiali), Academic Press, **2018**, pp. 321–353.
[237] C. S. McKay, M. G. Finn, *Chem. Biol.* **2014**, *21*, 1075–1101.
[238] E. M. Sletten, C. R. Bertozzi, *Angew. Chem. Int. Ed Engl.* **2009**, *48*, 6974–6998.
[239] D. M. Patterson, L. A. Nazarova, J. A. Prescher, *ACS Chem. Biol.* **2014**, *9*, 592–605.
[240] X. Chen, Y.-W. Wu, *Org. Biomol. Chem.* **2016**, *14*, 5417–5439.
[241] D. H. Dube, C. R. Bertozzi, *Curr. Opin. Chem. Biol.* **2003**, *7*, 616–625.
[242] H. Staudinger, J. Meyer, *Helv. Chim. Acta* **2004**, *2*, 635–646.

[243] J. M. Baskin, C. R. Bertozzi, *QSAR Comb. Sci.* **2007**, *26*, 1211–1219.
[244] F. L. Lin, H. M. Hoyt, H. van Halbeek, R. G. Bergman, C. R. Bertozzi, *J. Am. Chem. Soc.* **2005**, *127*, 2686–2695.
[245] R. Huisgen, *Angew. Chem.* **1963**, *75*, 604–637.
[246] C. W. Tornøe, C. Christensen, M. Meldal, *J. Org. Chem.* **2002**, *67*, 3057–3064.
[247] V. V. Rostovtsev, L. G. Green, V. V. Fokin, K. B. Sharpless, *Angew. Chem. Int. Ed Engl.* **2002**, *41*, 2596–2599.
[248] T. R. Chan, R. Hilgraf, K. B. Sharpless, V. V. Fokin, *Org. Lett.* **2004**, *6*, 2853–2855.
[249] V. Hong, N. F. Steinmetz, M. Manchester, M. G. Finn, *Bioconjug. Chem.* **2010**, *21*, 1912–1916.
[250] D. Soriano Del Amo, W. Wang, H. Jiang, C. Besanceney, A. C. Yan, M. Levy, Y. Liu, F. L. Marlow, P. Wu, *J. Am. Chem. Soc.* **2010**, *132*, 16893–16899.
[251] V. Hong, S. I. Presolski, C. Ma, M. G. Finn, *Angew. Chem. Int. Ed Engl.* **2009**, *48*, 9879–9883.
[252] R. B. Turner, A. D. Jarrett, P. Goebel, B. J. Mallon, *J. Am. Chem. Soc.* **1973**, *95*, 790–792.
[253] N. J. Agard, J. A. Prescher, C. R. Bertozzi, *J. Am. Chem. Soc.* **2004**, *126*, 15046–15047.
[254] C. P. Ramil, Q. Lin, *Chem. Commun.* **2013**, *49*, 11007–11022.
[255] X. Ning, J. Guo, M. A. Wolfert, G.-J. Boons, *Angew. Chem. Int. Ed Engl.* **2008**, *47*, 2253–2255.
[256] J. C. Jewett, E. M. Sletten, C. R. Bertozzi, *J. Am. Chem. Soc.* **2010**, *132*, 3688–3690.
[257] M. F. Debets, S. S. van Berkel, J. Dommerholt, A. (Ton) J. Dirks, F. P. J. T. Rutjes, F. L. van Delft, *Acc. Chem. Res.* **2011**, *44*, 805–815.
[258] R. van Geel, G. J. M. Pruijn, F. L. van Delft, W. C. Boelens, *Bioconjug. Chem.* **2012**, *23*, 392–398.
[259] R. A. Carboni, R. V. Lindsey, *J. Am. Chem. Soc.* **1959**, *81*, 4342–4346.
[260] B. L. Oliveira, Z. Guo, G. J. L. Bernardes, *Chem. Soc. Rev.* **2017**, *46*, 4895–4950.
[261] M. L. Blackman, M. Royzen, J. M. Fox, *J. Am. Chem. Soc.* **2008**, *130*, 13518–13519.
[262] A.-C. Knall, C. Slugovc, *Chem. Soc. Rev.* **2013**, *42*, 5131–5142.
[263] R. A. A. Foster, M. C. Willis, *Chem. Soc. Rev.* **2013**, *42*, 63–76.
[264] N. K. Devaraj, R. Weissleder, S. A. Hilderbrand, *Bioconjug. Chem.* **2008**, *19*, 2297–2299.
[265] M. T. Taylor, M. L. Blackman, O. Dmitrenko, J. M. Fox, *J. Am. Chem. Soc.* **2011**, *133*, 9646–9649.
[266] J. Yang, J. Seckute, C. M. Cole, N. K. Devaraj, *Angew. Chem. Int. Ed Engl.* **2012**, *51*, 7476–7479.
[267] D. M. Patterson, L. A. Nazarova, B. Xie, D. N. Kamber, J. A. Prescher, *J. Am. Chem. Soc.* **2012**, *134*, 18638–18643.
[268] C. M. Cole, J. Yang, J. Šečkutė, N. K. Devaraj, *ChemBioChem* **2013**, *14*, 205–208.
[269] F. Thalhammer, U. Wallfahrer, J. Sauer, *Tetrahedron Lett.* **1990**, *31*, 6851–6854.
[270] J. E. G. A. Dold, J. Pfotzer, A.-K. Späte, V. Wittmann, *ChemBioChem* **2017**, *18*, 1242–1250.
[271] K. Lang, L. Davis, S. Wallace, M. Mahesh, D. J. Cox, M. L. Blackman, J. M. Fox, J. W. Chin, *J. Am. Chem. Soc.* **2012**, *134*, 10317–10320.
[272] A.-K. Späte, Metabolic Engineering of Glycoproteins, PhD thesis, University of Konstanz, **2016**.
[273] N. Wu, L. Bao, L. Ding, H. Ju, *Angew. Chem. Int. Ed Engl.* **2016**, *55*, 5220–5224.
[274] L. Feng, S. Hong, J. Rong, Q. You, P. Dai, R. Huang, Y. Tan, W. Hong, C. Xie, J. Zhao, et al., *J. Am. Chem. Soc.* **2013**, *135*, 9244–9247.

[275] I. Nikić, T. Plass, O. Schraidt, J. Szymański, J. A. G. Briggs, C. Schultz, E. A. Lemke, *Angew. Chem. Int. Ed Engl.* **2014**, *53*, 2245–2249.
[276] Y. Liang, J. L. Mackey, S. A. Lopez, F. Liu, K. N. Houk, *J. Am. Chem. Soc.* **2012**, *134*, 17904–17907.
[277] G. A. Lemieux, C. L. De Graffenried, C. R. Bertozzi, *J. Am. Chem. Soc.* **2003**, *125*, 4708–4709.
[278] M. J. Hangauer, C. R. Bertozzi, *Angew. Chem. Int. Ed Engl.* **2008**, *47*, 2394–2397.
[279] J. Qi, C.-H. Tung, *Bioorg. Med. Chem. Lett.* **2011**, *21*, 320–323.
[280] P. Shieh, M. J. Hangauer, C. R. Bertozzi, *J. Am. Chem. Soc.* **2012**, *134*, 17428–17431.
[281] P. Shieh, M. S. Siegrist, A. J. Cullen, C. R. Bertozzi, *Proc. Natl. Acad. Sci. U. S. A.* **2014**, *111*, 5456–5461.
[282] J. C. Jewett, C. R. Bertozzi, *Org. Lett.* **2011**, *13*, 5937–5939.
[283] K. Yamagishi, K. Sawaki, A. Murata, S. Takeoka, *Chem. Commun. Camb.* **2015**, *51*, 7879–7882.
[284] N. K. Devaraj, S. Hilderbrand, R. Upadhyay, R. Mazitschek, R. Weissleder, *Angew. Chem. Int. Ed Engl.* **2010**, *49*, 2869–2872.
[285] J. C. T. Carlson, L. G. Meimetis, S. A. Hilderbrand, R. Weissleder, *Angew. Chem. Int. Ed Engl.* **2013**, *52*, 6917–6920.
[286] H. Wu, J. Yang, J. Šečkutė, N. K. Devaraj, *Angew. Chem. Int. Ed Engl.* **2014**, *53*, 5805–5809.
[287] A. Wieczorek, P. Werther, J. Euchner, R. Wombacher, *Chem. Sci.* **2017**, *8*, 1506–1510.
[288] J. F. W. Herschel, *Philos. Trans. R. Soc. Lond.* **1845**, *135*, 143–145.
[289] G. G. Stokes, *Philos. Trans. R. Soc. Lond.* **1852**, *142*, 463–562.
[290] G. G. Stokes, *Philos. Trans. R. Soc. Lond.* **1853**, *143*, 385–396.
[291] A. Jablonski, *Nature* **1933**, *131*, 839–840.
[292] J. R. Lakowicz, *Principles of Fluorescence Spectroscopy*, Springer, New York, **2006**.
[293] K. Suhling, P. M. French, D. Phillips, *Photochem. Photobiol. Sci.* **2005**, *4*, 13–22.
[294] E. Kuwana, E. M. Sevick-Muraca, *Biophys. J.* **2002**, *83*, 1165–1176.
[295] D. C. Prasher, V. K. Eckenrode, W. W. Ward, F. G. Prendergast, M. J. Cormier, *Gene* **1992**, *111*, 229–233.
[296] M. Chalfie, Y. Tu, G. Euskirchen, W. W. Ward, D. C. Prasher, *Science* **1994**, *263*, 802–805.
[297] H. Niwa, S. Inouye, T. Hirano, T. Matsuno, S. Kojima, M. Kubota, M. Ohashi, F. I. Tsuji, *Proc. Natl. Acad. Sci. U. S. A.* **1996**, *93*, 13617–13622.
[298] R. Y. Tsien, *Annu. Rev. Biochem.* **1998**, *67*, 509–544.
[299] M. Zimmer, *Chem. Rev.* **2002**, *102*, 759–781.
[300] M. Yang, E. Baranov, P. Jiang, F.-X. Sun, X.-M. Li, L. Li, S. Hasegawa, M. Bouvet, M. Al-Tuwaijri, T. Chishima, et al., *Proc. Natl. Acad. Sci. U. S. A.* **2000**, *97*, 1206–1211.
[301] R. Heim, R. Y. Tsien, *Curr. Biol.* **1996**, *6*, 178–182.
[302] B. P. Cormack, R. H. Valdivia, S. Falkow, *Gene* **1996**, *173*, 33–38.
[303] R. Heim, A. B. Cubitt, R. Y. Tsien, *Nature* **1995**, *373*, 663–664.
[304] P. Dedecker, F. C. De Schryver, J. Hofkens, *J. Am. Chem. Soc.* **2013**, *135*, 2387–2402.
[305] R. N. Day, M. W. Davidson, *Chem. Soc. Rev.* **2009**, *38*, 2887–2921.
[306] F. V. Subach, L. Zhang, T. W. J. Gadella, N. G. Gurskaya, K. A. Lukyanov, V. V. Verkhusha, *Chem. Biol.* **2010**, *17*, 745–755.
[307] N. C. Shaner, M. Z. Lin, M. R. McKeown, P. A. Steinbach, K. L. Hazelwood, M. W. Davidson, R. Y. Tsien, *Nat. Methods* **2008**, *5*, 545–551.
[308] M. A. Rizzo, M. W. Davidson, D. W. Piston, *Cold Spring Harb. Protoc.* **2009**, *2009*, pdb.top63.

[309] S. W. Hell, J. Wichmann, *Opt. Lett.* **1994**, *19*, 780–782.
[310] S. W. Hell, *Science* **2007**, *316*, 1153–1158.
[311] M. G. L. Gustafsson, *Proc. Natl. Acad. Sci. U. S. A.* **2005**, *102*, 13081–13086.
[312] M. J. Rust, M. Bates, X. Zhuang, *Nat. Methods* **2006**, *3*, 793–796.
[313] S. T. Hess, T. P. K. Girirajan, M. D. Mason, *Biophys. J.* **2006**, *91*, 4258–4272.
[314] F. Balzarotti, Y. Eilers, K. C. Gwosch, A. H. Gynnå, V. Westphal, F. D. Stefani, J. Elf, S. W. Hell, *Science* **2017**, *355*, 606–612.
[315] E. Betzig, G. H. Patterson, R. Sougrat, O. W. Lindwasser, S. Olenych, J. S. Bonifacino, M. W. Davidson, J. Lippincott-Schwartz, H. F. Hess, *Science* **2006**, *313*, 1642–1645.
[316] N. Naredi-Rainer, J. Prescher, A. Hartschuh, D. C. Lamb, *Fluorescence Microscopy: From Principles to Biological Applications, Kapitel 5 - Confocal Microscopy*, Wiley-Blackwell, Oxford, **2013**.
[317] A. K. Kenworthy, *Methods* **2001**, *24*, 289–296.
[318] P. Davidovits, M. D. Egger, *Appl. Opt.* **1971**, *10*, 1615–1619.
[319] P. Davidovits, M. D. Egger, *Nature* **1969**, *223*, 831.
[320] A. S. Buntz, Schnelle Fluoreszenzlebenszeitmikroskopie in Lebenden Zellen: Untersuchung von Proteininteraktionen, Proteinmodifikationen Und Proteinaktivität, PhD thesis, University of Konstanz, **2016**.
[321] C. Rosazza, Internalization and Intracellular Traficking of Plasmid DNA Delivered by Electroporation, PhD thesis, University of Konstanz, **2014**.
[322] T. Förster, *Naturwissenschaften* **1946**, *33*, 166–175.
[323] T. Förster, *Fluoreszenz Organischer Verbindungen*, Vandenhoeck & Ruprecht, Göttingen, **1951**.
[324] T. Förster, in (Ed.: O. Sinanoglu), Academic Press, New York, **1965**, pp. 93–173.
[325] R. E. Dale, J. Eisinger, W. E. Blumberg, *Biophys. J.* **1979**, *26*, 161–193.
[326] A. Periasamy, R. Day, *Molecular Imaging: FRET Microscopy and Spectroscopy*, Elsevier, **2011**.
[327] L. Ma, F. Yang, J. Zheng, *J. Mol. Struct.* **2014**, *1077*, 87–100.
[328] R. Roy, S. Hohng, T. Ha, *Nat. Methods* **2008**, *5*, 507–516.
[329] D. Shrestha, A. Jenei, P. Nagy, G. Vereb, J. Szöllősi, *Int. J. Mol. Sci.* **2015**, *16*, 6718–6756.
[330] S. Padilla-Parra, M. Tramier, *Bioessays* **2012**, *34*, 369–376.
[331] S. S. Vogel, C. Thaler, S. V. Koushik, *Sci. STKE* **2006**, *2006*, re2.
[332] J. Qian, B. Yao, C. Wu, *Exp. Ther. Med.* **2014**, *8*, 1375–1380.
[333] P. J. Verveer, O. Rocks, A. G. Harpur, P. I. H. Bastiaens, *CSH Protoc.* **2006**, *2006*, pdb.prot4597.
[334] J. van Rheenen, M. Langeslag, K. Jalink, *Biophys. J.* **2004**, *86*, 2517–2529.
[335] T. Zimmermann, J. Rietdorf, R. Pepperkok, *FEBS Lett.* **2003**, *546*, 87–92.
[336] C. Thaler, S. V. Koushik, P. S. Blank, S. S. Vogel, *Biophys. J.* **2005**, *89*, 2736–2749.
[337] F. S. Wouters, P. I. H. Bastiaens, K. W. A. Wirtz, T. M. Jovin, *EMBO J.* **1998**, *17*, 7179–7189.
[338] T. Zal, N. R. J. Gascoigne, *Biophys. J.* **2004**, *86*, 3923–3939.
[339] A. L. Mattheyses, A. D. Hoppe, D. Axelrod, *Biophys. J.* **2004**, *87*, 2787–2797.
[340] C. P. Toseland, *J. Chem. Biol.* **2013**, *6*, 85–95.
[341] M. A. Rizzo, D. W. Piston, *Biophys. J.* **2005**, *88*, L14–L16.
[342] I. Gautier, M. Tramier, C. Durieux, J. Coppey, R. B. Pansu, J. C. Nicolas, K. Kemnitz, M. Coppey-Moisan, *Biophys. J.* **2001**, *80*, 3000–3008.
[343] A. Squire, P. J. Verveer, O. Rocks, P. I. H. Bastiaens, *J. Struct. Biol.* **2004**, *147*, 62–69.

[344] E. A. Jares-Erijman, T. M. Jovin, *Nat. Biotechnol.* **2003**, *21*, 1387–1395.
[345] E. B. van Munster, T. W. Gadella, *Adv. Biochem. Eng. Biotechnol.* **2005**, *95*, 143–175.
[346] W. Becker, *J. Microsc.* **2012**, *247*, 119–136.
[347] W. Becker, A. Bergmann, M. A. Hink, K. König, K. Benndorf, C. Biskup, *Microsc. Res. Tech.* **2004**, *63*, 58–66.
[348] W. Becker, *Advanced Time-Correlated Single Photon Counting Techniques*, Springer Science & Business Media, Berlin, **2005**.
[349] Q. Zhao, I. T. Young, J. G. de Jong, *J. Biomed. Opt.* **2011**, *16*, 086007.
[350] M. Köllner, J. Wolfrum, *Chem. Phys. Lett.* **1992**, *200*, 199–204.
[351] K. Suhling, L. M. Hirvonen, J. A. Levitt, P.-H. Chung, C. Tregidgo, A. Le Marois, D. A. Rusakov, K. Zheng, S. Ameer-Beg, S. Poland, et al., *Med. Photonics* **2015**, *27*, 3–40.
[352] K. Dowling, S. C. W. Hyde, J. C. Dainty, P. M. W. French, J. D. Hares, *Opt. Commun.* **1997**, *135*, 27–31.
[353] G. Redford, R. M. Clegg, *Molecular Imaging, Chapter 11 - Real-Time Fluorescence Lifetime Imaging and FRET Using Fast-Gated Image Intensifiers*, Oxford University Press, New York, **2005**.
[354] K. Dowling, M. J. Dayel, M. J. Lever, P. M. French, J. D. Hares, A. K. Dymoke-Bradshaw, *Opt. Lett.* **1998**, *23*, 810–812.
[355] F. Doll, J. Hassenrück, V. Wittmann, A. Zumbusch, in *Methods Enzymol.* (Ed.: B. Imperiali), Academic Press, **2018**, pp. 283–319.
[356] T. W. J. Gadella Jr., T. M. Jovin, R. M. Clegg, *Biophys. Chem.* **1993**, *48*, 221–239.
[357] G. I. Redford, R. M. Clegg, *J. Fluoresc.* **2005**, *15*, 805–815.
[358] K. Kopp, A. Buntru, S. Pils, T. Zimmermann, R. Frank, A. Zumbusch, C. R. Hauck, *J. Biol. Chem.* **2012**, *287*, 39158–39170.
[359] M. Tramier, M. Zahid, J. C. Mevel, M. J. Masse, M. Coppey-Moisan, *Microsc. Res. Tech.* **2006**, *69*, 933–939.
[360] P. C. Schneider, R. M. Clegg, *Rev. Sci. Instrum.* **1997**, *68*, 4107–4119.
[361] P. C. Clegg, R. M. Schneider, in *Fluoresc. Microsc. Fluoresc. Probes* (Ed.: J. Slavik), Springer, Boston, MA, **1996**, pp. 15–33.
[362] J. R. Lakowicz, K. W. Berndt, *Rev. Sci. Instrum.* **1991**, *62*, 1727–1734.
[363] M. J. Booth, T. Wilson, *J. Microsc.* **2004**, *214*, 36–42.
[364] R. A. Colyer, C. Lee, E. Gratton, *Microsc. Res. Tech.* **2008**, *71*, 201–213.
[365] M. A. Digman, V. R. Caiolfa, M. Zamai, E. Gratton, *Biophys. J.* **2008**, *94*, L14-16.
[366] C. Buranachai, D. Kamiyama, A. Chiba, B. D. Williams, R. M. Clegg, *J. Fluoresc.* **2008**, *18*, 929–942.
[367] D. M. Grant, D. S. Elson, D. Schimpf, C. Dunsby, J. Requejo-Isidro, E. Auksorius, I. Munro, M. A. Neil, P. M. French, E. Nye, et al., *Opt. Lett.* **2005**, *30*, 3353–3355.
[368] K. Greger, M. J. Neetz, E. G. Reynaud, E. H. Stelzer, *Opt. Express* **2011**, *19*, 20743–20750.
[369] M. L. Hennrich, A.-C. Gavin, *Sci. Signal.* **2015**, *8*, re5.
[370] H. Goto, M. Inagaki, *Nat. Protoc.* **2007**, *2*, 2574–2581.
[371] B. G. Fuller, M. A. Lampson, E. A. Foley, S. Rosasco-Nitcher, K. V. Le, P. Tobelmann, D. L. Brautigan, P. T. Stukenberg, T. M. Kapoor, *Nature* **2008**, *453*, 1132–1136.
[372] F. Wang, J. Dai, J. R. Daum, E. Niedzialkowska, B. Banerjee, P. T. Stukenberg, G. J. Gorbsky, J. M. G. Higgins, *Science* **2010**, *330*, 231–235.
[373] J. Robertson, G. Jacquemet, A. Byron, M. C. Jones, S. Warwood, J. N. Selley, D. Knight, J. D. Humphries, M. J. Humphries, *Nat. Commun.* **2015**, *6*, 6265.
[374] H. Kimura, Y. Hayashi-Takanaka, T. J. Stasevich, Y. Sato, *Histochem. Cell Biol.* **2015**, *144*, 101–109.

[375] K. Kurita, T. Sakamoto, N. Yagi, Y. Sakamoto, A. Ito, N. Nishino, K. Sako, M. Yoshida, H. Kimura, M. Seki, et al., *Sci. Rep.* **2017**, *7*, 45894.
[376] Y. Fukata, A. Dimitrov, G. Boncompain, O. Vielemeyer, F. Perez, M. Fukata, *J. Cell Biol.* **2013**, *202*, 145–161.
[377] O. Söderberg, M. Gullberg, M. Jarvius, K. Ridderstråle, K.-J. Leuchowius, J. Jarvius, K. Wester, P. Hydbring, F. Bahram, L.-G. Larsson, et al., *Nat. Methods* **2006**, *3*, 995–1000.
[378] T. Conze, A. S. Carvalho, U. Landegren, R. Almeida, C. A. Reis, L. David, O. Söderberg, *Glycobiology* **2010**, *20*, 199–206.
[379] R. Pinto, A. S. Carvalho, T. Conze, A. Magalhães, G. Picco, J. M. Burchell, J. Taylor-Papadimitriou, C. A. Reis, R. Almeida, U. Mandel, et al., *J. Cell. Mol. Med.* **2012**, *16*, 1474–1484.
[380] M. Jarvius, J. Paulsson, I. Weibrecht, K.-J. Leuchowius, A.-C. Andersson, C. Wählby, M. Gullberg, J. Botling, T. Sjöblom, B. Markova, et al., *Mol. Cell. Proteomics* **2007**, *6*, 1500–1509.
[381] K.-J. Leuchowius, M. Jarvius, M. Wickström, L. Rickardson, U. Landegren, R. Larsson, O. Söderberg, M. Fryknäs, J. Jarvius, *Mol. Cell. Proteomics* **2010**, *9*, 178–183.
[382] G. J. Gu, D. Wu, H. Lund, D. Sunnemark, A. J. Kvist, R. Milner, S. Eckersley, L. N. G. Nilsson, K. Agerman, U. Landegren, et al., *J. Alzheimers Dis.* **2013**, *33*, 699–713.
[383] L. Elfineh, C. Classon, A. Asplund, U. Pettersson, M. Kamali-Moghaddam, S. B. Lind, *BMC Cancer* **2014**, *14*, 435.
[384] X. Gao, R. N. Hannoush, *Nat. Chem. Biol.* **2014**, *10*, 61–68.
[385] B. Zatloukal, I. Kufferath, A. Thueringer, U. Landegren, K. Zatloukal, J. Haybaeck, *PLoS ONE* **2014**, *9*, e96690.
[386] T. Förster, *Ann. Phys.* **1948**, *2*, 55–75.
[387] Y. Haga, K. Ishii, K. Hibino, Y. Sako, Y. Ito, N. Taniguchi, T. Suzuki, *Nat. Commun.* **2012**, *3*, 907.
[388] B. Belardi, A. de la Zerda, D. R. Spiciarich, S. L. Maund, D. M. Peehl, C. R. Bertozzi, *Angew. Chem. Int. Ed Engl.* **2013**, *125*, 14295–14299.
[389] W. Lin, Y. Du, Y. Zhu, X. Chen, *J. Am. Chem. Soc.* **2014**, *136*, 679–687.
[390] B. Yuan, Y. Chen, Y. Sun, Q. Guo, J. Huang, J. Liu, X. Meng, X. Yang, X. Wen, Z. Li, et al., *Anal. Chem.* **2018**, *90*, 6131–6137.
[391] P. J. Verveer, F. S. Wouters, A. R. Reynolds, P. I. Bastiaens, *Science* **2000**, *290*, 1567–70.
[392] A. R. Reynolds, C. Tischer, P. J. Verveer, O. Rocks, P. I. H. Bastiaens, *Nat. Chem. Biol.* **2003**, *5*, 447–453.
[393] T. Ng, A. Squire, G. Hansra, F. Bornancin, C. Prevostel, A. Hanby, W. Harris, D. Barnes, S. Schmidt, H. Mellor, et al., *Science* **1999**, *283*, 2085–2089.
[394] C. I. Maeder, M. A. Hink, A. Kinkhabwala, R. Mayr, P. I. H. Bastiaens, M. Knop, *Nat. Cell Biol.* **2007**, *9*, 1319–1326.
[395] H. E. Grecco, P. Roda-Navarro, A. Girod, J. Hou, T. Frahm, D. C. Truxius, R. Pepperkok, A. Squire, P. I. H. Bastiaens, *Nat. Methods* **2010**, *7*, 467–472.
[396] A. Bolbat, C. Schultz, *Biol. Cell* **2017**, *109*, 1–23.
[397] L. D. Carrillo, L. Krishnamoorthy, L. K. Mahal, *J. Am. Chem. Soc.* **2006**, *128*, 14768–14769.
[398] L. D. Carrillo, J. A. Froemming, L. K. Mahal, *J. Biol. Chem.* **2011**, *286*, 6650–6658.
[399] O. F. Sanchez, A. Mendonca, A. D. Carneiro, C. Yuan, *ACS Sens.* **2017**, *2*, 426–435.
[400] K. Sasaki, A. Ito, M. Yoshida, *Bioorg. Med. Chem.* **2012**, *20*, 1887–1892.
[401] C.-W. Lin, C. Y. Jao, A. Y. Ting, *J. Am. Chem. Soc.* **2004**, *126*, 5982–5983.

[402] T. V. Sekar, K. Foygel, R. Devulapally, R. Paulmurugan, *ACS Chem. Biol.* **2015**, *10*, 165–174.
[403] T. V. Sekar, K. Foygel, J. G. Gelovani, R. Paulmurugan, *Anal. Chem.* **2015**, *87*, 892–899.
[404] J. Zhang, Y. Ma, S. S. Taylor, R. Y. Tsien, *Proc. Natl. Acad. Sci. U. S. A.* **2001**, *98*, 14997–15002.
[405] K. Sasaki, M. Sato, Y. Umezawa, *J. Biol. Chem.* **2003**, *278*, 30945–30951.
[406] Y. Chen, L. Ding, W. Song, M. Yang, H. Ju, *Chem. Sci.* **2015**, *7*, 569–574.
[407] A. L. Santos, A. B. Lindner, *Oxid. Med. Cell. Longev.* **2017**, *2017*, 5716409.
[408] F. Doll, A. Buntz, A.-K. Späte, V. F. Schart, A. Timper, W. Schrimpf, C. R. Hauck, A. Zumbusch, V. Wittmann, *Angew. Chem. Int. Ed Engl.* **2016**, *55*, 2262–2266.
[409] H. Bußkamp, E. Batroff, A. Niederwieser, O. S. Abdel-Rahman, R. F. Winter, V. Wittmann, A. Marx, *Chem. Commun.* **2014**, *50*, 10827–10829.
[410] T. J. Ahern, A. M. Klibanov, *Science* **1985**, *228*, 1280–1284.
[411] R. A. Reeves, A. Lee, R. Henry, N. E. Zachara, *Anal. Biochem.* **2014**, *457*, 8–18.
[412] T. M. Gloster, W. F. Zandberg, J. E. Heinonen, D. L. Shen, L. Deng, D. J. Vocadlo, *Nat. Chem. Biol.* **2011**, *7*, 174–181.
[413] R. F. Ortiz-Meoz, J. Jiang, M. B. Lazarus, M. Orman, J. Janetzko, C. Fan, D. Y. Duveau, Z. W. Tan, C. J. Thomas, S. Walker, *ACS Chem. Biol.* **2015**, *10*, 1392–1397.
[414] H. M. Itkonen, S. S. Gorad, D. Y. Duveau, S. E. S. Martin, A. Barkovskaya, T. F. Bathen, S. A. Moestue, I. G. Mills, H. M. Itkonen, S. S. Gorad, et al., *Oncotarget* **2016**, *5*.
[415] M. Angelova, R. F. Ortiz-Meoz, S. Walker, D. M. Knipe, *J. Virol.* **2015**, *89*, 8474–8483.
[416] N. Shtraizent, C. DeRossi, S. Nayar, R. Sachidanandam, L. S. Katz, A. Prince, A. P. Koh, A. Vincek, Y. Hadas, Y. Hoshida, et al., *eLife* **2017**, *6*, e22477.
[417] Y. Liu, Y. Cao, X. Pan, M. Shi, Q. Wu, T. Huang, H. Jiang, W. Li, J. Zhang, *Cell Death Dis.* **2018**, *9*, 485.
[418] Y. Wang, J. Zhu, L. Zhang, *J. Med. Chem.* **2017**, *60*, 263–272.
[419] Y. Liu, Y. Ren, Y. Cao, H. Huang, Q. Wu, W. Li, S. Wu, J. Zhang, *Sci. Rep.* **2017**, *7*, 12334.
[420] S. A. Yuzwa, M. S. Macauley, J. E. Heinonen, X. Shan, R. J. Dennis, Y. He, G. E. Whitworth, K. A. Stubbs, E. J. McEachern, G. J. Davies, et al., *Nat. Chem. Biol.* **2008**, *4*, 483–490.
[421] C. Roth, S. Chan, W. A. Offen, G. R. Hemsworth, L. I. Willems, D. T. King, V. Varghese, R. Britton, D. J. Vocadlo, G. J. Davies, *Nat. Chem. Biol.* **2017**, *13*, 610–612.
[422] B. Li, H. Li, L. Lu, J. Jiang, *Nat. Struct. Mol. Biol.* **2017**, *24*, 362–369.
[423] M. Worth, H. Li, J. Jiang, *ACS Chem. Biol.* **2017**, *12*, 326–335.
[424] R. J. Konrad, J. F. Tolar, J. E. Hale, M. D. Knierman, G. W. Becker, J. E. Kudlow, *Biochem. Biophys. Res. Commun.* **2001**, *288*, 1136–1140.
[425] K. Kaasik, S. Kivimae, J. J. Allen, R. J. Chalkley, Y. Huang, K. Baer, H. Kissel, A. L. Burlingame, K. M. Shokat, L. J. Ptacek, et al., *Cell Metab.* **2013**, *17*, 291–302.
[426] L. Boglarka, S. A. Marsh, C. A. Brocks, W. Istvan, J. C. Chatham, *Am. J. Physiol. Heart Circ. Physiol.* **2010**, *299*, H1715–H1727.
[427] G. Tzivion, M. Dobson, G. Ramakrishnan, *Biochim. Biophys. Acta* **2011**, *1813*, 1938–1945.
[428] E. S. Nelson, A. W. Folkmann, M. D. Henry, K. A. DeMali, *Mol. Cancer Res.* **2011**, *9*, 712–723.
[429] X. A. Peng, E. S. Nelson, J. L. Maiers, K. A. DeMali, *Int. Rev. Cell Mol. Biol.* **2011**, *287*, 191–231.
[430] G. Wang, H. Zhang, L. Wang, Y. Wang, H. Huang, F. Sun, *Sci. Rep.* **2015**, *5*, 12126.

[431] W. B. Dias, W. D. Cheung, Z. Wang, G. W. Hart, *J. Biol. Chem.* **2009**, *284*, 21327–21337.
[432] H. Enslen, H. Tokumitsu, P. J. Stork, R. J. Davis, T. R. Soderling, *Proc. Natl. Acad. Sci. U. S. A.* **1996**, *93*, 10803–10808.
[433] L. Guo, M. Tang, L. Yang, L. Xiao, A. M. Bode, L. Li, Z. Dong, Y. Cao, *Int. J. Mol. Med.* **2012**, *29*, 574–80.
[434] Z. Gurel, B. W. Zaro, M. R. Pratt, N. Sheibani, *PLoS ONE* **2014**, *9*, e95561.
[435] K. T. Bieging, S. S. Mello, L. D. Attardi, *Nat. Rev. Cancer* **2014**, *14*, 359–370.
[436] D. Frescas, L. Valenti, D. Accili, *J. Biol. Chem.* **2005**, *280*, 20589–20595.
[437] M. P. Housley, J. T. Rodgers, N. D. Udeshi, T. J. Kelly, J. Shabanowitz, D. F. Hunt, P. Puigserver, G. W. Hart, *J. Biol. Chem.* **2008**, *283*, 16283–16292.
[438] M. P. Housley, N. D. Udeshi, J. T. Rodgers, J. Shabanowitz, P. Puigserver, D. F. Hunt, G. W. Hart, *J. Biol. Chem.* **2009**, *284*, 5148–5157.
[439] Y. Fardini, Y. Perez-Cervera, L. Camoin, P. Pagesy, T. Lefebvre, T. Issad, *Biochem. Biophys. Res. Commun.* **2015**, *462*, 151–158.
[440] A. Eijkelenboom, B. M. Burgering, *Nat. Rev. Mol. Cell Biol.* **2013**, *14*, 83–97.
[441] J. C. Gandy, A. E. Rountree, G. N. Bijur, *FEBS Lett.* **2006**, *580*, 3051–3058.
[442] S. Wang, X. Huang, D. N. Sun, X. L. Xin, Q. M. Pan, S. Y. Peng, Z. J. Liang, C. Luo, Y. M. Yang, H. L. Jiang, et al., *PLoS ONE* **2012**, *7*, e37427.
[443] E. S. Kang, D. Han, J. Park, T. K. Kwak, M. A. Oh, S. A. Lee, S. Choi, Z. Y. Park, Y. Kim, J. W. Lee, *Exp. Cell Res.* **2008**, *314*, 2238–2248.
[444] D. P. Brazil, B. A. Hemmings, *Trends Biochem. Sci.* **2001**, *26*, 657–664.
[445] G. Luboshits, D. Benayahu, *Gene* **2005**, *351*, 19–28.
[446] M. I. Mayr, S. Hümmer, J. Bormann, T. Grüner, S. Adio, G. Woehlke, T. U. Mayer, *Curr. Biol.* **2007**, *17*, 488–498.
[447] V. Varga, C. Leduc, V. Bormuth, S. Diez, J. Howard, *Cell* **2009**, *138*, 1174–1183.
[448] M. I. Mayr, M. Storch, J. Howard, T. U. Mayer, *PLoS ONE* **2011**, *6*, e27471.
[449] K. Jaqaman, E. M. King, A. C. Amaro, J. R. Winter, J. F. Dorn, H. L. Elliott, N. Mchedlishvili, S. E. McClelland, I. M. Porter, M. Posch, et al., *J. Cell Biol.* **2010**, *188*, 665–679.
[450] J. Stumpff, G. Von Dassow, M. Wagenbach, C. Asbury, L. Wordeman, *Dev. Cell* **2008**, *14*, 252–262.
[451] T. M. Kapoor, D. A. Compton, *J. Cell Biol.* **2002**, *157*, 551–556.
[452] J. Häfner, M. I. Mayr, M. M. Möckel, T. U. Mayer, *Nat. Commun.* **2014**, *5*, 4397.
[453] L. Wang, S. Yang, R. Sun, M. Lu, Y. Wu, Y. Li, *Chin. J. Gastrointest. Surg.* **2016**, *19*, 585–589.
[454] W. Liao, G. Huang, Y. Liao, J. Yang, Q. Chen, S. Xiao, J. Jin, S. He, C. Wang, *Oncotarget* **2014**, *5*, 10271–10279.
[455] Q. Chen, B. Cao, N. Nan, Y. Wang, X. Zhai, Y. Li, T. Chong, *Exp. Ther. Med.* **2016**, *12*, 377–383.
[456] M. Scales, D. Chubb, S. E. Dobbins, D. C. Johnson, N. Li, M. J. Sternberg, N. Weinhold, C. Stein, G. Jackson, F. E. Davies, et al., *Oncotarget* **2017**, *8*, 36203–36210.
[457] M. Zusev, D. Benayahu, *J. Cell. Physiol.* **2008**, *217*, 618–625.
[458] F. Yang, Y. Chen, W. Dai, *BMC Cancer* **2015**, *15*, 197.
[459] S. A. M. van der Laarse, A. C. Leney, A. J. R. Heck, *FEBS J.* **2018**, *285*, 3152-3167.
[460] L. Haiber, Analysis of Kif18A's O-GlcNAcylation inside Living Cells, Master's thesis, University of Konstanz, **2018**.
[461] H. A. Lashuel, C. R. Overk, A. Oueslati, E. Masliah, *Nat. Rev. Neurosci.* **2013**, *14*, 38–48.
[462] M. Emanuele, E. Chieregatti, *Biomolecules* **2015**, *5*, 865–892.

[463] C. C. Jao, B. G. Hegde, J. Chen, I. S. Haworth, R. Langen, *Proc. Natl. Acad. Sci. U. S. A.* **2008**, *105*, 19666–19671.
[464] N. Mizuno, J. Varkey, N. C. Kegulian, B. G. Hegde, N. Cheng, R. Langen, A. C. Steven, *J. Biol. Chem.* **2012**, *287*, 29301–29311.
[465] J. Varkey, J. M. Isas, N. Mizuno, M. B. Jensen, V. K. Bhatia, C. C. Jao, J. Petrlova, J. C. Voss, D. G. Stamou, A. C. Steven, et al., *J. Biol. Chem.* **2010**, *285*, 32486–32493.
[466] A. L. Fink, *Acc. Chem. Res.* **2006**, *39*, 628–634.
[467] Y. E. Lewis, A. Galesic, P. M. Levine, C. A. De Leon, N. Lamiri, C. K. Brennan, M. R. Pratt, *ACS Chem. Biol.* **2017**, *12*, 1020–1027.
[468] A. W. Schmid, B. Fauvet, M. Moniatte, H. A. Lashuel, *Mol. Cell. Proteomics* **2013**, *12*, 3543–3558.
[469] Z. Wang, K. Park, F. Comer, L. C. Hsieh-Wilson, C. D. Saudek, G. W. Hart, *Diabetes* **2009**, *58*, 309–317.
[470] Z. Wang, N. D. Udeshi, M. O'Malley, J. Shabanowitz, D. F. Hunt, G. W. Hart, *Mol. Cell. Proteomics* **2010**, *9*, 153–160.
[471] J. F. Alfaro, C.-X. Gong, M. E. Monroe, J. T. Aldrich, T. R. W. Clauss, S. O. Purvine, Z. Wang, D. G. Camp, J. Shabanowitz, P. Stanley, et al., *Proc. Natl. Acad. Sci. U. S. A.* **2012**, *109*, 7280–7285.
[472] M. Morris, G. M. Knudsen, S. Maeda, J. C. Trinidad, A. Ioanoviciu, A. L. Burlingame, L. Mucke, *Nat. Neurosci.* **2015**, *18*, 1183–1189.
[473] N. P. Marotta, Y. H. Lin, Y. E. Lewis, M. R. Ambroso, B. W. Zaro, M. T. Roth, D. B. Arnold, R. Langen, M. R. Pratt, *Nat. Chem.* **2015**, *7*, 913–920.
[474] J. Zhang, H. Lei, Y. Chen, Y.-T. Ma, F. Jiang, J. Tan, Y. Zhang, J.-D. Li, *Neurosci. Lett.* **2017**, *655*, 90–94.
[475] P. Chovancova, Metabolic Oligosaccharide Engineering for Visualization of Neurodegenerative and Neurodevelopmental Processes, PhD thesis, University of Konstanz, **in progress**.
[476] W. Lin, L. Gao, X. Chen, *ChemBioChem* **2015**, *16*, 2571–2575.
[477] A. R. Batt, B. W. Zaro, M. X. Navarro, M. R. Pratt, *ChemBioChem* **2017**, *18*, 1177–1182.
[478] A. H. Huber, W. J. Nelson, W. I. Weis, *Cell* **1997**, *90*, 871–882.
[479] Y. Xing, K.-I. Takemaru, J. Liu, J. D. Berndt, J. J. Zheng, R. T. Moon, W. Xu, *Structure* **2008**, *16*, 478–487.
[480] M. Ozawa, H. Baribault, R. Kemler, *EMBO J.* **1989**, *8*, 1711–1717.
[481] T. Valenta, G. Hausmann, K. Basler, *EMBO J.* **2012**, *31*, 2714–2736.
[482] O. Tetsu, F. McCormick, *Nature* **1999**, *398*, 422–426.
[483] N. Gavert, M. Sheffer, S. Raveh, S. Spaderna, M. Shtutman, T. Brabletz, F. Barany, P. Paty, D. Notterman, E. Domany, et al., *Cancer Res.* **2007**, *67*, 7703–7712.
[484] E. M. Verheyen, C. J. Gottardi, *Dev. Dyn. Off. Publ. Am. Assoc. Anat.* **2010**, *239*, 34–44.
[485] S.-Y. Lin, W. Xia, J. C. Wang, K. Y. Kwong, B. Spohn, Y. Wen, R. G. Pestell, M.-C. Hung, *Proc. Natl. Acad. Sci. U. S. A.* **2000**, *97*, 4262–4266.
[486] B. Vogelstein, K. W. Kinzler, *Nat. Med.* **2004**, *10*, 789–799.
[487] M. Bienz, H. Clevers, *Cell* **2000**, *103*, 311–320.
[488] W. Zhu, B. Leber, D. W. Andrews, *EMBO J.* **2001**, *20*, 5999–6007.
[489] R. Sayat, B. Leber, V. Grubac, L. Wiltshire, S. Persad, *Exp. Cell Res.* **2008**, *314*, 2774–2787.
[490] J. R. Ha, L. Hao, G. Venkateswaran, Y. H. Huang, E. Garcia, S. Persad, *Exp. Cell Res.* **2014**, *321*, 153–166.
[491] S. B. Harosh-Davidovich, I. Khalaila, *Exp. Cell Res.* **2018**, *364*, 42–49.

[492] P. Widder, Visualizing the O-GlcNAcylation of Beta-Catenin via FLIM-FRET Microscopy, Master's thesis, University of Konstanz, **2016**.
[493] S. Ganguly, A. H. A. Clayton, A. Chattopadhyay, *Biochem. Biophys. Res. Commun.* **2011**, *405*, 234–237.
[494] L. Joosen, M. A. Hink, T. W. J. Gadella, J. Goedhart, *J. Microsc.* **2014**, *256*, 166–176.
[495] J. Hassenrück, Untersuchungen Zur Anwendung Der Diels-Adler Reaktion Mit Inversem Elektronenbedarf Beim Metabolischen Glycoengineering, PhD thesis, University of Konstanz, **in progress**.
[496] C. Somerville, S. Bauer, G. Brininstool, M. Facette, T. Hamann, J. Milne, E. Osborne, A. Paredez, S. Persson, T. Raab, et al., *Science* **2004**, *306*, 2206–2211.
[497] R. Strasser, *Glycobiology* **2016**, *26*, 926–939.
[498] G. H. H. Borner, K. S. Lilley, T. J. Stevens, P. Dupree, *Plant Physiol.* **2003**, *132*, 568–577.
[499] E. P. Bennett, U. Mandel, H. Clausen, T. A. Gerken, T. A. Fritz, L. A. Tabak, *Glycobiology* **2012**, *22*, 736–756.
[500] M. Bar-Peled, M. A. O'Neill, *Annu. Rev. Plant Biol.* **2011**, *62*, 127–155.
[501] T. M. Thornton, S. M. Swain, N. E. Olszewski, *Trends Plant Sci.* **1999**, *4*, 424–428.
[502] L. M. Hartweck, C. L. Scott, N. E. Olszewski, *Genetics* **2002**, *161*, 1279–1291.
[503] N. E. Olszewski, C. M. West, S. O. Sassi, L. M. Hartweck, *Biochim. Biophys. Acta* **2010**, *1800*, 49–56.
[504] J. Alonso, M. Schimpl, D. M. F. van Aalten, *J. Biol. Chem.* **2014**, *289*, 34433–34439.
[505] E. Steiner, I. Efroni, M. Gopalraj, K. Saathoff, T.-S. Tseng, M. Kieffer, Y. Eshed, N. Olszewski, D. Weiss, *Plant Cell* **2012**, *24*, 96–108.
[506] R. Zentella, J. Hu, W.-P. Hsieh, P. A. Matsumoto, A. Dawdy, B. Barnhill, H. Oldenhof, L. M. Hartweck, S. Maitra, S. G. Thomas, et al., *Genes Dev.* **2016**, *30*, 164–176.
[507] S.-L. Xu, R. J. Chalkley, J. C. Maynard, W. Wang, W. Ni, X. Jiang, K. Shin, L. Cheng, D. Savage, A. F. R. Hühmer, et al., *Proc. Natl. Acad. Sci. U. S. A.* **2017**, *114*, E1536–E1543.
[508] M. Dumont, A. Lehner, B. Vauzeilles, J. Malassis, A. Marchant, K. Smyth, B. Linclau, A. Baron, J. Mas Pons, C. T. Anderson, et al., *Plant J. Cell Mol. Biol.* **2016**, *85*, 437–447.
[509] C. T. Anderson, I. S. Wallace, C. R. Somerville, *Proc. Natl. Acad. Sci. U. S. A.* **2012**, *109*, 1329–1334.
[510] R. M. Roberts, *Plant Physiol.* **1970**, *45*, 263–267.
[511] N. Khidekel, S. B. Ficarro, E. C. Peters, L. C. Hsieh-Wilson, *Proc. Natl. Acad. Sci. U. S. A.* **2004**, *101*, 13132–13137.
[512] J. E. Rexach, C. J. Rogers, S.-H. Yu, J. Tao, Y. E. Sun, L. C. Hsieh-Wilson, *Nat. Chem. Biol.* **2010**, *6*, 645–651.
[513] P. M. Clark, J. E. Rexach, L. C. Hsieh-Wilson, in *Curr. Protoc. Chem. Biol.*, John Wiley & Sons, Inc., **2009**, pp. 281–302.
[514] L. Camborde, A. Jauneau, C. Brière, L. Deslandes, B. Dumas, E. Gaulin, *Nat. Protoc.* **2017**, *12*, 1933–1950.
[515] Y. Long, Y. Stahl, S. Weidtkamp-Peters, M. Postma, W. Zhou, J. Goedhart, M.-I. Sánchez-Pérez, T. W. J. Gadella, R. Simon, B. Scheres, et al., *Nature* **2017**, *548*, 97–102.
[516] K. Celler, M. Fujita, E. Kawamura, C. Ambrose, K. Herburger, A. Holzinger, G. O. Wasteneys, *Methods Mol. Biol.* **2016**, *1365*, 155–184.
[517] R. P. Ladenson, S. O. Schwartz, A. C. Ivy, *Am. J. Med. Sci.* **1949**, *217*, 194–197.
[518] S. I. Hakomori, W. T. Murakami, *Proc. Natl. Acad. Sci. U. S. A.* **1968**, *59*, 254–261.
[519] B. N. Vajaria, P. S. Patel, *Glycoconj. J.* **2016**, 1–10.

[520] S. S. Pinho, C. A. Reis, *Nat. Rev. Cancer* **2015**, *15*, 540–555.
[521] S. Hakomori, *Proc. Natl. Acad. Sci. U. S. A.* **2002**, *99*, 10231–10233.
[522] M. N. Christiansen, J. Chik, L. Lee, M. Anugraham, J. L. Abrahams, N. H. Packer, *Proteomics* **2014**, *14*, 525–546.
[523] J. N. Arnold, R. Saldova, U. M. A. Hamid, P. M. Rudd, *Proteomics* **2008**, *8*, 3284–3293.
[524] N. T. Marcos, E. P. Bennett, J. Gomes, A. Magalhaes, C. Gomes, L. David, I. Dar, C. Jeanneau, S. DeFrees, D. Krustrup, et al., *Front. Biosci.* **2011**, *3*, 1443–1455.
[525] S. Julien, E. Adriaenssens, K. Ottenberg, A. Furlan, G. Courtand, A.-S. Vercoutter-Edouart, F.-G. Hanisch, P. Delannoy, X. Le Bourhis, *Glycobiology* **2006**, *16*, 54–64.
[526] R. Kannagi, J. Yin, K. Miyazaki, M. Izawa, *Biochim. Biophys. Acta* **2008**, *1780*, 525–531.
[527] S. Itzkowitz, T. Kjeldsen, A. Friera, S. Hakomori, U. S. Yang, Y. S. Kim, *Gastroenterology* **1991**, *100*, 1691–1700.
[528] R. Sewell, M. Bäckström, M. Dalziel, S. Gschmeissner, H. Karlsson, T. Noll, J. Gätgens, H. Clausen, G. C. Hansson, J. Burchell, et al., *J. Biol. Chem.* **2006**, *281*, 3586–3594.
[529] J. A. Ferreira, P. A. Videira, L. Lima, S. Pereira, M. Silva, M. Carrascal, P. F. Severino, E. Fernandes, A. Almeida, C. Costa, et al., *Mol. Oncol.* **2013**, *7*, 719–731.
[530] B. Davidson, A. Berner, J. M. Nesland, B. Risberg, G. B. Kristensen, C. G. Tropé, M. Bryne, *Hum. Pathol.* **2000**, *31*, 1081–1087.
[531] S. Pinho, N. T. Marcos, B. Ferreira, A. S. Carvalho, M. J. Oliveira, F. Santos-Silva, A. Harduin-Lepers, C. A. Reis, *Cancer Lett.* **2007**, *249*, 157–170.
[532] S. S. Pinho, P. Oliveira, J. Cabral, S. Carvalho, D. Huntsman, F. Gärtner, R. Seruca, C. A. Reis, C. Oliveira, *PLoS ONE* **2012**, *7*, e33191.
[533] A. Díaz-Fernández, R. Miranda-Castro, N. de-los-Santos-Álvarez, M. J. Lobo-Castañón, *Anal. Bioanal. Chem.* **2018**, *410*, 2059–2065.
[534] S. Mereiter, M. Balmaña, J. Gomes, A. Magalhães, C. A. Reis, *Front. Oncol.* **2016**, *6*, 55.
[535] F. M. S. de Oliveira, S. Mereiter, P. Lönn, B. Siart, Q. Shen, J. Heldin, D. Raykova, N. Karlsson, K. Polom, F. Roviello, et al., *New Biotechnol.* **2018**, *45*, 51-59.
[536] J. Zheng, H. Xiao, R. Wu, *Angew. Chem. Int. Ed Engl.* **2017**, *56*, 7107–7111.
[537] Z. L. Wu, A. Person, M. Anderson, B. Burroughs, T. Tatge, K. Khatri, Y. Zou, L. Wang, T. Geders, J. Zaia, et al., *Glycobiology* **2017**, *28*, 69–79.
[538] P. A. Gilormini, C. Lion, D. Vicogne, Y. Guérardel, F. Foulquier, C. Biot, *J. Inherit. Metab. Dis.* **2018**, *41*, 515–523.
[539] H. A. Badr, D. M. M. AlSadek, M. E. El-Houseini, C. T. Saeui, M. P. Mathew, K. J. Yarema, H. Ahmed, *Biomaterials* **2017**, *116*, 158–173.
[540] A. S. Carvalho, A. Harduin-Lepers, A. Magalhães, E. Machado, N. Mendes, L. T. Costa, R. Matthiesen, R. Almeida, J. Costa, C. A. Reis, *Int. J. Biochem. Cell Biol.* **2010**, *42*, 80–89.
[541] C. Gomes, H. Osório, M. T. Pinto, D. Campos, M. J. Oliveira, C. A. Reis, *PLoS ONE* **2013**, *8*, e66737.
[542] S. Mereiter, A. Magalhães, B. Adamczyk, C. Jin, A. Almeida, L. Drici, M. Ibáñez-Vea, C. Gomes, J. A. Ferreira, L. P. Afonso, et al., *Biochim. Biophys. Acta* **2016**, *1860*, 1795–1808.
[543] S. Mereiter, A. Magalhães, B. Adamczyk, C. Jin, A. Almeida, L. Drici, M. Ibáñez-Vea, M. R. Larsen, D. Kolarich, N. G. Karlsson, et al., *Data Brief* **2016**, *7*, 814–833.
[544] S. Ansar Ahmed, R. M. Gogal, J. E. Walsh, *J. Immunol. Methods* **1994**, *170*, 211–224.

[545] S. Perrot, H. Dutertre-Catella, C. Martin, J.-M. Warnet, P. Rat, *Cytom. Part J. Int. Soc. Anal. Cytol.* **2003**, *55*, 7–14.
[546] M. Ito, in *Anim. Cell Technol. Dev. 21st Century*, Springer, Dordrecht, **1995**, pp. 1005–1009.
[547] H. Zhou, A. C. Briscoe, J. W. Froehlich, R. S. Lee, *Anal. Biochem.* **2012**, *427*, 33–35.
[548] F. Maley, R. B. Trimble, A. L. Tarentino, T. H. Plummer, *Anal. Biochem.* **1989**, *180*, 195–204.
[549] W. Qin, K. Qin, X. Fan, L. Peng, W. Hong, Y. Zhu, P. Lv, Y. Du, R. Huang, M. Han, et al., *Angew. Chem. Int. Ed Engl.* **2018**, *57*, 1817–1820.
[550] K. Dinnell, J. M. Elliott, G. J. Hollingworth, D. E. Shaw, *Azaindole Derivatives and Their Use as Therapeutic Agents*, **2002**, US 2002/0022624 A1.
[551] Z. L. Marcsek, Z. Kocsis, B. Szende, A. Tompa, *Cell Biol. Int.* **2007**, *31*, 1214–1219.
[552] K. Sivakumar, F. Xie, B. M. Cash, S. Long, H. N. Barnhill, Q. Wang, *Org. Lett.* **2004**, *6*, 4603–4606.
[553] B. Devipriya, P. Kumaradhas, *Chem. Biol. Interact.* **2013**, *204*, 153–165.
[554] X. Yan, B. Pan, T. Lv, L. Liu, J. Zhu, W. Shen, X. Huang, J. Tian, *J. Biomed. Sci.* **2017**, *24*, 1.
[555] A. Jufvas, P. Strålfors, A. V. Vener, *PLoS ONE* **2011**, *6*, e15960.
[556] H. C. Beck, E. C. Nielsen, R. Matthiesen, L. H. Jensen, M. Sehested, P. Finn, M. Grauslund, A. M. Hansen, O. N. Jensen, *Mol. Cell. Proteomics* **2006**, *5*, 1314–1325.
[557] C. Choudhary, C. Kumar, F. Gnad, M. L. Nielsen, M. Rehman, T. C. Walther, J. V. Olsen, M. Mann, *Science* **2009**, *325*, 834–840.
[558] A. Bateman, M. J. Martin, C. O'Donovan, M. Magrane, E. Alpi, R. Antunes, B. Bely, M. Bingley, C. Bonilla, R. Britto, et al., *Nucleic Acids Res.* **2017**, *45*, D158–D169.
[559] S. Rokudai, O. Laptenko, S. M. Arnal, Y. Taya, I. Kitabayashi, C. Prives, *Proc. Natl. Acad. Sci. U. S. A.* **2013**, *110*, 3895–3900.
[560] Y.-H. Wang, Y.-G. Tsay, B. C.-M. Tan, W.-Y. Lo, S.-C. Lee, *J. Biol. Chem.* **2003**, *278*, 25568–25576.
[561] K. Sakaguchi, J. E. Herrera, S. Saito, T. Miki, M. Bustin, A. Vassilev, C. W. Anderson, E. Appella, *Genes Dev.* **1998**, *12*, 2831–2841.
[562] B. Bu, X. Tong, D. Li, Y. Hu, W. He, C. Zhao, R. Hu, X. Li, Y. Shao, C. Liu, et al., *ACS Chem. Neurosci.* **2017**, *8*, 2145–2151.
[563] P. Van Damme, M. Lasa, B. Polevoda, C. Gazquez, A. Elosegui-Artola, D. S. Kim, E. De Juan-Pardo, K. Demeyer, K. Hole, E. Larrea, et al., *Proc. Natl. Acad. Sci. U. S. A.* **2012**, *109*, 12449–12454.
[564] P. O. Hassa, S. S. Haenni, C. Buerki, N. I. Meier, W. S. Lane, H. Owen, M. Gersbach, R. Imhof, M. O. Hottiger, *J. Biol. Chem.* **2005**, *280*, 40450–40464.
[565] S. Gauci, A. O. Helbig, M. Slijper, J. Krijgsveld, A. J. R. Heck, S. Mohammed, *Anal. Chem.* **2009**, *81*, 4493–4501.
[566] V. Swaminathan, A. H. Kishore, K. K. Febitha, T. K. Kundu, *Mol. Cell. Biol.* **2005**, *25*, 7534–7545.
[567] J. Park, Y. Chen, D. X. Tishkoff, C. Peng, M. Tan, L. Dai, Z. Xie, Y. Zhang, B. M. M. Zwaans, M. E. Skinner, et al., *Mol. Cell* **2013**, *50*, 919–930.
[568] S. Das, R. Cong, J. Shandilya, P. Senapati, B. Moindrot, K. Monier, H. Delage, F. Mongelard, S. Kumar, T. K. Kundu, et al., *FEBS Lett.* **2013**, *587*, 417–424.
[569] S. Xie, Y. Yang, X. Lin, J. Zhou, D. Li, M. Liu, *J. Cell. Physiol.* **2018**, *233*, 2581–2589.
[570] P. Xia, Z. Wang, X. Liu, B. Wu, J. Wang, T. Ward, L. Zhang, X. Ding, G. Gibbons, Y. Shi, et al., *Proc. Natl. Acad. Sci. U. S. A.* **2012**, *109*, 16564–16569.

[571] K. Okumura, M. Mendoza, R. M. Bachoo, R. A. DePinho, W. K. Cavenee, F. B. Furnari, *J. Biol. Chem.* **2006**, *281*, 26562–26568.
[572] Z. Meng, L.-F. Jia, Y.-H. Gan, *Oncogene* **2016**, *35*, 2333–2344.
[573] T. Ikenoue, K. Inoki, B. Zhao, K.-L. Guan, *Cancer Res.* **2008**, *68*, 6908–6912.
[574] E. Landwehr, Towards Visualizing Protein-Specific Acetylation inside Single Cells, Bachelor's thesis, University of Konstanz, **2017**.
[575] R. L. Bartel, R. T. Borchardt, *Mol. Pharmacol.* **1984**, *25*, 418–424.
[576] X.-J. Cao, A. M. Arnaudo, B. A. Garcia, *Epigenetics* **2013**, *8*, 477–485.
[577] E. Bártová, A. H. Horáková, R. Uhlířová, I. Raška, G. Galiová, D. Orlova, S. Kozubek, *J. Histochem. Cytochem.* **2010**, *58*, 391–403.
[578] G. Cui, S. Park, A. I. Badeaux, D. Kim, J. Lee, J. R. Thompson, F. Yan, S. Kaneko, Z. Yuan, M. V. Botuyan, et al., *Nat. Struct. Mol. Biol.* **2012**, *19*, 916–924.
[579] J. Huang, J. Dorsey, S. Chuikov, X. Zhang, T. Jenuwein, D. Reinberg, S. L. Berger, *J. Biol. Chem.* **2010**, *285*, 9636–9641.
[580] Y. Yoshioka, T. Suzuki, Y. Matsuo, M. Nakakido, G. Tsurita, C. Simone, T. Watanabe, N. Dohmae, Y. Nakamura, R. Hamamoto, *Oncotarget* **2016**, *7*, 75023–75037.
[581] J. Seo, J. Jeong, Y. M. Kim, N. Hwang, E. Paek, K.-J. Lee, *J. Proteome Res.* **2008**, *7*, 587–602.
[582] K. Yamagata, H. Daitoku, Y. Takahashi, K. Namiki, K. Hisatake, K. Kako, H. Mukai, Y. Kasuya, A. Fukamizu, *Mol. Cell* **2008**, *32*, 221–231.
[583] S.-B. Seo, Y.-C. Chae, J.-Y. Kim, J. W. Park, K.-B. Kim, *Arch. Cancer Res.* **2017**, DOI 10.21767/2254-6081-C1-003.
[584] A. N. Iberg, A. Espejo, D. Cheng, D. Kim, J. Michaud-Levesque, S. Richard, M. T. Bedford, *J. Biol. Chem.* **2008**, *283*, 3006–3010.
[585] B. A. Garcia, S. B. Hake, R. L. Diaz, M. Kauer, S. A. Morris, J. Recht, J. Shabanowitz, N. Mishra, B. D. Strahl, C. D. Allis, et al., *J. Biol. Chem.* **2007**, *282*, 7641–7655.
[586] S. Pal, S. N. Vishwanath, H. Erdjument-Bromage, P. Tempst, S. Sif, *Mol. Cell. Biol.* **2004**, *24*, 9630–9645.
[587] M. Ananthanarayanan, S. Li, N. Balasubramaniyan, F. J. Suchy, M. J. Walsh, *J. Biol. Chem.* **2004**, *279*, 54348–54357.
[588] J. J. Coon, B. Ueberheide, J. E. P. Syka, D. D. Dryhurst, J. Ausio, J. Shabanowitz, D. F. Hunt, *Proc. Natl. Acad. Sci. U. S. A.* **2005**, *102*, 9463–9468.
[589] B. D. Strahl, S. D. Briggs, C. J. Brame, J. A. Caldwell, S. S. Koh, H. Ma, R. G. Cook, J. Shabanowitz, D. F. Hunt, M. R. Stallcup, et al., *Curr. Biol.* **2001**, *11*, 996–1000.
[590] J. J. Pesavento, H. Yang, N. L. Kelleher, C. A. Mizzen, *Mol. Cell. Biol.* **2008**, *28*, 468–486.
[591] W. Gao, R. Xiao, B. Peng, H. Xu, H. Shen, M. Huang, T. Shi, J. Yi, W. Zhang, X. Wu, et al., *Proc. Natl. Acad. Sci. U. S. A.* **2015**, *112*, E3327–E3336.
[592] H.-S. Cho, T. Shimazu, G. Toyokawa, Y. Daigo, Y. Maehara, S. Hayami, A. Ito, K. Masuda, N. Ikawa, H. I. Field, et al., *Nat. Commun.* **2012**, *3*, 1072.
[593] A. Guo, H. Gu, J. Zhou, D. Mulhern, Y. Wang, K. A. Lee, V. Yang, M. Aguiar, J. Kornhauser, X. Jia, et al., *Mol. Cell. Proteomics* **2014**, *13*, 372–387.
[594] S. Kernstock, E. Davydova, M. Jakobsson, A. Moen, S. Pettersen, G. M. Mælandsmo, W. Egge-Jacobsen, P. Ø. Falnes, *Nat. Commun.* **2012**, *3*, 1038.
[595] B. Lapeyre, H. Bourbon, F. Amalric, *Proc. Natl. Acad. Sci. U. S. A.* **1987**, *84*, 1472–1476.
[596] C. Uttamapinant, K. A. White, H. Baruah, S. Thompson, M. Fernández-Suárez, S. Puthenveetil, A. Y. Ting, *Proc. Natl. Acad. Sci. U. S. A.* **2010**, *107*, 10914–10919.

[597] R. R. Ramos, A. J. Swanson, J. Bass, *Proc. Natl. Acad. Sci. U. S. A.* **2007**, *104*, 10470–10475.
[598] S. J. Watton, J. Downward, *Curr. Biol.* **1999**, *9*, 433–436.
[599] J. Park, Y. Hu, T. V. Murthy, F. Vannberg, B. Shen, A. Rolfs, J. E. Hutti, L. C. Cantley, J. Labaer, E. Harlow, et al., *Proc. Natl. Acad. Sci. U. S. A.* **2005**, *102*, 8114–8119.
[600] X. Shen, J.-S. Park, Y. Qiu, J. Sugar, B. Y. J. T. Yue, *Genes Cells* **2009**, *14*, 1133–1139.
[601] G. Martínez-Noël, J. T. Galligan, M. E. Sowa, V. Arndt, T. M. Overton, J. W. Harper, P. M. Howley, *Mol. Cell. Biol.* **2012**, *32*, 3095–3106.
[602] L. Trinkle-Mulcahy, J. E. Sleeman, A. I. Lamond, *J. Cell Sci.* **2001**, *114*, 4219–4228.
[603] F. T. Kolligs, G. Hu, C. V. Dang, E. R. Fearon, *Mol. Cell. Biol.* **1999**, *19*, 5696–5706.
[604] A. E. Witt, L. M. Hines, N. L. Collins, Y. Hu, R. N. Gunawardane, D. Moreira, J. Raphael, D. Jepson, M. Koundinya, A. Rolfs, et al., *J. Proteome Res.* **2006**, *5*, 599–610.
[605] L. Tou, Q. Liu, R. A. Shivdasani, *Mol. Cell. Biol.* **2004**, *24*, 3132–3139.
[606] X.-C. Zeng, S. Bhasin, X. Wu, J.-G. Lee, S. Maffi, C. J. Nichols, K. J. Lee, J. P. Taylor, L. E. Greene, E. Eisenberg, *J. Cell Sci.* **2004**, *117*, 4991–5000.
[607] W. Wang, A. Budhu, M. Forgues, X. W. Wang, *Nat. Cell Biol.* **2005**, *7*, 823–830.
[608] J. Hageman, H. H. Kampinga, *Cell Stress Chaperones* **2009**, *14*, 1–21.
[609] J.-J. Hao, Y. Liu, M. Kruhlak, K. E. Debell, B. L. Rellahan, S. Shaw, *J. Cell Biol.* **2009**, *184*, 451–462.
[610] E. Tresse, F. A. Salomons, J. Vesa, L. C. Bott, V. Kimonis, T.-P. Yao, N. P. Dantuma, J. P. Taylor, *Autophagy* **2010**, *6*, 217–227.
[611] M. Takagi, M. J. Absalon, K. G. McLure, M. B. Kastan, *Cell* **2005**, *123*, 49–63.
[612] R. A. Furlong, Y. Narain, J. Rankin, A. Wyttenbach, D. C. Rubinsztein, *Biochem. J.* **2000**, *346*, 577–581.
[613] F. Liu, S. Wagner, R. B. Campbell, J. A. Nickerson, C. A. Schiffer, A. H. Ross, *J. Cell. Biochem.* **2005**, *96*, 221–234.
[614] T. Schmitter, F. Agerer, L. Peterson, P. Münzner, C. R. Hauck, *J. Exp. Med.* **2004**, *199*, 35–46.
[615] H. C. Birnboim, J. Doly, *Nucleic Acids Res.* **1979**, *7*, 1513–1523.
[616] N. Campo, M.-L. Daveran-Mingot, K. Leenhouts, P. Ritzenthaler, P. Le Bourgeois, *Appl. Environ. Microbiol.* **2002**, *68*, 2359–2367.
[617] D. Stepensky, *Biochem. Biophys. Res. Commun.* **2007**, *359*, 752–758.
[618] E. B. van Munster, T. W. J. Gadella, *Cytometry A* **2004**, *58A*, 185–194.
[619] D. Magde, R. Wong, P. G. Seybold, *Photochem. Photobiol.* **2002**, *75*, 327–334.
[620] Y. Sun, R. N. Day, A. Periasamy, *Nat. Protoc.* **2011**, *6*, 1324–1340.
[621] W. Schrimpf, A. Barth, J. Hendrix, D. C. Lamb, *Biophys. J.* **2018**, *114*, 1518–1528.

11. Appendix

The appendix includes ^{1}H NMR and ^{13}C NMR spectra of compounds synthesized within this thesis.

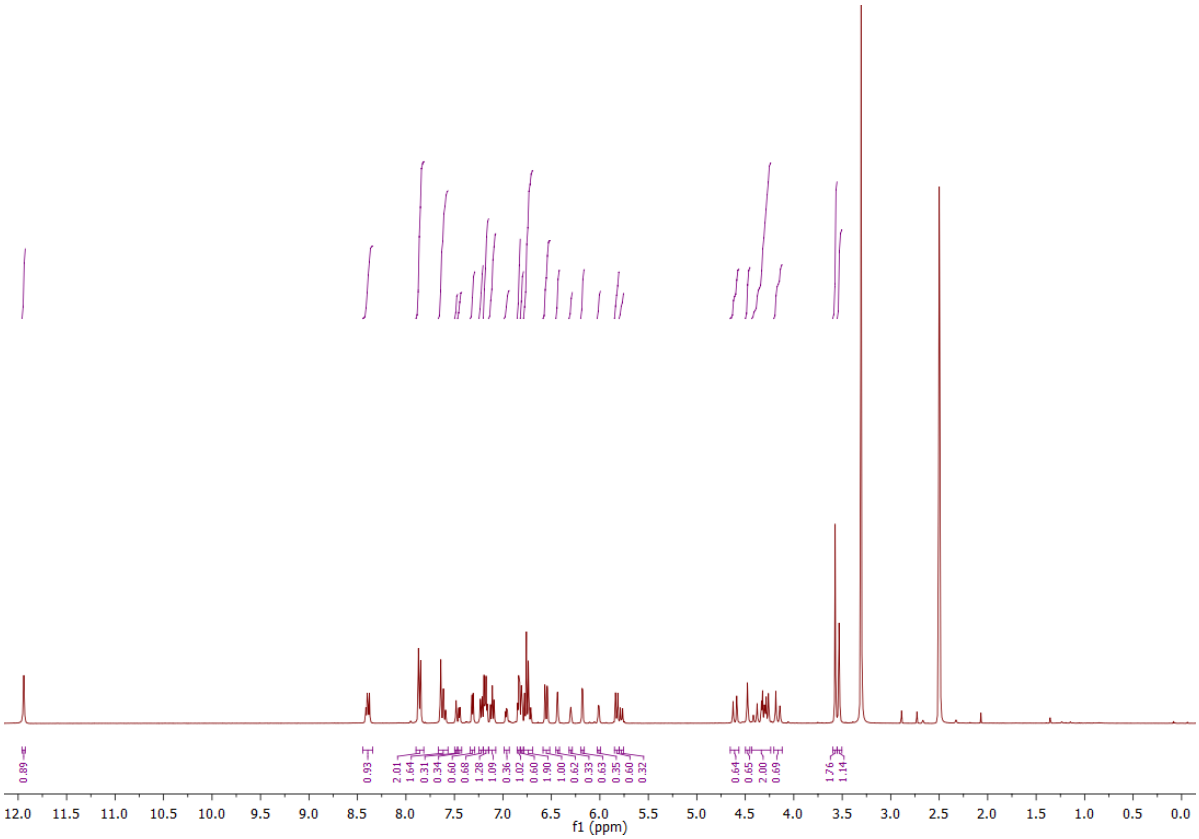

Figure 11.1: ^{1}H NMR spectrum (DMSO-d6, 400 MHz) of OSMI-1.

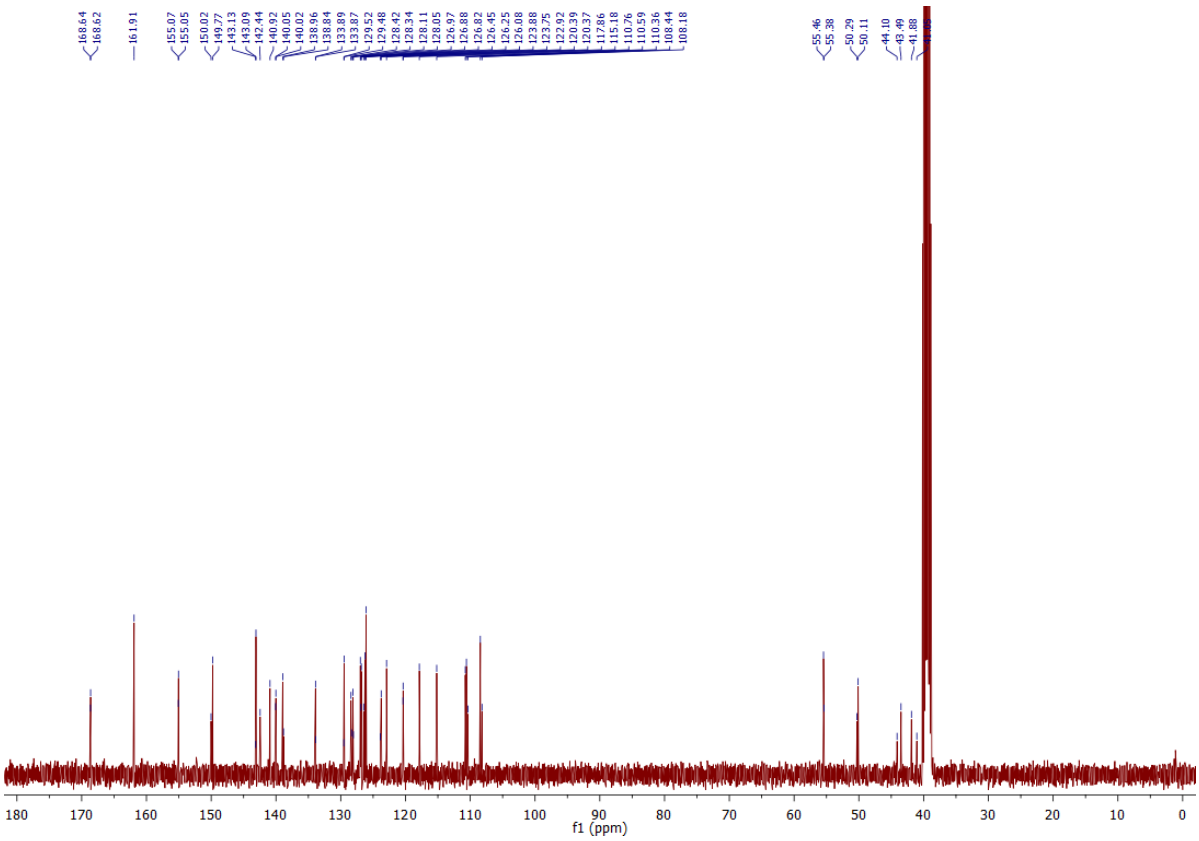

Figure 11.2: ^{13}C NMR spectrum (DMSO-d6, 101 MHz) of OSMI-1.

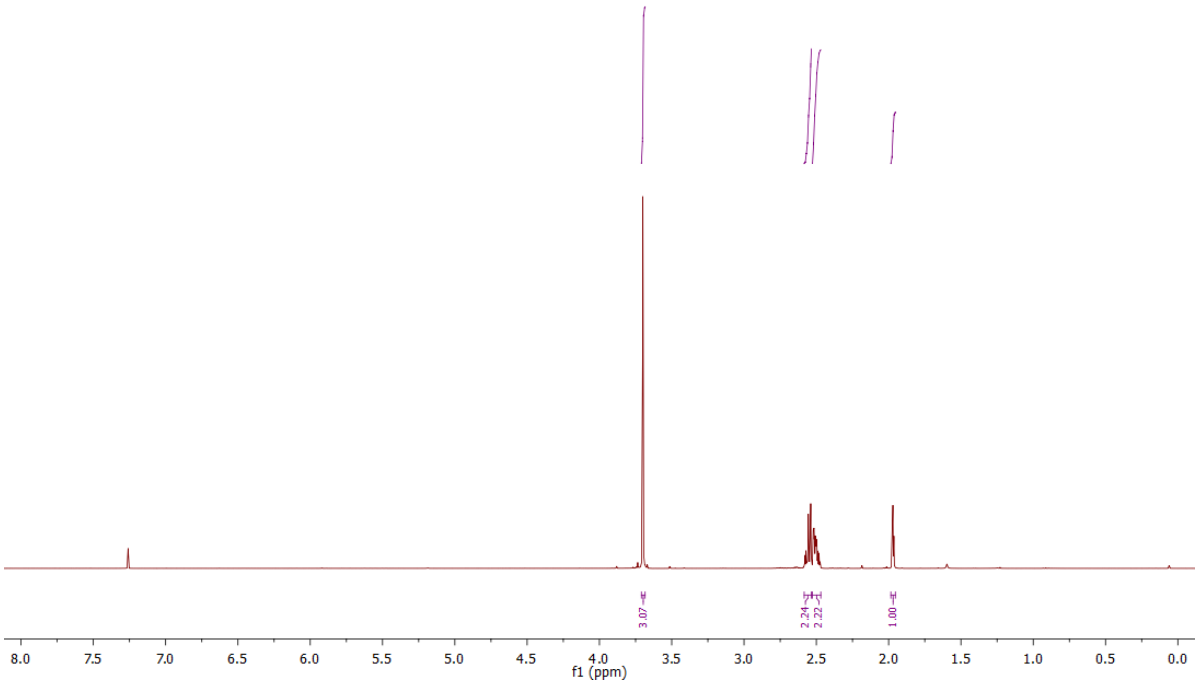

Figure 11.3: ^{1}H NMR spectrum ($CDCl_3$, 400 MHz) of M4P.

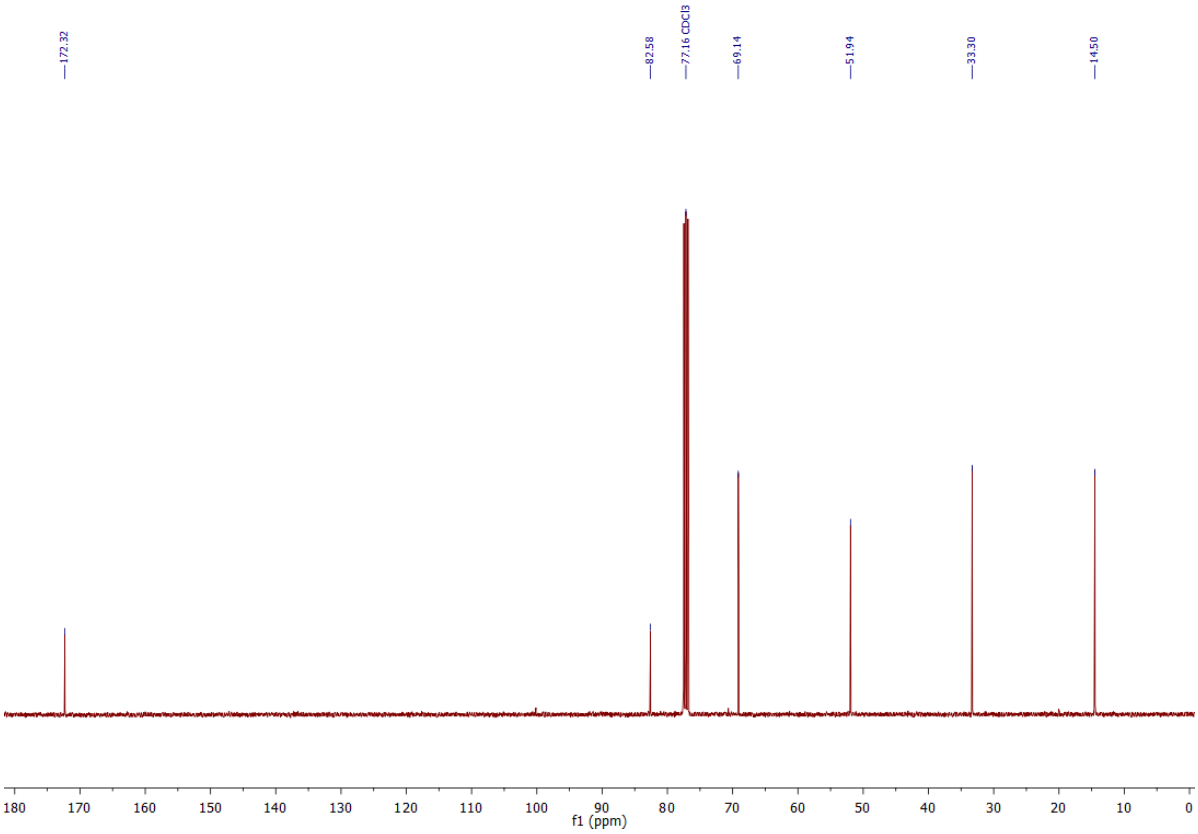

Figure 11.4: ^{13}C NMR spectrum ($CDCl_3$, 101 MHz) of M4P.

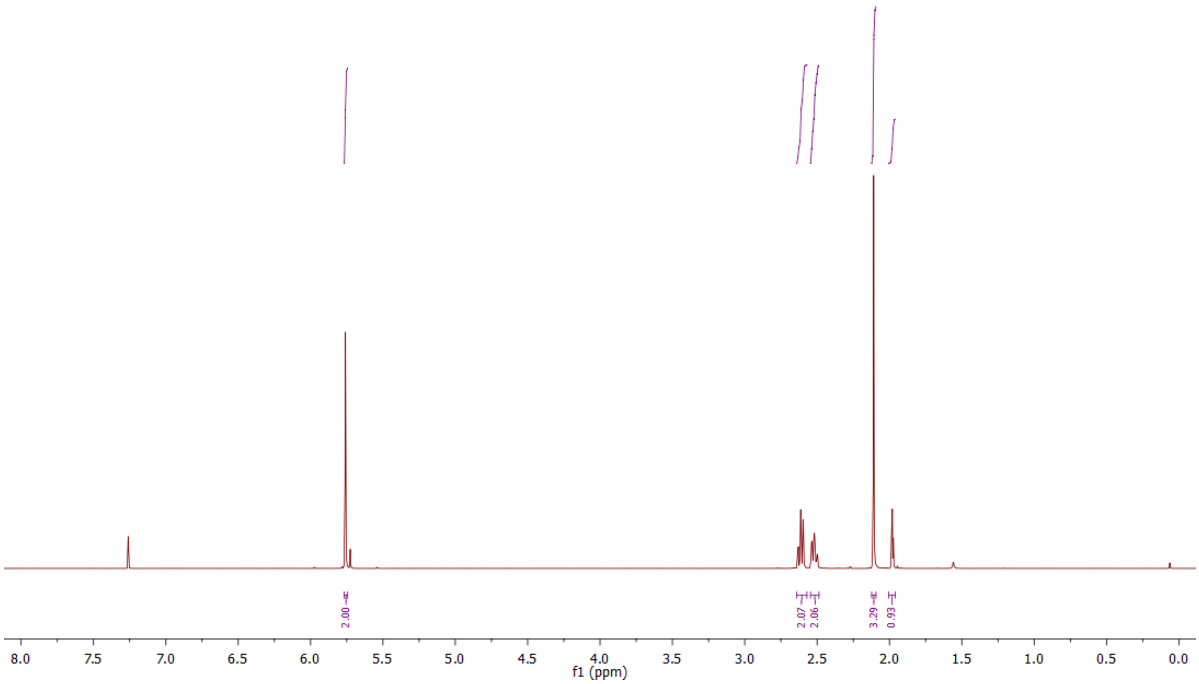

Figure 11.5: ^{1}H NMR spectrum ($CDCl_3$, 400 MHz) of AM4P.

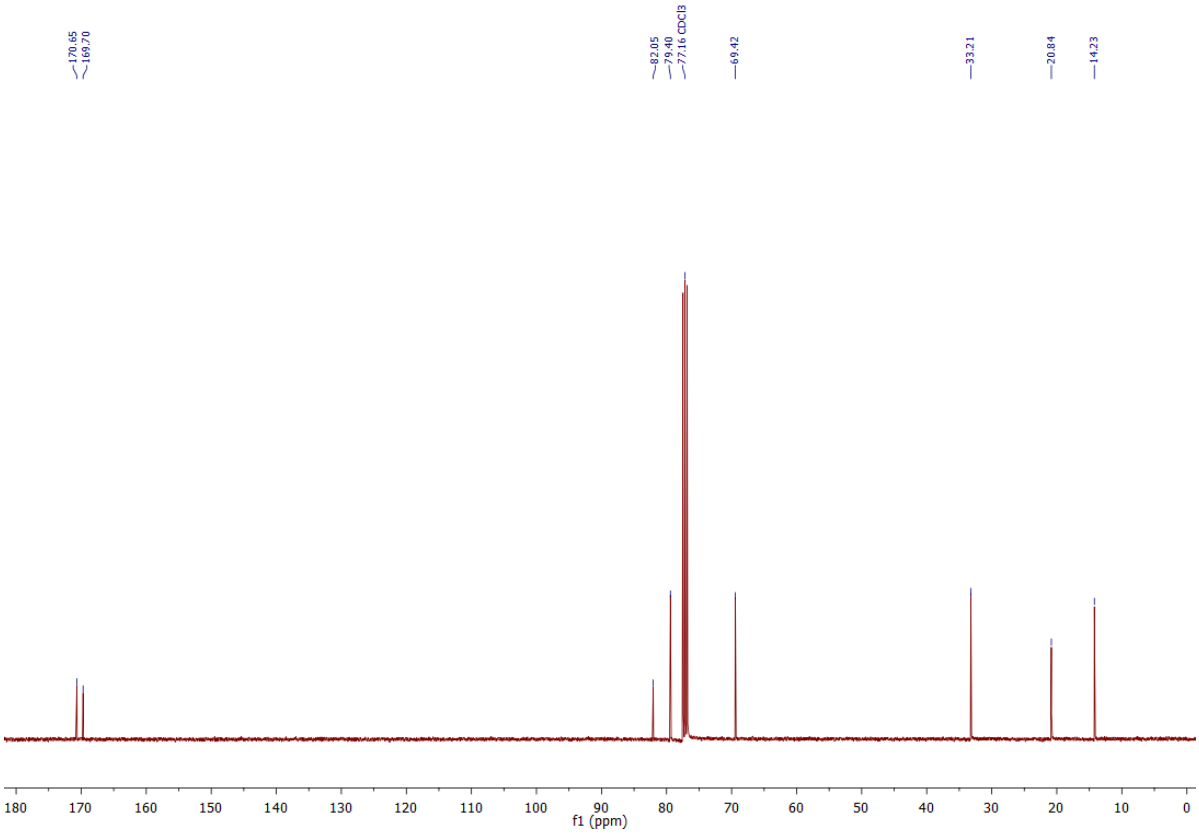

Figure 11.6: ^{13}C NMR spectrum ($CDCl_3$, 101 MHz) of AM4P.